A Light Scattering Study of the Soft Modes in DKDP and DADP.

Kenneth I. White

Ph.D

University of Edinburgh

1972

Acknowledgement

I should like to acknowledge the help given by Dr.S.M.Kay during the early part of this work and the personal financial support of the Dewar Research Fund of the University of Edinburgh.

ABSTRACT

The introductory chapter gives a brief review of ferroelectricty, including the 'soft' mode theory,with particular reference to tunnelling theories of the transition in potassium dihydrogen phosphate and its isomorphs. The theory of light scattering from polar modes of phonon or tunnelling character is dealt with in chapter two. A number of light scattering experiments on ferroelectric crystals are then discussed to show the wide applicability of this experimental technique. Several experiments on KDP-type crystals by other methods are also mentioned. The apparatus used in the present experiment is described in chapter four. Chapter five starts with a discussion on the analysis of the recorded data and continues with a presentation of the results. In particular, a Debye relaxation function fit to the spectra of the four modes under study, which appear as broad wings on the Rayleigh peak, yields the following values for their half-widths :-

DKDP	B_2 wing	$\omega_{\frac{1}{2}} = 0.029\ (T - T_c)$	cm^{-1}
DKDP	E wing	$\omega_{\frac{1}{2}} = 8.45$	cm^{-1}
DADP	B_2 wing	$\omega_{\frac{1}{2}} = 10.6$	cm^{-1}
DADP	E wing	$\omega_{\frac{1}{2}} = 20.3 \dfrac{T - T_c}{T}$	cm^{-1}

The results of the present experiment are compared with those of other experiments on the KDP family in chapter six, while some suggestions for further work are given in the final chapter.

CONTENTS

Introduction		1
Chapter One	- Introduction	2
	The thermodynamic theory of ferroelectricty	4
	The soft mode theory	6
	Ferroelectricty of KDP and its isomorphs	13
	Antiferroelectricty and ADP	38
Chapter Two	- Introduction	41
	Theory of light scattering by polar modes	45
	Forms of the dielectric susceptibility	60
Chapter Three	- Review of light scattering experiments on soft modes	69
	Light scattering experiments on KDP and its isomorphs	93
	Other experiments on KDP crystals	102
Chapter Four	- The experimental apparatus	112
Chapter Five	- Introduction	135
	Data reduction	138
	Results :- DKDP B_2 wing	154
	DKDP E wing	164
	DADP B_2 wing	167
	DADP E wing	169
Chapter Six	- Comparison of present experiment with other work	173
Chapter Seven	- Suggestions for further work	195
Appendix One	- Some properties of KDP	201
Appendix Two	- Physics Letters Paper	202
References		203

INTRODUCTION

A crystal is said to be a ferroelectric if, over some range of temperature, it exhibits a spontaneous polarization which can be reversed by an externally applied electric field. These materials are so called because, phenomenologically, they form the electric analogue of the ferromagnets. In particular, at high temperatures there is no spontaneous polarization and the crystal is in the paraelectric phase while at a lower temperature the crystal undergoes a phase transition to a structure of lower symmetry which is truly ferroelectric. The transition from the paraelectric to ferroelectric phase can often be described by a theory due to Cochran in which, out of all the normal modes present, a transverse optic mode near the centre of the Brillouin zone shifts to very low frequencies as the transition is approached from above. This mode is said to be the ferroelectric or 'soft' mode. The crystal finally becomes unstable against this mode and transforms to the ferroelectric phase whose structure is the static deformation of the high temperature phase corresponding to the dynamical motion of the soft mode.

Soft modes have been studied by numerous experimental methods. The work that follows involved the Raman effect - a process which measures the frequencies of some of the zone centre phonons. Thus Raman scattering is a particularly useful technique in the study of the dynamics of ferroelectric phase transitions.

It was one of those fortunate coincidences that, at approximately the same time, there was a renewed interest in both ferroelectric transitions and Raman scattering due to Cochran's theory on the one hand and the advent of the laser on the other.

CHAPTER ONE

The properties of ferroelectrics in general, and in particular, have been extensively reviewed by several authors including Megaw (1·1), Kanzig (1·2) and Jona and Shirane (1·3).

Out of the 32 crystal point groups 11 are centrosymmetric and thus cannot have a net dipole moment. Of the remaining 21, 20 are piezoelectric and therefore have a moment in the presence of applied stress. A further 10 of these are simultaneously pyroelectric - that they exhibit a spontaneous polarization whose magnitude is temperature dependent. Where this moment is reversible under an applied field the crystal is in a ferroelectric phase. While pyroelectricity can be established on grounds of symmetry alone, ferroelectricity can only be verified by experiment. Such an experiment could involve a Sawyer and Tower circuit (1·4) with an oscilloscope display which would show the characteristic hysteresis loop for the relation between polarization and applied field. In the paraelectric phase where there is no spontaneous polarization the hysteresis loop degenerates into a line.

In the paraelectric phase most ferroelectrics have a Curie-Weiss type anomaly in the low frequency dielectric constant $\epsilon(o)$

$$\epsilon(o) = \epsilon_1 + \frac{C}{T - T_c} \qquad (1\cdot1)$$

T_c is the Curie temperature and may be different from the transition temperature T_T. Since $C \sim 10^3$ or 10^5, ϵ_1, which is typically ~ 5 can be neglected near the transition where $\epsilon(o)$ becomes anomalously large.

The dielectric constant is related to the dielectric susceptibility χ, which is also anomalous, by

$$\chi = \frac{\epsilon - 1}{4\pi} \qquad (1\cdot2)$$

Certain other 'constants' eg elastic, piezoelectric, electro-optic constants, may also show strong temperature dependence near the transition.

Ferroelectric transitions are often classed as first or second order. At a first order transition there are discontinuities in the temperature dependence of the static susceptibility, spontaneous polarization, unit cell volume, specific heat etc and $T_c < T_T$. A second order transition is characterised by a discontinuity in the temperature gradient of these properties and $T_c = T_T$. Diagrams illustrating the above are in fig (1·1).

Schemes for classifying ferroelectrics are often neither particularly definitive or useful. It is, however, common to refer to 'displacive' or 'order-disorder' ferroelectrics. In displacive ferroelectrics, certain atoms undergo small (ie 1-2% of unit cell dimension) shifts in equilibrium position at the transition. The resulting separation of the centres of positive and negative charge produces the spontaneous polarization. The perovskites eg. $BaTiO_3$ typify this class. Order-disorder ferroelectrics, on the other hand, have an atom, or group of atoms which can occupy either of two equilibrium sites above the transition but assume an ordered configuration in the ferroelectric phase. The displacements involved are somewhat larger than for displacive ferroelectrics. $NaNO_2$ and triglycine sulphate are among the order-disorder types.

Fig. 1.1

First order

Second order

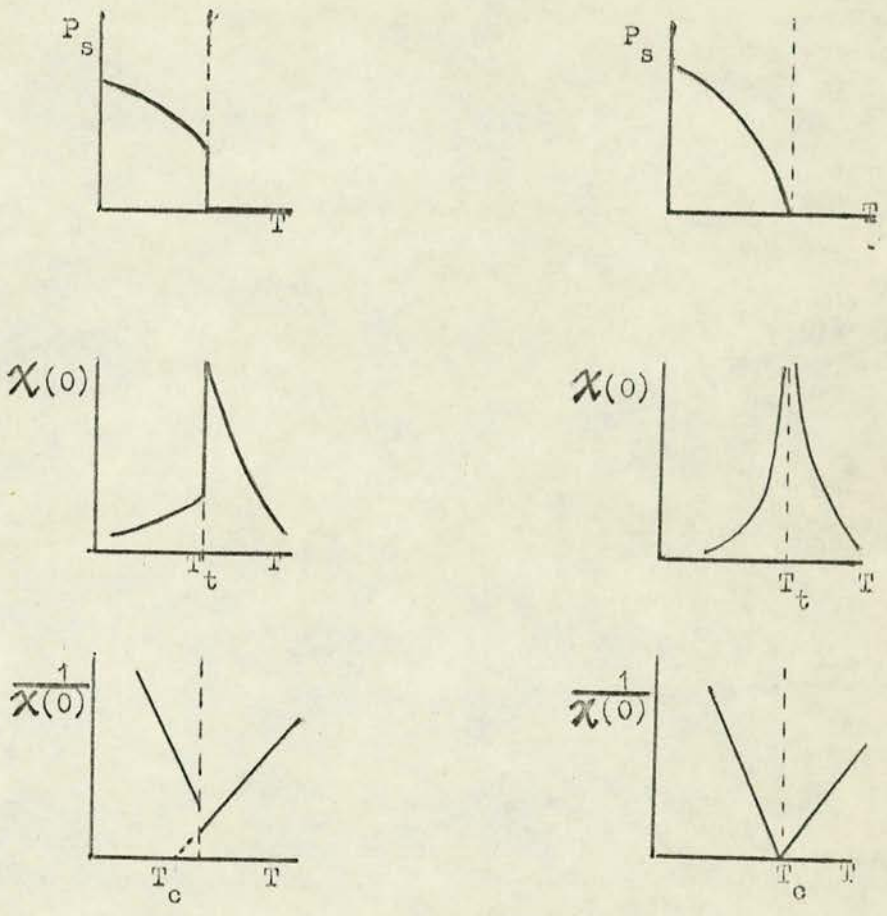

The temperature variation of the spontaneous polarization, P_s, the static susceptibility, $\chi(0)$, and its reciprocal in the region of a ferroelectric transition.

Potassium dihydrogen phosphate - KDP - and its isomorphs form an interesting group intermediate between these two classes and shall be discussed later.

THERMODYNAMIC THEORY OF FERROELECTRICITY

Since, in general, the bulk properties of all ferroelectrics are similar it is useful to consider ferroelectricity from a thermodynamic viewpoint. The development of such a phenomenological theory owes much to Landau (1·5) and Devonshire (1·6). In the Devonshire theory it is assumed that the free energy of the crystal can be expanded as a power series in polarization and strain - $A(P, x)$ - or field and stress $A(E, X)$ or even $A(P, X)$ and $A(E, x)$. It is further assumed that the crystal is always in a minimum of free energy and that, since only a small deformation occurs at the transition, the same function can be applied in both phases. An example of such a function is

$$A(P, x) = \tfrac{1}{2} k^{(x)}_{\alpha\beta} P_\alpha P_\beta + \tfrac{1}{3} k^{(x)}_{\alpha\beta\gamma} P_\alpha P_\beta P_\gamma + \ldots. \quad (1\cdot3)$$
$$+ \tfrac{1}{2} C^{(P)}_{\alpha\beta} x_\alpha x_\beta$$
$$+ a_{\alpha\beta} x_\alpha P_\beta + \tfrac{1}{2} g_{\alpha\beta\gamma} x_\alpha P_\beta P_\gamma$$

$\frac{1}{k}$ = dielectric susceptibility (linear)

$\frac{1}{k}$ = " " (non linear)

c = elastic constant

a = piezoelectric constant

g = electrostrictive constant

The Voigt notation has been used ($x_4 = x_{yz}$) and there is implied summation over repeated indices. The temperature dependence of $A(P, x)$ is included through the Constants; usually just $k_{\alpha\beta}^{(x)}$. In piezoelectric crystals care must be taken to denote the appropriate mechanical and electrical boundary conditions, since $C^{(P)}$ and $C^{(E)}$ are not necessarily equal and neither are $k^{(x)}$ and $k^{(X)}$. In the ferroelectric phase terms up to P^6 may well be needed to obtain a good fit between experiment and theory. As the crystal is always assumed to obey Hooke's Law, terms above quadratic in strain are omitted.

By forming the various partial derivatives of the four forms of the free energy mentioned above it is possible to obtain relations between the various constants involved. While this can be done for any crystal its value in the case of a ferroelectric is that one can predict which components, if any, of the elastic, piezoelectric etc constants will show an anomaly in parallel with the dielectric constant.

By expanding $A(X=0, P)$ up to P^6, for a crystal centrosymmetric in the paraelectric phase, it can be shown that the transition will be first or second order depending on whether the coefficient P^4 is less than or greater than zero.

A recent extension of Devonshire's theory by Draegert and Singh (1·7) shows that while near the transition the ratio of the slopes of the inverse susceptibility below and above the transition is -2 for second order and -8 for first order, both ratios tend to -4 far from the transition. That is

$$\frac{\left(\frac{\partial \underline{1}}{\partial T}\right)_{T < T_c}}{\left(\frac{\partial \underline{1}}{\partial T}\right)_{T > T_c}} = \begin{cases} \leqslant -4 & \text{first order} \\ \geqslant -4 & \text{second order} \end{cases} \qquad (1\cdot4)$$

These predictions compare reasonably well with experiment and provide a basis for distinguishing between first and second order transitions over a wide range of temperature, rather than from measurements taken close to the transition, as is usually the case.

While Devonshire's theory is useful for predicting the macroscopic behaviour of ferroelectrics in general, it does not tell us about the mechanism of ferroelectricity in specific materials.

THE SOFT MODE THEORY

While the idea that a ferroelectric transition is due to the instability of a crystal against a normal mode of vibration owes its extensive development to Cochran (1·8), the connection between structural phase transitions and lattice dynamics had occurred to others before him. This point has recently been discussed by Cochran (1·9) who traces the idea back to Raman and Nedungadi in 1940 (1·10). They noted that, in the Raman spectrum of quartz, the mode near 220 cm^{-1} became broader and shifted to lower frequencies as the transition at 573°C was approached from below. They inferred that this was to a large extent responsible for the transition. Although this transition is not infact ferroelectric, their experiment probably represents the first observation of a soft mode. The idea was also

familiar to Ginzburg (1·11) and Fröhlich (1·12) who pointed out that the Lyddane-Sachs-Teller relation (1·13)

$$\frac{\omega_L^2}{\omega_T^2} = \frac{\epsilon(o)}{\epsilon(\infty)} \qquad (1·5)$$

might imply a lattice dynamical instability resulting from the dielectric anomaly. ω_L and ω_T denote the longitudinal and transverse optic mode frequencies in an ionic diatomic crystal having low and high frequency dielectric constants $\epsilon(o)$, $\epsilon(\infty)$, Anderson (1·14) also discussed the topic in 1960 although he had done the work some years before.

While the phenomenological theory of Devonshire links the anomalies in various crystal properties to that in the dielectric constant, the central idea of Cochran's theory is that the transition itself and all the anomalies that precede it result from the instability of the paraelectric crystal structure against a long wavelength transverse optic mode of vibration.

The simplest structure for which a ferroelectric transition could be envisaged is that of sodium chloride. This has the necessary polar transverse optic mode whose dynamic displacements could 'freeze' in at the transition to give the spontaneous polarization in the ferroelectric phase. Although NaCl is not in fact a ferroelectric the closely related system $Sn_xSe_{1-x}Te$ can be (1·15) (1·16).

Modes of long wavelength propagating parallel to the crystal axes are essentially those of a linear diatomic chain. The ionic displacements then result from crystal symmetry rather than interatomic forces and the modes are thus purely transverse or longitudinal. With the rigid ion approximation in which the ions of types 1 and 2 are represented by point charges $\pm$ z, the equations of motion are given by

$$M_1\ddot{U}_1 = R(U_2-U_1) + \frac{4\pi P}{3} z \quad \text{for transverse optic modes} \qquad (1\cdot6)$$

$$M_1\ddot{U}_1 = R(U_2-U_1) + \frac{4\pi P}{3} z - 4\pi P z \quad \text{for longitudinal optic modes} \qquad (1\cdot7)$$

$$\text{With } M_1\ddot{U}_1 = -M_2\ddot{U}_2 \quad \text{for both} \qquad (1\cdot8)$$

Where $M_{1,2}$ is the mass of ion of type 1,2 having displacements $U_{1,2}$

R represents short range forces between nearest neighbours only

$$P = \frac{z}{v}(U_1-U_2) \qquad (1\cdot9)$$

is the polarization associated with the ionic displacements in a unit cell of volume v.

$\frac{4\pi P}{3}$ is the Lorentz field acting on an ion of charge z due to all the other dipoles in the crystal

$-4\pi P$ is the macroscopic dipolarizing field due to the displacements involved in a longitudinal optic mode.

Solving equations (1·6) to (1·9) gives the longitudinal and tranverse optic (LO and TO) frequencies as

$$\mu \omega_L^2 = R + \frac{8\pi z^2}{3V} \qquad (1\cdot10)$$

$$\mu \omega_T^2 = R - \frac{4\pi z^2}{3V} \qquad (1\cdot11)$$

$$\mu = \frac{M_1 M_2}{M_1 + M_2} \qquad \text{the reduced mass} \qquad (1\cdot12)$$

Born and Huang (1·17) have shown that a crystal will remain stable against a normal mode of vibration provided that its frequency remains real. An instability could occur for the transverse optic mode of equation (1·11) if the short range and electrostatic forces cancel. A mode which becomes unstable in this way is said to be 'soft'. When the soft mode has zerofrequency the ions move to new positions of equilibrium that are related to the dynamical motions involved in the soft mode. This allows the corresponding mode in the new structure to have a real frequency.

The longitudinal mode frequency, on the other hand, is little affected. The difference in frequency between the longitudinal and transverse optic modes, or LO-TO splitting, arises from the depolarizing field associated with the polar longitudinal modes. While $\omega_L > \omega_T$ for polar modes, they are degenerate for longwave length non-polar modes.

To determine the dielectric response of the crystal a sinusoidal electric field is imagined applied to the crystal. A term $zE_o e^{-i\omega t}$ is thus added to the right hand side of equation (1·6), which is solved with equation (1·8) and $P = P_o e^{-i\omega t}$ to give

$$\frac{P_o}{E_o} = \frac{\frac{\mathfrak{z}^2}{\mu V}}{\omega_T^2 - \omega^2} \qquad (1\cdot13)$$

but $$\frac{P_o}{E_o} = \chi(\omega) = \frac{\epsilon(\omega) - 1}{4\pi} \quad \text{by definition} \qquad (1\cdot14)$$

$\chi(\omega)$ can be made a little less unrealistic near ω_T by including a damping term in the equation of motion (1·6), but the result we require does not need that.

Equations (1·13) and (1·14) give $\epsilon(o) = 1 + \frac{4\pi\mathfrak{z}^2}{\mu V \omega_T^2}$ (1·15)

While (1·10) and (1·11) yield $\omega_L^2 = \omega_T^2 + \frac{4\pi\mathfrak{z}^2}{\mu V}$ (1·16)

Thus $$\left(\frac{\omega_L}{\omega_T}\right)^2 = \frac{\epsilon(o)}{1} \qquad (1\cdot17)$$

This is the LST relation in the rigid ion approximation. Since the ions have not been considered polarizable, the response of the electrons has been neglected and the high frequency dielectric constant $\epsilon(\infty)$ is unity. The form of the LST relation and the experimental observation that $\epsilon(o) \propto (T-T_c)^{-1}$ near the transition makes Cochran's assumption that $\omega_T^2 \propto (T-T_c)$ as a result of a linear temperature dependence of force constants and/or unit cell volume seem indeed plausible, since it has already been remarked that ω_L is little affected by the transition and $\epsilon(\infty)$, the square of the refractive index, is known to be ordinarily a weak function of temperature. Hence ferroelectricity arises from the ionic rather than electronic properties of a crystal.

Thus, on the basis of a very simple model the transition is seen to result from an unstable long wavelength transverse optic mode which is also responsible for the dielectric anomaly.

Cochran (1·8), using more than nearest neighbour interactions and treating the ions as being polarizable within the shell model (1·18) approximation, deals firstly with Barium Titanate ($BaTiO_3$) and subsequently extends the theory to crystals of lower symmetry which may be piezoelectric in the paraelectric phase, taking the zinc blende structure as an example. By considering the propagation of appropriate acoustic modes, the elastic and piezoelectric constants, for instance, can be found in terms of the force constants, charges and other microscopic parameters. Thus the anomalies in certain properties of crystals approaching ferroelectric phase transitions are all seen to result from the lattice instability rather than, as was once thought, from a 'special' anomaly e.g. that in the static dielectric constant. The soft mode theory has been particularly successful in dealing with displacive ferroelectrics.

Although the relation originally derived by Lyddane, Sachs and Teller (1·13), equation (1·5), applies only to diatomic crystals in which each atom is surrounded by at least tetrahedral symmetry, the applicability of this useful relation has been extended by Cochran and Cowley (1·9) who derived a generalised LST relation

$$\prod_i \left(\frac{\omega_{L_i}}{\omega_{T_i}} \right)^2 = \frac{\epsilon(o)}{\epsilon(\infty)} \qquad (1·18)$$

The product is over all long wavelength optic modes which have

atomic displacements along the direction for which $\epsilon(o)$ and $\epsilon(\infty)$ have been measured. Near a ferroelectric transition equation (1·18) can be approximated by $\omega_o^2 . \epsilon(o)$ = temperature independent constant, eqn. (1·19), where o denotes the soft mode. This relation is often used to make comparison between measurements of the soft mode frequency and static dielectric constant.

Although the soft mode theory, as discussed above, has only been applied above the transition, there will also be a soft mode in the ferroelectric phase. By virtue of the LST relation, ω_o^2 will increase again on cooling below the transition as $\epsilon(o)$ falls to lower values.

However, since we noted while discussing the thermodynamic theory that the ratio of $\left(\frac{\partial \frac{1}{\chi}}{\partial T}\right)$ above and below the transition was temperature dependent, ω_o^2 will not in general be proportional to $(T_c - T)$ over a large temperature range in the ferroelectric phase.

In discussing ferroelectric transitions the term 'long wavelength mode' is often used. This wavelength is taken to be long compared to the unit cell dimension but short compared to the crystal dimensions. Similarly, the equivalent term 'zone centre mode' ie $|\underline{q}| \equiv \frac{2\pi}{\lambda} = 0$ is intended to refer to phonons having small but finite values of $\underline{q}$, just beyond the region of polariton dispersion.

Crystals may become unstable to modes at points in the zone other than at $\underline{q} = o$. A zone boundary instability involving an anti-polar mode, induces a transition to an anti-ferroelectric phase in which adjacent dipoles are anti-parallel. There is no net spontaneous polarization.

Figure (1·2) shows zone centre and zone boundary modes appropriate for ferro- and anti-ferroelectric transitions in a two-dimensional crystal. Antiferroelectricity is defined only by analogy with ferroelectricity and does not give rise to a macroscopically measurable quantity. It is a microscopic property which can be verified only by structural analysis.

Transitions are also possible for mode instabilities that involve no dipoles at all, e.g. the $\alpha \leftrightarrow \beta$ transition in quartz, the 106°K transition in strontium titanate. The term 'anti ferroelectric transition' is often extended to include such structural transitions.

THE FERROELECTRICITY OF POTASSIUM DIHYDROGEN PHOSPHATE AND ITS ISOMORPHS

Ferroelectricity was discovered in potassium dihydrogen phosphate - KDP - by Busch and Scherrer (1·20) in 1935. Since then the isomorphs formed by replacing potassium by rubidium or caesium, or phosphorous by arsenic, together with the isotopes obtained on deuteration have all been shown to exhibit similar ferroelectric properties. A discussion of KDP therefore suffices for them all. The substitution of ammonium for potassium gives a series of anti-ferroelectric isomorphs which shall be discussed in a later section. While details of the structure of KDP are listed in appendix 1, some of the main features are discussed below.

In the paraelectric phase KDP is usually referred to a tetragonal unitcell having twice the volume of the primitive cell. The structure, due to West (1·21), is shown in figure (1·3). The K and P ions, separated by half a unit cell dimension, form chains parallel to the

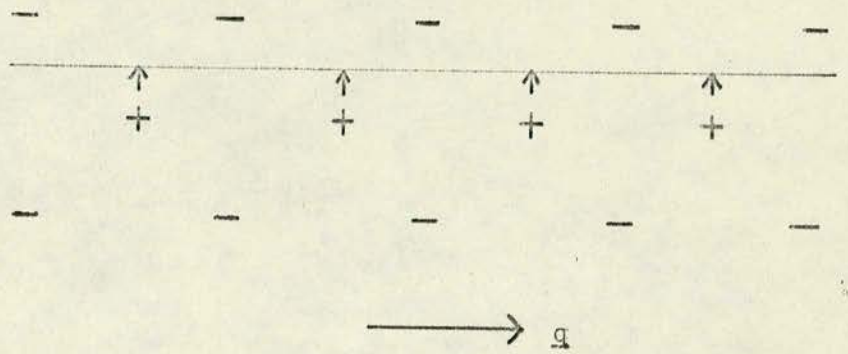

Fig. 1.2a

A transverse optic mode of q = 0.
Such a mode can lead to a ferroelectric transition.

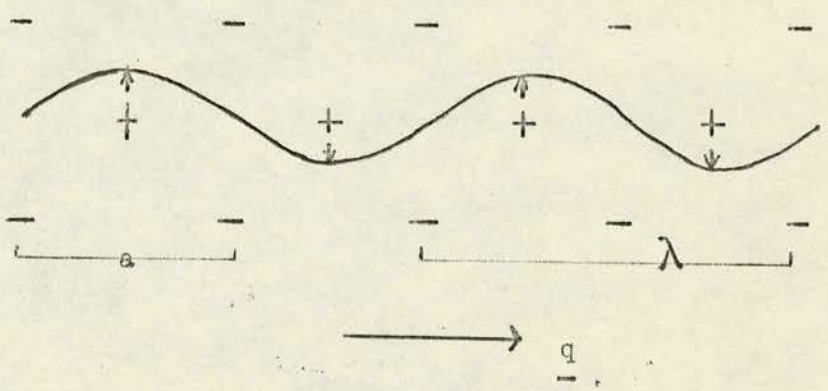

Fig. 1.2b

A transverse optic mode of $q = \frac{\pi}{a}$. i.e. $\lambda = 2a$.
Such a mode can lead to an anti-ferroelectric transition.

+ − denote ions of opposite charge.

Fig. 1.3

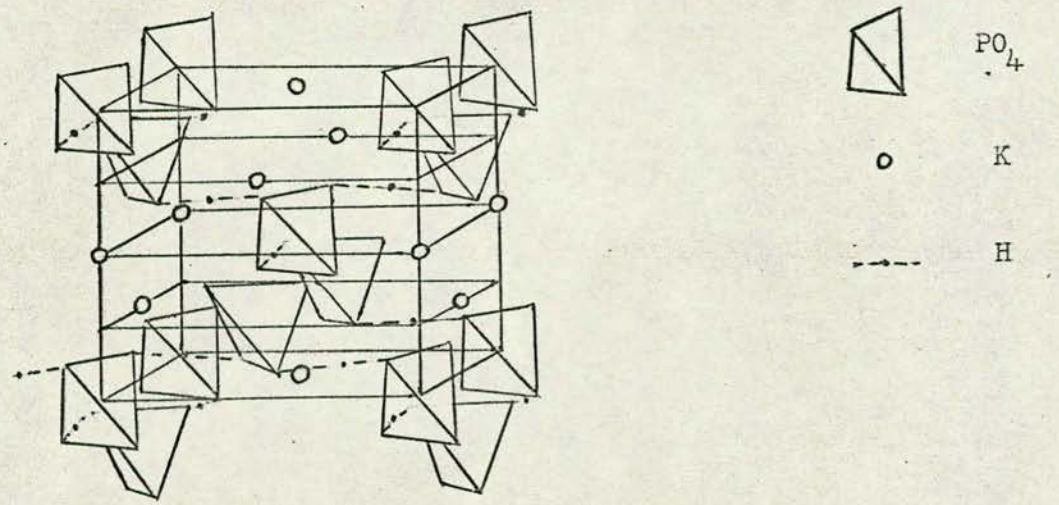

The structure of paraelectric KDP - after West

tetrad, C, axis. Each of the PO_4 groups, which form tetrahedra, is linked to the four nearest PO_4 groups by hydrogen bonds running between the top of one group and the bottom of the next. The crystal is imagined to have its C axis vertical. The hydrogen bonds are approximately parallel to the a and b axis. A view of the crystal looking down the C axis is shown in figure (1·4).

Detailed structural studies by Frazer and Pepinsky (1·22) using x-rays, and by Bacon and Pease (1·23) with neutron diffraction, just above and below the transition show that the spontaneous polarization which develops along the former C axis is due to opposite displacements of the K and P ions of about 0·05 Å from their equilibrium positions in the paraelectric phase. This, together with a small xy shear (27′ at 20° below T_T), takes the crystal into the orthorhombic ferroelectric phase. The relation between the unit cells in both phases is shown in figure (1·5). The neutron diffraction experiments further showed that in the ferroelectric phase, the hydrogens were ordered on off-centre positions on the bonds - by about 0·2 Å - in such a way that there were two hydrogens at the end of each PO_4 group from which the K and P ions had departed. This ordering is shown in figure (1·4). A sufficiently strong electric field produces the shifts in the positions of the K and P ions necessary to reverse the sponteneous polarization, and causes each hydrogen to move to the other equilibrium position on the bond. Above the transition the hydrogens were either undergoing oscillations along the bond between the two possible low temperature sites, or were randomly distributed between them. The terms 'hydrogen' and 'proton' are used interchangably to denote a proton with most of an electrons charge, as observed in structural studies.

Fig. 1.4

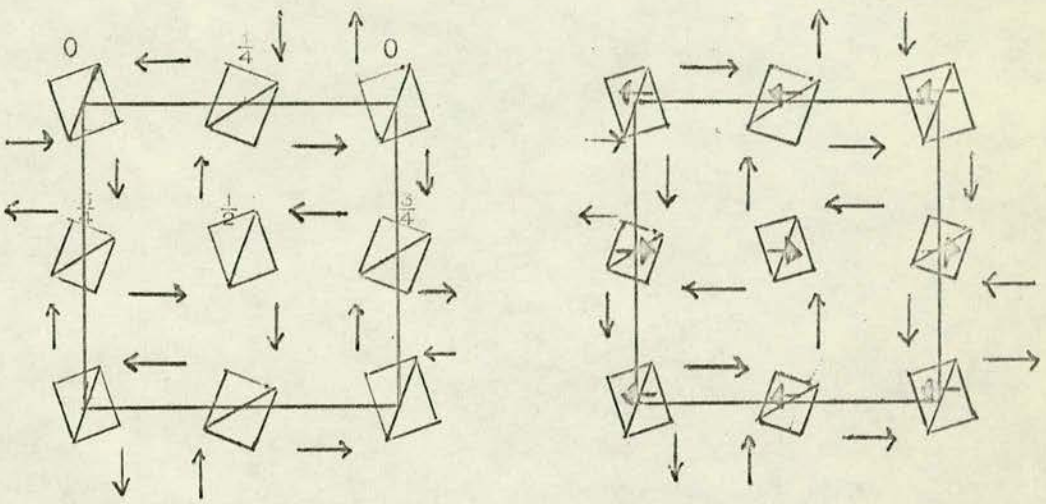

a. b.

The arrows represent the proton motions in the (a) ferroelectric (b) anti-ferroelectric modes of KDP. The protons 'freeze in' at the arrow heads to give dipoles for the H_2PO_4 groups all out of the page in (a) but forming oppositely directed chains in (b) - denoted by solid head arrows.

The relative height of the PO_4 groups  are noted in (a).

Fig. 1.5

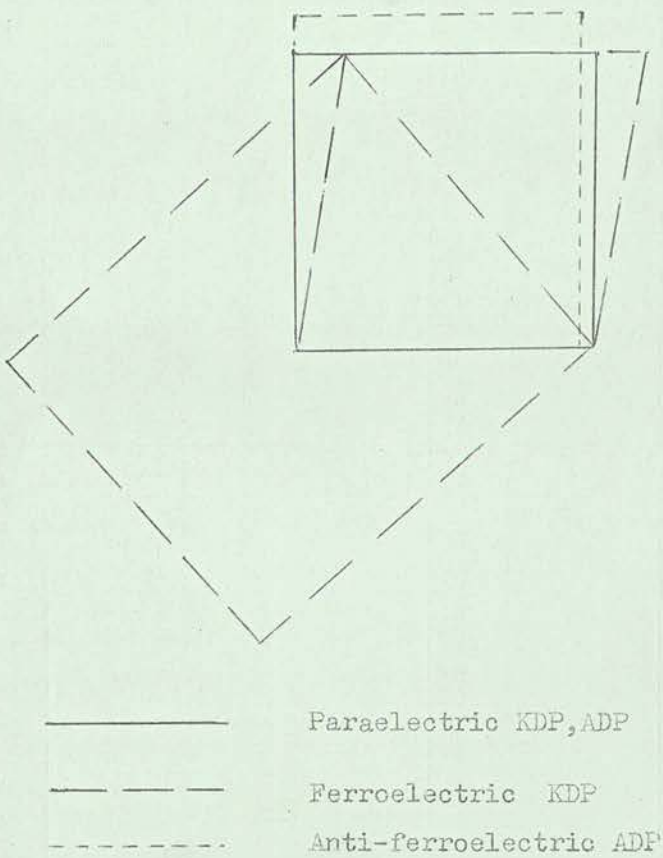

A comparison of the unit cells of KDP and ADP.

As the spontaneous polarization can be accounted for by the displacements of the P,K,O ions on assuming plausible effective charges, the transition has the appearance of the displacive type as in the perovskites. However, the hydrogens must play an important role in the transition since their order is related to that of the heavy ions and also since on deuteration the transition temperature increases by about 70% for the isomorphs as a whole. The spontaneous polarization and Curie Constant are little changed, however. This situation is to be compared with Rochelle salt or lithium ammonium tartrate, two hydrogen bonded ferroelectrics that have the hydrogens centrally situated on the bond and have little or no isotope effect on the transition temperature. Further, in KDP, the entropy change at the transition is comparable to that found in order-disorder transitions and much larger than is usual for displacive ones. Thus any theory of KDP must have as its aim a satisfactory explanation of the appearance of the spontaneous polarization along the c axis and the importance of the hydrogen bonds lying the ab plane.

THEORIES OF FERROELECTRICITY IN KDP

In an attempt to explain the dielectric anomaly in KDP, early theories, which have been reviewed by Baumgartner et.al. (1·24), applied the Langevin-Weiss theory of ferromagnetism to the permanent dipoles present in the ferroelectric phase. That the theory gave a poor fit to experimental results was taken to show that it was unsatisfactory to assume a solely Coulomb nature for the dipole-dipole interactions as implied by using a Lorentz field.

Following the early structural work by West (1·21) but before that by Bacon and Pease (1·23), Slater (1·25) developed a model of KDP in which only short range interactions were important. Assuming one proton per bond, he considered distributions of hydrogens in which two of the equilibrium sites near a PO_4 group were filled. All other configurations were neglected since their supposed higher energy made their occurrence less likely. The two configurations having both protons at the top or bottom of a PO_4 group were assumed to be the ferroelectric ground state and to give a dipole pointing along the $\pm$ c directions for that H_2PO_4 group. The four other configurations were assumed to have higher energy and to produce dipoles pointing along $\pm$ a or $\pm$ b. Slater's model accounts well for the observed eutropy change at the transition. The spontaneous polarization is a step function but other quantities vary smoothly.

Takagi (1·26) extended Slater's theory to allow a small proportion of configurations having one or three protons per PO_4 group. This improved the general agreement with experiment for thermodynamic properties, rounded off the step function for the spontaneous polarization and predicted a first or second order transition depending on the values of certain parameters.

The main objections to the Slater-Takagi theory are that the spontaneous polarization is assumed due to the configurations of protons which move in a plane perpendicular to the polar axis, and that the transition temperature which is taken to depend on the energy difference between the two sets of configurations having two protons near one PO_4 group, is unlikely to have a strong enough mass dependence to agree with the isotope effect on the Curie temperature.

By introducing long range dipole-dipole interactions into the Slater theory, Senko (1·27) obtained isotope effects for the Curie temperature and, unfortunately, the spontaneous polarization for which he obtained poor temperature dependence. He also treated the temperature and field dependence of the dielectric constant. Further extensions to the Slater-Takagi theory were made by Silsbee et al (1·28) who introduced dynamical aspects by considering deuteron interbond and intrabond jumps both theoretically and in resonance experiments.

As distinct from the Slater approach, Pirenne (1·29) proposed a model in which the kinetic energy of the proton motion was important. The protons were assumed to move in an anharmonic potential well whose levels were lowered on deuteration to give an isotope effect on the Curie temperature and spontaneous polarization. Dipole-dipole interactions were taken to give the spontaneous polarization which Pirenne treated in two parts - one due to the displaced protons and another, larger, contribution from the rest of the crystal.

Blinc (1·30) developed Pirenne's ideas to a model in which the protons tunnelled between the two equilibrium positions in a symmetric double minima potential well. He also considered interactions between an isolated proton and the lattice in the strong and weak coupling limits. While the isotope effect on the Curie temperature can be explained by assuming that the heavier particle is less likely to tunnel, the model also gives an isotope effect to the spontaneous polariziation which has the protons as its source.

Following work by de Gennes (1·31), Brout, Müller and Thomas (1·32) Villain and Stamenkovic (1·33) and Tokunaga and Matsubara (1·34) all showed that the proton system had collective excitations that had soft behaviour; that is the frequency of the proton mode tends to zero at the temperature at which the proton system becomes ordered. Tokunaga and Matsubara linked the proton behaviour to t he spontaneous polarization by assuming that the K-PO_4 system under went an order disorder transition in parallel to that of the proton system. There is however no evidence to support such a disordering of the K-PO_4 system above the transition. They also discuss the relation of their model to those of Slater and Blinc which are seen as its limiting cases.

Cochran (1·8) has applied the soft mode theory to KDP. He considered coupling between a mode involving the K and P ions, similar to the soft mode in purely displacive ferroelectrics, and a mode involving a re-ordering of the protons which becomes more complete as the transition is approached. While this leads naturally to the observed change in structure at the transition, and hence the spontaneous polariziation, by putting the driving force behind the transition into the K-P ion vibration,it deals little with the isotope effect on Curie temperature.

Further theories in which there was proton-phonon coupling were developed by Novakovic (1·35) who considered the proton motion to be slow enough for the other atoms to be at positions of equilibrium relative to the proton system, - the adiabatic approximation. This leads to a lattice excitation spectrum unaffected by the proton mode, which itself has the same general behaviour as it had without the interaction but with renormalized parameters. Kobayashi (1·36)

considered coupling of the proton mode, which, because of the isotope effect on the transition temperature, is assumed to be the driving force behind the transition, to the optic mode involving the K, P ions which produce the spontaneous polarization below the transition. Thus Kobayashi, like Cochran, treats the dynamics of the transition in KDP as a problem in lattice dynamics, but with the emphasis on the proton rather than phonon modes.

Before considering the full theory involving phonons, proton modes and their interaction due to Kobayashi (1·36), it is perhaps useful to review the work of Tokunaga and Matsubara (1·34) on the proton motion alone. The work of the above authors in the paraelectric phase has been reviewed by Cochran (1·37) whom we now follow.

The motion of protons along the bond, proposed by Blinc (1·30) to be an oscillation in a double minima potential well, is considered by analogy to the hydrogen molecule ion. As shown in figure (1·6), the lowering of the infinite barrier between two similar potential wells causes their originally identical energy levels to split. The magnitude of the ground state splitting, designated 2Ω, is determined by the extent of the overlap between the two wavefunctions, $\phi^{(a)}$ and $\phi^{(b)}$, appropriate to protons situated in the initially separate wells. In the double well the general wavefunction is given by

$$\Phi = a\,\phi^{(a)} + b\,\phi^{(b)} \qquad (1\cdot19)$$

where the a and b are Fermi operators. If it is assumed that there is only one proton associated with each bond and that the splitting, 2Ω, is small compared with the energy of the first excited state, the Fermi operators may be represented by a further set of operators

Fig. 1.6

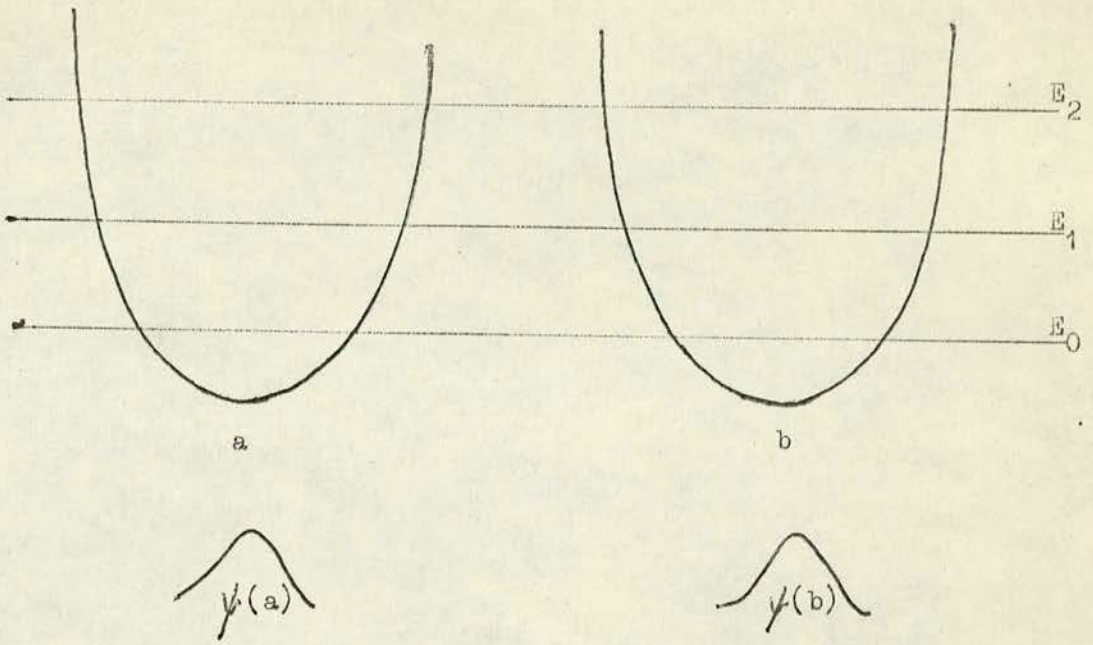

Two infinite potential wells and their energy levels.

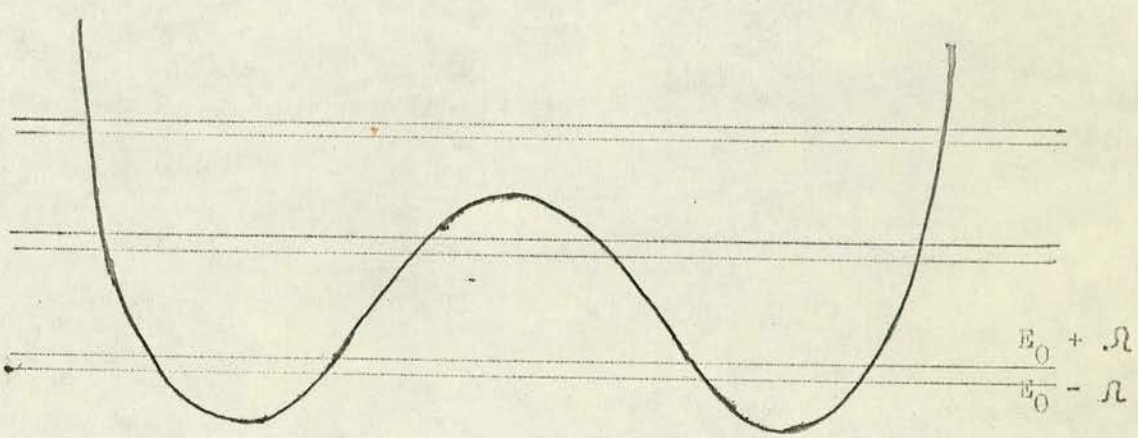

$$\Psi = a\psi(a) + b\psi(b)$$

A double minima potential well derived from those above.

X, Y, Z, which satisfy the commutation relation $[X, Y] = iZ$, and cyclically. Thus, this two level system can be treated as a fictitious or pseudo spin $\frac{1}{2}$ system. This was first suggested in 1962 (1·38) and published by de Gennes in 1963 (1·31).

Extending the treatment from one bond to a crystal having one proton per unit cell, labelled l, the Hamiltonian for the protons is given by

$$H = -2\Omega \sum_{l} X_{l} - \frac{1}{2} \sum_{ll'} J_{ll'} Z_{l} Z_{l'} \qquad (1\cdot20)$$

The first term represents the kinetic energy of a system of isolated protons where the spin components, $X_{l} = \pm \frac{1}{2}$, cause the proton to move to the other minimum on the bond. The second term represents an unspecified interaction between pairs of protons. $J_{ll'}$ is the interaction constant and $Z_{l} = \pm \frac{1}{2}$ denotes at which minima on the l^{th} bond the proton is situated. Note that $J_{ll} = 0$ since there is no self interaction. Since interactions of the form $Z_{l} Z_{l'} Z_{l''}$ and higher order have been omitted, the Hamiltonian is within the harmonic approximation. Small terms due to interaction between the tunnelling motion and the proton-proton interaction have also been neglected.

For $\Omega = 0$, i.e. a static model in which there is no tunnelling, the Hamiltanian is that of the Ising model successfully used by Yamada and Yamada (1·39) for the purely order disorder transition in $NaNO_2$.

The problem is made less intractable by the application of the Mean (or Molecular) Field Approximation (MFA). In this all pair-wise interactions are assumed to have the same strength and thus the motion of each proton is due to the average behaviour of all the others. This is a good approximation for long range interactions but is poor for

nearest neighbour ones.

Approximating $\frac{1}{2} \sum_{ll'} J_{ll'} Z_l Z_{l'}$ by $\sum_l J \langle Z \rangle Z_l$ (1·21)

where $J = \sum_{l'} J_{ll'}$ (1·22)

and $\langle Z \rangle$ is the thermal average of Z

gives $H = - \sum_l \left\{ 2\Omega X_l + J \langle Z \rangle Z_l \right\}$ (1·23)

The pseudo spin, $S^o = (X_l, 0, Z_l)$, can be thought of as precessing around the mean field, $\underline{w}$, whose components are $(2\Omega, 0, J\langle Z \rangle)$ and whose magnitude is $|\underline{w}| = [(2\Omega)^2 + (J\langle Z \rangle)^2]^{\frac{1}{2}}$ (1·24)

From figure (1·7), for a self consistent solution having $\langle S^o \rangle$ pointing along $\underline{w}$, we require

$$\frac{\langle S^o \rangle}{|\underline{w}|} = \frac{\langle Z \rangle}{J \langle Z \rangle} = \left(\frac{\langle X \rangle}{2\Omega} \right) \quad (1·25)$$

which has solutions $\langle Z \rangle = 0$ (1·26)

$$\langle S^o \rangle = \frac{|\underline{w}|}{J} \quad \text{for } \langle Z \rangle \neq 0 \quad (1·27)$$

where $\langle S^o \rangle = \frac{1}{2} \tanh \frac{1}{2} \beta w \; ; \beta = \frac{1}{k_B T}$ (1·28)

a standard result for average alignment of spins.

Equation (1·26) holds above the transition where the protons are randomly distributed with equal numbers on the two possible sites. $\langle S^o \rangle$ then points along X. Below the transition where the protons are ordered $\langle Z \rangle \neq 0$ and the solution (1·27) holds.

Fig. 1.7

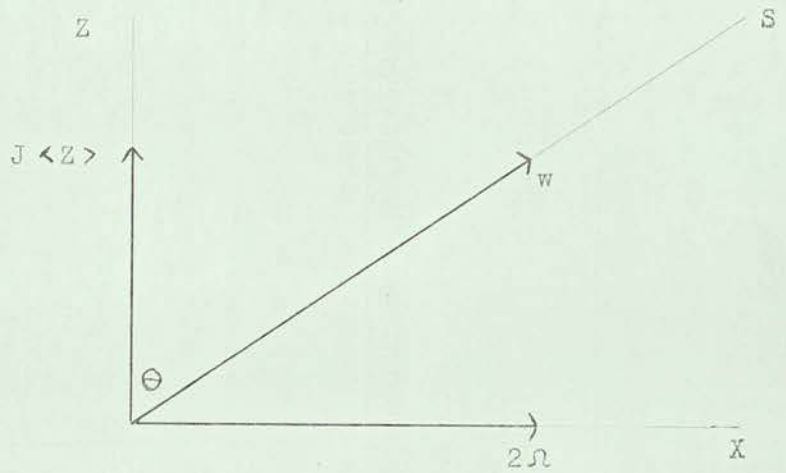

The components of the pseudo spin.

The transition between the disordered and ordered phases takes place at a temperature T_1, given, on putting $\langle Z \rangle = 0$ in equation (1·27), with (1·24) and (1·28), by

$$\frac{4\Omega}{J} = \tanh \frac{\Omega}{k_B T_1} \qquad (1\cdot29)$$

T_1 thus marks the onset of order, which builds up as $\langle Z \rangle$ given by equations (1·27) and (1·24).

Having shown that the system of interacting protons can exhibit a phase transition, it is of interest to derive its elementary excitations. For convenience we shall follow Tokunaga and rotate the coordinate system. This simplifies the treatment of the ferroelectric phase by diagonalising the MFA Hamiltonian, but is not necessary for the paraelectric phase to which the discussion is limited.

Thus, with θ as in figure (1·1) put

$$X_l = S_l^o \operatorname{Sin}\theta + S_l^x \operatorname{Cos}\theta \qquad (1\cdot30)$$

$$Z_l = S^o{}_l \operatorname{Cos}\theta - S_l^x \operatorname{Sin}\theta$$

and introduce S_l^+ and S_l^-, which rotate oppositely in a plane perpendicular to S_l^o, defined by $S_l^{\pm} = S_l^x \pm S_l^y$ (1·31)

and further define $S_l = S_l^+ + S_l^- = 2S_l^x$

In the paraelectric phase, $\langle Z \rangle = 0$ and thus $\theta = \frac{\pi}{2}$ giving as the relations between the operators in the two frames of reference

$$X_l = S^o{}_l$$

$$Z_l = -\tfrac{1}{2} S_l \qquad (1\cdot32)$$

It is also helpful to transform S^{o}_{l}, S^{+}_{l}, S^{-}_{l} and thus S_{l} from real to reciprocal space using Fourier components of the form

$$S = N^{-\frac{1}{2}} \sum_{\underline{q}} S(\underline{q}) \; e^{i\underline{q}\cdot\underline{r}_{l}} \qquad (1\cdot33)$$

where N = number of protons in the crystal.

The Hamiltonian (1·23) then becomes

$$H = -2\Omega N^{\frac{1}{2}} S^{o}(o) - \frac{1}{8} \sum_{\underline{q}} J(\underline{q}) S(\underline{q}) S(-\underline{q}) \qquad (1\cdot34)$$

where $J(\underline{q}) = \sum_{l'} J_{ll'} e^{i\underline{q}(\underline{r}_{l}-\underline{r}_{l})}$ (1·35)

and $S^{o}(o) = S^{o}(\underline{q} = 0)$

The equations of motion for $S^{o}(\underline{q})$, $S^{+}(\underline{q})$ and $\bar{S}(\underline{q})$ are obtained from

$$i\hbar \dot{S}^{o}(\underline{q}) = -[H, S^{o}(\underline{q})]$$

with $$i\hbar \dot{S}^{o}(\underline{q}) = -\hbar\omega S^{o}(\underline{q})$$

and similarly for $S^{+}(\underline{q})$ and $S^{-}(\underline{q})$.

On neglecting terms representing torques acting on the spin components due to fluctuations of the Z component of a spin about its equilibrium value, which would give finite life times to the excitations of the system, the frequency spectrum of these excitations is given in the high temperature phase, by

$$\Omega^{2}(\underline{q}) = \frac{2\Omega}{\hbar^{2}} \cdot \left(2\Omega - \langle S^{o} \rangle J(\underline{q}) \right) \qquad (1\cdot36)$$

Since $\langle S^o \rangle = \frac{1}{2} \tanh \beta\Omega$ in the disordered phase (1·37)

then $\Omega^2(\underline{q}) = \left(\frac{2\Omega}{\hbar}\right)^2 \left(1 - \frac{J(\underline{q})}{4\Omega} \tanh \beta\Omega\right)$ (1·38)

$\Omega(\underline{q})$ is the frequency of the proton tunnelling mode.

Whereas for a system of isolated protons, each would have the same frequency, $\frac{2\Omega}{\hbar}$, due to the ground state splitting in the double well, the inclusion of interactions between the protons produces a spectrum of elementary excitations given by the dispersion relation (1·38). $\Omega(\underline{q})$ is $\underline{q}$ and temperature dependent through $J(\underline{q})$ and β respectively.

If $J_{11'}$ is a long range interaction it will be 'spread out' in real space but $J(\underline{q})$ will be compressed in reciprocal space, having a maximum at $q = 0$. Thus $\Omega(\underline{q})$ will have a minimum at $\underline{q} = 0$ and go to zero at a temperature T_o given by

$$\frac{4\Omega}{J(\underline{q}=0)} = \tanh \frac{\Omega}{k_B T_o} \qquad (1·39)$$

Since from equations (1·35) and (1·22), $J(\underline{q}=0) = J$, equation (1·39) is identical with equation (1·29) on taking $T_o = T_1$.

Thus the ordering of the protons below the transition can be seen as a consequence of the instability of the proton system against a $\underline{q}=0$ tunnelling mode.

Since $\tanh x \leqslant 1$ we require $J \geqslant 4\Omega$ to get a transition for $T \geqslant 0^oK$.

If $\Omega << k_B T_1$, then $\tanh \frac{\Omega}{k_B T_1}$ can be approximated by $\frac{\Omega}{k_B T_1}$ and equations (1·38) and (1·39) reduce, at $\underline{q} = 0$, to

$$\Omega^2(o) = \left(\frac{2\Omega}{\hbar}\right)^2 \left(\frac{T - T_1}{T}\right) \qquad (1\cdot40)$$

$$T_1 = \frac{J}{4k_B} \qquad (1\cdot41)$$

Being independent of Ω, equation (1·41) shows that a transition is still possible for $\Omega = 0$ - the Ising model. Thus the low temperature phase results from the ordering of the protons, with tunnelling necessary only to move the protons to the 'correct' end of the bond.

The result corresponding to equation (1·40) for displacive ferroelectrics is, reference (1·8), $\omega_o^2 \propto (T-T_c)$. Equation (1·41) is similar to this near the transition.

On the tunnelling model the isotope effects result from the decrease in Ω, with increasing mass, due to the reduction in the overlap of the wavefunctions appropriate to the heavier particle. In equation (1·29) decreasing Ω will cause the left hand side to be reduced more rapidly than the right hand side, and thus T_1 must rise to maintain the equality.

In order to deal adequately with the spontaneous polarization which appears along the C axis, we follow Kobayashi (1·36) and consider coupling between the phonon and tunnelling modes.

The Hamiltonian for the coupled system having one spin per unit cell is given, in the harmonic approximation, by

$$H = H_p + H_L + H_{pL} \qquad (1.42)$$

where

$$H_p = -2\Omega \sum_l X_l - \tfrac{1}{2} \sum_{ll'} J_{ll'} Z_l Z_{l'} \qquad (1.43)$$

$$H_L = \tfrac{1}{2} \sum_{\substack{lk \\ l'k'}} \left[\frac{p^2_{lk}}{M_k} + \underline{U}_{lk} \cdot \underline{\Phi} \begin{pmatrix} l & l' \\ k & k' \end{pmatrix} \cdot \underline{U}_{l'k'} \right] \qquad (1.44)$$

$$H_{pL} = -2 \sum_{ll'k} G_{ll'k} \cdot \underline{U}_{l'k} Z_l \qquad (1.45)$$

H_p is the Hamiltonian of the proton system alone, as already discussed.

H_L is the lattice Hamiltonian. $\underline{U}_{lk}$ is the displacement from equilibrium of the k atom of mass M_k in the l^{th} cell, while $\underline{p}_{lk}$ is the corresponding momentum - Reference (1·40). The sum over k probably includes the protons, since their motions can be decomposed into a small vibration around each equilibrium site, included in H_L, and the larger tunnelling oscillation included in H_p.

H_{pL} is the interaction Hamiltonian relating the small atomic motions to the larger oscillation of the protons along the bond.

Then, as with the proton system only, on rotating the coordinate axes and transforming to reciprocal space with

$$\underline{U}_{lk} = (NM_k)^{-\frac{1}{2}} \sum_{j\underline{q}} e_{kj}(\underline{q})\, Q_j(\underline{q}) \exp i(\underline{q} \cdot \underline{r}_{lk}) \qquad (1.46)$$

from reference (1·40), the mean field Hamiltonian in the disordered phase is

$$H_p = -2\Omega N^{\frac{1}{2}} S^o(o) - \frac{1}{8} \sum_{\underline{q}} J(\underline{q})\, S(\underline{q})\, S(-\underline{q}) \qquad (1.47)$$

$$H_L = \frac{1}{2} \sum_{jq} \left\{ P_j(-q)\, P_j(q) + \omega_j^2(q)\, Q_j(-q)\, Q_j(q) \right\} \quad (1\cdot48)$$

$$H_{PL} = \sum_{jq} G_j(q)\, S(-q)\, Q_j(q) \quad (1\cdot49)$$

where $P_j(q)$ and $Q_j(q)$ are conjugate momentum and normal coordinates.

$$G_j(q) = \sum_{ll'k'} G_{ll'k'}\, e_{k'j}(q)\, M_{k'}^{-\frac{1}{2}} \exp i\, q.(r_{ll'k'} - r_l) \quad (1\cdot50)$$

The spectrum of elementary excitations can be obtained by solving the equations of motion

$$i\hbar \dot{S}^o(q) = -[H,\ S^o(q)] \quad (1\cdot51)$$

$$i\hbar \dot{S}(q) = -[H, S(q)] \quad (1\cdot52)$$

$$\frac{\partial H}{\partial Q_j(-q)} = i\omega P_j(q) = \omega_j^2(q)\, Q_j(q) + G_j(-q)\, S_j(q) \quad (1\cdot53)$$

where terms representing torques acting on spins have been neglected.

This yields the excitation spectrum for a single tunnelling mode coupled to j phonons that are not directly coupled to each other, viz:-

$$\omega^2 = \Omega^2(q) + \sum_j \frac{8\Omega}{\hbar^2} \frac{|G_j(q)|^2 < S^o >}{\omega^2 - \omega_j^2(q)} \quad (1\cdot54)$$

Where there is no proton lattice interaction, $|G_j(q)|^2 = 0$, the solutions of (1·54) are the uncoupled lattice and tunnelling mode frequencies $\omega_j(q)$, $\Omega(q)$

Considering the case of coupling to just one optic phonon - j - gives

$$\omega^2 = \frac{1}{2} \left[(\omega_j^2(q) + \Omega^2(q)) \pm (\omega_j^2(q) - \Omega^2(q) \sqrt{1 + \frac{32\Omega |G_j(q)|^2 < S^o >}{\hbar^2 (\omega_j^2(q) - \Omega^2(q)^2}} \right] \quad (1\cdot55)$$

If the interaction is weak enough for the approximation

$\sqrt{1+x} = 1+\frac{1}{2}x$ to be valid, the two solutions of equation (1·55)

$\omega_+^2(\underline{q})$ and $\omega_-^2(\underline{q})$ are

$$\omega_+^2(\underline{q}) = \omega_j^2(\underline{q}) + \frac{8\Omega \left| G_j(\underline{q}) \right|^2 < S^o >}{\hbar^2(\omega_j(\underline{q})^2 - \Omega(\underline{q})^2)} \qquad (1\cdot56)$$

$$\omega_-^2(\underline{q}) = \Omega^2(\underline{q}) - \frac{8\Omega \left| G_j(\underline{q}) \right|^2 < S^o >}{\hbar^2(\omega_j(\underline{q})^2 - \Omega^2(\underline{q}))} \qquad (1\cdot57)$$

Since, in the absence of the interaction, $G_j(\underline{q})$, $\Omega^2(\underline{q})$ has been shown to tend to zero as the transition is approached, it is assumed that $\Omega^2(\underline{q}) << \omega_j^2(\underline{q})$ in this region, and thus

$$\omega_+^2(\underline{q}) = \omega_j^2(\underline{q}) \qquad (1\cdot58)$$

$$\omega_-^2(\underline{q}) = \Omega^2(\underline{q}) - \frac{8\Omega}{\hbar^2} \frac{\left| G_j(\underline{q}) \right|^2 < S^o >}{\omega^2_j(q)} \qquad (1\cdot59)$$

Of these two mixed modes $\omega_+(\underline{q})$ is substantially of phonon character and little affected by the interaction, while $\omega_-(\underline{q})$ has predominately tunnelling character.

Substituting for $\Omega(\underline{q})$ from equation (1·36) gives (1·59) as

$$\omega_-^2(\underline{q}) = \left(\frac{2\Omega}{\hbar}\right)^2 \left[1 - \frac{< S^o >}{2\Omega} (J(\underline{q}) + J_L(\underline{q}))\right] \qquad (1\cdot60)$$

where $J_L(\underline{q}) = \left[\frac{2 \left| G_j(\underline{q}) \right|}{\omega_j(\underline{q})}\right]^2 \geqslant 0 \qquad (1\cdot61)$

Thus the effect of coupling to the lattice is to increase the direct proton - proton interaction by $J_L(\underline{q})$. Proceeding by analogy with pure tunnelling mode if $J(\underline{q}) + J_L(\underline{q})$ has a maximum at $\underline{q}=0$, the crystal will become unstable against the zone centre coupled tunnelling mode given by (1·60) with $\underline{q}=0$ at a temperature T_2 defined by

$$\frac{4\Omega}{J + J_L(o)} = \tanh \frac{\Omega}{k_B T_2} \qquad (1\cdot62)$$

In the limit $\Omega << k_B T$

$$\omega_-^2(o) = \left(\frac{2\Omega}{\hbar}\right)^2 \frac{T-T_2}{T} \qquad (1\cdot63)$$

$$T_2 = \frac{J + J_L(o)}{4k_B} \qquad (1\cdot64)$$

It is perhaps useful to summarize the results of Kobayashi's theory.

1) The system exhibits a transition to an ordered phase at a temperature T_2 whose increase on deuteration can be explained as in the uncoupled mode case.
2) By coupling the tunnelling mode to the K-P ion optic phonon, the ionic motion associated with the ω_- mode will 'freeze in' at the transition to give the spontaneous polariziation. Although the Kobayashi theory does not give an expression for the spontaneous polarization, it is unlikely to have an isotope effect since it has its origin in the heavy ions.
3) The soft mode frequency ω_- is proportional to Ω and should thus be reduced on deuteration.
4) From equations 1·41, 1·61 and 1·64 $T_2 - T_1 = \frac{|G_j(o)|^2}{k_B \omega_j^2(o)}$ (1·65)

On the basis of this equation, Cochran (1·37) estimates that $T_2 >> T_1$ and thus the ordering arises mainly from the proton lattice interaction $J_L(o)$ rather than the direct proton-proton interaction J. Kobayashi however estimates $T_2-T_1 = \frac{J_L(o)}{4k_B}$ at only $\sim 10^oK$. This seems unlikely since a strong proton-lattice interaction must be required to produce the spontaneous polarization in parallel with proton ordering. This is in contrast to the situation in the perovskite displacive ferroelectrics where the transition results from a cancellation of long and short range forces.

5) It has been found more convenient to postpone derivation of the static susceptibility due to the two coupled modes discussed above until the next chapter, where it is shown, equation (2·81) that

$$\chi(o) \propto 1 + \frac{T_2-T_1}{T-T_2} \qquad (2\cdot81)$$

If $T_2 >> T_1$, then near the transition $T_2-T_1 >> T-T_2$ and $\chi(o) \propto \frac{T_2-T_1}{T-T_2}$. This has the observed Curie-Weiss behaviour. Since $T_2-T_1 \propto J_L(o)$, the Curie constant is unlikely to be much affected by deuteration, as it is the proton-proton interaction, J, that will be the more strongly dependent on isotope effects. If, as Kobayashi suggests, $T_2-T_1 \sim 10^oK$ equation (2·81) gives a Curie-Weiss type behaviour only for a very few degrees above T_2.

6) Whereas both Cochran (1·8) and Kobayashi (1·36) predict the same atomic motions in the ferroelectric mode - illustrated in figure (1·8) - the emphasis is on the phonon character in the former model and the tunnelling character in the latter.

Fig. 1.8

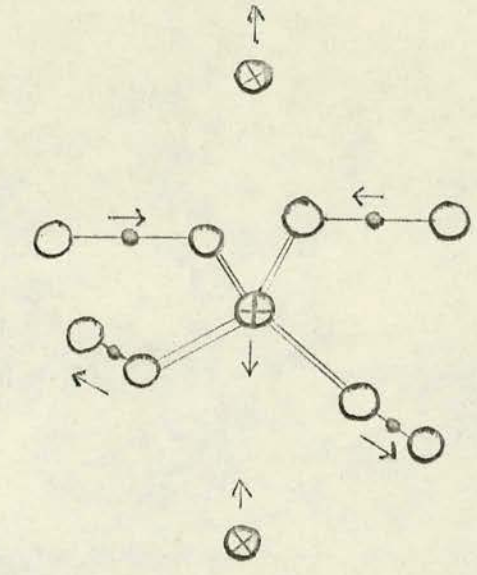

K O

P H

The soft ω_- mode.

In the ω_+ mode the motions of the K and P ions are π out of phase with that of the protons.

7) As we have seen, a zone centre instability results from $J(\underline{q}) + J_L(\underline{q})$ having a maximum at $\underline{q}=0$. Maxima are, however, also possible at other values of $\underline{q}$. If $J(\underline{q}) + J_L(\underline{q})$ have a maximum at the zone boundary an antiferroelectric transition could occur.

Further comparison of Kobayashi's theory with experiment will be discussed later, but only qualitative agreement can be hoped for due to limitations imposed by the mean field approximation and as a result of dealing with only one, instead of four, spins per primitive KDP cell.

Note In parallel with equation (1·35) which applies to the direct proton-proton interaction, we can write for the indirect interaction through the lattice

$$J_L(o) = \sum_{1'} J_{11'}^{(L)}$$

From equations (1·61) and (1·50)

$$J_L(o) = \sum_{1k'} \frac{2\,|G_{11k'}|^2 \;\; |e_{k'j}(o)|^2}{M_{k'}\;\omega_j^2(o)}$$

Since the self interaction term does not contribute to the coupling

$$J_{11}^{(L)} = 0 \quad \text{and thus} \quad G_{11k'} = 0$$

Elliot (1·41) had discussed this point from a different standpoint and finds that the coupling constant, on omitting the self interaction term which Kobayashi includes is not $\frac{|G_j(o)|^2}{\omega_j^2(o)}$ but

$$\frac{|G_j(o)|^2}{\omega_j^2(o)} - \frac{1}{N}\sum_{\underline{q}} \frac{|G_j(\underline{q})|^2}{\omega_j^2(\underline{q})}$$

While the correction affects detailedcalculation of the coupling constant it does not alter the general results of the theory outlined above. Bearing this in mind, we will continue to denote the coupling constant by $G_j(o)$ for simplicity.

The change of structure at the transition in KDP involves an xy shear. This indicates an instability in the corresponding zone centre acoustic mode. The thermodynamic theory shows that this shear is related to the polarization along the c axis by the piezoelectric constant d_{36}. Just as Kobayashi's theory shows that it is the tunnelling mode that drives the polarization, we show below, following Coombs (1·42), that the acoustic instability is likewise driven by coupling to the proton system.

If the tunnelling mode is coupled to two lattice modes, one optic and the other acoustic, the excitations of the coupled systen near $\underline{q}=0$ have frequencies given by equation (1·54) as

$$\omega^2(o) = \Omega^2(o) + \frac{8\Omega\langle S^o\rangle |G_o(o)|^2}{\hbar^2(\omega^2(o)-\omega_o^2(o))} + \frac{8\Omega\langle S^o\rangle |G_a(o)|^2}{\hbar^2(\omega^2(o)-\omega_a^2(o))} \qquad (1\cdot65)$$

The subscripts o and a refer to optic and acoustic modes respectively.

Although the coupling terms, G , are essentially $\underline{q}$ dependent we are looking for solutions near $\underline{q}=0$ and can thus take

$$G_o(o) = A \text{ , independent of } \underline{q} \qquad (1\cdot66)$$

for the optic mode since its dispersion relations are flat near $\underline{q}=0$, and

$$G_a(o) = B\,\omega_a(o) \quad , \quad \text{with B independent of } \underline{q} \qquad (1\cdot67)$$

for the acoustic mode since its dispersion relations are linear near $\underline{q}=0$ and $G_a \propto q \propto \omega_a$ near $\underline{q}=0$.

It simplifies the notation to write

$$\frac{8\Omega}{\hbar^2} \langle S^o \rangle \left|A\right|^2 = \alpha^2$$
$$\frac{8\Omega}{\hbar^2} \langle S^o \rangle \left|B\right|^2 = \beta^2 \qquad (1\cdot68)$$

The uncoupled, $\alpha^2 = \beta^2 = 0$, solutions of 1·65 are $\omega_o^2(o)$, $\Omega^2(o)$ and $\omega_a^2(o)$. When coupling is introduced, since $\omega_o(o) >> \Omega(o)$ and $\omega_o(o) >> \omega_a(o)$ the solution at high frequencies is approximately

$$\omega_1^2(o) = \omega_o^2(o) \qquad (1\cdot69)$$

This is to be expected since the optic mode was little affected by coupling to the tunnelling mode in the previous section, and even now there is no direct interaction with the acoustic mode.

The other two solutions are then given by the quadratic

$$\omega^4(o) - (\omega_-^2(o) + \omega_a^2(o) + \beta^2)\,\omega^2(o) + \omega_-^2(o)\,\omega_a^2(o) = 0 \qquad (1\cdot70)$$

where $\omega_-^2(o)$ is the frequency of the coupled optic tunnelling mode.

Thus $w^2(o) = \frac{1}{2}\left[(w_-^2(o)+w_a^2(o)+\beta^2) \pm (w_-^2(o)-w_a^2(o)+\beta^2)\sqrt{1+\frac{4\beta^2 w_a^2(o)}{(w_-^2(o)-w_a^2(o)+\beta^2)^2}}\right]$ (1·71)

which in the weak coupling limit where $\sqrt{1+x} \rightarrow 1+\frac{1}{2}x$ gives

$$w_2^2(o) = w_-^2(o) + \beta^2 + \frac{\beta^2 w_a^2(o)}{(w_-^2(o) - w_a^2(o) + \beta^2)} \qquad (1\cdot72)$$

$$w_3^2(o) = w_a^2(o) - \frac{\beta^2 w_a^2(o)}{(w_-^2(o) - w_a^2(o) + \beta^2)} \qquad (1\cdot73)$$

Where the approximation $w_-^2(o) + \beta^2 >> w_a^2(o)$ is valid (1·74)

$$w_2^2(o) = w_-^2(o) + \beta^2 \qquad (1\cdot75)$$

$$w_3^2(o) = w_a^2(o) \frac{w_-^2(o)}{w_2^2(o)} \qquad (1\cdot76)$$

On comparing equations (1·60) and (1·75) it can be seen that the effect of coupling to the acoustic mode is to reduce the interaction term $J + J_L(o)$ by $J_A(o) = 4|B|^2 \geq 0$ (1·77)

Thus in the approximation $\Omega << k_B T$ the coupled optic-tunnelling-acoustic mode of predominately tunnelling character, w_2, will have a temperature dependent frequency given by

$$\omega_2^2(o) = \left(\frac{2\Omega}{\hbar}\right)^2 \left(\frac{T-T_3}{T}\right) \qquad (1\cdot78)$$

where $T_3 = \dfrac{J + J_L(o) - J_A(o)}{4k_B}$ (1·79)

The mainly acoustic coupled mode, ω_3, on the other hand, has a temperature dependence

$$\omega_3^2(o) = \left(\frac{T - T_2}{T - T_3}\right) \omega_a^2(o) \qquad (1\cdot80)$$

From equations (1·78) and (1·64) and (1·76) $T_2 - T_3 = \dfrac{J_A(o)}{4k_B} =$

$$\frac{|B|^2}{k_B} > o \qquad (1\cdot81)$$

Thus, when coupling to the acoustic mode is included, the transition to the ferroelectric phase takes place at a temperature T_2 due to an acoustic mode instability. Since $\omega_a \propto \underline{q}$ it can be seen from equation (1·80) that the slope, $\dfrac{\partial \omega_3(q)}{\partial q}$, of the coupled acoustic mode goes to zero at $\underline{q}=0$ at the transition.

Since in the absence of coupling to the acoustic mode, the crystal is in effect 'clamped', while with that coupling it is 'free', T_2 and T_3 can be taken to be the 'clamped' and 'free' Curie temperatures, which it is known (1·3) differ by about $4 \sim 5^{\circ}K$ in KDP. The approximation (1·74) will be least good at the transition where it reduces to $\left(\dfrac{2\Omega}{\hbar}\right)^2 \dfrac{T_2 - T_3}{T_2} >> \omega_a^2(o)$ (1·82)

which, for KDP, implies $\left(\dfrac{2\Omega}{\hbar}\right) \dfrac{1}{5} > \omega_a(o)$.

It seems likely that the pure tunnelling mode at high temperatures, or equivalently, the isolated proton, will have a frequency greater that 5 times that of the acoustic mode.

It can be further shown that near $\underline{q}=0$, $\omega_2^2(o) >> \omega_3^2(o)$, and thus the modes do not cross. The temperature dependence of the three coupled modes is shown in figure (1·9).

Finally, it is of interest to discuss the elastic constant c_{66}. For the xy shear mode under study, $\omega(\underline{q}) = v\,\underline{q}$ near $\underline{q}=0$ (1·83)

with $v = \sqrt{\frac{c_{66}}{\rho}}$; ρ = density (1·84)

Since the transverse optic mode $\omega_o(o) \approx \omega_1(o)$ has no macroscopic field associated with it equation (1·80) gives

$$\sqrt{\frac{c_{66}^{E=0}}{\rho}} = \left.\frac{\partial\omega_3(\underline{q})}{\partial\underline{q}}\right|_{\underline{q}=0} = \left(\frac{T-T_2}{T-T_3}\right)^{\frac{1}{2}} \left.\frac{\partial\omega_a(\underline{q})}{\partial\underline{q}}\right|_{\underline{q}=0} \qquad (1·85)$$

The elastic constant at constant polarization is obtained by suppressing the optic mode, but maintaining the coupling between tunnelling and acoustic modes. The requisite equations are obtained by replacing $\omega^2(o)$ by $\Omega^2(o)$ from equation (1·70) onwards.

This leads to the coupled tunnelling-acoustic mode frequency $\omega_4(o)$ being given by

$$\omega_4^2(o) = \frac{T - T_1}{T - \left(T_1 - \frac{J_A(o)}{4k_B}\right)}\,\omega_a^2(o) \qquad (1·86)$$

Fig, 1.9

(a)

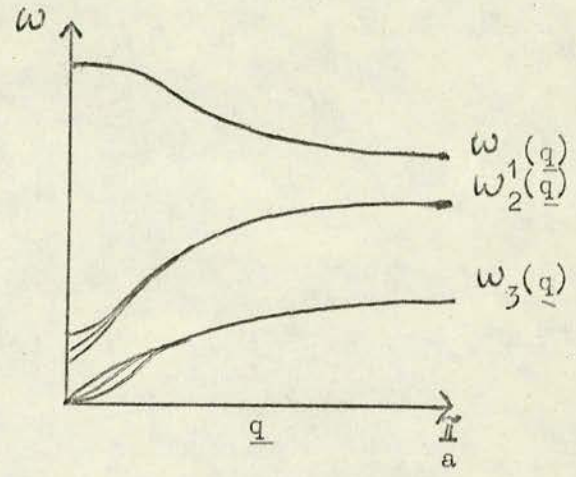

(b)

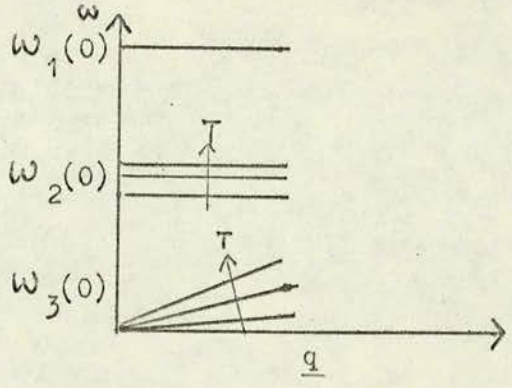

(a) shows possible dispersion curves for the three coupled modes whose temperature dependence near $\underline{q}=0$, as derived in the theory, is shown in figure (b).

This is equation (1·80), with $J_L(o)$ set to zero in the expressions for T_2 and T_3.

Thus $$\sqrt{\frac{c_{66}^{p=0}}{\rho}} = \left.\frac{\partial \omega_L^2(\underline{q})}{\partial \underline{q}}\right|_{\underline{q}=0} = \sqrt{\frac{T-T_1}{T-T_1-\left(\frac{J_A(o)}{4k_B}\right)}} \left.\frac{\partial \omega_a^2(\underline{q})}{\partial \underline{q}}\right|_{\underline{q}=0} \quad (1\cdot87)$$

In the paraelectric phase $T \geqslant T_2$ and $T_2 >> T_1$ or $\frac{J_A(c)}{4k_B}$, so equation (1·87) can be approximated by

$$\sqrt{\frac{c_{66}^{p=0}}{\rho}} = \left.\frac{\partial \omega_a(\underline{q})}{\partial \underline{q}}\right|_{\underline{q}=0} \quad (1\cdot88)$$

and hence (1·85) becomes

$$c_{66}^{E=0} = \frac{T-T_2}{T-T_3} c_{66}^{p=0} \quad (1\cdot89)$$

Thus $c_{66}^{E=0}$ goes to zero at the transition temperature T_2, while $c_{66}^{p=0}$ is largely temperature independent.

Equation (1·89) can be cast in the form

$$c_{66}^{E=0} = c_{66}^{p=0} - c_{66}^{p=0}\left[\frac{T_c^{x=0} - T_c^{x=0}}{T - T_c^{x=0}}\right] \quad (1\cdot90)$$

which agrees with a result of the thermodynamic theory.

This leads support to the requirement that $T_2 >> T_1$ which is essential if equation (1·87) is to reduce to (1·88) and thus lead to a formula consistent with the thermodynamic theory.

ANTIFERROELECTRICITY AND AMMONIUM DIHYDROGEN PHOSPHATE

All KDP type crystals are tetragonal above the transition temperature. However, unlike the other KDP isomorphs, ammonium dihydrogen phosphate (ADP) and arsenate (ADA) and their deuterated isotopes (DADP, DADA) undergo an antiferroelectric transition.

The phase transition in ADP was first observed by Busch (1·43). X-ray and optical studies by Wood et al (1·44) which showed the crystal was orthorhombic below the transition temperature but without the shear observed in KDP, led to Mason and Matthias (1·45) suggesting a structure compatible with their data. This was also suggested independently by Nagamiya (1·46).

In the tetragonal phase there are symmetry axes along the a and b axes and along the base diagonals of this unit cell. In the ferroelectric transition the base diagonals retain their symmetry operations while the a and b axes do not. The opposite occurs at an antiferroelectric transition. While the orthorhombic ferroelectric unit cell is at 45^{o} to the paraelectric tetragonal cell and has twice the volume, the antiferroelectric orthorhombic cell has neither the rotation or volume doubling. The body centre and cell corner positions are, however, no longer equivalent. Whereas for KDP, in the ferroelectric phase, there are two protons at the top of each PO_4 group (1·23), the structure proposed for ADP (1·44) (1·45) has one proton at the top and one at the bottom of each PO_4 group ordered in such a way that adjacent dipoles of H_2PO_4 groups point oppositely in the ab plane. The emphasis on proton ordering in the antiferro-

electric structure stems from the observations that, as with KDP, ADP has an entropy change at the transition typical of an order-disorder transition and a large ($148^{o}K \rightarrow 242^{o}K$) increase of the transition temperature on deuteration.

It is perhaps not too surprising that of the KDP isomorphs some are ferroelectric while others are antiferroelectric. Since the spontaneous polarization is reversible, the interatomic forces must be finely balanced, so that isomorphic changes can lead to potentials favouring antiferroelectric transitions. $PbZrO_3$ is an antiferroelectric that becomes ferroelectric under an applied stress.

While ADP is not a ferroelectric,it does exhibit larger than average a and c-axis static susceptibilities which increase on reducing the temperature. This indicates that, if the antiferroelectric transition were somehow suppressed, the crystal would undergo a ferroelectric transition at a much lower temperature.

Nagamiya (1.46) on the basis of Mason and Matthias' (1.45) results has fitted a Curie-Weiss dependence for the a and c-axis static dielectric constants of ADP to their data, and obtains

$$\epsilon_a^{x=0} = 7 + \frac{18000}{T - (-55)} \qquad (1.91)$$

$$\epsilon_a^{x=0} = 7 + \frac{2690}{T - (-17)} \qquad (1.92)$$

The clamped Curie temperatures are substantially lower, eg.

$$\epsilon_a^{x=0} = 6.8 + \frac{2510}{T - (-67)} \qquad (1.93)$$

Although $\varepsilon_a^{x=0} > \varepsilon_c^{x=0}$ at all temperatures $> -10^{o}K$, the c-axis instability, if it existed, would develop before that along the a-axis. The corresponding result in KDP (1·47) is

$$\varepsilon_c^{x=0} = 4{\cdot}5 + \frac{3122}{T - 122} \qquad (1{\cdot}94)$$

Apart from a substantial increase in Curie temperature KDP and ADP have similar behaviour for $\varepsilon_c^{x=0}$.

The present interest in DADP is in the zone centre behaviour that heralds the thwarted ferroelectric transition.

Although only one tunnelling mode per unit cell was needed in KDP to qualitatively explain the appearanceof the spontaneous polarization and the transition, there are in fact four tunnelling modes since there are four spins in the primitive cell. Blinc has shown that two of these are degenerate. In ADP the a and c-axis instabilities could both be treated as arising from coupled proton lattice modes as in Kobayashi's theory.

CHAPTER TWO

INTRODUCTION

Although it was Leonardo da Vinci who suggested that the blue colour of the sky might be due to the scattering of light by air molecules, it was not until after Newton and Tyndall had attempted to solve the problem, that Lord Rayleigh (2.1), following a suggestion by Maxwell, finally did so. He showed that the intensity of light scattered independently be small dielectric spheres varied as the fourth power of the frequency. Continuous media were first treated by von Smoluchowski (2.2) and Einstein (2.3) who found that the phenomenon of critical opalescence was due to the density fluctuations in the liquid becoming anomalously large when the bulk modulus tended to zero at the critical point.

Following Debye's (2.4) theory of specific heat, which identified the thermal content of a body with the excitation of density waves, Brillouin (2.5) predicted that sidebands would appear in the spectrum of monochromatic light scattered by these waves. Brillouin scattering was first observed by Gross (2.6). Since

$$\Delta \rho = \left(\frac{\partial \rho}{\partial P}\right)_S \Delta P + \left(\frac{\partial \rho}{\partial S}\right)_P \Delta S \qquad (2.1)$$

where ρ = density

P = pressure

S = entropy

as well as the Brillouin doublet there is also scattering by isobaric entropy fluctuations which, since they are non-propagating, is centred on the incident frequency. This feature was explained by Landau and Placzek (2.7) who also related the intensities of the central and

Brillouin components to the difference between the specific heats at constant pressure and volume.

Smekal (2.8) and later Kramers and Heisenberg (2.9) considered the scattering of light by a system having two quantised energy levels and predicted the effect discovered by Raman (2.10) which now bears his name. Landsberg and Mandlestam (2.11) independently discovered the same effect in Russia.

Following an early and comprehensive review by Placzek (2.12), many authors have since extended the theory to deal with the various solid state excitations. The theory of Brillouin scattering has been reviewed in papers by Benedek and Fritsch (2.13), and by Griffin (2.14) which are good sources of references to earlier work. The Raman effect has been treated by Born and Huang (2.15) and by Loudon (2.16) in his now classic paper. A more recent paper by Mills and Burstein (2.17) properly deals with the photons in the solid as polaritons.

Light is scattered away from its original direction of propagation by fluctuations in the polarizability of the medium in which it is travelling. Since these polarizability fluctuations have as their source numerous other fluctuating parameters in solids, liquids and gases, the Raman effect is indeed a widespread one.

The scattering process in solids can be treated as the creation or annihilation of elementary excitations of the system (eg phonons, magnons etc) on interaction with the light beam. Thus, the equations of conservation of energy and wavevector for a process involving one phonon are

$$\omega_o = \omega_s \pm \omega(\underline{q}) \qquad (2.2)$$

$$\underline{k}_o = \underline{k}_s + \underline{q} \,. \qquad (2.3)$$

where ω_o, $\underline{k}_o$ and ω_s, $\underline{k}_s$ are the frequency and wavevector of the incident and scattered beams respectively, while $\omega(\underline{q})$ and $\underline{q}$ refer to the phonon. The wavevector, $|\underline{k}| = \frac{2\pi n}{\lambda}$, where n is the refractive index and λ the wavelength of the light. The $\pm$ in equation (2.2) denotes creation (+) and annihilation (-) of a phonon. A typical experimental scattering geometry and corresponding wavevector conservation diagram are shown in figures (2.1) and (2.2).

Multiphonon processes are also possible for which conservation equations similar to (2.2) and 2.3) must hold

$$\omega_o = \omega_s + \sum_j (\pm \omega(\underline{q}_j)) \qquad (2.4)$$

$$\underline{k}_o = \underline{k}_s + \sum_j \underline{q}_j \qquad (2.5)$$

Returning to equation (2.2), it can be seen that each phonon that scatters light gives rise to a pair of peaks in the scattered spectrum positioned symmetrically about the indcident frequency. Finite lifetimes for the excitations result in finite linewidths. The change in frequency of the light upon scattering leads directly to the phonon frequencies.

Conventionally, the peak having lower frequency than the incident light is called the Stokes peak, while the other is the anti-Stokes. Although the Raman effect really encompasses all forms of inelastic light scattering by elementary excitations, that by acoustic modes (and density waves in fluids) is still known as Brillouin scattering. The distinction probably arose because Brillouin scattering was predicted first, and has persisted because a Brillouin scattering experiment usually involves a Fabry-Perot interferometer whereas the normally higher frequency Raman scattering is usually analysed by a grating spectrometer.

Fig. 2.1

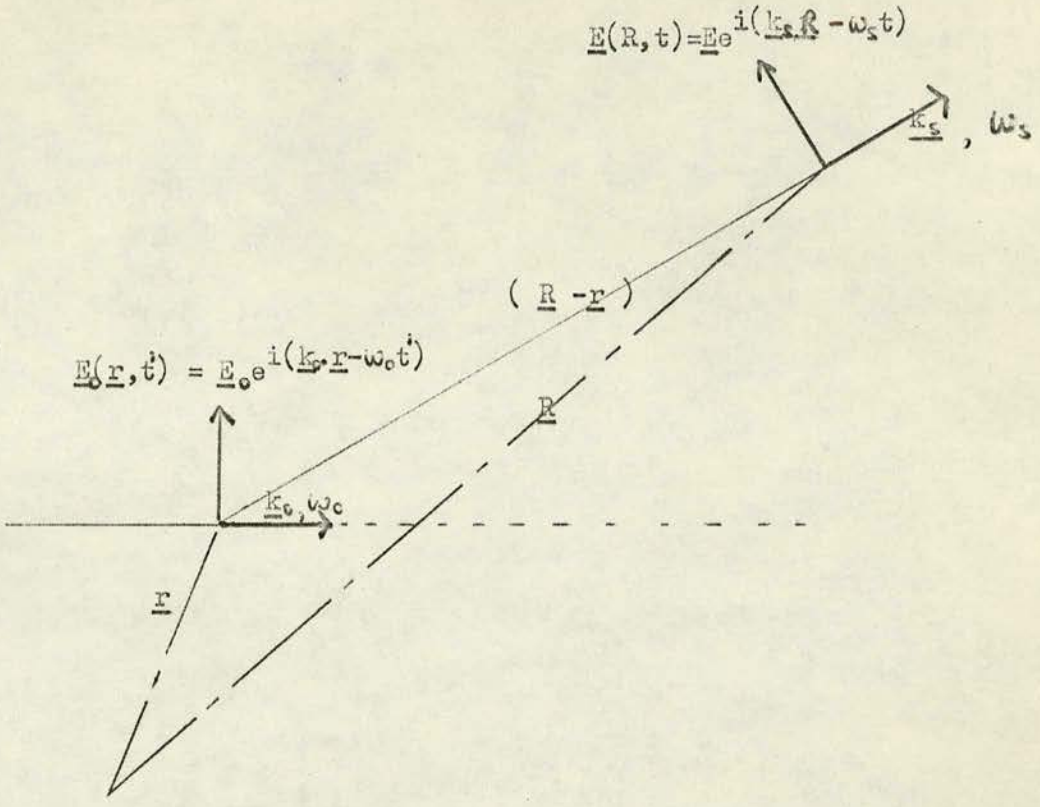

A typical scattering geometry.

Fig. 2.2

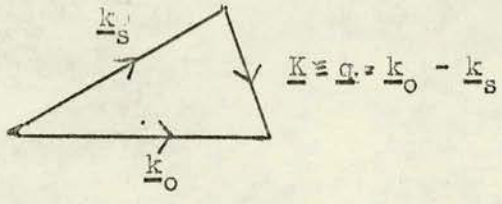

Wavevector conservation.

It is customary in light scattering to denote modes and their frequencies by the difference in wavenumber, $\omega = \frac{1}{\lambda}$ cm^{-1}, between the light scattered by the mode and the incident beam. On this scale the acoustic mode frequencies are of the order of 1 cm^{-1} while the optic modes generally lie in the 100-500 cm^{-1} range. By comparison, the centre of the visible spectrum at 5000 Å is 2.10^4 cm^{-1} in wavenumbers. Thus the change in frequency and hence wavevector, of the scattered light is small. Taking $|\underline{k}_o| \approx |\underline{k}_s|$ we find from figure (2.2) that

$$|\underline{q}| = 2 |\underline{k}_o| \sin \frac{\theta}{2} \qquad (2.6)$$

where θ is the scattering angle.

It is interesting to compare the maximum phonon wavevector that can take part in a scattering process - $|\underline{q}|_{max} = 2 |\underline{k}_o| = \frac{4\pi n}{\lambda_o}$ - with the wavevector at the zone boundary - $|\underline{q}|$ (z.b.) = $\frac{\pi}{a}$ - where a is the unit cell dimension

$$\therefore \frac{|\underline{q}|_{max}}{|\underline{q}|_{zb.}} = \frac{4a\,n}{\lambda_o} \sim 5.10^{-3} \qquad 2.7$$

Since the unit cell dimensions are much less than the wavelength of visible light, light scattering experiments measure the phonon frequency near $\underline{q} = o$. This makes Raman scattering a particularly valuable tool in the study of ferroelectric and other structural phase transitions that involve the instability of a zone centre mode. While inelastic neutron scattering, with thermal neutrons having wavelengths comparable to the unit cell dimensions, can investigate the dispersion relations throughout the zone, the resolution near $\underline{q} = o$ is poorer than is possible with light scattering. Reducing the photon wavelength to that of the unit cell dimension gives thermal diffuse x-ray scattering which yields the total intensity scattered by all modes, with a $\frac{1}{\omega_j^2(q)}$ weighting factor, at

all points in the zone. The energy distribution of the scattered beam is however too narrow to be resolved.

Although they do not involve a scattering process, infra red reflectivity experiments might seem a more powerful technique in the study of soft modes which are always infra red active but not necessarily Raman active, as will be shown later. However, infra red experiments are difficult at low frequencies and the analysis of the data for phonon frequencies may be complicated by uncertain contributions from multi-phonon processes.

Although the theory derived below is initially perfectly general, an explicit solution will be found for the case of polar modes which include the soft optic, tunnelling and coupled tunnelling-optic modes which are of particular interest in the present work.

THEORY OF LIGHT SCATTERING BY CONTINUOUS MEDIA - POLAR MODES

The spectral distribution of the light scattered by a system is determined by the time dependence of the fluctuations of the scattered field amplitude. The Weiner-Khintchine Theorem (2.18) shows that the spectral distribution function $S(\underline{K}, \omega^1)$ is the Fourier transform of the autocorrelation function of the scattered field $\underline{E}\ (\underline{K},t)$

$$S(\underline{K},\omega^1) = \frac{1}{2\pi} \int_{-\infty}^{\infty} < \underline{E}\ (\underline{K}, t + \tau). \underline{E}^*\ (\underline{K},t) > e^{i\omega^1 \tau} d\tau \qquad (2.8)$$

where

$$< \underline{E}\ (\underline{K},t + \tau). \underline{E}^*\ (\underline{K}, t)> = \underset{T \to \infty}{\text{Lim}} \frac{1}{2T} \int_{-T}^{T} \underline{E}\ (\underline{K}, t + \tau).\underline{E}^*(\underline{K},t)\ dt. \qquad (2.9)$$

and $$\int_{-\infty}^{\infty} S(\underline{K}, \omega^1)\, d\omega = < \left| \underline{E}\ (\underline{K}, t) \right|^2 > \qquad (2.10)$$

* = complex conjugate

ω^1 = frequency of scattered light

$\underline{K} = \underline{k}_o - \underline{k}_s = \underline{q}$, the scattering vector.

While for neutron inelastic scattering $\underline{K}$ and $\underline{q}$ may differ by a vector of the reciprocal lattice, they are identically equal in light scattering.

$\underline{E}\ (\underline{K},t)$ is the field at a point $\underline{R}$ at a time t due to a scattering process having scattering vector $\underline{K}$.

As the wavelength of light - λ - is large compared to atomic dimensions, there being $\sim 10^9$ tetragonal KDP unit cells in a volume λ^3 for $\lambda \approx 6328 \mathring{A}$, a solid can be considered a continuum as regards light scattering. The incident field can thus be assumed constant over an elementary volume $|d\underline{r}|$ which is large compared with the unit cell volume but small compared to λ^3. Thus, the scattered field $d\underline{E}\ (\underline{R},t)$, at $\underline{R}$, at a time t, due to an oscillating dipole $\underline{P}(\underline{r}, t^1)d|\underline{r}|$ produced at $\underline{r}$ at the retarded time $t^1 = t - \frac{|\underline{R} - \underline{r}|n}{C}$ by an incident field $\underline{E}\ (\underline{r}, t^1)$ is given by

$$d\underline{E}\ (\underline{R},t) = \left. \frac{\hat{\underline{i}}_{\underline{R}-\underline{r}} \times \left[\hat{\underline{i}}_{\underline{R}-\underline{r}} \times \ddot{\underline{P}}\ (\underline{r},t^1)\ |d\underline{r}| \right]}{C^2\ |\underline{R} - \underline{r}|} \right|_{t^1 = t - \frac{|\underline{R}-\underline{r}|n}{C}} \qquad (2.12)$$

The scattering geometry is illustrated in figure (2.1)

n is the refractive index in the direction $(\underline{R} - \underline{r})$

C is the velocity of light in vacuum

$\hat{\underline{i}}_{\underline{R} - \underline{r}}$ is a unit vector in the direction $(\underline{R} - \underline{r})$

The polarization $\underline{P}(\underline{r},t^1)$ is related to the incident field $\underline{E}_o(\underline{r},t^1)$ by the 3x3 polarizability tensor $\underset{\sim}{\alpha}(\underline{r},t^1)$

$$\underline{P}(\underline{r},t^1) = \underset{\sim}{\alpha}(\underline{r},t^1).\ \underline{E}_o(\underline{r},t^1) \tag{2.13}$$

$$\underline{E}_o(\underline{r},t^1) = \underline{Eo}\ e^{i(\underline{k}_o.\underline{r} - \omega_o t^1)} \tag{2.14}$$

Since the time dependence of the polarizability arises through the normal modes whose frequencies are small compared to that of the incident field, the time dependence of the polarization is, to a first approximation, that of the field.

$$\therefore\ \ddot{\underline{P}}(\underline{r},t^1) = -\omega_o^2\,\underline{P}(\underline{r},t^1) \tag{2.15}$$

Using equations (2.13), (2.14), (2.15) the total scattered amplitude at $\underline{R}$ is found by integrating equation (2.12) over the illuminated volume, V, to be

$$\underline{E}(\underline{R},t) = -\left[\frac{\omega_o}{C}\right]^2 \frac{1}{R}\, e^{i(\underline{k}_{os}.\underline{R} - \omega_o t)}\ \hat{\underline{i}}_{\underline{k}_s} \times \left[\hat{\underline{i}}_{\underline{k}_s} \times \int_V \underset{\sim}{\alpha}(\underline{r},t^1).\ \underline{E}_o\, e^{i(\underline{k}_o - \underline{k}_{os}).\underline{r}}\, |d\underline{r}|\right] \tag{2.16}$$

It has been assumed that the origin of coordinates is near the centre of the illuminated volume and that the point of observation, $\underline{R}$, is far from it though still within the medium. This avoids consideration of reflection and refraction at the surfaces, which can be accounted for later, and simplifies the treatment of time retardation. Hence the explicit approximations used in obtaining equation (2.16) are

in the denominator $$|\underline{R} - \underline{r}| \approx |\underline{R}| = R \tag{2.17}$$

and in the time retardation
$$\left.\begin{aligned} \hat{\underline{i}}_{\underline{R}-\underline{r}} &\approx \hat{\underline{i}}_{\underline{k}_s} \\ |\underline{R} - \underline{r}| &= \hat{\underline{i}}_{\underline{k}_s}.(\underline{R} - \underline{r}) \\ \frac{n\omega_o}{C}\,\hat{\underline{i}}_{\underline{k}_s} &= \underline{k}_{os} \end{aligned}\right\} \tag{2.18}$$

$\underline{k}_{os}$ has the magnitude of the incident wavevector and the direction of the scattered one. Note that $\underline{\underline{\alpha}}(\underline{r},t')$ is still at the retarded time.

In order to proceed further, explicit account must be taken of the fluctuations of the polarizability tensor. It is usual to expand the polarizability tensor as a Taylor series in terms of some suitable set of coordinates for the system $\{\underline{X}_i(\underline{r},t)\}$ eg atomic displacements, normal mode coordinates.

$$\therefore \underline{\underline{\alpha}}(\underline{r},t') = \underline{\underline{\alpha}}^{(0)} + \sum_i \left[\frac{\partial \underline{\underline{\alpha}}(\underline{r},t')}{\partial \underline{X}_i(\underline{r},t')}\right]_o \underline{X}_i(\underline{r},t') + \frac{1}{2}\sum_{ii'}\left[\frac{\partial^2 \underline{\underline{\alpha}}(\underline{r},t')}{\partial \underline{X}_i(\underline{r},t')\partial \underline{X}_{i'}(\underline{r},t')}\right]_o \underline{X}_i(\underline{r},t')\underline{X}_{i'}(\underline{r},t') +$$

$$= \underline{\underline{\alpha}}^{(0)} + \sum_i \underline{\underline{\alpha}}_i^{(1)} \underline{X}_i(\underline{r},t') + \sum_{ii'} \underline{\underline{\alpha}}_{ii'}^{(2)} \underline{X}_i(\underline{r},t')\underline{X}_{i'}(\underline{r},t') + \cdots \quad (2.19)$$

The validity of this expansion, due to Placzek, depends on the Born-Oppenheimer separation of electronic and nuclear motions. The electronic structure is taken to adjust adiabatically to the instantaneous nuclear configuration expressed through the coordinates $\underline{X}_i(\underline{r},t')$. In equation (2.19), $\underline{\underline{\alpha}}^{(o)}$ is the average polarizability, constant in time and space, which can always be diagonalised. In the remaining terms the derivatives are evaluated at equilibrium, as denoted by the subscript o, and are thus constants as is emphasised by writing

$$\left[\frac{\partial \underline{\underline{\alpha}}(\underline{r},t')}{\partial \underline{X}_i(\underline{r},t')}\right]_o \equiv \underline{\underline{\alpha}}_i^{(1)} \quad \text{etc} \quad (2.20)$$

The fluctuations in the polarizability have thus been expressed in the set of coordinates that represent their source.

The form of the scattered field for each term in the expansion (2.19) is considered in turn. The average polarizability, $\underline{\underline{\alpha}}^{o}$, gives in

equation (2.16).

$$\underline{E}^{(o)}(\underline{R},t) = -\left[\frac{2\pi\omega_o}{C}\right]^2 \frac{2\pi}{R}\, e^{i(\underline{k}_o\cdot\underline{R}-\omega_o t)}\; \hat{\underline{i}}_{\underline{k}_s} \times \left[\hat{\underline{i}}_{\underline{k}_s} \times \underline{\underline{\alpha}}^{(o)}\cdot\underline{E}_o\right] \tag{2.21}$$

where the result

$$\int_V e^{i(\underline{k}_o-\underline{k}_{os})\cdot\underline{r}} \left|d\underline{r}\right| = (2\pi)^3\, \delta(\underline{k}_o-\underline{k}_{os}) \tag{2.22}$$

has been used. Thus there will only be a scattered field for $\underline{k}_o = \underline{k}_{os}$. $\underline{E}^{(o)}(\underline{R},t)$ therefore represents a scattered beam passing undeviated through the medium with the same frequency and wavevector as the incident beam. If the medium is anisotropic, $\underline{\underline{\alpha}}^{o}.\underline{E}_o$ will not in general be parallel to $\underline{E}_o$.

In agreement with observation, it has been assumed that scattering is a very weak effect - only a small part of the incident energy interacts with each dipole in the illuminated volume. The incident beam is taken to propagate unattenuated through the medium and scattering of light out of the scattered beams is neglected. The total field in the forward direction, within the approximations used, is $\underline{E}\ o(\underline{R},t) + \underline{E}^{(o)}(\underline{R},t)$.

To determine the scattered field due to the next term in equation (2.19) itis useful to express $\underline{X}_i\ (\underline{r},t^1)$ in terms of its spatial Fourier components:-

$$\underline{X}_i\ (\underline{r},t^1) = \left(\frac{1}{2\pi}\right)^{\frac{3}{2}} \sum_j \int \underline{X}_j^{(i)}(\underline{q})\, e^{-i(\underline{q}.\underline{r} \pm \omega_j(q)t^1)} \left|d\underline{q}\right| \tag{2.23}$$

The sum over j provides for a number of branches in the dispersion relation connecting $\underline{q}$ and $\omega(\underline{q})$. The time dependence has been taken out of $\underline{X}_j^{(i)}(\underline{q},t^1)$ to leave $\underline{X}_j^{(i)}(\underline{q})$, and the double $(\pm)$ sign accounts for the degeneracy in the dispersion relations for positive and negative running waves.

Thus for each coordinate $\underline{X}_i$, the scattered field due to $\underset{\sim}{\alpha}_i^{(1)}$ is obtained from equation (2.16) with (2.19) and (2.21) as

$$\underline{E}_i^{(1)}(\underline{R},t) = -\left(\frac{\omega_o}{C}\right)^2 \frac{1}{R}\left[\frac{1}{2\pi}\right]^{\frac{3}{2}} \sum_j \int_{\underline{q}} e^{i(\underline{k}_s\cdot\underline{R} - \omega_s t)} \; \underline{X}_j^{(i)}(\underline{q}) \; \hat{\underline{i}}_{\underline{k}_s}$$

$$\times \left[\hat{\underline{i}}_{\underline{k}_s} \times \underset{\sim}{\alpha}_i^{(1)} \cdot \underline{E}_o\right] \int_V e^{i(\underline{k}_o - \underline{q} - \underline{k}_s)\cdot\underline{r}} \; |d\underline{r}| \; |d\underline{q}| \qquad (2.24)$$

where $\omega_s = \omega_o \mp \omega_j(\underline{q})$ (2.25)

$$\underline{k}_s = \frac{n\omega_s}{C} \hat{\underline{i}}_{\underline{k}_s} \qquad (2.26)$$

and since $\int_V e^{i(\underline{k}_o - \underline{q} - \underline{k}_s)\cdot\underline{r}} \; |d\underline{r}| = (2\pi)^3 \delta(\underline{k}_o - \underline{q} - \underline{k}_s)$

$$\therefore \underline{k}_o = \underline{k}_s + \underline{q} \qquad (2.27)$$

Hence

$$\underline{E}_i^{(1)}(\underline{R},t) = -\left[\frac{\omega_o}{C}\right]^2 \frac{1}{R}(2\pi)^{\frac{3}{2}} \sum_j e^{i(\underline{k}_s\cdot\underline{R} - \omega_s t)} \; \underline{X}_j^{(1)}(\underline{q})$$

$$\hat{\underline{i}}_{\underline{k}_s} \times \left[\hat{\underline{i}}_{\underline{k}_s} \times \underset{\sim}{\alpha}_i^{(1)} \cdot \underline{E}_o\right] \qquad (2.28)$$

The scattered field at $\underline{R}$ has wavevector $\underline{k}_s$ and frequency ω_s defined by equations (2.25) and (2.26), and results from scattering by those fluctations in the coordinate $\underline{X}_i$ whose Fourier components have wavevector $\underline{q}$ and frequency $\omega_j(\underline{q})$, where $\underline{q}$ is selected by the scattering geometry through equation (2.29).

Comparing equations (2.25) and (2.27) with (2.2) and (2.3) shows that the second term in the expansion of $\underset{\sim}{\alpha}(\underline{r},t')$ gives rise to the one-phonon cross-section. The third term, involving the change of $\underset{\sim}{\alpha}(\underline{r},t')$ with two coordinates $\underline{X}_i$, $\underline{X}_{i'}$ gives the two -phonon cross-section and so on.

To determine the spectral density of the first order, or one phonon, Raman scattering we write $\underline{E}_i^{(1)}(\underline{R},t) = \underline{E}_i^{(1)}(\underline{K},t)$ to emphasise the dependence of the scattered field on scattering vector - the point $\underline{R}$ unambiguously defines the vector $\underline{K}$ - and reabsorb $\pm\omega_j(\underline{q})\ t^1$ into $\underline{X}_j^{(i)}(\underline{q})$ to give $\underline{X}_j^{(i)}(\underline{q},t^1)$. Then putting equation (2.28) into (2.8) gives, for each coordinate $\underline{X}_i(\underline{r},t^1)$

$$S_i^{(1)}(\underline{K},\omega^1) = \left[\frac{\omega_o}{C}\right]^4\left[\frac{2\pi}{R}\right]^2\left[\hat{\underline{i}}_{\underline{k}_s} \times \left[\hat{\underline{i}}_{\underline{k}_s} \times \underset{\sim}{\alpha}_i^{(1)} \cdot \underline{E}_o\right]\right]^2 \sum_j \int \langle \underline{X}_j^{(i)}(\underline{q},\ t^1+\tau) \cdot \underline{X}_j^{(i)^*}(\underline{q},t^1)\ e^{i(\omega^1-\omega_o)\tau}\ d\tau \qquad (2.29)$$

Terms involving $\underset{\sim}{\alpha}^{(0)} \cdot \underset{\sim}{\alpha}^{(1)}$ do not contribute to the cross-section since they include an odd number of $\underline{X}_j(\underline{q},t)$ terms whose time average is zero.

From equation (2.29) it can be seen that

$S_i^{(1)}(\underline{K},\omega^1) \sim \omega_o^4$ the fourth power of the incident frequency

$\frac{1}{R^2}$ the inverse square law

$\left[\underset{\sim}{\alpha}_i^{(1)}\right]^2$ this is not included in the correlation since it is evaluated at equilibrium.

$\underline{E}_o^2$ the incident intensity.

The nature of the double cross product can best be seen by using the identy of vector algebra

$$\hat{\underline{i}}_{\underline{k}_s} \times \left[\hat{\underline{i}}_{\underline{k}_s} \times \underset{\sim}{\alpha}_i^{(1)} \cdot \underline{E}_o\right] = \left[\hat{\underline{i}}_{\underline{k}_s} \cdot \underset{\sim}{\alpha}_i^{(1)} \cdot \underline{E}_o\right]\hat{\underline{i}}_{\underline{k}_s} - \left[\hat{\underline{i}}_{\underline{k}_s} \cdot \hat{\underline{i}}_{\underline{k}_s}\right]\underset{\sim}{\alpha}_i^{(1)} \cdot \underline{E}_o$$

$$= -\sum_{\hat{\underline{i}} \neq \hat{\underline{i}}_{\underline{k}_s}} \left[\underset{\sim}{\alpha}_i^{(1)} \cdot \underline{E}_o\right]_{\hat{\underline{i}}}\ \hat{\underline{i}} \qquad (2.30)$$

The set of unit vectors $\hat{\underline{i}}$ form an orthogonal basis, and the subscript $\hat{\underline{i}}$ denotes the component of $\underset{\sim}{\alpha}^{(1)}_{i} \cdot \underline{E}_o$ in the direction $\hat{\underline{i}}$. Thus in light scattering experiment observations are made on the components of $\underset{\sim}{\alpha}^{(1)}_{i} \cdot \underline{E}_o$ that lie in the plane perpendicular to the direction of the scattered beam.

The geometrical factors involved in the scattering process thus give

$$\underline{E}_i^{(1)}(\underline{K},t) \propto \sum_{\hat{\underline{i}} \neq \hat{\underline{i}}_{k_s}} \left[\underset{\sim}{\alpha}_i^{(1)} \cdot \underline{E}_o \right] \hat{\underline{i}} \qquad \hat{\underline{i}} \tag{2.31}$$

Apart from verifying that polarization of the scattered field is normal to its direction of propagation, equation (2.31) shows that a particular component of the Raman tensor - say $\left[\underset{\sim}{\alpha}^{(1)}_{i}\right]_{ij}$ - is selected by having the incident beam polarized along $\hat{\underline{j}}$ and the scattered beam along $\hat{\underline{i}}$. (or vice versa since the tensor is symmetric).

This leads to a notation for defining the scattering geometry due to Damen, Porto and Tell (2.19) eg $\mathbf{x}(\mathbf{yx})\mathbf{z}$. The terms outside the bracket refer to the direction of propagation of the incident and scattered light respectively and hence define the phonon propagation direction, while the terms inside refer to the direction of polarization of the incident and scattered light.

To proceed further it is necessary to be explicit about the coordinates involved in the expansion of the polarizability. Born and Huang (2.15) have expanded the polarizability in terms of the normal mode coordinates $Q_j(\underline{q},t)$. The $\underset{\sim}{\alpha}^{(1)}$ tensors obtained in this way are similar to those derived by Louden (2.16), who used a quantum mechanical approach. Louden's paper includes a table showing which components of the polarizability tensor fluctuate under a given normal mode. A mode that causes such fluctuations is said to be Raman active.

Since $\underset{\sim}{\alpha}^{(1)}$ is a second rank tensor, its components, in the language of group theory, transform like the products xy, z^2 etc. Thus as the $\alpha^{(1)}$ tensors are constants, only modes transforming as xy, z^2 etc can be first order Raman active.

Because in light scattering modes near the zone centre are studied, these long wavelength acoustic and polar optic modes can be considered as strain and polarization waves respectively. If the polarizability is expanded in terms of strain or polarization the $\underset{\sim}{\alpha}^{(1)}$ tensors are the elasto-optic and electro-optic tensors respectively. These tensors are discussed by Nye(2.20). This approach has been followed for acoustic modes by Benedek and Fritsch (2.13). In the treatment below the polarizability is expanded in terms of the polarization associated with polar modes. This leads to a form of $S(\underline{K},\omega^1)$ that is useful when dealing with experimental results.

Following a suitable text on lattice dynamics (2.21), consider the simplest model of a crystal - the rigid ion model in which the electronic polarizability is neglected. When the atoms are displaced under thermal excitation there is a polarization at $\underline{r}$ at a time t given by

$$\underline{P}(\underline{r},t) = \sum_{l\ k} \frac{Z_k\, \underline{U}_{lk}(t)}{V} \quad \delta(\underline{r} - \underline{r}_{lk}) \qquad (2.32)$$

where Z_k is the ionic charge of the kth ion in the lth unit cell of a crystal whose volume is V. $\underline{U}_{lk}$ and $\underline{r}_{lk}$ are the corresponding displacement and position coordinates of that ion. The polarization is assumed proportional to the displacement.

The displacement $\underline{U}_{lk}(t)$ can be expressed in terms of the normal coordinates using the standard result

$$\underline{U}_{lk}(t) = \frac{1}{\sqrt{NM_k}} \sum_{\underline{q}j}' \underline{e}_{kj}(\underline{q})\, Q_j(\underline{q},t) \exp i(\underline{q}.\underline{r}_{lk}) \qquad (2.33)$$

where N is the number of unit cells in the crystal, M_k the mass of the k th atom and $\underline{e}_{kj}(\underline{q})$ the eigenvectors of the lk th atom in that mode.

The spatial Fourier transform of equation (2.32) can be obtained as

$$\underline{P}(\underline{q},t) = \sum_j \underline{P}_j(\underline{q},t) = N^{\frac{1}{2}} \sum_j \underline{P}_j(\underline{q})\, Q_j(-\underline{q},t) \qquad (2.34)$$

This is an exact result. The approximations lie in the explicit form of $\underline{P}_j(\underline{q})$ which , on the present model, is

$$\underline{P}_j(\underline{q}) = \frac{1}{(2\pi)^{\frac{3}{2}}} \sum_k \frac{Z_k}{V\, M_k^{\frac{1}{2}}}\, \underline{e}_{kj}(-\underline{q}) \qquad (2.35)$$

where use has been made of the fact that, in light scattering, small values of $\underline{q}$ are important and that $\sum_l 1 = N$

For the expansion of $\underline{\alpha}(\underline{r},t^1)$ in terms of $\underline{P}(\underline{r},t^1)$

$$\underline{X}_j(\underline{q},t) \equiv \underline{P}_j(\underline{q},t) \qquad (2.36)$$

The summation over i henceforth vanishes since there is only one vector $\underline{P}$ at $\underline{r}$. The autocorrelation function of equation (2.29) thus becomes

$$\int \langle \underline{P}(\underline{q},\tau).\, \underline{P}(-\underline{q},0) \rangle\, e^{i(\omega^1 - \omega_o)\tau}\, d\tau = \sum_j N \left|\underline{P}_j(\underline{q})\right|^2 \int \langle Q_j(-\underline{q},\tau).Q_j(\underline{q},0) \rangle\, e^{i(\omega^1-\omega_o)\tau}\, d\tau \qquad (2.37)$$

where it has been assumed that the system is in equilibrium and the autocorrelation function thus depends only on the time difference τ. In the harmonic approximation, the normal mode coordinates can be expressed in terms of annihilation (a^+) and creation (a) operators,

$$Q_j(\underline{q},t) = \left[\frac{\hbar}{2\omega_j(\underline{q})}\right]^{\frac{1}{2}} \left[a_j^{+}(-\underline{q})\, e^{i\omega_j(\underline{q})t} + a_j(\underline{q})\, e^{-i\omega_j(\underline{q})t} \right] \quad (2.38)$$

and the autocorrelation functation evaluated by standard methods to give

$$\int \langle \underline{P}(\underline{q},\tau).\underline{P}(-\underline{q},0)\rangle\, e^{i(\omega^1 - \omega_o)}\, d\tau$$

$$= \sum_j \frac{N\left|\underline{P}_j(\underline{q})\right|^2 \hbar\pi}{\omega_j(\underline{q})}\, n(\omega^1 - \omega_o) \left[\delta(\omega^1 - \omega_o - \omega_j(\underline{q})) - \delta(\omega^1 - \omega_o + \omega_j(\underline{q}))\right] \quad (2.39)$$

where $n(\omega^1 - \omega_o)$, the phonon population factor, is given by

$$n(\omega^1 - \omega_o) = \left[\exp \frac{\hbar(\omega^1 - \omega_o)}{k_B T} - 1\right]^{-1} \quad (2.40)$$

where ω is in units of radians per second.

To determine the dielectric response of the crystal at the frequency $(\omega^1 - \omega_o)$, consider the effect of an applied electric field having this frequency. The equation of motion of the normal mode coordinate $Q_j(-\underline{q},t)$ having natural frequency $\omega_j(\underline{q})$ but being driven by the applied field of frequency $(\omega^1 - \omega_o)$ is

$$\ddot{Q}_j(-\underline{q},t) + \omega_j^2(\underline{q})\, Q_j(-\underline{q},t) = \frac{\partial(\underline{P}_j^*(\underline{q},t).\underline{E})\, V}{\partial Q_j^*(-\underline{q},t)}$$

$$= N^{\frac{1}{2}} V\, \underline{P}_j^*(\underline{q}).\underline{E} \quad (2.41)$$

Multiplying by $N^{\frac{1}{2}}\, \underline{P}_j(\underline{q})$ and summing over j gives, as the solution for $\underline{P}(\underline{q},t)$

$$\underline{P}(\underline{q},t) = N V \sum_j \frac{\underline{P}_j(\underline{q})\, \underline{P}_j^*(\underline{q}).\underline{E}}{\omega_j^2(\underline{q}) - (\omega^1 - \omega_o)^2} \quad (2.42)$$

If the components of the susceptability tensor are defined as

$$P_x(\underline{q},t) = \sum_y \chi_{xy}(\underline{q}, \omega^1 - \omega_o)\, E_y \qquad (2.43)$$

then

$$\chi'_{xy}(\underline{q}, \omega^1 - \omega_o) = N V \sum_j \frac{P_{xj}(\underline{q}) P_{yj}^{*}(\underline{q})}{\omega_j(\underline{q})^2 - (\omega^1 - \omega_o)^2} \qquad (2.44)$$

This is the ionic contribution to the susceptability. The rigid ion model neglects the electronic contribution.

As the above derivation has been entirely in the harmonic approximation χ'_{xy} is purely real - this is denoted by the prime $'$. However, through the Kramers- Krönig relations, reference (2.22), an imaginary part, $\chi''(\underline{q}, \omega^1 - \omega_o)$, can be defined by, for example

$$\chi''_{xx}(\underline{q}, \omega^1 - \omega_o) = \frac{\pi}{2} N V \sum_j \frac{\left|P_{xj}(\underline{q})\right|^2}{\omega_j(\underline{q})} \left[\delta(\omega^1 - \omega_o - \omega_j(\underline{q})) - \delta(\omega^1 - \omega_o + \omega_j(\underline{q})) \right] \qquad (2.45)$$

Comparision with (2.39) yields

$$\int \langle \underline{P}(\underline{q}, \tau) \cdot \underline{P}(-\underline{q}, 0) \rangle \, e^{i(\omega^1 - \omega_o)\tau} \, d\tau$$

$$= \frac{2\pi}{V} n(\omega^1 - \omega_o) \sum_{xyz} \chi''_{xx}(\underline{q}, \omega^1 - \omega_o) \qquad (2.46)$$

Thus, the power spectrum of the fluctuations of the polarization is related to the imaginary part of the dielectric susceptability.

Although equation (2.46) has been derived in a special case, it is in fact a perfectly general result and is an expression of the Fluctuation Dissipation Theorem, (2.22) and references therein.

The derivation above has been for transverse fluctuations driven by a (transverse) electric field. Thus the applied field is also the local field and therefore

$$\chi = \frac{P}{E} = \frac{\epsilon-1}{4\pi} \tag{2.47}$$

$$\therefore \chi'' = \frac{1}{4\pi} \epsilon'' \tag{2.48}$$

For longitudinal fluctuations the driving force is a longitudinal displacement field $E-4\pi P$.

Thus, since $\frac{P}{E-4\pi P} = \frac{\epsilon-1}{4\pi}$ (2.49)

$$\chi = \frac{P}{E} = \frac{1}{4\pi}\left(1 - \frac{1}{\epsilon}\right) \tag{2.48}$$

$$\therefore \chi'' = -\frac{1}{4\pi} \operatorname{Im}\left(\frac{1}{\epsilon}\right)$$

Only transverse contributions to χ'' will be considered hereafter.

Substituting equation (2.46) into (2.29) gives the spectral density function $S^{(1)}(\underline{K},\omega)$ as

$$S^{(1)}(\underline{K},\omega) = \left(\frac{\omega_o}{C}\right)^4 \left(\frac{2\pi}{R}\right)^2 \frac{2\hbar}{V} \left[\hat{\underline{i}}_{\underline{ks}} \times \left[\hat{\underline{i}}_{\underline{ks}} \times \underset{\sim}{\alpha}^{(1)} . \underline{Eo}\right]\right]^2 n(\omega)\, \chi''(\omega) \tag{2.49}$$

Where $w = \omega' - \omega_o$, the change in frequency between scattered and incident beams; this emphasises the fact that the scattered spectrum is centred on the incident frequency. $\chi''(\omega)$ denotes that component of the susceptability tensor selected by the scattering arrangement employed. The $\underline{q}$ dependence has been dropped from the susceptibility since $\underline{q} \simeq 0$ for Raman scattering and geometrical factors are accounted for by the double cross product.

Since $\chi''(-\omega) = -\chi''(\omega)$ (2.50)

and $\quad -\, n(-\omega) = n(\omega) + 1 \qquad (2.51)$

$$n(-\omega)\,\chi''(-\omega) > n(\omega)\,\chi''(\omega) \qquad (2.52)$$

Thus the light scattered with a smaller frequency than the incident beam is more intense than the corresponding anti-Stokes component. This arises since in thermal equilibrium there are more phonons in the ground state than the first excited state.

While it might appear from (2.49) that $S^{(1)}(K,\omega) \propto \frac{1}{V}$ this is not so since $\chi''(\omega) \propto NV = \frac{V^2}{v}$ and thus $S^{(1)}(K,\omega) \propto \frac{V}{v}$. The scattered signal is thus proportional to the illiminated volume V and inversely proportional to the unit cell volume v.

Although one would normally ascertain whether or not a mode was Raman active by reference to Louden's tables (2.16), it is instructive to investigate the Raman tensor $\underset{\sim}{\alpha}^{(1)}$ which, for the expansion of $\underset{\sim}{\alpha}(\underline{r},t)$ that has been performed is

$$\underset{\sim}{\alpha}^{(1)} = \left[\frac{\partial \underset{\sim}{\alpha}(\underline{r},t)}{\partial \underline{P}\,(\underline{r},t)}\right]_0 \qquad (2.53)$$

The electro-optic tensor related to $\underset{\sim}{\alpha}^{(1)}$ above is defined by

$$\left[\frac{\partial \epsilon_{\mu\nu}}{\partial\, Pi}\right]_0 = -\sum_{\mu\sigma} \epsilon_{\mu\rho}\, \gamma_{\rho\sigma i}\, \epsilon_{\sigma\nu} \qquad (2.54)$$

where $\epsilon_{\alpha\beta}$ and $\gamma_{\alpha\beta\gamma}$ are components of the dielectric constant and electro-optic tensors respectively. The link between dielectric constant and polarizability gives

$$\partial\alpha_{\mu\nu} = \frac{1}{4\pi}\quad \partial\epsilon_{\mu\nu}$$

If the principal axes of the dielectric constant tensor are parallel to

the Cartesian axes used, the above equations simplify to give

$$\mathcal{Q}^{(1)} = \left[\frac{\partial \alpha_{\mu\nu}(\underline{r},t)}{\partial\, Pi\ (\underline{r},t)}\right]_0 = -\frac{1}{4\pi} \sum_{\mu\nu} \epsilon_\mu \epsilon_\upsilon \wp_{\mu\nu i} \qquad (2.56)$$

The symmetry properties of the electro-optic tensors are the same as those of the piezoelectric tensors which are discussed by Nye (2.20). Thus from the known non-zero components of the electrooptic tensor one can find those components of $\underset{\sim}{\alpha}(\underline{r},t)$ which fluctuate under a given component of fluctuating polarization. Also, there can be no Raman scattering from polar modes in non-piezoelectric, ie centrosymmetric, crystals.

Since the dielectric constant appropriate in the definition of the electro-optic tensor is that at optical frequencies, the scattered intensity depends on no less than the eighth power of the refractive index of the scattering medium. Even so, the temperature dependence of the refractive index is often so weak that it gives a negligible contribution to the temperature dependence of the spectrum. The electro-optic tensor defined by equation (2.54) shows no anomaly near a ferroelectric transition, although that defined as $(\frac{\partial \epsilon_{\mu\nu}}{\partial Ei})$ does. Thus the temperature dependence of the scattered intensity lies mainly in the term $n(\omega)\chi''(\omega)$. The spectral density function appropriate to first order Raman scattering by polarization fluctuations can thus be written

$$S(\underline{K},\omega) = A\, n(\omega)\ \chi''(\omega) \qquad (2.57)$$

where A can be obtained from (2.49).

FORMS OF THE SUSCEPTIBILITY

In equation (2.45), $\chi^{11}(\omega)$ consisted of a pair of δ-function peaks for each polar phonon. This was a consequence of dealing with a loss free system. Finite lifetimes for the phonons and hence spectral linewidths can be introduced phenomenologically by adding a dissipative, or damping, term $2\Gamma Q_j(-\underline{q},t)$ to the left hand side of equation (2.41). This leads to components of a complex dielectric susceptibility tensor

$$\chi_{xx}(\omega) = \sum_j \frac{NV\,|P_{xj}(0)|^2}{\left[\omega_j(0)^2 - \omega^2\right] + i\left[2\Gamma\omega\right]} \qquad \text{for } q \approx o \tag{2.58}$$

Thus each mode is assumed behaving as an independent damped harmonic oscillator with $\omega_j(o)$ the undamped mode frequency and Γ the damping constant. Both of these parameters may be temperature dependent. Substantially the same result was obtained rigorously by Cowley (2.23) on considering an-harmonic effects on the dielectric properties.

If $\hbar\omega << k_B T$, $n(\omega)$ can be approxmated by

$$n(\omega) \approx \frac{k_B T}{\hbar\omega} \tag{2.59}$$

and thus the spectral profile resides in $\frac{\chi^{11}(\omega)}{\omega}$ from equation (2.57). The contribution of each mode to the total spectrum is thus given by

$$\frac{\chi^{11}_{xx}(\omega)}{\omega} = \frac{NV\,|P_{xj}(0)|^2}{\left[\omega_j^2(0) - \omega^2\right]^2 + \left[2\Gamma\omega\right]^2}\,2\Gamma \tag{2.60}$$

The form of $\frac{\chi^{11}_{xx}(\omega)}{\omega}$ as $\frac{\Gamma}{\omega_j(0)}$ increases is illustrated in figure (2.3) and discussed below.

Since for $\Gamma = 0$ there would be δ-function peaks at $\omega = \pm\,\omega_j(o)$, it is assumed that for small $\frac{\Gamma}{\omega_j(o)}$ that the spectrum has peaks substantially

Fig. 2.3

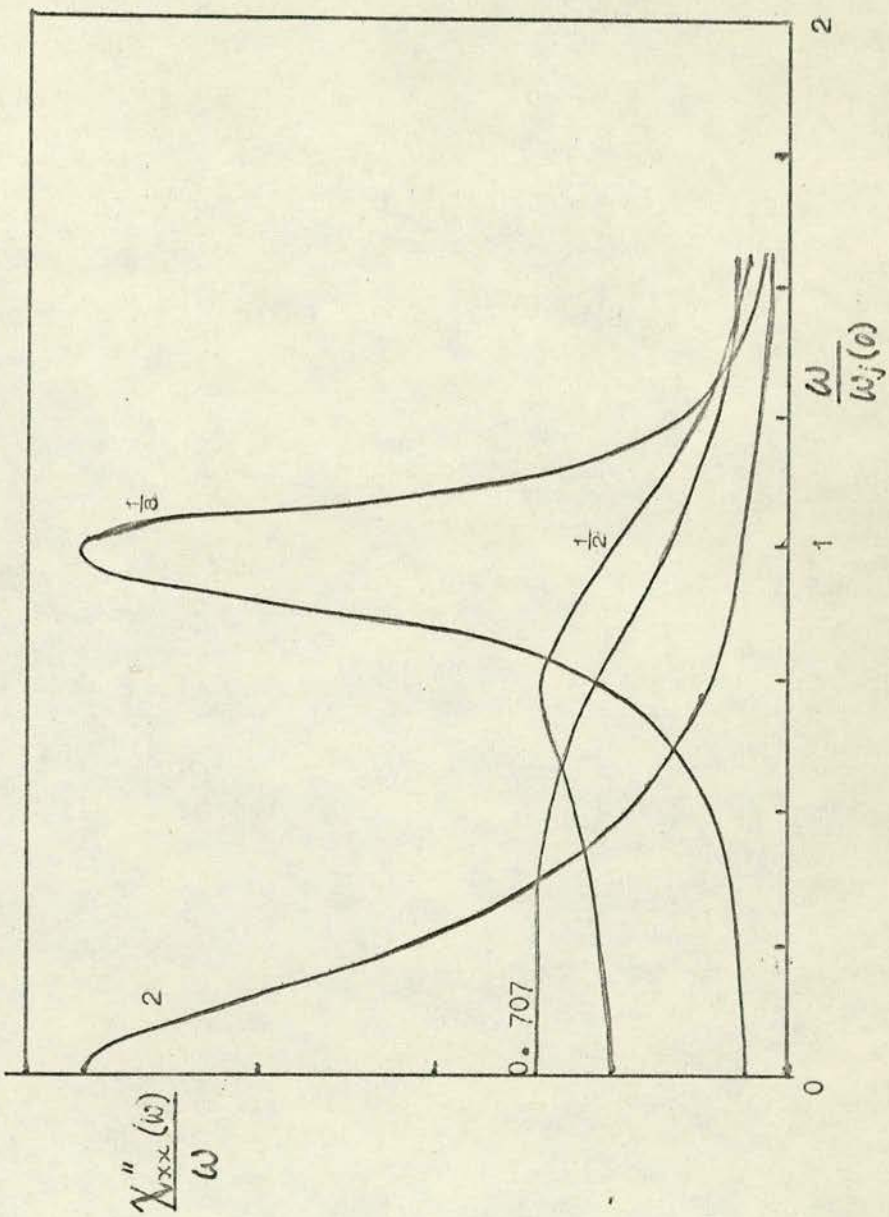

The Raman lineshape as a function of $\frac{\omega}{\omega_j(0)}$ for various values of $\frac{\Gamma}{\omega_j(0)}$ on the damped harmonic oscillator model.

at $\pm\omega_{j(o)}$.

Then, with the approximations

$$\omega_j^2(o) - \omega^2 = 2\omega_j(o)\,(\omega_j(o)-\omega)$$

$$2\omega\Gamma = 2\,\omega_j(o)\Gamma \qquad (2.61)$$

$$\frac{\chi''_{xx}(\omega)}{\omega} = \frac{NV\,\left|P_{xj}(o)\right|^2\,\dfrac{\Gamma}{2\omega_j^2(o)}}{\left[\omega_j(o)-\omega\right]^2+\Gamma^2} \qquad (2.62)$$

Thus, for a lightly damped mode the lineshape is Lorentzian with full width at half maximum of 2Γ and maxima at $\omega = \pm\omega_j(o)$. $\omega_j(o)$ and Γ can therefore be extracted directly from the spectral profile. Most modes have this type of lineshape.

The peak of spectral response occurs at a frequency ω_{max} given by $\frac{\partial}{\partial\omega}\left(\frac{\chi''_{xx}(\omega)}{\omega}\right) = o$ as

$$\omega^2_{max} = \omega_j^2(o)\left(1 - \frac{2\Gamma^2}{\omega_j(o)^2}\right) \qquad \text{for } 1 \geq \sqrt{2}\left[\frac{\Gamma}{\omega_j(o)}\right] \qquad (2.63)$$

$$= o \qquad 1 \leq \sqrt{2}\left[\frac{\Gamma}{\omega_j(o)}\right]$$

Thus as $\frac{\Gamma}{\omega_j(o)}$ increases, the peak moves to lower frequencies and the mode becomes 'overdamped' for $\sqrt{2}\left[\frac{\Gamma}{\omega_j(o)}\right] \geq 1$ when the spectrum appears as a broad non-resonant wing on the central, Rayleigh, peak. The full formula given by (2.60) must be fitted to the experimental data in order to extract $\omega_j(o)$ and Γ. Barker (2.24) has shown that for such modes $\omega_j(o)$, the undamped frequency, is the appropriate frequency to insert in the Lyddane-Sachs-Teller relation.

If $\frac{\Gamma}{\omega_j(o)}$ increases still further so that $2(2\Gamma^2-\omega_j(o)^2) >> \omega^2$ in the region of appreciable intensity then equation (2.60) reduces to a Debye Relaxation formula

$$\frac{\chi''_{xx}(\omega)}{\omega} = \frac{NV\,|P_{xj}(o)|^2\,\frac{\tau}{\omega_j^2(o)}}{1+(\omega\tau)^2} \qquad (2.64)$$

where $\tau = \frac{2\Gamma}{\omega_j^2(o)}$

Fitting to such a spectrum yields only the ratio $\frac{2\Gamma}{\omega_j^2(o)}$ and not Γ and $\omega_j^2(o)$ individually.

The static susceptibility can be obtained from equation (2.58) as

$$\chi_{xx}(o) = \sum_j \frac{NV\,|P_{xj}(o)|^2}{\omega_j^2(o)} \qquad (2.65)$$

This is the contribution from the lattice. There is also small electronic contribution which has been neglected. In ferroelectrics the susceptibility has an anomaly due to the soft mode and is given by

$$\chi_{xx}(o) = \chi_x + \frac{C}{T-T_c} \qquad (2.66)$$

$$= \sum_{j\neq o} \frac{NV|P_{xj}(o)|^2}{\omega_j^2(o)} + \frac{NV\,|P_{xo}(o)|^2}{\omega_o^2(o)} \qquad (2.67)$$

Where the first term in each equation is assumed temperature independent and the Curie-Weiss behaviour restricted to the last terms in which the subscript o denotes the soft mode. Since $\chi(o) \alpha \frac{1}{\omega_j^2(o)}$, low frequency modes contribute most to the static susceptibility.

Thus the spectral profiles of a soft mode described by a damped harmonic oscillator or a Debye relaxation time formula are given respectively by

$$\frac{\chi''_{xx}(\omega)}{\omega} = \frac{\frac{C_x}{T-T_c}\,2\Gamma\,\omega_o^2(o)}{\left[\omega_o^2(o)-\omega^2\right]^2+\left[2\omega\Gamma\right]^2} \qquad (2.68)$$

$$\frac{\chi''_{xx}(\omega)}{\omega} = \frac{\frac{Cx}{T-T_c}\ \tau}{1 + (\omega\tau)^2} \qquad (2.69)$$

These forms of $\frac{\chi''(\omega)}{\omega}$ have been used by many authors in analysing their data. Examples of such experiments will be discussed later.

It is perhaps worth noting that while the response to a disturbance of a system described by a harmonic oscillator has a time dependence $e^{-i\omega t}$, it is $e^{-i\omega t}\ e^{-\Gamma t}$ for a damped harmonic oscillator and $e^{\frac{t}{\tau}}$ for a Debye relaxation process.

The contribution to the susceptibility of a pure tunnelling mode, like that discussed in chapter one, can be derived in parallel with the phonon case. For protons tunnelling in a double minima potential well the polarization is

$$\underline{P}(\underline{r},t) = \frac{1}{V} \sum_{1} 2\,\underline{U}\ \mathcal{Z}\ Z_1(t)\ \delta(\underline{r}-\underline{r}_1) \qquad (2.70)$$

where $2\underline{U}$ is the separation of the minima and $\mathcal{Z}$ isthe effective charge of the one hydrogen or deuterium per unitcell of a crystal of volume V. The Fourier transform of $\underline{P}(\underline{r},t)$ is

$$\underline{P}(\underline{q},t) = -N^{\frac{1}{2}}\ \underline{\mathfrak{p}}\ S(-\underline{q},t) \qquad (2.71)$$

where
$$\underline{\mathfrak{p}} = \frac{\mathcal{Z}\,\underline{U}}{V} \qquad (2.72)$$

For a tunnelling mode the general result expressed by equation (2.46) yields

$$n(\omega)\ \chi''_{zz}(\omega) = \frac{NV}{2\hbar}\ |\mathfrak{p}_z|^2 \int \langle S(-\underline{q},\tau)\ S(\underline{q},o)\rangle e^{i\omega\tau}\, d\tau \qquad (2.73)$$

The form of the autocorrelation function has been discussed by Brout (2.25) and is

$$\int \langle S(-\underline{q},\tau)\, S(\underline{q},o)\rangle\, e^{i\omega\tau}\, d\tau = \frac{4\pi\Omega \tanh\beta\Omega}{\hbar\,\Omega(o)}\, n(\omega)\left[\delta(\omega-\Omega(o)) - \delta(\omega+\Omega(o))\right] \qquad (2.74)$$

$\Omega(o)$ is the $\underline{q} = o$ tunnelling mode frequency.

Thus

$$\chi''_{zz}(\omega) = \frac{NV\, 2\pi\, \Omega \tanh\beta\Omega}{\hbar^2\, \Omega(o)} \left|p_z\right|^2 \left[\delta(\omega-\Omega(o)) - \delta(\omega+\Omega(o))\right] \qquad (2.75)$$

This has obvious simlarities to the corresponding equation in the phonon case, namely equation (2.45), where

Phonon mode		Tunnelling Mode
$\left\|P_{zj}(o)\right\|^2$	$\longleftrightarrow$	$\left\|p_z\right\|^2 \frac{4\Omega \tanh\beta\Omega}{\hbar^2}$
$\omega_j(o)$	$\longleftrightarrow$	$\Omega(o)$

(2.76)

Use of the Kramers-Krönig relations allows the real part of the susceptibility to be obtained from (2.75). The tunnelling mode will experience damping due to torques, acting on the pseudo-spins, which were omitted in the derivation of chapter one. This damping can be introduced phenomenologically as in the phonon case to give the tunnelling contribution to the complex susceptibility as

$$\chi_{zz}(\omega) = \frac{NV \left|p_z\right|^2 \frac{4\Omega \tanh\beta\Omega}{\hbar^2}}{\left[\Omega^2(o)-\omega^2\right] + i\left[2\Gamma\omega\right]} \qquad (2.78)$$

For $\Omega \ll k_B T$ using equation (1.40)

$$\Omega^2(o) = \left(\frac{2\Omega}{\hbar}\right)^2 \left(\frac{T-T_1}{T}\right)$$

gives

$$\chi_{zz}(o) = \frac{\frac{NV}{k_B}\left|p_z\right|^2}{T - T_1} \qquad (2.79)$$

Thus, a tunnelling mode associated with proton ordering has a static susceptibility having a Curie Weiss behaviour.

The Curie Constant $C_z = \frac{NV}{k_B} \left| p_z \right|^2$ (2.80)

Further

$$\frac{\chi^{11}_{zz}(\omega)}{\omega} = \frac{\frac{C_z}{T} 2\Gamma \frac{(2\Omega)^2}{\hbar^2}}{\left[\Omega^2(o)-\omega^2\right]^2 + \left[2\Gamma\omega\right]^2} = \frac{\frac{C_z}{T-T_c} 2\Gamma \Omega^2(o)}{\left[\Omega^2(o)-\omega^2\right]^2+\left[2\Gamma\omega\right]^2} \quad (2.81)$$

This is similar to the corresponding equation for the phonon case and has identical temperature dependence if $\omega_b^2 \alpha \frac{T-T_c}{T}$ in (2.68)

Of the two coupled phonon tunnelling modes dealt with in chapter one, the mode of mostly phonon character can be treated as the phonons discussed above. Near the transition the frequency, ω_-, of the predominately tunnelling coupled mode, is small and equation (1.53) gives

$$Q_j(\underline{q},t) = - \frac{G_j(-\underline{q})\, S(\underline{q},t)}{\omega_j^2(\underline{q})} \quad (2.82)$$

The phonon coordinate adiabatically follows the spin coordinate.

If, as is likely in KDP type crystals, it is assumed that the polarization due to the coupled tunnelling mode arises from the motion of the potassium and phosphrous ions rather than the proton, equation (2.34) gives

$$\underline{P}(\underline{q},t) = - \frac{N^{\frac{1}{2}}\, \underline{P}_j(\underline{q})\, G_j(\underline{q})\, S(\underline{q},t)}{\omega_j(\underline{q})^2} \quad (2.83)$$

Comparison with the pure tunnelling mode case yields:-

Pure tunnelling mode	Coupled tunnelling mode
$\underline{p}$	$\frac{P_j(o)\, G_j(o)}{\omega_j^2(o)}$
$\Omega(o)$	$\omega_-^2(o)$

(2.84)

for the $\underline{q} \approx o$ modes applicable in Raman scattering. With these modifications, the formulae derived for the pure tunnelling mode carry over into the coupled mode situation. In particular, the susceptibility components are of the form

$$\chi_{zz}(\omega) = \frac{N V \left|P_{zj}(o)\right|^2 \left|G_j(o)\right|^2 \; 4\Omega \tanh \beta\Omega}{\omega_j(o)^4 \hbar^2 \; (\omega_-(o)^2 - \omega^2 + i2\Gamma\omega)} \qquad (2.85)$$

The damping includes anharmonic coupling to other modes as well as torques acting on spins.

The static susceptibility of the two coupled modes, can be obtained from equations (2.65) and (2.85) as

$$\chi_{zz}(o) = \frac{NV\left|P_{zj}(o)\right|^2}{\omega_j^2(o)} \left[1 + \frac{\left|G_j(o)\right|^2 \; 4\Omega \tanh \beta\Omega}{\omega_j^2(o) \; \hbar^2 \omega_-^2(o)} \right] \qquad (2.86)$$

The first term arises from the mostly phonon coupled mode, and the other from the tunnelling one.

Equation (2.86) on using equations (1.63, 1.65) with $\tanh \beta\Omega \approx \beta\Omega$ reduces to

$$\chi_{zz}(o) = \frac{NV\left|P_{zj}(o)\right|^2}{\omega_j^2(o)} \left[1 + \frac{T_2 - T_1}{T - T_2} \right] \qquad (2.87)$$

a result already discussed in Chapter one. The first term gives a constant contribution to the susceptibility, while the second provides

the Curie Weiss behaviour having Curie Constant

$$C_z = \frac{NV\,(T_2 - T_1)\,\left|P_z j(o)\right|^2}{\omega_j^2(o)} \qquad (2.88)$$

Further, for the coupled tunnelling mode,

$$\frac{\chi^{11}_{zz}(\omega)}{\omega} = \frac{\frac{C_z}{T}\,2\Gamma\,\left(\frac{2\Omega}{\hbar}\right)^2}{\left[\omega_-^2(o) - \omega^2\right]^2 + \left[2\Gamma\omega\right]^2} = \frac{\frac{C_z}{T-T_2}\,2\Gamma\,\omega_-^{-2}(o)}{\left[\omega_-^2(o) - \omega^2\right]^2 + \left[2\Gamma\omega\right]^2} \qquad (2.89)$$

This is the same equation as (2.81) but C_z has the value appropriate to the coupled mode. In regions where the Debye relaxation formula is valid

$$\frac{\chi^{11}_{zz}(\omega)}{\omega} = \frac{\frac{C_z}{T-T_2}\,\tau}{1 + (\omega\tau)^2} \qquad (2.90)$$

where $\tau = \frac{2\Gamma}{\omega_-^2(o)}$ (2.91)

$$\omega_-^2(o) = \left(\frac{2\Omega}{\hbar}\right)^2 \left(\frac{T - T_2}{T}\right) \qquad (1.63)$$

Thus $\frac{\chi^{11}(\omega)}{\omega}$ is seen to have the same form for a soft phonon, equations (2.68, 2.69), tunnelling mode (2.81) and coupled tunnelling mode (2.89 2.90). Thus any distinction between these modes must be based on the behaviour of the parameters. $\omega(o)^2$, and hence $\frac{1}{\tau}$, if Γ is temperature independent, is proportional to (T-Tc) for a soft phonon but $\left(\frac{T-Tc}{T}\right)$ for a soft coupled tunnelling mode. It may be difficult to distinguish these temperature dependennes except in the region far from Tc. However a sharp drop in $\omega(o)^2$ or $\frac{1}{\tau}$ on deuteration would indicate a mode of tunnelling origin.

The effect of further coupling the coupled tunnelling mode to the acoustic shear mode involved in the transition in KDP can be accounted for in the above by replacing T_2 by T_3.

The Raman activity of the $\omega-$ mode is assured if the $\omega+ \approx \omega j(\underline{q})$ mode is Raman active, because only modes of the same symmetry can couple. Another way of saying that is that, in a piezoelectric crystal, the $\omega-$ and ω_+ modes will be Raman active if the polarization fluctuations associated with them can couple to the polarizability through the electrooptic tensor.

Silverman (2.26) has recently derived the dielectric susceptibility from Kobayashi's model in a related manner, but has only obtained solutions for specific examplesof the parameters of the phonon and tunnelling modes eg $\omega o(o) = \Omega(o)$ - uncoupled modes having the same frequency and damping constant. He finds $\chi''(\omega)$ has only one peak encompassing both modes. This is to be expected since for the phonon mode, equation (2.63) gives

$$\omega^2_{max} = \omega_j^2(o) \quad (1 - \frac{2\Gamma}{\omega_{j2(o)}})$$

for the maximum $\frac{\chi''(\omega)}{\omega}$. Since $\frac{\chi''(\omega)}{\omega}$ has the same ω dependence for both phonon and tunnelling coupled modes, equations (2.60) and (2.89), $\left.\frac{\chi''(\omega)}{\omega}\right|_{MAXIMUM}$ will occur at the same frequency for both modes in the unlikely event of their uncoupled frequencies and damping constants being equal.

CHAPTER THREE

A number of light scattering experiments which have given interesting information about soft modes in a variety of crystals, including KDP, are reviewed. Reference is made to measurements by other experimental techniques.

POTASSIUM TANTALATE AND STRONTIUM TITANATE, $KTaO_3$, $SrTiO_3$.

It is unfortunate that a number of interesting crystals have soft modes, which, due to symmetry, are not Raman active. This is the case in the cubic perovskite $KTaO_3$ - a crystal having inversion symmetry at each atomic site. The higher order Raman effects are - as always - present.

Fleury and Worlock (3.1, 3.2) have induced first order Raman scattering in $KTaO_3$ by applying an electric field which removes the crystal inversion symmetry. They applied the field in the form of a square wave, and by means of synchronous detection rejected the more intense, but non-modulated, second order scattering. Investigation of the field dependence of the soft mode is relatively simple since the field, when applied, has a constant value. By varying the pulse length they were able to control sample heating at low temperatures.

In the experiment, Fleury and Worlock investigated the frequency, linewidth and cross section of the soft mode as a function of temperature and applied field in the ranges 8-300°K and 0.2 to 1.5 KV/cm respectively. They observed a temperature dependence of the soft mode frequency at the lowest field values in agreement with inelestic neutron scattering (3.3) and infra-red reflectivity (3.4) measurements. Although the soft mode frequency decreases as absolute zero is approached, the frequency does

not become zero nor does a transition to a ferroelectric phase appear to take place. The mode frequency and linewidth are respectively $85cm^{-1}$ and $20cm^{-1}$ at $300^{o}K$, reducing to $18cm^{-1}$ and $11cm^{-1}$ at $8^{o}K$. The mode is underdamped at all temperatures. The linewidth varies approximately linearly with temperature, while the frequency behaves as $(T - Tc)^{\frac{1}{2}}$ above $40^{o}K$ but decreases less rapidly below this temperature. The integrated intensity increased by a factor of 10 both on cooling from $300^{o}K$ to $80^{o}K$ and from $80^{o}K$ to $8^{o}K$. This results from an increased response of the crystal to a given field as $\epsilon(o)$ increases on reducing the temperature. Although able to determine the soft mode frequency, the neutron experiment lacked the resolution to determine the line width, while the infra red measurements gave linewidths markedly larger than those observed in the Raman experiment. As the infra red data has to be fitted by a model in which correct account of the multiphonon background may be difficult, the more direct Raman measurements are expected to be the more reliable.

Fleury and Worlock discuss their results in terms of the Lyddane-Sachs-Teller relation in the form of equation (1.19) viz. $\omega_o^2(o) \times \epsilon(o) = \text{Constant}$. Their own Raman data together with Wemple's (3.5) dielectric work gives a good fit down to $15^{o}K$. Below this the situation is not well understood.

Increasing the field from low values increases the soft mode frequency. At $8^{o}K$ the mode shifts from $18cm^{-1}$ at 1Kv/cm to $37cm^{-1}$ at 15 Kv/cm. This effect decreases on increasing the temperature, being barely detectable at $75^{o}K$. The frequency, linewidth and cross section of the mode were all observed to increase with the square of the field for low field values. The centrosymmetry of the crystal prohibits a linear

dependence. At high fields, due to the non linear response of the crystal, these parameters increased less rapidly and saturation was observed.

To interpret the field dependence of their data, Fleury and Worlock (3.6) assumed the validity of the LST relation under applied fields and used a thermodynamic argument to obtain the field dependence of the dielectric constant. By expanding the free energy as a power series in polarization

$$A(T,P) = \tfrac{1}{2}\chi(T)\,P^2 + \tfrac{1}{4}\xi(T)\,P^4 + \ldots\ldots \qquad (3.1)$$

(where $\chi(T)$ and $\xi(T)$ are linear and non-linear inverse dielectric susceptibilities, and odd even powers of P are prohibited by symmetry), the dielectric constant can be found from $\frac{\partial^2 A}{\partial P^2}$ and combined with the LST relation. This gives the field dependence, at high fields, of the soft mode frequency as

$$\omega_o^2(E) = \omega_o^2(E=0) + 3.10^6\,\varepsilon_o\left[3\xi(T)E^2\right]^{\frac{2}{3}} \qquad (3.2)$$

where ε_o is the permittivity of vacuum.

Equation (3.2) was found to fit their data fairly well, but gave discrepancies with previous values of $\xi(T)$. This could be due to a difference in the dielectric response to pulsed and static fields.

It should be noted that the applied field also causes the soft mode to be split into two components, polarized parallel and perpendicular to the applied field. The parallel component has a larger shift and is more intense. It is this component that has been discussed above.

Although in principle all the modes are Raman active under an applied

field, only the soft mode and transverse optic modes appearing at $198cm^{-1}$ and $556cm^{-1}$ at $10^{o}K$ had sufficient crossection to be observed. A maximum of 8 modes could have been observed with the scattering geometry used by Fleury and Worlock.

Although the above has dealt exclusively with $KTaO_3$, Worlock and Fleury (3.2, 3.6) were at the same time investigating induced scattering from the corresponding soft mode in Sr TiO_3. The situation in Sr TiO_3 is complicated by the non-ferroelectric transition at $110^{o}K$ which, at the time of their experiments, was thought to involve only a slight change of the unit cell from cubic to tetragonal form. As the c/a ratio in the tetragonal phase was only 1.00056, the dielectric properties were expected to be essentially those of the cubic crystal. Worlock and Fleury indeed found that the field induced soft mode scattering in Sr TiO_3 was substantially similar to that in K TaO_3, both in field and temperature dependence. At no temperature did the soft mode frequency go to zero nor did it show any anomaly at $110^{o}K$, confirming that the transition was unlikely to be ferroelectric. Apart from the soft mode, 4 other modes were observed in the field induced spectrum of Sr TiO_3. One of these was a silent mode, neither intrinsically Raman nor infra red active. This further show the power of this technique in crystals of high symmetry.

Davies (3.7) has studied both the Raman spectra field induced in the paraelectric perovskite phase of the system $K_x Na_{1-x} TaO_3$ and natural scattering from those members of the family having a truely ferroelectric phase.

THE $110^{o}K$ TRANSITION IN STRONTIUM TITANATE

In this section it is convenient to use the term 'ferroelectric mode' to

designate that mode, apparent in the field induced spectrum of $SrTiO_3$, which shifts to low frequencies as absolute zero is approached and is responsible for the high dielectric constant. The term 'soft mode' will refer to the mode causing the 110°K transition.

At room temperature, $SrTiO_3$ has the cubic perovskite structure with one formula group per unit cell. The structure at lower temperatures was in doubt for some time. Following the observation by Gräincher (3.8) of anisotropy in the dielectric constant below 110°K, the electron spin resonance (ESR) experiments of Müller (3.9) and later Rimai and de Mars (3.10) demonstrated the presence of a cubic to tetragonal phase transition. Distinct anomalies in the sound velocities at the transition were found by Bell and Rupprecht (3.11), While, in an X-ray study, Lytle (3.12) determined the c/a ratio as only 1.00056, with no change in the unit cell volume at the transition. This suggested a second order phase change. Several groups (3.13-3.16) had obtained Raman spectra of $SrTiO_3$ in which several first order type peaks appeared below 110°K on top of a strong multiphonon background. None of themodes was expected to be Raman active in the postulated tetragonal structure in which all the atoms were thought to remain at inversion centres. (The field induced tetragonal distortion involves opposite movement of positive and negative ions and thus breaks the inversion symmetry). The modes observed in the field induced spectrum had frequencies in good agreement with those obtained in infra-red experiments but differing markedly from those observed in the zero field spectrum. These peaks were variously interpreted as being due to imperfections or strains.

Little progress on the detailed structure below 110°K was made until

the further ESR work of Unoki and Sakudo (3.17) and Müller, Berlinger and Waldner (3.18), where it was proposed that a doubling of the unit cell took place at the transition. This was verified in a Raman scattering experiment by Fleury, Scott and Worlock (3.19). They pictured the transition as arising from a soft zone corner mode involving counter rigid rotations of adjacent oxygen octahedra about the three equivalent (100) directions. This motion 'freezes out' below 110°K to give the static distortion predicted by Unoki and Sakudo (3.17). This involves a doubling of the unit cell and hence a halving of the Brillouin zone. As a result, the zone boundary modes above 110°K are folded over to appear at the zone centre below 110°K, thus doubling the number of zone centre modes. In this new structure some of the zone centre modes are indeed expected to be Raman active and the five peaks observed (3.13-3.16) do in fact come from first order scattering. In particular, the triply degenerate soft F_{2u} zone corner mode, inaccessible to Raman scattering above 110°K, appears as two Raman active zone centre modes below 110°K. One is an A_{1g} mode polarized parallel to the C axis while the other is a doubly degenerate Eg mode with polarization perpendicular to the C axis. Due to domain structure in the low temperature phase, the C axis has no unique direction for the crystal as a whole. Both the A_{1g} and E_g modes exhibited soft behaviour as the transition temperature (T_o) was approached from below with $\omega \alpha (T_o - T)^n$, where n = 0.3 for the best fit for both modes. The soft behaviour of these modes is a strong indication of their first order character.

Ginz burg (3.20), from the point of view of the Landau thermodynamic theory of second order phase transitions in solids (3.21), has concluded that a soft mode should be a general feature of such transitions. Although $\omega \alpha (T - T_o)^n$ will hold in general for the modes involved in structural transitions, it is only when a ferroelectric transition is approached from

Fig. 3.1

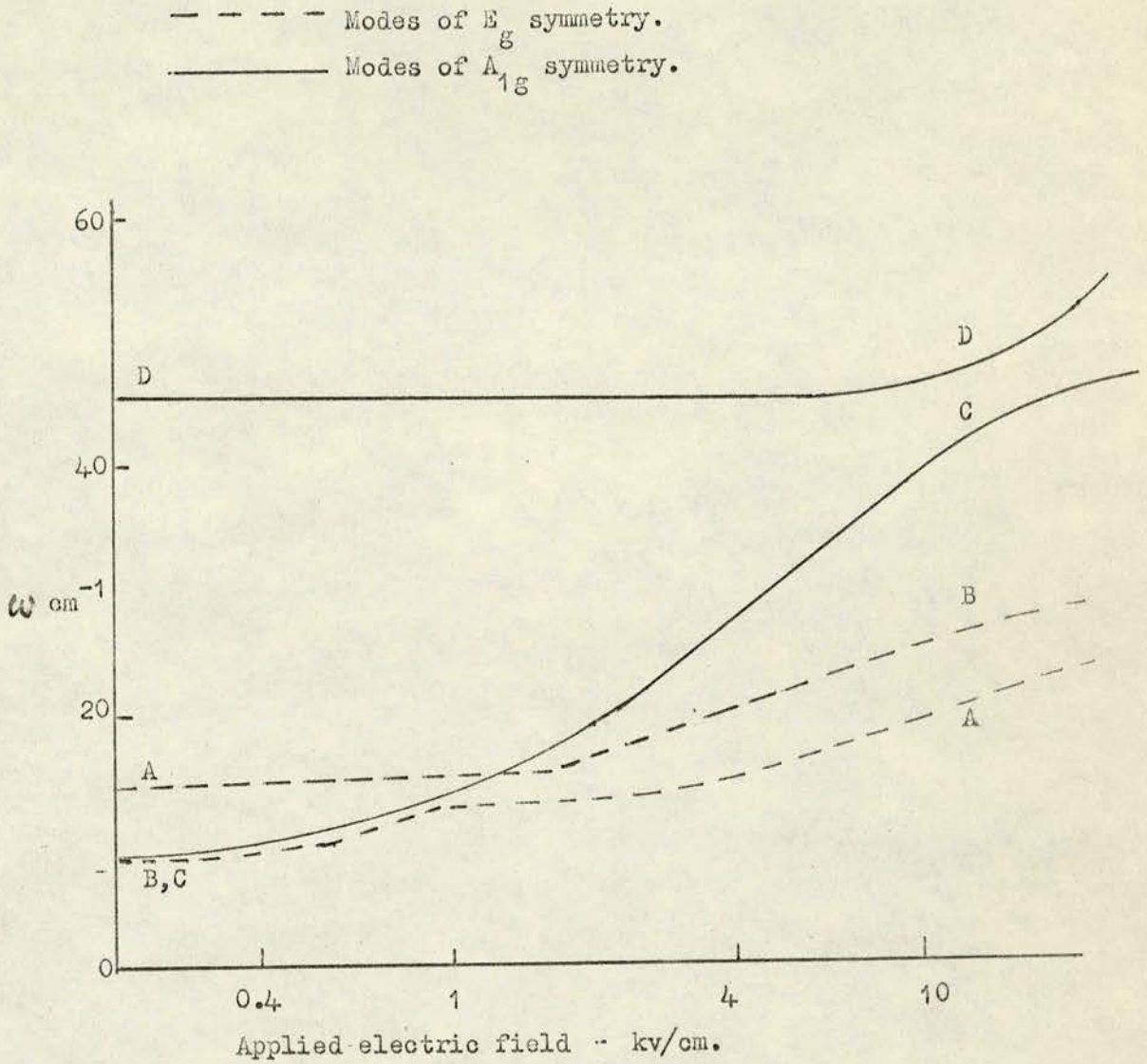

The electric field dependence of the four lowest modes in the field induced Raman spectra of $SrTiO_3$ at 10°K. Anticrossing is evident between the two components of the 'ferroelectric' mode - B & C - and the modes A and D respectively, as the 'ferroelectric' mode frequency is swept by the electric field.

above that we require n = $\frac{1}{2}$. to satisfy the LST relation (1.19), $\omega_o^2(o)\epsilon(o)$ = constant, since $\epsilon(o) \propto \frac{1}{T-Tc}$ in such a case. For a non-ferroelectric transition, as the 110°K transition in $SrTiO_3$, the modes involved are non polar and there is no related dielectric anomaly. Thus the LST relation is not involved, since there is no LO-TO splitting for these modes, and n can have any value. Here n = 0.31.

Fleury, Scott and Worlock (3.19) also showed that as the frequencies of the two components of the field induced ferroelectric mode were varied by sweep ing the magnitude of the applied field at a given temperature, each of these modes exhibited 'anti crossing' effects with one or other of the intrinsic soft modes near the point where the pair of modes might be expected to have the same frequency. Fig (3.1), taken from reference (3.19), illustrates this point. As the symmetry properties of the induced spectrum are known (3.2 3.7), and since only excitations having the same frequency, wavevector and symmetry can exhibit anticrossing, this experiment shows that the two soft mode components are real excitations having the symmetry required by the proposed 'double' structure and are not due to strain or imperfections as was once thought.

Neutron scattering experiments (3.22-3.24) have subsequently shown the presence of the soft F_{2u} zone corner mode in agreement with Fleury Scott and Worlock's interpretation of the transition. This mode has $\omega\alpha(T-To)^{\frac{1}{2}}$ with To = 107°K, the transition occurring at 110°K due to the prior instability of an acoustic mode (3.11). The temperature dependence of the A_{1g} and E_g modes below 110°K and of the ferro-electric

mode at all temperatures was found to be in close agreement with the results of thevarious Raman experiments.

In a Brillouin scattering experiment on Sr TiO_3, Kaiser and Zurek (3.25) observed a sharp drop, of about 3%, in the frequency of a zone centre (100) transverse acoustic mode at the transition. This was followed by a gradual rise to its pre-transition value on further cooling. Fleury,Scott and Worlock (3.19) picture this as being due to an interaction with the soft mode. Above the transition the soft mode is at the zone corner and there is no interaction. At the transition the soft mode appearsat the zone centre,depressing the acoustic frequency . As the soft mode frequency rises on lowering the temperature further, the strength of the interaction decreases and the acoustic frequency recovers. The appearance of a second transverse mode below $110^{o}K$ is indicative of the change of crystal structure.

Kaiser and Zurek also observe critical Rayleigh scattering close to $110^{o}K$ involving a three-fold increase in intensity of the central component. A discussion of ultra sonic studies in this critical region has recently been given by Berre and Fossheim (3.26).

THE RARE EARTH ALUMINATES

Lanthanum Aluminate - La AlO_3 - is a perovskite that undergoes a transition at $820^{o}K$ from a cubic to a low temperature trigonal structure. Cochran and Zia (3.27) have shown that the atomic displacements involved at the transition could be due to the softening of a F_{2u} zone corner mode. X-ray (3.28) and ESR (3.18) studies have been consistant with this view, with the suggestion that the transition is second order. As a result of Raman scattering experiments by Scott

(3.29), and inelastic neutron scattering work by Axe, Shirane and Müller (3.30), the transition in $LaAlO_3$ is thought to be very similar to the 110°K transition in $SrTiO_3$. The trigonal structure in $LaAlO_3$ results from a rigid counter rotation of oxygen octehedra about the (111) directions, rather than the (100) directions as in $SrTiO_3$. There are no Raman active modes in the cubic phase, but the unit cell doubling at the transition makes some modes of the trigonal structure active, including the E_g and A_{1g} modes descended from the F_{2u} zone corner soft mode. Investigating the temperature dependence of these two modes, Scott finds that $\omega \propto (To-T)^{0.5}$ is a good fit above 600°K. Below this temperature the frequency increases less rapidly. The linewidth of these modes increases as the frequency decreases on approaching the transition from below, in such a way that the mode becomes overdamped near the transition. This, coupled with the fact that the intensity goes smoothly to zero at the transition, makes the experiment difficult in the region near To.

The neutron data (3.30) in the cubic phase, shows that the F_{2u} soft mode is overdamped near the transition but the damping decreases as the frequency and temperature rise from the transition. It is estimated that $\omega \propto (T-To)^{0.5}$ for the undamped frequency.

Further Raman work by Scott (3.29) on Praseodymium and Neodymium Aluminates, $PrAlO_3$ $NdAlO_3$, shows that these crystals behave similarly to $LaAlO_3$, and gives an estimate of their previously unknown transition temperatures as 1320°K and 1640°K respectively.

A transition similar to those in $SrTiO_3$ and $LaAlO_3$ has been observed in potassium manganese fluoride, $KMnF_3$, by neutron scattering (3.31), but no Raman scattering from a soft mode has been observed.

Thus, structural transitions involving oxygen octahedra rotations seem to be a general property of perovskite class crystals. The different structures below the transition are thought to result from different linear combinations of the three degenerate F_{2u} modes.

Sr TiO_3 is only just tetragonal since relatively weakstresses in the (111) direction cause a transition to the trigonal structure of La AlO_3 (3.32). Recently, Wall, Rokui and Schawlow (3.33) have observed Raman scattering from the A_{1g} and Eg soft modes in stress induced Sr TiO_3. They find the stress dependence of these modes to be in agreement with a theory due to Slonczewski.

BARIUM TITANATE

In contrast to Sr TiO_3, Ba TiO_3 is a perovskite that does undergo a ferroelectric transition. It has the cubic perovskite structure at high temperatures changing to tetragonal, orthorhombic and rhombohedral structures near 133°C, 7°C and -90°C respectively. The precise transition temperatures depend on crystal quality. The last three structures are all ferroelectric and can be viewed as deformations of the high temperature cubic structure along cube edge, face diagonal and body diagonal respectively. The dielectric constant exhibits Curie Weiss behaviour above 133°C as expected at a ferroelectric transition. Below 133°C the tetragonal C axis dielectric constant rapidly assumes small values and shows negligible anomaly at the 7°C transition. The a - axis dielectric constant, while falling from the high values at 133°C, does rise again to give a large anomaly at 7°C, though smaller than that at 133°C. The temperature dependence of the dielectric constants of Ba TiO_3 are reviewed by, for example, Jona and Shirane (3.35).

Although, as usual, the symmetry of the cubic phase precludes any mode being Raman active, all the modes are active in the tetragonal phase. Following a number of experiments which suffered from the use of multidomain samples, undefined scattering geometries and mode assignments that were inconsistant with the LST relation, Di Domenico et al (3.36,3.37) performed an extensive study of the Raman spectra of single domain tetragonal Ba TiO_3. Their measurements were confined to the range $10^{o}C$-$60^{o}C$ since the crystal becomes multidomain above this temperature. Of particular interest is the behaviour of the lowest frequency E and A_1 symmetry modes which are descended from the ferroelectric mode in the cubic phase.

The scattering from the soft E mode, which was first observed at room temperature by Pinczuk (3.38) but not interpreted as such, appears as a broad wing on the Rayleigh peak having maximum intensity at $0cm^{-1}$ and extending to 70 cm^{-1}. Di Domenico et al (3.36) analyse the spectrum by treating the mode as a damped harmonic oscillator, equation (2.60), and extract a temperature dependent undamped frequency -$\omega_o(o)$- and a damping constant -Γ, in good agreement with the infra red data of Barker (3.39) and Ballentyne (3.40). The undamped frequency decreased from $50cm^{-1}$ at $60^{o}C$ to 34 cm^{-1} at $10^{o}C$. This is consistent with the anomaly in the a-axis dielectric constant - $\epsilon_a(0)$. Using the observed frequencies of the appropriate modes and a value of $\epsilon_a(0)$ obtained from the same crystal, they find a good fit to the generalised LST relation, equation (1.18). The damping constant increased with temperature from 35 cm^{-1} at $10^{o}C$ to 68 cm^{-1} at $60^{o}C$. Di Domenico et al (3.36) speculate that the damping constant would increase through the transitionto agree with Barker's observation of a

heavily overdamped low frequency mode at 200°C.

Since the c-axis dielectric constant, $\epsilon_c(0)$, has a low value and little temperature dependence in the tetragonal phase, the lowest frequency A_1 mode is not expected to exhibit 'soft' behaviour or to be at an unusually low frequency. Since the second order scattering is particularly intense, relatively speaking, in the perovskites, the lowest frequency A_1 (TO) mode could not clearly be distinguished. By using the other observed mode frequencies and dielectric constant data in the generalized LST relation, they estimated the mode to be at 180 cm^{-1}. This is in rough agreement with the infra red work of Barker (3.39) who observed a broad A_1 mode spreading between 100cm^{-1} and 200cm^{-1}.

Further Raman studies of the A_1 modes have been carried out in the polariton region by Pinczuk, Burstein and Ushioda (3.41). By varying the scattering angle in the 0.65-8.5° range theywere able to trace out the polariton dispersion curves and conclude that peaks at 170cm^{-1}, 270cm^{-1} and 520cm^{-1} are all first order. The bands at 270 and 520cm^{-1}, which are broad, were considered by Di Domenico et. al. (3.36) to be second order while they assigned first order scattering to weaker features. Parsons and Rimai (3.42) show that above the transition, the spectrum, which can only arise from higher order processes, has features near 270 and 520cm^{-1}. Taking the frequencies of the modes to which they assign first order character and the value of the static dielectric constant obtained from the initial slope of the lowest frequency polariton branch, Pinczuk et al (3.41) claim agreement with the LST relation. They feel that their dielectric constant is more reliable than that of Di Domenico et al who used a capacitance method which is sensitive to spurious effects in

ferroelectrics. Thus while there is some doubt as to correct A_1 mode assignments there is general agreement that the lowest A_1 mode is near $175cm^{-1}$.

Neutron scattering experiments on Ba TiO_3 have been carried out by Shirane et. al. (3.43, 3.44). These show the presence of a soft mode in the cubic phase having $\omega_o(o) \propto (T-T_c)^{\frac{1}{2}}$, where $T_c = 120^oC$. Since the transition temperature is at 132^oC for their crystal, the transition is clearly first order. In the tetragonal phase, the soft mode dispersion curve was found to be highly dependent on phonon direction. Although in certain directions at finite values of $\underline{q}$ the mode was underdamped, near $\underline{q} = o$ the mode always appeared overdamped in agreement with Raman and infra red observations.

Fleury and Lazay (3.45) have investigated the soft E mode in tetragonal $BaTiO_3$ in an experiment similar to that of Di Domenico et. al.(3.36) but at higher resolution and to lower frequencies. They observe both the overdamped soft mode and the transverse acoustic mode. Just below the lowest frequencies observed by Di Domenico, Fleury and Lazay find that the broad E mode intensity falls and then rises rapidly to an exceptionally intense transverse acoustic mode, about 1000times stronger than normal for perovskites. While the intensity and linewidth increase on cooling, the frequency decreases somewhat. The temperature dependence of the frequency shift is a consequence of the temperature dependence of certain elastic constants, while that of the intensity, as Brody and Cummins (3.46) have shown for KDP, is due to the anomaly in the Pockels elasto-optic constants. The dielectric, elastic and elasto-optic anomalies at the 7^oC transition in Ba TiO_3 can all be linked via the thermodynamic theory and are a consequence of the lattice instability that preceeds the onset of the orthorhombic phase. Fleury and Lazay

accounted for the spectral profile they observed by using a model, originally due to Barker and Hopfield (3.47) which involves a linear piezoelectric coupling of thepolarization and strain modes. They take the uncoupled polarization and strain susceptibilities to be given by

$$\chi_R = (\omega_R^2 - \omega^2 + i2\Gamma\omega)^{-1} \qquad (3.3)$$

where R = P (Polarization) or S (Strain) respectively.

In a similar notation, the coupled polarization and strain susceptibilities are given by

$$\chi_R^{\text{coupled}} = \frac{\chi_R}{1-A^2\chi_P\chi_S} \qquad (3.4)$$

where A is the coupling constant. At the frequencies of interest, the spectral profile for each coupled mode is given by

$$I_R(\omega) \alpha \frac{\chi''^{\text{coupled}}_R(\omega)}{\omega}$$

These formulae provide a good fit to Fleury and Lazay's data

LEAD TITANATE $PbTiO_3$

$PbTiO_3$ undergoes a first order ferroelectric transition from a cubic perovskite to tetragonal structure near 490°C. Unlike $BaTiO_3$, there are no other transitions on further cooling.

Burns and Scott (3.48) have investigated the spectrum from room temperature to the transition. The lowest frequency E mode, which is descended for the soft ferroelectric mode in the cubic phase, was found to have appreciable width near the transition although it was not overdamped. Burns and Scott fitted the lineshape to the damped harmonic oscillator function (2.60) to obtain the undamped mode

frequency and damping constant. The frequency decreases from $90cm^{-1}$ at $30^{o}C$ to $50cm^{-1}$ at $490^{o}C$ - it need not tend to zero at the transition since it is first order in nature. As in $Ba\ TiO_3$, in $Pb\ TiO_3$ the damping constant increases with temperature. Similarly the lowest frequency A_1 mode is masked by strong second order scattering, but is observed at $127cm^{-1}$ in a spectrum of mixed polarization. The absence of low frequency data on the clamped dielectric constants precludes the use of the LST relation as a test of mode frequencies.

In a neutron scattering experiment on $Pb\ TiO_3$, Shirane et al (3.44) have studied the soft mode in the cubic phase, where it is underdamped, and the A_1 and E modes at $22^{o}C$ in the tetragonal phase, obtaining reasonable agreement with the Raman data.

Burns and Scott (3.49) have extended their work to the mixed system $Pb\ Ti_{(1-x)}Zr_x\ O_3$ which, at room temperature, is tetragonal and ferroelectric for $x < 0.52$. It is very difficult to produce a single crystal of this material. However, they show that the peaks in the Raman spectra of powdered or ceramic samples occur at the same frequencies as the modes propagating along the principle axes of the corresponding single crystal. This interesting technique is only of limited usefulness in the study of soft modes, since the intense elastic scattering from the powdered sample makes observation of shifts less than about $50cm^{-1}$ difficult. Burns and Scott find that on increasing x from 0 to 0.25 the soft E mode frequency drops from $90cm^{-1}$ to $50cm^{-1}$. Since the decrease of this frequency is more rapid than the decrease of the ferroelectric transition temperature, it is postulated that the transition approaches second order as x increases,

frequency and damping constant. The frequency decreases from $90cm^{-1}$ at $30^{o}C$ to $50cm^{-1}$ at $490^{o}C$ - it need not tend to zero at the transition since it is first order in nature. As in $BaTiO_3$, in $PbTiO_3$ the damping constant increases with temperature. Similarly the lowest frequency A_1 mode is masked by strong second order scattering, but is observed at $127cm^{-1}$ in a spectrum of mixed polarization. The absence of low frequency data on the clamped dielectric constants precludes the use of the LST relation as a test of mode frequencies.

In a neutron scattering experiment on $PbTiO_3$, Shirane et al (3.44) have studied the soft mode in the cubic phase, where it is underdamped, and the A_1 and E modes at $22^{o}C$ in the tetragonal phase, obtaining reasonable agreement with the Raman data.

Burns and Scott (3.49) have extended their work to the mixed system $Pb\ Ti_{(1-x)}Zr_x\ O_3$ which, at room temperature, is tetragonal and ferroelectric for $x < 0.52$. It is very difficult to produce a single crystal of this material. However, they show that the peaks in the Raman spectra of powdered or ceramic samples occur at the same frequencies as the modes propagating along the principle axes of the corresponding single crystal. This interesting technique is only of limited usefulness in the study of soft modes, since the intense elastic scattering from the powdered sample makes observation of shifts less than about $50cm^{-1}$ difficult. Burns and Scott find that on increasing x from 0 to 0.25 the soft E mode frequency drops from $90cm^{-1}$ to $50cm^{-1}$. Since the decrease of this frequency is more rapid than the decrease of the ferroelectric transition temperature, it is postulated that the transition approaches second order as x increases,

in agreement with dielectric and thermal expansion studies (3.50).

The same workers (3.51) have applied the powder Raman technique to the system $Pb_{(1-x)}Ba_x TiO_3$, which is a tetragonal ferroelectric at room temperature for all x. On increasing x the transition temperature decreases linearly. There is also a smooth change of soft E mode lineshape from the underdamped mode of $PbTiO_3$ to the overdamped mode of $BaTiO_3$ - the undamped frequency decreases with x while the damping constant increases. Although in single crystals of $PbTiO_3$ the lowest frequency $A_1(TO)$ mode is observed at $127cm^{-1}$ in a mixed polarization, it cannot be resolved from the background in spectra obtained using a powdered sample. Thus, the benefits to be gained by observing the variation of the spectrum with composition from $PbTiO_3$ to the less well understood $BaTiO_3$ are cancelled by the lack of polarization and low frequency data inherent in the powder technique.

LITHIUM NIOBATE AND TANTALATE, $LiNbO_3$ $LiTaO_3$

$LiNbO_3$ and $LiTaO_3$ are ferroelectric at room temperature undergoing second order transitions at $\sim 1485^{\circ}K$ and $\sim 900^{\circ}K$ respectively. The low temperature structure is trigonal with two formula groups per unit cell.

Johnston and Kaminow (3.52) have investigated the temperature dependence of the frequency, linewidth and cross-section of all the Raman active modes over the range 90 to $1000^{\circ}K$, in both crystals. Analysis of the data is complicated by the fact that the soft A_1 mode crosses initially lower lying E modes. Although modes of different symmetry should not couple, the 'anti crossing' effects observed as the soft mode descends are attributed to a lowering of the crystal

symmetry caused by temperature dependent strain perturbations. Although the soft mode becomes broader on heating, as in $PbTiO_3$, Johnston and Kaminow do not treat the mode as a damped harmonic oscillator but instead extract a 'centre of gravity' frequency. Near the transition this frequency is found to have a $(T_c-T)^{\frac{1}{2}}$ temperature dependence. This is in agreement with the thermodynamic theory which predicts

$$\epsilon(o) = \frac{C}{T-Tc} \qquad T > Tc$$

$$= \frac{C}{2(Tc-T)} \qquad T < Tc \qquad (3.5)$$

and thus $\omega_o(o) \alpha (Tc-T)^{\frac{1}{2}}$ for the soft mode below the transition by virtue of the LST relation.

The soft mode frequency increases less rapidly below 300^oK due to polarization saturation. Similar behaviour was noted in $La AlO_3$.

The scattering crossections of themodes that remain active in the paraelectric phase are found to be temperature independent. The modes that become inactive decrease in intensity as (Tc-T) going to zero continuously at the transition, with the exception of the soft mode which has a $\sqrt{Tc-T}$ dependence due to the effect of a $\frac{1}{\omega}$ phonon term in the cross-section.

Johnston and Kaminow also observed a large increase in the unresolved Rayleigh-Brillouin peak near Tc. They report Ginzburg (3.53) to have derived a relation connecting non propagating polarization and dielectric constant fluctuations which are linked by the linear electro-optic effect below Tc and the much weaker quadratic effect above it. Thus the intensity does not follow the same temperature dependence as the dielectric anomaly - it decreases much more rapidly above the transition due to the weaker coupling.

QUARTZ

Quartz undergoes a non-ferroelectric transition from a high temperature hexagonal β phase, to a low temperature trigonal α phase at 573°C, for which a soft mode is thought to be responsible.

Kleinman and Spitzer (3.54) have shown that a mode at 207 cm^{-1} at room temperature, which is Raman active and infra red inactive, has the dynamical motions corresponding to the static structural changes at the transition and is likely to be the soft mode. Group theory predicts that, in the α phase, 3 further A_1 modes and 8 doubly degenerate E modes will be Raman active.

An early Raman experiment by Narayanaswang (3.55) indeed revealed a soft temperature dependence for the 207 cm^{-1} mode as the transition is approached from below. In a more recent experiment, Shapiro, O'Shea and Cummins (3.56) observed an 'extra' feature at 147 cm^{-1} in addition to the four expected A_1 modes at 207 cm^{-1}, 355 cm^{-1}, 446 cm^{-1} and 1080 cm^{-1}, (room temperature values). While the 207 cm^{-1} mode shifts to somewhat lower frequencies as the temperature rises, it is the 147 cm^{-1} feature that, growing in intensity, approaches zero frequency at the transition. The 207 cm^{-1} mode persists (at 162 cm^{-1}) above the transition, as does the 466 cm^{-1} line although group theory predicts that 'only one of the four A_1 modes' is Raman active in the β phase. Shapiro et.al.insist that the 147 cm^{-1} line must be first order since it plays so fundamental a role in the transition.

Scott (3.57) doubts whether the 147 cm^{-1} feature is first order both because at low temperatures it is broad, assymmetric and has several maxima, and because inelastic neutron scattering measurements have failed to detect such a mode (3.58). Scott's interpretation is

that the 207 cm^{-1} mode is indeed the soft mode whose frequency tends to zero as the transition is approached. The 147 cm^{-1} feature is essentially temperature independent and second order in nature, consisting of two oppositely directed zone edge acoustic phonons, and it persists through the transition. Thus the number of first order peaks observed is thus consistent with the predictions of group theory. Because of anharmonic coupling between the soft mode and the two phonon excitation, the system exhibits 'anti-crossing' effects not unlike those observed in $SrTiO_3$ (3.19). As the temperature is increased, the 207 cm^{-1} mode softens slightly to about 162 cm^{-1} and maintains this frequency, but with two - phonon character, through the transition, while the two-phonon feature at 147 cm^{-1} picks up the soft mode character and thus goes to zero at the transition. The temperature dependence of the soft mode is found to be $\omega \alpha (To-T)^n$ with $n = 0.3$. A similar value was found at the 110°K transition in $SrTiO_3$. That $n \neq 0.5$ implies that the force constants of the mode are not linearly dependent on (To-T).

The success of this experiment is due to the fact that at the extremes of the temperature range used (6 - 840°K), the two features are well separated and thus reveal their true nature. This helps in the analysis of the more complicated spectra in the anti-crossing region.

Above the transition the soft mode is both Raman and infra-red inactive. However a neutron scattering experiment by Axe and Shirane (3.59) has revealed an overdamped zone centre transverse optic mode with a Curie-Weiss dependence for the total intensity.

Scott (3.60) has performed a similar Raman experiment in $AlPO_4$ whose structure is closely related to that of quartz. A similar transverse optic mode - two phonon interaction is observed but it occurs closer to

the transition.

ANTIMONY SULPHO-IODIDE,SbSI.

SbSI is a ferroelectric with a transition temperature of 288°K. It is orthorhombic above Tc, while structural studies (3.60) indicate that the transition to the ferroelectric phase is accompanied by displacements of Sb and S along the C axis. Thus the corresponding mode of vibration is expected to be a soft mode.

Perry and Agrawal(3.61) and Chisler et.al.(3.62) have carried out a mode assignment for the lines observed in the Raman spectra of both phases. They have also studied the temperature dependence of the soft A_1 mode which is Raman active below the transition. The correct interpretation of the soft mode behaviour is probably due to Harbeke, Steigmeier and Welmer (3.63) who believe that two coupled A_1 modes are involved. Far from the transition ($Tc-T \sim 200^{\circ}K$) there is a strong mode at 50 cm^{-1} and a weak one at 30 cm^{-1}. On approaching the transition the 50 cm^{-1} mode descends to lower frequencies transferring its character, strength and temperature dependence at about $Tc-T \sim 50^{\circ}K$ to the 30 cm^{-1} mode whose frequency subsequently tends to zero at the transition. They find $\omega_o(o) \propto (Tc-T)^{0.33}$. As the pair of modes are broad compared to their separation and as intensity is transferred from one to the other, it was perhaps not surprising that the first experiments (3.61, 3.62) had incorrect interpretation.

As SbSI is opaque the experiment must be performed in the awkward backscattering configuration. There is an overall increase in intensity as the temperature is lowered from the transition. This is due to a resonant Raman process which accompanies the rise in optical

absorption edge above the laser frequency as the temperature is reduced.

A Brillouin scattering study of the acoustic modes has recently been carried out by Sandercock (3.64). The 9 elastic constants, at constant displacement, derived from the frequency shifts, all change step wise by about 1-3% over an interval of 0.25°C at the transition. No large anomalies are observed. His present work involves a study of the elastic constants at constant field since C^{E}_{33} is expected to be soft below Tc.

Experimental difficulties arise in measuring these small frequency shifts in the presence of the intense elastic scattering inevitable with the backscattering geometry. Sandercock has very successfully overcome this by passing the light twice through the Fabry-Perot Interferometer, giving a significant improvement in the contrast.

GERMANIUM TELLURIDE GeTe

Inelastic neutron scattering experiments on SnTe (3.65) have shown the presence of a soft mode whose frequency decreases with decreasing temperature but is still finite at absolute zero, as in $KTaO_3$. All members of the system $Ge_x Sn_{1-x} Te$ have a high static dielectric constant and, except for small values of x, undergo a structural transition at temperatures up to 625K for $x=1$. The low temperature phase is a rhombohedral distortion of the high temperature NaCl structure. Although GeTe is a semiconductor and does not exhibit a spontaneous polarization the transition is like that of a displacive ferroelectric from the view point of lattice dynamics. This is the first example of a diatomic 'ferroelectric', the simplest type possible.

Steigmeier and Harbeke (3.66) in a Raman scattering experiment on GeTe have observed both the expected modes in the low temperature α phase.

At low temperatures, the Γ_1 mode is at 140cm^{-1} and the doubly degenerate Γ_2 mode at 98 cm^{-1}. Although the Γ_1 mode is always of higher frequency it has the dynamic motions corresponding to the structural changes at the transition and thus appears to be soft mode. Both modes show soft behaviour in fact but the Γ_1 mode increases in line width as the temperature is raised, possibly becoming overdamped near the transition at 625°K. Loss of tellurium from the surface at temperatures above 500°K prevent verification of this. Steigmeier and Harbeke propose that the electric field associated with infra-red active modes, which gives rise to LO-TO splitting in an ionic crystal, is completely screened by the conduction electrons in this narrow band gap semi-conductor. The mode at 98cm^{-1} is LO-TO degenerate, while that at 140 cm^{-1} is split from the 98 cm^{-1} mode by crystal anisotropy. Thus GeTe undergoes a displacive phase transition as a result of a lattice instability.

Apart from theusual difficulties involved in performing a back scattering experiment on an opaque sample, local heating of the illuminated volume by the laser beam requires that the temperature be deduced from the Stokes/anti-Stokes intensity ratio.

THE RARE EARTH MOLYBDATES

Aizu (3.67) has recently distinguished a class of materials which, below a certain temperature, possess a spontaneous strain which may be reversed by application of an external stress. These crystals are called ferroelastics since they are the mechanical analogy of the ferroelectrics. The rare earth molybdates eg. Gadolinium Molybdate $Gd_2(MoO_4)_3$ - 'GMO' - are both ferroelectric and ferroelastic, having a transition near 155°C. The spontaneous strain and polarization found in the low temperature orthorhombic phase can both be reversed by either

an applied stress or an electric field.

The nature of the transitions in these crystals has recently been clarified in a neutron scattering experiment by Axe, Dorner and Shirane (3.68) in the paraelectric phase of $Tb(MoO_4)_3$ - TMO. Since there is no dielectric or elastic anomaly above the transition, a $\underline{q} = o$ phonon is unlikely to be of prime importance. Consideration of the structural change at the transition - tetragonal to orthorhombic with a 45° rotation about the C-axis and a unit cell volume doubling - strongly suggests that a zone boundary mode is involved. Neutron scattering has been observed from such a mode which appears as a broad damped peak, with the bulk of the intensity occurring at lower frequencies as the transition is approached from above. An analysis in terms of a damped harmonic oscillator gives a temperature independent damping constant and an undamped frequency with a $(T-Tc)^{\frac{1}{2}}$ temperature dependence. These observations are in accord with a theory due to Pytte (3.69) who believes that the soft mode is anharmonically coupled to the strain fluctuations which, in turn, are linked to the polarization fluctuations by the normal piezoelectric coupling. It is of note that the mode causing the transition is neither zone centre nor polar as was previously thought essential for a displacive ferroelectric transition.

As a result of the unit cell doubling, the soft mode appears at the zone centre below thetransition where it is Raman active. Thisis similar to the $110^\circ K$ transition in $SrTiO_3$. Fleury (3.70) has observed Raman Scattering from this, the lowest frequency A1 mode, which appears as a broad peak whose intensity shifts to lower frequencies as the transition is approached from below. A damped harmonic oscillator analysis shows that, in fact, the undamped mode frequency at $50\ cm^{-1}$ is substantially temperature independent in agreement with the low

frequency dielectric constant to which it is linked through the LST relation. The damping constant increases rapidly as the transition is approached so that the mode becomes overdamped near the transition. The lack of a dielectric anomaly is also responsible for the temperature independence of the total scattered intensity.

In contrast to its temperature independent nature in the paraelectric phase, Cross, Fouskova and Cummins (3.71) have observed soft behaviour for the C^{E}_{66} elastic constant in the low temperature phase as it recovers from a sharp 50% drop at the transition. Fleury (3.70) states that the small variation in undamped A_1 mode frequency is quite unable to account for this large elastic anomaly by means of normal piezoelectric coupling alone and that higher order interactions are the more important.

SODIUM TRIHYDROGEN SELENITE $NaH_3(SeO_3)_2$

$Na\ H_3(SeO_3)_2$ transforms from a paraelectric monoclinic phase to a ferroelectric triclinic phase at 194°K and to a further ferroelectric monoclinic phase at 100°K.

A Raman scattering study by Peercy (3.72) failed to detect soft behaviour among any of the modes observed in the paraelectric phase. The spectra in the ferroelectric phases are considerably more complicated, but no strong temperature dependence was found for any mode at either transition.

The tail of the Rayleigh peak appears to extend to $\sim 35cm^{-1}$ in Peercy's published spectra, so the possibility exists that the soft mode is highly overdamped and not resolved from the Rayleigh peak in this particular experiment. Other hydrogen bonded ferroelectrics eg KDP (3.73) do have over-damped soft modes.

POTASSIUM DIHYDROGEN PHOSPHATE AND ITS ISOMORPHS

Early experiments were performed with a mercury arc lamp, single grating or prism spectrometer and photographic detection. The presence of other emission lines, grating ghosts and a strong background, together with lack of sensitivity, made these experiments difficult and were no doubt the source of discrepencies between the observations of different workers. However a number of modes were observed at room temperature by Chappelle (3.74) for KDP and ADP, Landsberg and Baryshanskaya (3.75) for KDP, and Narayanan (3.76) for KDP and ADP.

Photo-electric detection was employed by Aref'ev and Bazhulin (3.71) who studied the spectra from KDP and ADP between 25 and 135 cm^{-1} at 6 temperatures above the transition and one below. Apart from the slight ($3cm^{-1}$) shift of a line at 34 cm^{-1} which appeared on a broad Rayleigh wing, the spectra they obtained showed no temperature dependence and were the same for both ADP and KDP, contrary to the observations of other workers. An extensive study by Stekhanov and Popova (3.78) over the range 25-4000 cm^{-1} showed an increase in the number of modes below the transition. At low frequencies their spectra are in disagreement with those of Aref'ev and Bazhulin but do show a low frequency wing whose intensity increases markedly on cooling from room temperature to the transition and then falls appreciably below the transition.

The advent of the laser with its highly directional and polarized beam enabled the scattering by the various polarizability tensor components to be separated, thus simplifying normal mode analysis. Kaminow, Leite and Porto (3.79) observed the first laser Raman spectra of KDP which were in qualitative agreement with the results of earlier workers. In a later experiment (3.80) they studied an 80% deuterated

sample. Three strong broad (250 cm^{-1}) lines appear at 2705, 2360 and 1790 cm^{-1} forKDP. Because of the high frequencies involved these are assumed due to the lightest nucleus in the unit cell - the proton. The corresponding lines in the deuterated sample are at 1990, 1770, 1370 cm^{-1}. The ratio of these frequencies is sufficiently near $\sqrt{2}$ to conclude that the protons are involved in a phonon, rather than tunnelling, motion. Since $\omega \propto m^{-\frac{1}{2}}$, where m is the particle mass, the isotope effect on these frequencies is solely due to the increased mass of the deuteron. On the Kobayashi model, these modes involve oscillations of the protons at one site on the bond only, and thus the frequencies represent transitions between the energy levels of a single well.

The greatly increased suppression of light elastically scattered at the laser frequency, afforded by the tandem grating spectrometer, enabled Kaminow and Damen (3.73) to make a quantative study of the soft mode in KDP. This mode has B_2 symmetry. They identify as the soft mode a broad wing on the Rayleigh line extending from its maximum at 0 cm^{-1} to beyond 140 cm^{-1}. The presence of this mode had been deduced from far infra-red measurements (3.81)(3.82), but due to the low frequencies involved both the experiment and the analysis of the results had proved difficult. The wing becomes narrower and more intense as the transition is approached from above, while cooling below the transition causes a rapid decrease in intensity in an unpoled crystal. Kaminow and Damen treat the soft mode as a damped harmonic oscillator. Using equation (2.57)

$$I(\omega) = A\, n(\omega)\, \chi''(\omega)$$

they obtain the imaginary part of susceptibility from the intensity

distribution, and fit $\chi''(\omega)$ with equation (2.68)

$$\chi''(\omega) = \frac{\chi_o(o)\ 2\Gamma\omega_o^2(o)\ \omega}{[\omega_o^2(o)-\omega^2]^2 + [2\omega\Gamma]^2} \qquad (3.5)$$

where $\chi_o(o)$ is the contribution of the soft mode to the static susceptibility. They find

$$\chi_o(o) \propto \frac{1}{T-Tc} \quad ; \quad Tc = 117^oK$$

$$\omega_o(o) = 99\sqrt{\frac{T-Tc}{T}}\ cm^{-1} \qquad (3.6)$$

$$\Gamma = 85\ cm^{-1}$$

That $\chi_o(o)$ has a Curie-Weiss form indicates that the soft mode is responsible for the dielectric anomaly in KDP. $\omega_o(o)$ has the form predicted by Kobayashi - equation (1.63) - for a coupled tunnelling mode. For an isolated proton, the tunnelling frequency is thus 99 cm^{-1}. This mode extrapolates to zero at 117°K, the Curie temperature of the clamped crystal. Due to an acoustic instability the transition occurs at 122°K, the Curie temperature of the free crystal. The damping constant is essentially temperature independent but there is a wide (±20%) scatter in the points. Kaminow and Damen claim agreement with their previous (3.83) microwave measurements of the complex dielectric constant $\epsilon_c(\omega)$ in as much that Γ is temperature independent, but do not find the LST relation $-\epsilon_c(o)\ \omega_o(o)^2 =$ constant - a particularly good fit. This is hardly surprising since $\chi_o(o) \propto \frac{1}{T-Tc}$ and $\omega_o(o)^2 \propto \frac{T-Tc}{T}$. They go on to develop 'a modified LST relation that applies to heavily damped oscillators' which is satisfied by their data. This modified relation only applies relatively near the transition where there is little difference between

$\omega_o^2(o) \propto \frac{T-Tc}{T}$ and $\frac{T-Tc}{Tc}$. The latter expression obviously satisfies the LST relation. In a later paper (3.84), Kaminow says that the corresponding longitudinal mode frequency would have to rise from 100 cm^{-1} to 200 cm^{-1} over the temperature range 417°K to 127°K, to satisfy the generalised LST relation. He has not been able to positively identify this mode experimentally.

Although the crystal was not poled in the ferroelectric phase Kaminow and Damen found that both $\omega_o(o)$ and $\frac{1}{\chi(o)}$ increased rapidly on cooling below the transition. Γ remained constant through the transition.

In a more recent Raman experiment on KDP, Wilson (3.85) extensively discusses the problem of fitting both a Debye Relaxation function (DRF) and a Damped Harmonic Oscillator (DHO) to his own soft mode data. He found that both fitted the data equally well below ~45 cm^{-1}, while at higher frequencies the damped harmonic oscillator gave the better fit. It should be noted that as he fits to $\chi''(\omega)$, which is approximately proportional to $\omega.I(\omega)$, the high frequency points will be subject to the largest error. He does not have error bars on his data so it is hard to judge whether the two fits can be distinguished within experimental error.

Wilson finds that the temperature dependence of the parameters $\chi_o(o)$, $\omega_o^2(o)$, Γ depends somewhat on the temperature range considered.

For $122 \leq T \leq 290°K$

$$\chi_o(o) \propto \frac{1}{T - 109.0}$$

$$\omega_o^2(o) = 118.2\ (T - 115.6)^{0.76} \quad (cm^{-1})^2 \qquad (3.7)$$

$$\Gamma = 73\ cm^{-1}$$

While for $122 \leq T \leq 480^{\circ}K$

$$\chi_o(0) = 1.76 + \frac{1098.9}{T-116.8}$$

$$\omega_o^2(0) = 227.3\,(T - 120.7)^{0.63} \qquad (cm^{-1})^2 \qquad (3.8)$$

$$\Gamma = 73 \ cm^{-1}$$

Both of these fits are in disagreement with Kaminow and Damen's results. Wilson also finds that, at higher temperatures, the damped harmonic oscillator becomes a poorer fit. This seems strange because in such circumstances there is proportionately more intensity at higher frequencies. The DRF andDHO fits should be more distinct, and hence parameter interaction in the latter reduced, leading to a more confident fit. Thus, there still seems to be doubt as to which function fits the soft mode best in KDP.

Wilson extended his work to perform a normal mode analysis of all the observable Raman lines in paraelectric KDP, ADP, DKDP and ferroelectric KDP. His results confirm those of earlier infra-red and Raman studies and also yield tentatively a few previously unobserved weak lines.

Two further pionts of interest in Wilson's work are noted below - their significance will be discussed in a later chapter.

1) Wilson's data for the low frequency modes of E symmetry in KDP shows an interesting feature for which he has no explanation. this is a band of almost constant intensity extending from the Rayleigh line to the two modes near 100 cm^{-1}. If anything the intensity rises as the frequency increases.

2) Wilson, as Kaminow (3.84), has obtained the spectrum for B_2 modes in KDP and DKDP above the transition. Both find the hint of a wing extending beyond the Rayleigh line in DKDP. Kaminow notes that it appears to have little temperature dependence, while Wilson makes no comment at all although the feature is just visible in his published graphs.

Another Raman study of KDP and DKDP has been carried out by Blinc et. al. (3.86) who claim that a B_1 mode at 397 cm^{-1} and an E mode at 80 cm^{-1} in KDP are not apparent in DKDP. They presume that the corresponding modes in DKDP lie within the Rayleigh peak which, in their experiment, extends to 40 cm^{-1}. This is interpreted as due to coupling to the proton system similar to the soft mode on Kobayashi's theory, which predicts an isotope effect on the tunnelling mode frequencies. These findings are in line with previous work by Blinc (3.87) which shows that, as there are four protons in the unit all of KDP, there will be four proton tunnelling modes: one of B_2 symmetry - the soft mode -, one of B_1 symmetry and two degenerate modes of E symmetry. However, Wilson's results show that the 397 cm^{-1} mode has B_2, not B_1, symmetry and it is also present in DKDP. Further, neither Wilson's or Blinc's data shows a distinct E mode at 80 cm^{-1}. The validity of the results of Blinc's experiment appears doubtful.

Recent work in our own laboratory by Katiyar, Ryan and Scott (3.88) has led to interesting results for cesium and potassium dihydrogen arsenates - CsDA, KDA. These crystals have heavily overdamped soft modes, similar to that in KDP, but with the next mode of B_1 symmetry at much lower frequencies than in the phosphate, presumably due to the greater mass of the arsenic ion. This mode is much broader in the arsenates than the phosphates. The reduction in frequency

and increase in width of this mode leads to a coupled mode spectrum reminiscent of that due to the soft mode and two phonon band in quartz and $AlPO_4$ (3.59) which have been analysed by Zawadowski and Ruvalds, (3.89). The analysis used by Katiyar, Ryan and Scott shows that, for CsDA, the uncoupled soft mode is best fitted by a Debye relaxation function having a half width $\omega_{\frac{1}{2}} = \frac{1}{\tau}$ of 7.0 cm^{-1}, while the other coupled mode is a damped harmonic oscillator having uncoupled frequency (ω) and linewidth (Γ) given by 67 cm^{-1} and 107 cm^{-1} respectively. The effect of coupling, on the two uncoupled modes given by the above parameters, is for the wing intensity to be depleted below the lattice mode and enhanced above.

Another interesting feature in CsDA is that τ, from the DRF fit, which is the high damping limit of $\frac{2\Gamma}{\omega_o^2}$ from the DHO fit, has a $\frac{T}{T-To}$ temperature dependence. Similar behaviour was found in KDP for ω_o^2 (3.73). However in contrast to KDP where ω_o^2 extropolates to zero 4-5°K below the transition temperature, in CsDA To is approximately half the transition temperature, a difference of some 75°K. A similar though smaller effect was noted in KDA. Such a difference is hard to explain since experiments by other techniques have shown that the transition is at least close to being second order and that the difference between clamped and free Curie temperatures is only a few degrees. Cowley et. al. (3.90) believe that in piezoelectric paraelectric materials, the damped harmonic oscillator is no longer an adequate model due to a contribution to the self energy of the soft mode at low frequencies arising from fluctuations in the phonon density. They give for the susceptibility

$$\chi(\omega) = \frac{A}{\omega_o^2(o) - \omega^2 + i\omega\Gamma - \frac{\alpha T}{1 - i\omega\tau'}}. \qquad (3.9)$$

The term $-\frac{\alpha T}{1-i\omega\tau'}$ has been added to the denominator of the usual damped harmonic oscillator function. α is a positive constant and τ' is the lifetime of modulations introduced into the phonon distribution by fluctuations of the soft mode. The above formula was developed from work by Maradudin and Fein (3.91) who showed that for a weakly anharmonic crystal $\omega_o^2(o) \propto$ T-Tc and $\Gamma \propto$ T. In the limit that $\omega\tau' \gg 1$, equation (3.4) reduces to the standard damped oscillator form but has $\omega_o^2(o) = K\,(T-T_o)$ (3.10). When $\omega\tau \ll 1$, $\chi(o) = \frac{A}{\omega_o^2(o) - \alpha T}$

which is proportional to $(T-Tc)^{-1}$. Thus

$$To = \left(1 - \frac{\alpha}{K}\right) Tc \qquad (3.11)$$

The difference between high and low frequency response arises because while fluctuations in the phonon distribution caused by the ferroelectric mode can decay within a period of that wave at low frequencies, they cannot at high freqnencies. While $\frac{\alpha}{K}$ is small ~ 0.01 for KDP it is much larger ~0.5 for CsDA.

Brody and Cummins (3.92) have observed temperature dependence in the frequency of the transverse acoustic mode which corresponds to the xy shear that occurs at the transition. The velocity of this mode is $\sqrt{\frac{C^E_{66}}{\rho}}$. Mason (3.93) has shown that C^E_{66} has an anomaly as the transition is approached, but C^P_{66} has not. This is in agreement with a result of the thermodynamic theory:-

$$C^{E}_{66} = C^{P}_{66} - \frac{a^{2}_{36}}{\chi_{3}(o)} \qquad (3.12)$$

where a_{36} is a non-anomalous piezoelectric constant relating strain and polarization, and $\chi_3(o)$ is the static susceptibility which is known to have Curie -Weiss behaviour. Brody and Cummins consider piezoelectric coupling between the acoustic strain wave and the soft polarization wave, and find that the mostly acoustic coupled mode has a frequency ω_2 given by

$$\omega_2^2 = \omega_a^2 - \frac{q^2}{m^*}\frac{1}{\rho}\frac{a^2_{36}}{\omega_o^2} \qquad (3.13)$$

m^* and q are the 'mass density' and wavevector associated with the acoustic mode of frequency ω_a. From their data and equation (3.13) they find, for the optic mode, $\omega_o^2(o) \propto (T - 117.7)$ (3.14)

This is in contradiction to the temperature dependence found by Kaminow and Damen (3.73). The trouble with Brody and Cummins interpretation is that they have taken the coupling between the acoustic mode and a soft phonon mode. The acoustic mode, on Kobayashi's theory will be coupled to a soft tunnelling mode. This coupling is not piezoelectric in nature. The coupling between acoustic and tunnelling modes on the Kobayashi theory was discussed in chapter 1, where equation (3.12) was derived, in a slightly different form as equations (1.89), (1.90). Brody and Cummins data do indeed satisfy these equations, but they are wrong in thinking that from the temperature dependence of the acoustic mode, thebehaviour of the soft mode can be determined.

Brody and Cummins (3.94) extend their work to show that not only does the transverse acoustic mode related to C^{E}_{66} tend to zero frequency at the transition but the intensity of the scattering from this mode becomes anomolously large as the transition is approached from above. On the basis of the thermodynamic theory, they show that there will be an anomaly in the elasto-optic constant p^{E}_{66}. The scattered intensity depends on p^{E}_{66} and C^{E}_{66} in such a way that both lead to increased intensity at low temperatures.

The next section in this chapter consists of a brief review of some experiments performed on KDP and its isomorphs by a variety of techniques.

INFRA-RED REFLECTIVITY EXPERIMENTS

Barker and Tinkham (3.95) have studied the C-AXIS IR reflectivity spectra of KDP and DKDP in the ranges 2.5-1500 cm^{-1} and 75-320 cm^{-1} respectively. They found a low frequency temperature dependent mode in KDP which was difficult to analyse. This was later identified as the soft mode in Kaminow and Damen's (3.73) Raman experiment. In the frequency range that they investigated, no corresponding mode was observed in DKDP. However, comparing the observed mode strengths with the known value of $\epsilon c(o)$ for DKDP suggested the presence of a polar mode below the limit of their experiment - 75 cm^{-1}. In general the spectra for KDP and DKDP were similar.

Kawamura, Mitsuishi and Yoshinaga (3.96) have obtained $\epsilon_{a}^{11}(\omega)$ and $\epsilon_{c}^{11}(\omega)$ for KDP and ADP in the range 20-500 cm^{-1}. The results are clearly in agreement with Wilson's Raman experiment in which the intensity is related to $\frac{\epsilon^{11}(\omega)}{\omega}$. All four spectra show low frequency modes. In particular, at low frequencies in KDP,

$\epsilon''_a(\omega) \propto \omega$, which is equivalent to the flat spectral response observed by Wilson.

The temperature dependence of the low frequency $\epsilon''_c(\omega)$ in KDP has been determined by Sugawara and Nakamura (3.97) in the range 16 cm^{-1} to 400 cm^{-1}. With decreasing temperature, the soft mode peak moves to lower frequencies and becomes more intense, in agreement with Raman work (3.73), while the first phonon peak gathers some strength and moves to slightly higher frequencies.

INELASTIC NEUTRON SCATTERING

In order to avoid the high incoherent background due to uncompensated spins in the protons, Paul et.al. (3.95) studied inelastic neutron scattering in deuterated KDP. None of the undamped modes observed had any anomalous frequency or intensity behaviour as the transition was approached from above. However, strongly temperature dependent quasi-elastic scattering was observed in the range 226°K - 300°K. As the width of this peak was that of the instrumental resolution - 4 cm^{-1} full width at half maximum - the width of the scattered peak was taken to be very much less than this. While the total scattered intensity varied from one reciprocal lattice point to another, the temperature variation was the same at all of them. This indicated that the quasi-elastic scattering was from a collective motion. The temperature dependence of the total quasi-elastic scattered intensity was found to vary as $\frac{T}{T - T_c}$, where T_c is the Curie temperature of the free crystal ie. the

transition temperature. The q-dependence of the quasi-elastic scattering has, in the reciprocal ac plane, a dumbell appearance with marked elongation along the reciprocal a-axis. This indicates that the scattering is related to polarization fluctuations predominately along the real C axis ie. to the soft mode.

The temperature and $\underline{q}$ dependence of the intensity was fitted to both a simple Ising model of an order-disorder transition and to a damped harmonic oscillator whose undamped frequency was found to be $\omega_o = 5(T-Tc)^{\frac{1}{2}}$ cm^{-1}. The order-disorder model is prefered since the deuterons are known to be ordered below the transition and have large displacements above it.

Paul et.al.also observed the acoustic mode whose velocity is proportional to $\sqrt{C_{66}}$. No anomaly was observed in the mode frequency which Brody and Cummins (3.92) found in a Brillouin experiment to be strongly anomalous. The explanation given is that, at the $\underline{q}$ values used in the neutron experiment, the acoustic mode has higher frequency than the soft mode and can thus follow the ferroelectric fluctuations. The experiment therefore measures the free crystal properties and the acoustic mode velocity depends on C^P_{66} which Mason (3.93) has shown to be non-anomalous. Conversely, light scattering experiments take place at small $\underline{q}$ values, and thus the acoustic mode frequency is less than the soft mode frequency and so the clamped crystal properties are determined. The acoustic mode velocity is then related to C^E_{66}, which is anomalous.

In another neutron experiment on DKDP, Skalyo, Frazer and Shirane (3.99) have determined the atomic motions involved in the ferroelectric mode in DKDP from thevariation of the quasi-elastic intensity in $\underline{q}$-space. This is possible since the scattered neutron intensity is related

to the structure factor which in turn depends, among other things, on the atomic displacements. While the atomic motions are basically those proposed by Cochran - fig (1.8) -, Skalyo et. al. observed, in addition, a large distortional motion of the oxygen tetrahedra and a component of deuteron motion along the C axis. The extent of the deuteron motion is ~ 1% of the unit cell dimension in the C direction and about 5% in the a (or b) direction. It is not known why the tetrahedral distortion and the deuteron C-AXIS motion do not condense at the transition. Such displacements would have been detected by Bacon and Pease (1.23) in their structural study on KDP which is expected to behave similarly to DKDP.

The zone boundary mode thought responsible for the anti-ferroelectric transition in DADP has been investigated by Meister et. al. (3.100). Although this mode is highly overdamped, its width is greater than the spectrometer's resolution. The linewidth was found to vary as $(T-To)^{\frac{1}{2}}$ with To = 210°K. As the transition temperature is 234°K, this is clearly a first order transition. The $\underline{q}$-dependence of the scattered intensity was strongly elliptical with its major axis along the reciprocal C axis, indicating that the anti-polarization fluctuations are in the real ab plane. The integrated intensity was analysed by a Debye fit with a relaxation time having a $(\frac{T}{T-To})$ temperature dependence, where To = 195°K. Although Meister et. al. found their results compatible with a lattice dynamical interpretation of the anti-ferroelectric transition in DADP, they were unable to determine anti-ferroelectric mode motions due to insufficient data.

Meister et al note that the values of To that they obtained were much closer to the transition than that obtained in dielectric measurements (3.101), which extrapolate to give To $\simeq 80^{o}K$. No relation between these temperatures should be expected, however, since the neutron experiment studied a zone boundary instability while the dielectric measurements refer to the thwarted zone centre instability.

DIELECTRIC MEASUREMENTS

The a and c static dielectric constants of KDP, ADP and DADP have been determined over a wide range of temperature by Mason (3.101). In KDP the C-AXIS dielectric constant $\epsilon_c(o)$ is strongly temperature dependent, while $\epsilon_a(o)$ is only slightly so, but has a reasonably large value of $\sim$ 50-60. In ADP the situation is reversed with $\epsilon_a(o)$ being temperature dependent and $\epsilon_c(o)$ almost constant at a value of 20.

The microwave dielectric properties of KDP, ADP and partially deuterated KDP have been studied by Kaninow (3.102) at 9.2 GHz ($0.31 cm^{-1}$) as a function of temperature. The behaviour of ϵ^{1}(9.2 GHz) shows little dispersion compared to the static dielectric constants. At all levels of deuteration in KDP $\epsilon^{1}a > \epsilon^{1}c$ for (T-Tc)> 60. In ADP, $\epsilon^{1}a > \epsilon^{1}c$ at all temperatures used in the experiments. While the main effect of increasing deuteration on $\epsilon^{1}c$ in KDP is to shift the curves to higher temperatures in step with the rise of Curie temperature, $\epsilon^{11}c$ has additionally an increase in its value at a given T-Tc. $\epsilon^{11}a$ has similar behaviour although its temperature dependence is much weaker.

Hill and Ichiki (3.103) have measured the clamped complex dielectric constant of DKDP and TGS (triglycine sulphate) as a function of frequency, temperature and applied field both above and below the transition. They found for each crystal that the points lay on a common curve when plotted as $\epsilon''_c(\omega).(T-Tc) \sim \frac{\omega}{T-Tc}$, and similarly for $\epsilon'_c(\omega)$, in the paraelectric phase. Hill and Ichiki analysed their data in terms of a Gaussian distribution of Debye Relaxation times. Their results have been treated in a different manner by Ishibashi, Sawada and Takagi (3.104) who found

$$\epsilon(\omega) - \epsilon(\infty) = \frac{\epsilon(o) - \epsilon(\infty)}{(1+i\omega\tau)^{\alpha}} \quad ; \quad \alpha = 0.6 \qquad (3.15)$$

to give a better fit. Hill and Ichiki's experiment will be discussed more fully in a later chapter with reference to the results of the present experiment.

ULTRASONIC EXPERIMENTS

The ultra-sonic studies in KDP and DKDP are mainly due to Garland, Novotny, Litov and Uehling (3.105-3.108). These experiments investigate the temperature and frequency dependence of the velocity and attenuation, of the x_y shear mode associated with the transition in these crystals. The velocity measurements lead directly to the anomalous elastic constant C^E_{66} from which $\chi_3(o)$ can be calculated using equation (3.7). By inserting velocity and attenuation data into an equation derived phenomenologically by Landau and Khalatnikov (3.109), the polarization relaxation time, τ_p, can be found.

Litov and Uehling (3.107, 3.108) interpret their data on DKDP in terms of the development of the Slater model due to Silsbee, Uehling and Schmidt (SUS) (1.28) but do not get a particularly good fit. They thus predict that certain features of a collective mode model should be included in the SUS approach.

The values of C^E_{66} as a function of (T-Tc) are much the same for KDP and 84% DKDP. This is in agreement with Kobayashi's theory which predicts no isotape effect on C^E_{66}. Further, the ultrasonic (3.105) and Brillouin (3.92) measurements of C^E_{66} in KDP are in very close agreement, indicating a lack of velocity dispersion over an appreciable range of $\underline{q}$.

In KDP Garland and Novotny (3.105) obtain $\tau p \alpha (T-Tc)^{-1}$ on the basis of a theory due to Geguzina and Krivoglaz (3.110), while Litov and Uehling (3.108) obtain $\tau p \alpha \frac{T}{T-Tc}$ for DKDP from the SUS model. Over temperatures up to 15°K above the transition temperature there is likely to be little difference between $\frac{Tc}{T-Tc}$ and $\frac{T}{T-Tc}$. A useful quantity to note is the initial slope of $\frac{1}{\tau p}$ viz $(\frac{\partial \frac{1}{\tau p}}{\partial T})_{T_c}$;

$$\left[\frac{\partial \frac{1}{\tau p}}{\partial T}\right]_{Tc} = 4.2\ 10^{10}\ \text{sec}^{-1}\text{deg}^{-1} \text{ for KDP for } T > Tc \quad (3.105)$$

$$2.8 \ldots\ldots \quad (3.106)$$

$$1.6 \ldots\ldots \quad T < Tc \quad (3.106)$$

$$0.4 \ldots\ldots \quad 84\% \text{ DKDP for } T > Tc \quad (3.108)$$

$$3.0 \ldots\ldots \quad T < Tc \quad (3.108)$$

In the paraelectric phase $\left[\frac{\partial \frac{1}{\tau p}}{\partial T}\right]_{Tc}$ for DKDP is approximately an order of magnitude smaller than that for KDP. This is compatible with the strong reduction of soft mode frequency on deuteration predicted by Kobayashi. The initial slope of $\frac{1}{\tau}$ is similar in both crystals below the transition since the absence of tunnelling in the ferroelectric phase implies the absence of isotope effect.

For both KDP and DKDP the ratio of the Curie Constants in both phases, obtained from velocity data and equation (3.12), is about ~12. The work of Draegert and Singh (1.7), expressed by equation (1.4), would

tend to place the transition in these crystals at first, rather than second, order.

Further work on KDP and DKDP has been carried out by Shimshoni and Harnik (3.111). In order to avoid both the complication of suppressing domain wall scattering in the ferroelectric phase by the application of an electric field and also the loss of signal due to high attenuation near the transition where the xy shear wave and polarization fluctuations are strongly coupled, Shimshoni and Harnik used a Zz longitudinal wave as the probe. This wave couples weakly to polarization fluctuations along the C-axis below Tc and not at all above Tc. They studied the velocity and attenuation of this wave from Tc-0.2°K to Tc-0.005°K. C^{E}_{66} had a definite discontinuity at Tc for both crystals, indicating a first order transition. They found $\left[\frac{\partial \frac{1}{\tau_p}}{\partial T}\right]_{Tc} = 400.10^{10}$ sec^{-1}deg^{-1} for KDP, $T<T_c$. $\left[\frac{\partial \frac{1}{\tau_p}}{\partial T}\right]_{T_c} = 3.6\ 10^{10}$ sec^{-1}deg^{-1} for KDP $T<Tc$.

While there is good agreement for DKDP with the result found using the x y shear wave (3.108), for KDP there is a difference of two orders of magnitude. This discrepancy is unexplained.

Inoue (3.112) has considered the sound attenuation of waves travelling along the C-axis which are coupled to the soft mode, on the bases of Kobayashi's theory. Shimshoni and Harnik make no reference to Inone's work.

SPECIFIC HEAT MEASUREMENTS

In a series of experiments on KDP and DKDP, Reese and May (3.113) finally concluded that the transition in these crystals was first order.

Latent heat was detected at the transitions, and simultaneous measurements of the dielectric constant showed that the free Curie temperature was $0.1^{c}K$ below the transition temperature. The entropy change at the transition is similar for both crystals and has a magnitude indicative of an order-disorder transition. In contrast to thepredictions of the SUS development of Slater's theory of KDP, no sizeable contribution to the specific heat due to the protons, in excess of the normal lattice contributions, was found at reasonable temperatures above the transition eg $T > Tc+20^{o}K$. This lends support to the lattice dynamical approach of Kobayashi.

The specific heat anomaly, which reflects the amount of energy, required to overcome the saturated polarization, is very sharp in KDP, indicating that short and long range order are destroyed above Tc.

In their first experiment on KDP, the polycrystalline nature of the sample caused the transition to be 'smeared into a second order one'. This would arise if the crystals in the sample had a range of transition temperatures or if some of the crystals were under the electric field produced by others via the pyroelectric effect as the sample was heated.

"MOSSBAUER EXPERIMENT

Brunstein et.al.(3.114) have doped KDP and DKDP with ^{57}Co, which takes up K sites, and detected the ^{57} Fe Mössbauer line. They detect an increase in the width of this line within $0.4^{o}K$ of the transition in KDP and $1.2^{o}K$ in DKDP. From the data in these temperature ranges an average soft mode frequency is deduced for KDP, of $4 10^{6}$ Hz with a

width of 1.5 10^6 Hz. The amplitude of the Mössbauer ion motion is 0.15 Å; similar to the displacements of the K and P ions on going into the ferroelectric phase. No link is given with other experiments which indicate much higher frequencies for the ferroelectric fluctuations.

CHAPTER FOUR

THE EXPERIMENTAL APPARATUS

Most of the observations were obtained using a Fabry-Perot interferometer system, which will be described in detail. A few remarks will be made about a grating spectrometer system used for preliminary measurements.

THE FABRY-PEROT LIGHT SCATTERING APPARATUS

The arrangement of the apparatus is shown in figure (4.1). The experiment was set up on an 8' by 4' steel table having anti-vibration mountings which reduce the effect of disturbances on the stability of the interferometer. The light source was a Spectra Physics Model 125 helium-neon laser producing up to 70mW of vertically polarized light at 6328Å. The beam, proceeding via a mirror M_1 and passing through a half wave plate if horizontal polarization is required, is brought to a focus in the crystal by a lens, L_1, of focal length 20cms. Due to losses at the various components some 60mW of vertically, or 50mW of horizontally polarized light, are incident on the crystal. On emerging from the sample, the laser beam may be dumped in a matt black tube or reflected back through the crystal to increase the intensity. A system comprising lens L_2 with mirror M_2 can be used to trap the laser beam between this mirror and the laser output mirror. A goniometer adjustment on mirror M_2 allows accurate alignment of the multiply reflected beams, This arrangement approximately doubles the intensity in the crystal. Since the light is incident on the crystal from opposite directions, scattering at right angles to the incident beam will take place from phonons

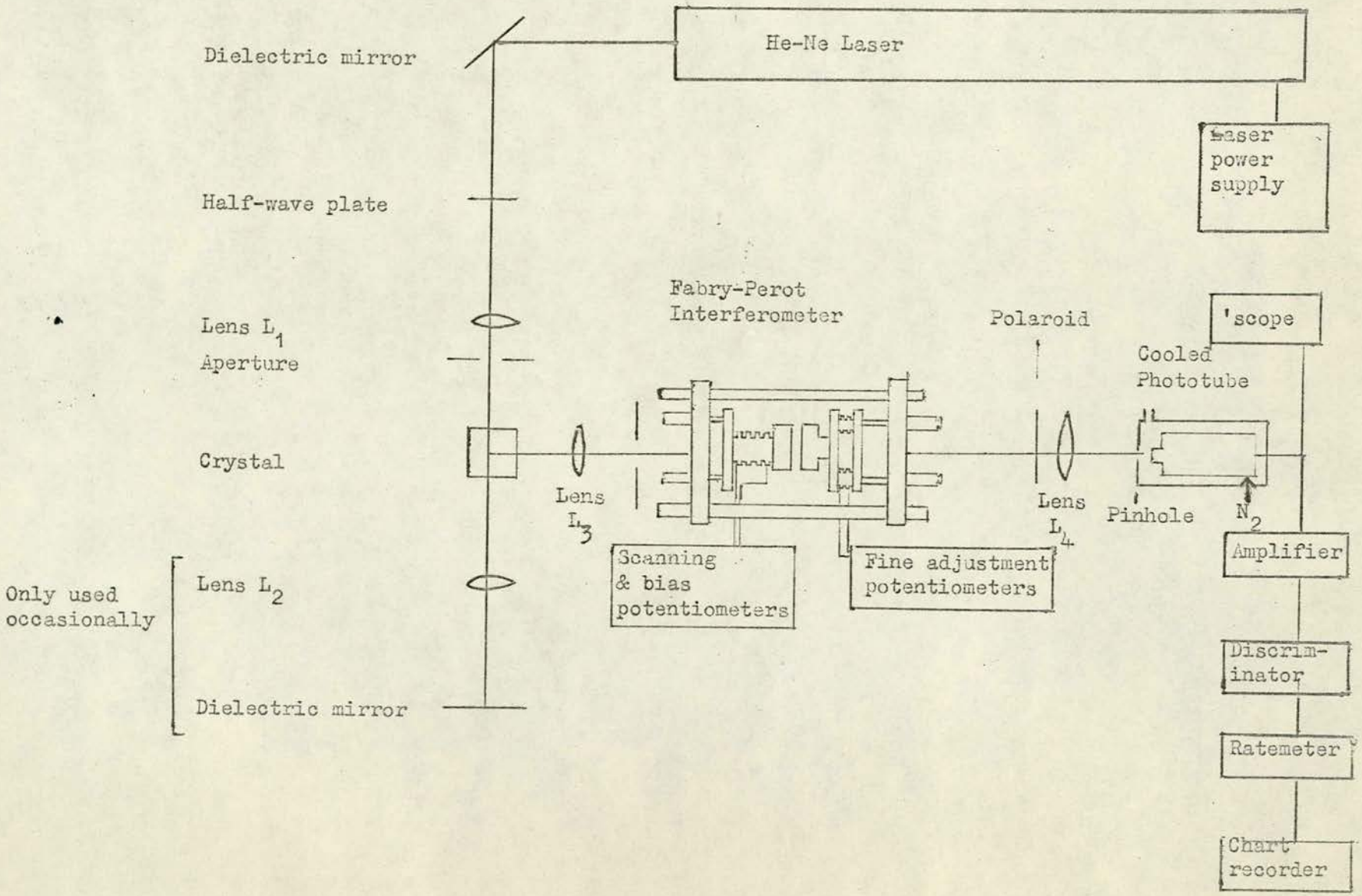

Fig. 4.1

The Fabry-Perot light scattering apparatus.

propagating at right angles to each other. When these phonons are not equivalent by crystal symmetry, this method can not be used to increase the intensity. Due to difficulties in maintaining the alignment of this system, it is only used in cases of the weakest intensities.

The light scattered at right angles to the incident beam is collected by a lens, L_3, of focal length 10cms. This lens is positioned to give a beam of parallel light incident normally on the mirrors of a piezo-electrically scanned Fabry-Perot interferometer. The light transmitted by the interferometer is analysed for horizontal or vertical polarization and then focussed by a lens, L_4, of focal length 20cms onto a plate having a pinhole, typically 1mm in diameter, drilled through it. This pinhole is positioned at the centre of the ring system formed by lens L_4, and allows light transmitted parallel to the axis of the interferometer to fall on the photo-cathode of a cooled photo-multiplier tube. The pulses on the load resistor of the photomultiplier are amplified, passed through a discriminator to give a standard output pulse, and fed into a ratemeter whose output is displayed on a chart recorder. For intense scatterers, the output current from the photomultiplier, possibly smoothed by some capacitance, can be displayed directly on an oscilloscope.

THE FABRY PEROT INTERFEROMETER

Essentially, the interferometer is the cavity formed by a pair of parallel, flat, semi-reflecting mirrors. As the theory of such a system is dealt with fully in standard texts on optics (4.1), only the results will be discussed here.

For each wavelength of light from an extended source, the interference pattern, produced at the focus of a lens, is a set of concentric rings whose intensity maxima are given by

$$2\mu t \cos\theta = n\lambda \qquad (4.1)$$

where μ = the refractive index of the medium in the cavity.

t = the separation of the mirrors.

θ = the angle of incidence of the light on the etalon.

n = the order of interference. It is an integer.

λ = the wavelength of light.

The intensity as a function of wavelength may be determined by varying θ, μ or t. A photographic method, in which the ring diameters are measured, essentially involves a variation of θ, but is inapplicable to the low light intensities in the present experiment. The interferometers normally used employ a variation either of the refractive index of the cavity gas with pressure (pressure scanning) or of the mirror separation by moving one mirror on a piezoelectric transducer (piezoelectric scanning).

As both pressure and piezoelectrically scanned interferometers are used near normal incidence - $\theta \approx 0^{\circ}$ - the interference maxima occur at the centre of the ring system for

$$2\mu t = n\lambda. \qquad (4.2)$$

Varying μt by $\frac{\lambda}{2}$ results in the wavelength λ transmitted at the beginning of the scan, being transmitted again, but in an adjacent order. Such a scan covers a range of wavelengths known as the Free Spectral Range - f - given by

$$f = \frac{1}{2\mu t} \quad cm^{-1} \qquad (4.3)$$

$(1\ cm^{-1} = 30\ MHz)$.

It is more usual, as here, to express the free spectral range in terms of wavenumber, where it appears independent of the incident wavelength, than in terms of wavelength, where it does not. Thus the mirror spacing defines the range covered in an order to order scan, while $\Delta(\mu t) = \frac{\lambda}{2}$ gives the change in optical path necessary to produce this scan. It should be noted that the wavelength of the transmitted light varies linearly with μt.

While proponents of pressure scanned systems claim better linearity and stability for their instruments compared with piezoelectric types, nonlinearities can be accounted for in piezoelectric instruments, and stability need not be a problem if they are well built. On the other hand piezoelectric instruments are more easily and more accurately aligned for parallelism (tuning) - always an important consideration - and the spacing between the mirrors may readily be varied over a large range without the need for accurate spacers for each separation of the mirrors - an important consideration in the present experiment where the spectra under study extend over a wide range of frequencies.

For piezoelectrically scanned interferometers, the mirror movement Δt is given by $\Delta t = \frac{1}{\mu} \frac{\lambda}{2}$. (4.4)

and is independent of the mirror spacing, while for pressured scanned systems $\Delta\mu = \frac{1}{t} \frac{\lambda}{2}$ (4.5)

and the refractive index, and hence pressure, change required depends inversely on the spacing. A pressure change of some 17

atmospheres would be needed to scan a nitrogen gas (μ = 1.0003) interferometer through 80cm^{-1} - the maximum free spectral range of the present piezoelectric instrument.

Confocal Fabry-Perot interferometers, while having significant advantages over plane parallel systems at large separations, when the mirror separation exceeds their diameter, are inappropriate in the present experiment because they operate only at a single free spectral range and only relatively small spacings are used.

The choice of mirror coating and flatness play a crucial role in the optical performance of the instrument. The three main operational parameters of a Fabry-Perot are maximum transmission, finesse and contrast. For perfectly flat and parallel mirrors, these parameters depend only on the reflectivity, transmission and hence absorption of the mirrors.

If R = reflectivity

T = transmission

A = absorption, scatter and other losses

I_o = incident intensity

then the maximum transmitted intensity of the interferometer is

$$I_{max} = \left[\frac{T}{1-R}\right]^2 I_o = \frac{I_o}{(1+A/T)^2} = \left[\frac{1-R-A}{1-R}\right]^2 I_o \qquad (4.6)$$

The finesse, F, the ratio of the full width at half height of a transmitted peak, due to a monochromatic beam, to the free spectral range, is given by

Fig. 4.2

$\left[1 - \frac{A}{1-R}\right]^2 \sim R$; for various values of absorption A

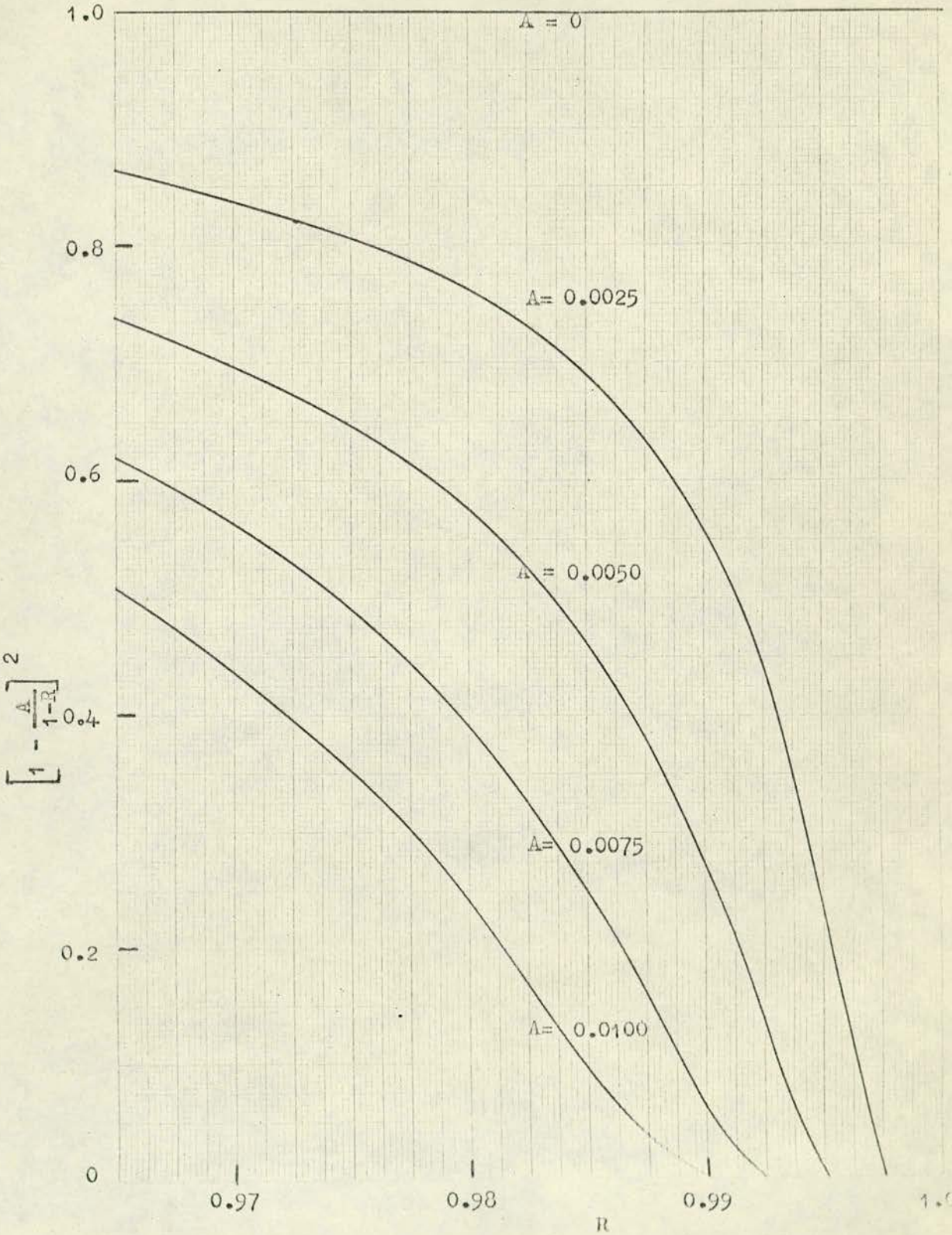

Fig. 4.3

Finesse as a function of reflectivity.

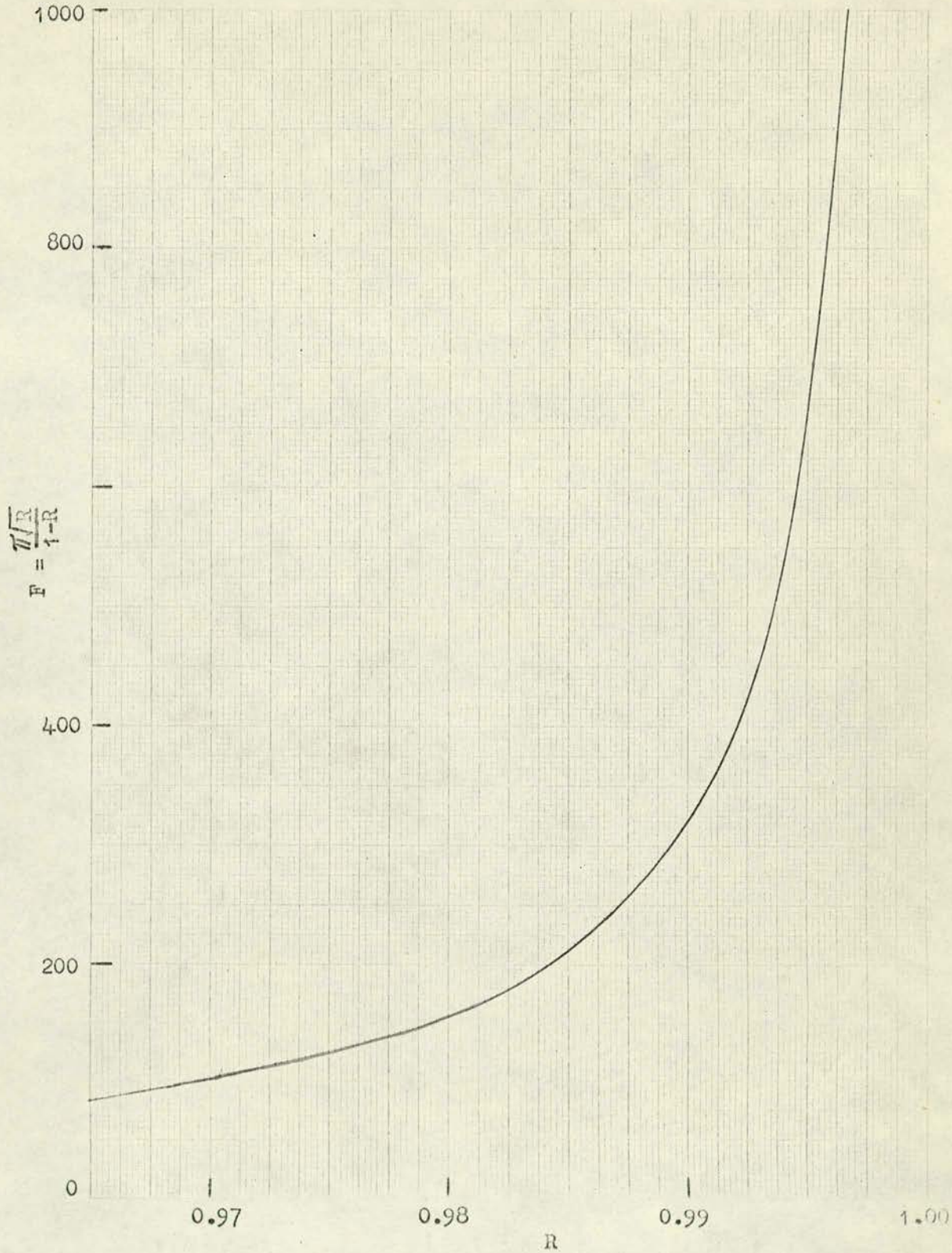

Fig. 4.4

$\frac{\tan^{-1}(x)}{x}$ v x

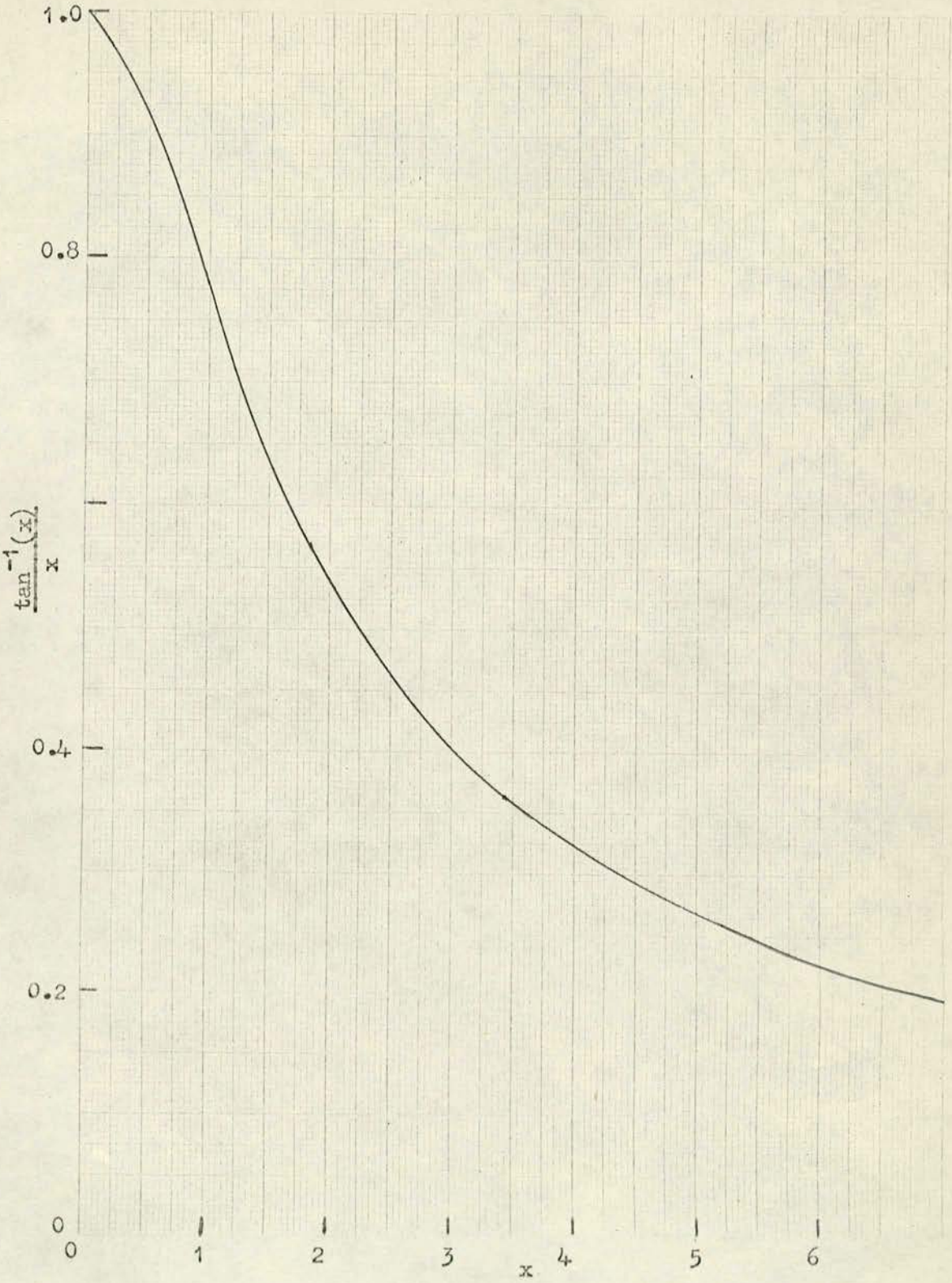

$$F = \frac{\pi\sqrt{R}}{1-R} \qquad (4.7)$$

The contrast, C, the ratio of maximum to minimum interferometer transmission, is

$$C = \left[\frac{2F}{\pi}\right]^2 \qquad (4.8)$$

In practice, the detector has a finite spectral width, $\Delta\omega_D$. Taking this into account, I have found that

(a) the maximum collected signal, S_{max} , is

$$S_{max} = A_p I_o \left[\frac{1-R-A}{1-R}\right]^2 \frac{\tan^{-1}\left[\frac{2F.\Delta\omega_D}{f}\right]}{\left[\frac{2F\Delta\omega_D}{f}\right]} \qquad (4.9)$$

where A_p is the geometrical area of the pinhole through which the collected light passes. Since it is fixed by $\Delta\omega_D$, A_p is not an independent variable.

(b) the contrast C' is, $C' = \left[\frac{2F}{\pi}\right]^2 \frac{\tan^{-1}\left[\frac{2F.\Delta\omega_D}{f}\right]}{\left[\frac{2F.\Delta\omega_D}{f}\right]}$ (4.10)

(c) the apparent finesse F' is given by

$$\frac{1}{F'} = \sqrt{\left[\frac{1}{F}\right]^2 + \left[\frac{\Delta\omega_D}{f}\right]^2} = \frac{1}{F}\sqrt{1 + \left[\frac{F.\Delta\omega_D}{f}\right]^2} \qquad (4.11)$$

where F' is defined as the ratio of observed peak width to free spectral range. The effect on the linewidth of the finite spectral integration has been assumed to be approximately described by equation (4.11).

The behaviour of the contrast, finesse and transmission can be judged from figures (4.2 , 4.3 , 4.4) which show

a) $\left[1-\frac{A}{1-R}\right]^2$ as a function of R for various values of A

b) F as a function of R

c) $\frac{\tan^{-1}x}{x}$ as a function of x .

In the case of zero spectral width for the detector, the good contrast required to observe weak signals in the presence of a strong Rayleigh peak is produced by using highly reflecting mirrors. This also gives good finesse. However as R tends to (1-A) the transmitted intensity can suffer markedly. The transmitted intensity, contrast and finesse all decrease when spectral integration by the detector is considered. Increasing F much beyond $(\frac{2\ \Delta\omega_D}{f})^{-1}$ leads to a sizeable loss of transmitted signal, but this is often the price one has to pay to get adequate contrast and finesse. It is of note that the contrast and finesse are independent of mirror absorption.

The value chosen for the reflectivity is necessarily a compromise both between the requirements of transmission, contrast and finesse, and the individual characteristics of the various spectra understudy.

In practice, the maximum transmission of the interferometer is reduced by destructive interference, between the multiply reflected beams, arising from deviations from plate flatness. At high reflectivities, any losses in addition to absorption may affect the peak transmission critically.

Three pairs of mirrors were used on the present interferometer. The first set had an excessively high reflectivity resulting in only 1% peak transmission. The second pair had lower reflectivity but also poor flatness - $\frac{\lambda}{10}$. These gave an increased transmission of 8% with a low finesse of 15. A third pair, which took almost six months to be delivered, were flat to $\frac{\lambda}{200}$ and each mirror had a transmission

of 1%. The total transmission of the interferometer rose to 35% and finesses of over 100 were observed. Taking 0.25% as an estimate of the losses in good multilayer dielectric mirrors, an ideal interferometer, whose mirrors each had 1% transmission, would have finesse, contrast and maximum transmission of 250, 3.10^4 and 64% respectively. The mirrors used are thus seen to give a reasonably efficient interferometer.

Another factor which reduces the observed finesse is the finite linewidth of the laser ~ 0.025 cm^{-1}. This places a lower limit on the free spectral range that can be effectively investigated. In nearly all cases, the observed finesse is due to the spectral width of the detector and laser linewidth rather than the fundamental interferometer finesse.

The optical flats used have aslight wedge angle of 10 minutes of arc so that the non-coated surfaces do not produce spurious interference patterns. However,as figure 4.5 shows, internal reflection in the exit flat produces a displaced ring system, identical to the main system but much weaker. Although the outside surfaces of the flats were given anti-reflection coatings, a ghost of some 0.1% of the intensity of the main system appears. The ghost of a strong feature in the spectrum can still therefore be comparable to a weak feature in the main system. Fortunately, this problem can largely be avoided because, since the source is a linear focussed laser beam and not an extended area, only a diametrical line across the centre of the ring system is illuminated. By arranging the wedge angle to shift the ghost above the main ring system, rather than displace it horizontally, the ghost ring system will not cross the pinhole as the interferometer is scanned.

Fig. 4.5

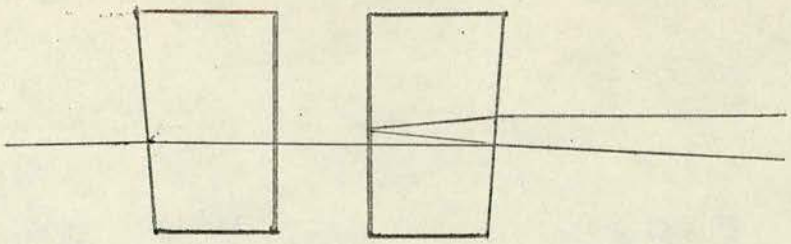

Formation of ghost ring system by mirror wedge angle.

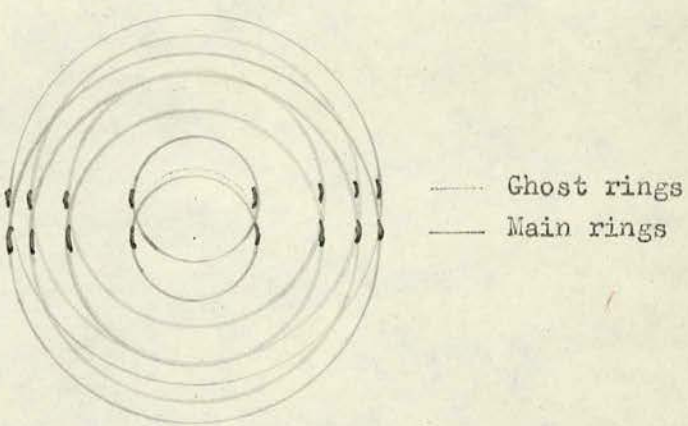

The displacement of the main and ghost ring systems by the mirror wedge angle. Those segments illuminated by a linear source are shown in heavy print.

Poorly polished crystal surfaces may produce spurious light over an extended area and thus give a ghost system of complete rings, part of which will cross the pinhole. Good sample preparation is the only cure for this.

The interferometer used is shown in figure 4.6. It is built on a chassis of 4 $\frac{1}{2}$" invar rods and $\frac{1}{2}$" steel end plates. The position of the end plates on the rods determines the mirror separation. Three micrometers provide rough adjustment for each of the mirror mounts, which are held in place by 12 high rate springs. Both the translation of the scanning mirror and the final alignment of the stationary mirror are produced by applying a voltage across a stack of piezoelectric discs. The stacks are made by gluing alternate layers of piezoelectric and non-piezoelectric materials.

A hollow stack of 8 discs, across each of which a voltage varying linearly in the range 0-140 volts is applied, gives a displacement of about 4000Å - a little greater than the $\frac{\lambda}{2}$ movement necessary for an order to order scan. The scanning voltage may be supplied from the sawtooth output on an oscilloscope, whose display is then synchronous with the scan, or, for slower scan rates of 10 minutes or more, a motor driven potentiometer with H T batteries as the voltage source. A further voltage of up to 120v may be applied to position the spectrum suitably on the scan.

Three stacks of two discs, a cross each of which a voltage in the range $-400 < V < 400$ volts can be applied from potentiometers, produce the fine adjustment necessary to align the mirrors for parallelism. These alignment stacks do not suffer from the slow relaxation found in any of the metal leaf springs used initially. The stability of

Fig. 4.6

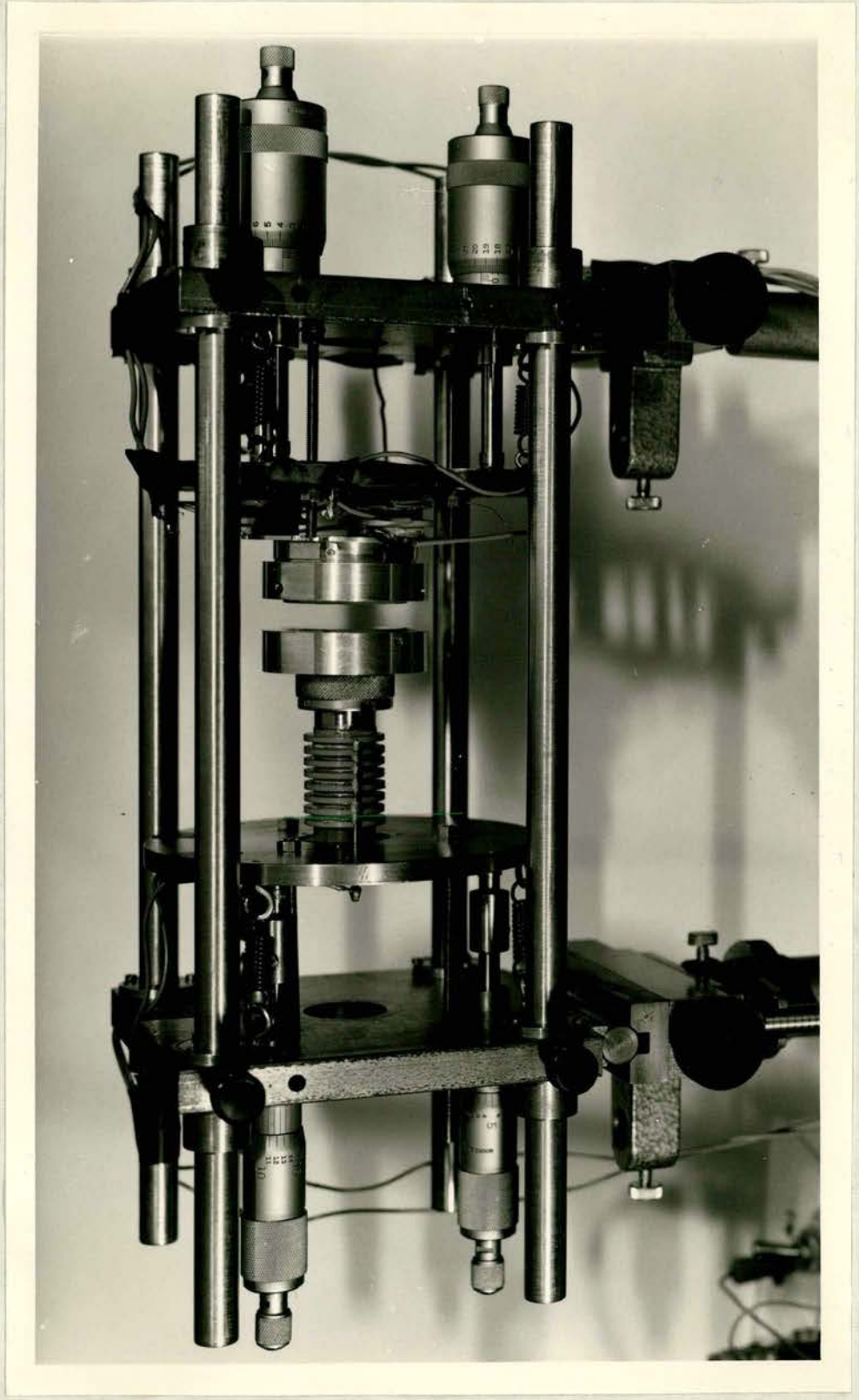

The Fabry-Perot Interferometer.

the instrument derives from its rigid construction and the use of many springs with the high initial rate of 50 lbs/inch. The optical flats are glued into their mounts to maintain rigidity.

Apart from design factors related to rigidity, the stability of the interferometer also depends on temperature fluctuations. Isobaric changes of the temperature of the air in the cavity, affect the optical path length between the mirrors. It is known (4.2) that for the refractive index of air

$$\mu(T) = 1 + \frac{\mu(0^{\circ}C) - 1}{1 + \alpha T} \frac{P}{760} \qquad (4.12)$$

where P = the constant pressure of the air

$\alpha = 3.7\ 10^{-3}$

$\mu(0^{\circ}C) - 1 = 2.9\ 10^{-4}$.

This leads to the result that the change of order of interference, Δn, is $3 10^{-2}/^{\circ}C$/cm. spacing. Temperature variations of the cavity gas are thus unlikely to be a serious problem at the small spacings used.

Larger fluctuations arise from the expansion of the components of the interferometer. The expansion of the long invar rods is opposite to the greater expansion in the micrometers. The net effect is for a change in the order of interference of $1.5/^{\circ}C$. Stable ambient temperatures are thus essential for the successful operation of the instrument. Monitoring the position of a Rayleigh peak over a period of several hours showed that the interferometer was largely stable against detuning and drifting.

It should be remembered that in a scanning Fabry-Perot any linear changes in optical path length due to temperature fluctuations etc, do not adversely

affect the performance of the instrument. Their effect is to alter the scan rate. Only quadratic and higher order fluctuations degrade the spectrum produced.

The interferometer has an aperture of $\frac{1}{2}$" and a maximum usable free spectral range of $\sim 80\ cm^{-1}$ corresponding to a plate separation of 7.10^{-3}cms.

THE TEMPERATURE CONTROL SYSTEM

It was necessary in the present experiment to establish crystal temperatures in the range $220^{o}K$ - $370^{o}K$. The system used is shown in figure (4.7). There are only slight differences in the systems used above and below room temperature. The individual components of the cryostat are described below.

THE CRYSTAL HOLDER

The crystal is mounted in a holder slung beneath a goniometer head which is attached to an adjustable stand. The crystal, having six degrees of freedom, can be oriented accurately relative to the incident beam and be positioned so that the scattering volume is free from occlusions. Elastic scattering from occlusions may be intense enough for the residual intensity far from the laser line to swamp a weak feature of the spectrum.

THE LIQUID BATH

The crystal is immersed in a rectangular glass trough of liquid which serves two purposes. Firstly, heating or cooling the liquid changes the crystal temperature as there is good thermal contact between the crystal and the liquid. Secondly, by choosing a liquid whose refractive index is close to that of the crystal, surface scattering is minimised. Surface scattering also can obscure weak spectral features and give rise to the ghost peaks mentioned earlier. Even when immersed in a liquid, the crystals still need to be well polished. A mixture of jewellers'

Fig. 4.7

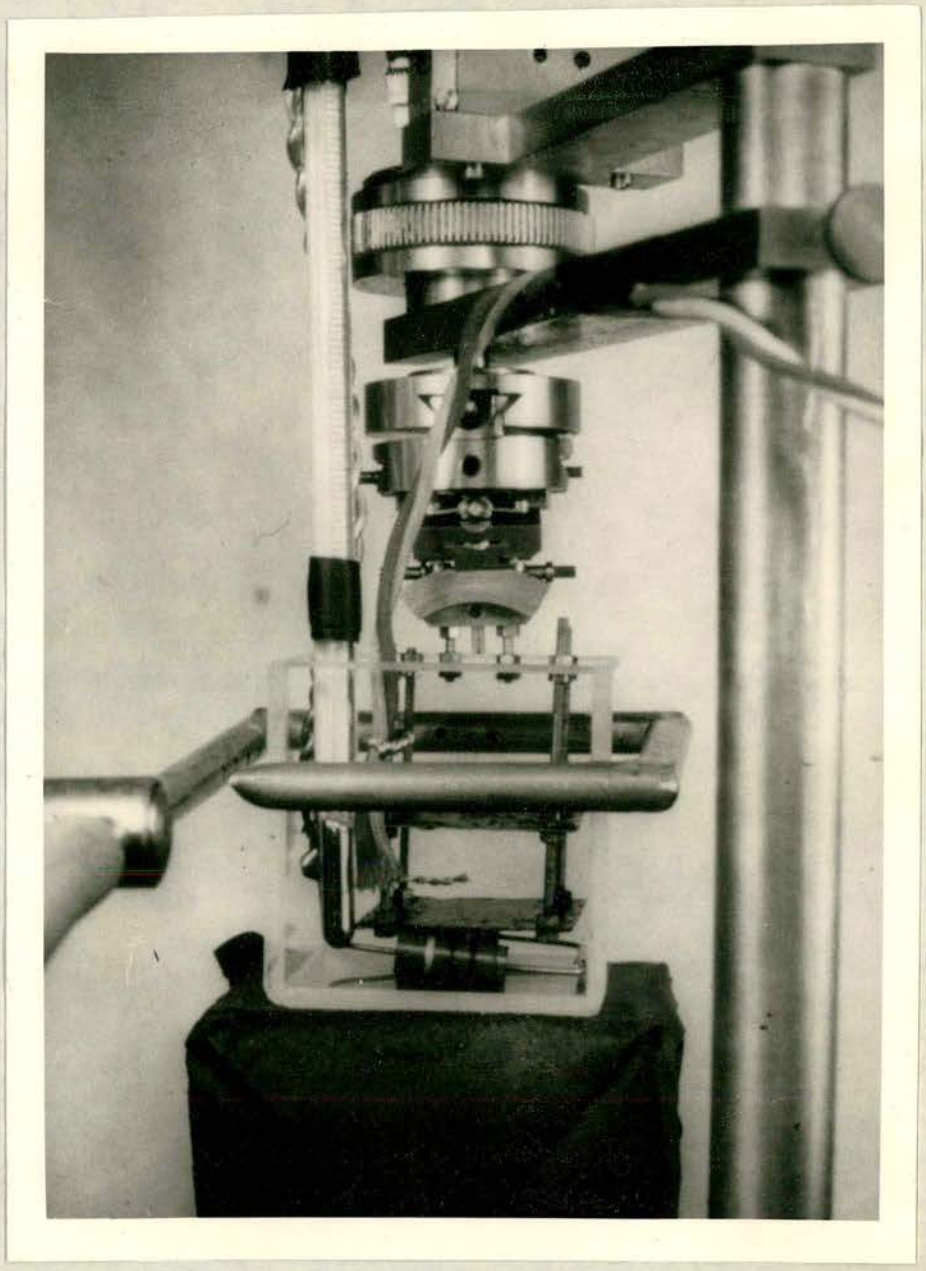

The Cryostat.

rouge and a light oil on a chamois leather over a glass flat was found suitable. The trough was painted matt black internally to absorb spurious light. Small 'windows' were left unpainted on each face for the passage of the beams and for viewing the crystal.

During heating, the crystal was immersed in one of Rayner's refractive index oils, which did not boil off when heated and matched the crystal well. The requirements for the liquid used for cooling are more stringent. It must be liquid and transparent down to 220°K, must not evaporate rapidly at room temperature and should match the refractive index of the crystal. The oils used for heating became opaque and very viscous below 270°K. Of the other liquids tested, chloroform was the most suitable. Its evaporation was minimal below about 270°K and the refractive index of ~1.48 provided a good match which improved on cooling. Care must be taken to avoid chloroform or oil that has absorbed water, as this easily damages the surface of the hydroscopic crystals used in this experiment.

TEMPERATURE MEASUREMENT

A chromel-alumel thermocouple, having its reference junction in an ice-water slurry, was used. Its emf is displayed on the chart recorder. There were, in addition, mercury and alcohol thermometers used while heating and cooling the crystal respectively.

The thermocouple's reading at the liquid nitrogen and steam points agreed with publish calibration curves (4.3). The alcohol thermometer was calibrated for total immersion. As only 5 cms of it were immersed, correction was made for the length of the alcohol column above the liquid surface. The mercury thermometer was calibrated for 3 inch immersion, so needed little correction.

HEATING THE CRYSTAL

The crystal was heated by passing current from a 'Variac' transformer through two 10 ohm carbon resistors placed in the oil at the foot of the trough. Convection ensures that the contents of the trough are eventually heated to the same temperature. Tests failed to detect any spatial variation in the temperature throughout a heated trough of liquid, indicating that any temperature variation must be less than 0.05degree. The presence of the crystal and its holder is unlikely to alter the uniform temperature distribution, provided time is allowed for the steady state to be reached. Heat loss from the trough is minimised by placing it on a block of expanded polystyrene and by having 2 narrow 10BA threaded rods as the only heat path to the goniometer.

COOLING THE CRYSTAL

The trough, chloroform and crystal are cooled by blowing cold nitrogen gas onto the outside of the trough. A piece of copper tube, $\frac{1}{4}$" in diameter, encircles the trough. Cold nitrogen boiled off from a 25 litre Dewar is directed at the top of the trough by a number of 1/16" holes in the copper tube. The temperature in the trough becomes uniform due to convection. Tests did not show any spatial temperature variation in the steady state. The temperature of the crystal depends on the rate of gas flow which is controlled by varying the current through resistors in the Dewar, by means of a Variac.

Condensation of water vapour on the sides of the trough, which would prove disasterous, is prevented by placing a perspex box around the trough, crystal holder etc. By flushing the box with a rapid flow of nitrogen before cooling, the box can be kept full of dry nitrogen by the gas

cooling the trough and by the exhaust from the cold nitrogen used to cool the photomultiplier tube. Initially the laser beam is visible in the box due to scattering from dust in the air. Once flushed with nitrogen, the beam is no longer visible. The box has small holes drilled in a pair of opposite faces for entrance and exit of the laser beam. Provided the box is taped to the bench to minimise nitrogen leakage, there is sufficient flow out of the laser beam ports to prevent the entry of water vapour. Since a much larger opening is required to allow the scattered light out of the box, a double window was made from two 2" square slide glasses with a polystyrene spacer. Even though there is condensation on the outside of thebox at depressed temperatures, the double window remains clear. With the exception of 'windows' through which the sample and thermometer may be viewed, the box is painted matt black internally.

Cooling crystals of the KDP family near their transition is difficult, since, due to the anomalously high values of the specific heat, a very vigorous flow of nitrogen is required. Furthermore, on passing through the transition, the specific heat rapidly falls, and, unless the gas flow is reduced, so does the temperature. This sudden change in temperature may crack the crystal.

The system outlined above has proved suitable for cooling crystals down to ~ 200^{o}K without condensation problems, provided care is taken to expel the water vapour and maintain a dry nitrogen atmosphere.

TEMPERATURE CONTROLLER

Apart from the Variac, there was no temperature controller. However, once a steady state had been reached no fluctuations could be detected in the temperature, indicating a stability of better than 0.05 of a degree.

The laboratory was heated by a thermostatically controlled convection heater, and, being situated in the basement of an old thick stone walled building, a steady ambient temperature was maintained. This no doubt had considerable effect on the stability of the cryostat.

COMMERCIAL CRYOSTAT

Originally, a commercial cryostat was purchased, but this instrument suffered from numerous faults. On several occasions leaks developed between vacuum and liquid nitrogen chambers, necessitating its return to the manufacturers for repair. The thermocouple, with junctions near a liquid nitrogen chamber and in the cold finger, gave a false reading possibly due to the thermocouple wires themselves conducting heat from the cold finger to nitrogen chamber. Since it was thought undesirable to glue the crystal to the cold finger, as stresses on cooling or going through the transition might crack the crystal, it was held against the cold finger by a spring. The thermal constact was not sufficient to allow a rate of cooling the crystal that would permit the required range of temperature to be covered in a day's experimenting. The rate of improvement on this instrument was so slow that the cryostat described above was built. The use of a liquid bath gave good thermal contact with the crystal and as a result restored faith in the accuracy of the temperature measurement. The marked reduction in elastic scattering, that resulted from index matching the liquid and crystal, made experiments possible at low frequencies.

THE PHOTOMULTIPLIER TUBE

The photomultiplier tube is an ITT FW130 with an S-20 photocathode. Pulses developed across the load resistor are amplified, standardised by a discriminator and fed into a rate meter whose output is displayed on a chart recorder. The amplifier and discriminator were manufactured by Nuclear Enterprises, the chart recorder by Smiths.

The main feature of this photomultiplier tube is the small effective area of the photocathode, $\sim \frac{1}{10}$ square inch. This gives a marked reduction in dark current compared to a similar tube with a full 2 inch window. Since the Fabry-Perot is used near normal incidence the illuminated area of the photocathode is less than the effective area, so that the reduction in dark current is not accompanied by a reduction in signal. The dark current of the tube used was about 200 counts/sec at room temperature, falling to ~1/count/sec on cooling. The low dark count rate is essential in the present experiment where signal count rates of less than 50 counts/sec are often encountered, with 150 counts/sec being average.

The tube is cooled by boiling off liquid nitrogen in a Dewer and passing the cold gas through a copper tube wound round the cylindrical brass housing of the photomultiplier tube. This not only reduces the dark current but also causes water vapour to condense on the inside of the housing, thus preventing misting of the photomultiplier window. The only opeining from the housing being the pinhole, through which the collected light passes, there is little flow of moist air towards the tube. Tests have shown no fall in signal over long periods of cooling, indicating an absence of misting. Experience has also shown that 1840v across the tube are sufficient to collect all the photo-electrons, as no gain in count rate occurs on increasing the voltage beyond this level. The quantum efficiency of the tube was measured to be 2%.

Originally an EMI 9558B tube was used with the voltage developed across the load resistor displayed directly on the chart recorder. While this successfully recorded Brillouin spectra from organic liquids like toluene, it was insufficiently sensitive where crystals were used, since the scattered intensity can be weaker by a factor of 10^3 or more.

Also, having a 2 inch diameter photocathode, this tube gave the high dark current of ~1000 counts/second even when cool. To improve the sensitivity and reduce the effect of dark current, a phase sensitive detection system was employed. However, the mechanical chopping of the beam necessary for phase sensitive detection, causes a 50% loss in intensity and the airborne vibration from the chopper adversely affects the stability of the interferometer. The present photon counting system overcomes these problems. Unfortunately, there was a five months delivery time for the FW130 photomultiplier.

CHOICE OF LENS FOCAL LENGTHS AND PINHOLE DIAMETER

The pinhole diameter and focal length of lens L_4 are intimately related since it is the angular, rather than linear, radius of the pinhole that determines the spectral width of the detector. The frequency width of the pinhole $-\Delta\omega_D$ - is

$$\Delta\omega_D = \frac{1}{2\lambda_L}\left[\frac{R_p}{F_4}\right]^2 \qquad (4.13)$$

where R_p = Radius of the pinhole

F_4 = Focal length of lens L_4 ; λ_L = Laser wavelength

The pinholes used most had diameters of 1.08mm and 0.66mm, giving, with a 20 cm lens, spectral widths of $\Delta\omega_D = 0.06\text{cm}^{-1}$ and $0.02\ \text{cm}^{-1}$ respectively. The smaller pinhole was used for $f \lesssim 2\text{cm}^{-1}$ to maintain reasonable observed finesse, although with decreased transmission. Both pinholes were small enough so that the ghost 'ring' system from a linear source did not cross the pinhole during a scan.

The choice of focal length for lens 3 depends on two factors. The length of the beam in the sample from which scattered light is collected, L, is given by

$$\frac{L}{2F_3} = \frac{R_p}{F_4} \qquad (4.14)$$

where F_3 is the focal length of lens L_3. Thus the effective length of beam is proportional to F_3. However, the solid angle subtended by the interferometer aperture, of radius R_a, at beam is $\pi \left[\frac{R_a}{F_3}\right]^2$. Combining these two effects shows that maximum collected intensity occurs for a minimum value of F_3. Physical factors limit F_3 to 10cms in the present experiment. Thus light is collected from a length of beam equal to the pinhole radius. It is thus possible to isolate a part of the crystal having good optical quality, for the scattering measurements.

Since the frequency of light scattered by optic phonons is, to a first approximation, independent of θ, the scattering angle, the relatively large collection solid angle of the short focal length lens used, does not appreciably degrade resolution. In the case of acoustic modes whose scattered frequency depends on $\sin \frac{\theta}{2}$, and, especially Rayleigh linewidths having a $\sin^2\left[\frac{\theta}{2}\right]$ dependence, broadening by collection solid angle must be accounted for.

The region of focus of a laser beam can be considered approximately as a cylinder of diameter $\lambda(\frac{F1}{a})$ and length $3\lambda(\frac{F1}{a})^2$, (4.3), where a is the laser beam diameter and F_1 the focal length of the lens. For F_1 = 20cms, a = 0.2cm $\lambda = 6.10^{-5}$cm, the cylinder has diameter 6.10^{-3}cms and length 1.8cms. Since the image of the pinhole at the scattering region is a circle of diameter R_p, the focussed beam gives a line source of

scattered light. Very short focal length lenses indeed would have to be used before the focussed beam was wider than the image of the pinhole, with the resultant loss in collected intensity.

The focal length of lens L_2, if used, can have any value but is chosen as small as practicable to produce a compact system.

OPTICAL ALIGNMENT

Due to the small size of the scattering volume, it is important that the various components are positioned correctly on their respective optic axes.

Mirror M_1 positions the incident beam parallel to both the surface and end of the bench. The scattering angle of 90° is established, with an accuracy better than 0.1°, by means of auto-collination of this incident beam by a right angle prism placed in the crystal holder. The lenses L_3 and L_4, the interferometer, pinhole and photomultiplier tube, which can all be adjusted both horizontally and vertically, are centred on the beam transmitted by the prism. The interferometer is further aligned with its front mirror normal to this beam. Due to the wedge angle on the interferometer flats, this optic axis is not a continuous straight line. This must be taken into account when positioning the components that follow the interferometer. Finally, lens L_1 is centred on the incident beam.

On replacing the prism by a sample, slight adjustments to the positions of lenses L_1 and L_3 may be needed to compensate for the change in focal length due to the refractive index of the crystal. By viewing the beam in the crystal and its image formed by the interferometer mirror, a parallex method can be used to check that the incident beam is at the focus of lens L_3. Illuminating the pinhole should then produce a sharp image, central in the interferometer aperture, at the same height as the incident beam.

Alignment of the interferometer mirrors for parallelism is best performed with a screen illuminated with laser light to form an extended source. Using the micrometers, the exit mirror is adjusted to produce a good ring system. By rapidly scanning the interferometer and displaying the photomultiplier output on an oscilloscope, the fine piezoelectric adjustments can be used to optimize the two observed peaks which correspond to adjacent orders of interference. The fine tuning of the interferometer is checked by this method before each slow scan when data is being collected.

Rapid scanning with an extended source enables the pinhole to be positioned in the centre of the ring system. Correct pinhole alignment is of the utmost importance.

As the adjustment of one component, necessarily effects those that follow, the overall optical alignment is an iterative process.

LINEARITY OF MIRROR SCAN

The recorded spectra show transmitted intensity as a function of time. Tests have revealed that the dependence of transmitted wavelength on time is not strictly linear, even when the scanning voltage varies linearly with time.

As might be expected, when scanning the interferometer rapidly by the oscilloscope sawtooth, there are non-linearities due to the rapid flyback. However, non-linearities still exist on slow scans in which the mirror starts from rest. These non-linearities were investigated by running Brillouin spectra with the interferometer spacing set to give a frequency shift of typically 7% of the free spectral range. This shift is small enough to show variations in dispersion while being large enough for these variations to be measured. By altering the bias voltage on the stack, the spectrum can be positioned anywhere on the scan, and the variation in dispersion of the interferometer can thus be monitored. These tests show that the variation

in the observed shift of an acoustic mode from the laser frequency, depends only on the position of that shift from the beginning of the trace, ie. the scanning voltage, and not on the bias voltage, nor the scan rate, nor the free spectral range.

As a result of very many measurements, a calibration curve was drawn showing the correction that need be applied at any point on the trace to account for non linearities in the frequency scale.

It is thus possible to obtain scattered intensity as a function of transmitted wavelength.

DETERMINATION OF MIRROR SEPARATION

In order that frequency shifts analysed by the interferometer may be known absolutely in terms of cm^{-1} or Hz and not just as a fraction of the free spectral range as they are initially measured, the mirror separation, which determines the free spectral range, must be known.

For free spectral ranges greater than $\sim 2cm^{-1}$, a rough estimate of the plate separation can be obtained from direct measurement of the diameters of the first three rings produced by passing the laser beam through the interferometer. This value of the free spectral range is used to determine the relative orders of interference of the sodium D lines, whose known separation of 17.19 cm^{-1} is used to determine the free spectral range accurately.

The frequency shift of a spectral feature determined by the above method can often be used to calibrate free spectral ranges less than $\sim 2cm^{-1}$ where the width of the sodium D lines, and uncertainty in order, would seriously affect the accuracy of the measurement.

The mirror separation can also be determined by running a known spectrum under the same conditions, eg temperature, as the original measurement.

It is also possible to determine the free spectral range by photographing the ring system produced by an extended source of laser light and measuring the ring diameters. This method is inapplicable at large free spectral ranges where only one or two rings are visible. The width of the developed film must be checked against an unexposed portion in case there has been shrinkage during processing. The main disadvantage of this method is the time taken to determine a mirror spacing.

The mirror spacing can be measured and maintained with an accuracy of $\sim \frac{1}{2}\%$.

THE GRATING SPECTROMETER SYSTEM

This apparatus was available for light scattering experiments. In principle, the experimental arrangement was similar to the Fabry-Perot system described above, but with the interferometer replaced by a spectrometer. The spectrometer was a Spex 1401 double grating instrument. The light source was a Laser Associates Argon Ion laser. This latter instrument proved extremely unreliable in spite of several overhauls by the manufacturer. There were long periods when it did not lase satisfactorily. In use, it often delivered a mere 5mW at 4880Å, only a few percent of its specified output. 50% changes in power output while recording in spectrum were not uncommon. Due to the short amount of time available on this apparatus and the low power output when it did work, it was of only limited usefulness in the present experiment. A good grating spectrometer system would have

been invaluable.

Some results were obtained on the spectrometer, however, using the helium-neon laser as a source.

Note. Over the limited range of frequencies studied in this experiment the photocathode sensitivity, spectral slit width and mirror reflectivity show negligible ($< 1\%$) variation.

CHAPTER FIVE

INTRODUCTION

The experiment was an investigation of the temperature dependence of the spectral distribution of the light scattered by the lowest frequency zone centre modes of B_2 and E symmetry in DKDP and DADP.

It is useful to summarise the reasons behind performing these experiments.

(1) A neutron scattering experiment on DKDP (3·98) had shown the presence of a quasi-elastic feature whose width was much less than the 4 cm^{-1} resolution function of the spectrometer. In order to agree with the high C-axis dielectric constant in DKDP, Barker and Tinkham (3·95) postulated the presence of a mode at frequencies lower than they could study in their infra-red reflectivity experiment. The results of a microwave dielectric experiment (3·103), which measured $\epsilon''_c(\omega)$ for $0{\cdot}001 \leq \omega \leq 1$ cm^{-1}, predict a quasi-elastic B_2 mode in DKDP of half width 0·007 (T-Tc) cm^{-1}.

Light scattering experiments are able to probe, with sufficient resolution, that frequency region which the above methods could not, and thus study that feature whose presence they have indicated.

(2) A Raman experiment on KDP (3·73) had revealed a soft, highly overdamped B_2 mode. Tunnelling theories of the transition in crystals of the KDP class predict a reduction in the frequency of this mode on deuteration. The corresponding Raman experiment on DKDP would provide direct evidence on this point.

(3) As the a-axis dielectric constant in DKDP is also relatively high, but having little temperature dependence, it is of interest to ask whether there is a corresponding low frequency polar mode of E symmetry, and if it too is of tunnelling origin.

(4) Although DADP undergoes an antiferroelectric transition, it also has high a and c-axis dielectric constants which increase as the temperature is decreased. By performing a similar experiment to that on DKDP, the behaviour of possible soft modes related to thwarted a and c-axis instabilities could be studied.

THE SCATTERED INTENSITY AND EXPERIMENTAL GEOMETRY

From equations (2·49) and (2·56), the first order scattered intensity is seen to be given by

$$S'(\underline{K},\omega) = \left(\frac{\omega_0}{C}\right)^4 \left(\frac{2\pi}{R}\right)^2 \frac{2\hbar}{V} \left[\sum_{\underline{i}\neq\underline{i}_s} \frac{1}{4\pi} \left\{ \sum_{\mu\nu j} \epsilon_\mu \, \epsilon_\nu \int_{\mu\nu j} \underline{E}_o \right\} \hat{\underline{i}} \right]^2$$

$$n(\omega)\, \chi''(\omega) \qquad (5\cdot1)$$

As has been remarked, the scattered intensity depends on the eighth power of the refractive index through the $\left[\epsilon_\mu \, \epsilon_\nu\right]^2$ terms in equation (5·1). The refractive indices for both o and e rays for various crystals of the KDP class have been determined over a wide range of temperature by Phillips (5.1). He finds that they depend very weakly on temperature and that there is no anomalous behaviour near the transition. A typical value for the fractional change in scattered intensity per unit degree change in temperature is $1{\cdot}3\ 10^{-4}$. Thus, over the temperature range $220 \leqslant T \leqslant 370^{\circ}K$ used in this experiment, a 2% change in intensity, due to the temperature dependence of the

refractive indices, can be expected. This can be neglected in comparison with the intensity variation due to the soft nature of the B_2 mode in DKDP. It is also less than the noise fluctuations on the signals generally detected in these experiments.

The components of the electro-optic tensor, $\int_{\mu\nu i}$, do not exhibit an anomaly at the transition. Little is known of any weak temperature dependence they may have. $\int_{123}$ for KDP is said (5·2) to have no marked temperature dependence. Some data for $\int_{123}$ in ADP is available (5·3) and is shown in figure 5·1. Although both experiments show an increase in $\int_{123}$ on decreasing the temperature, they are not in good agreement. No data could be found for DKDP or DADP.

Nye (2·20) gives the two non-zero components of the electro-optic tensor in KDP crystals as

$$\int_{321} = \int_{231} = \int_{132} = \int_{312}$$

$$\text{and } \int_{123} = \int_{213} \qquad (5\cdot2)$$

$$\text{where } \int_{\mu\nu i} \propto \frac{\partial \varepsilon_{\mu\nu}}{\partial P_i}$$

Thus c-axis (i = 3) polarization fluctuations are studied by observing their effect on ε_{xy} - the suffices are interchangeable - while for the degenerate a or b axis fluctuations ε_{xz}, ε_{yz} are appropriate. Hence, by equation 2·31, arranging the experimental geometry so that the polarizations of the incident and scattered beams are parallel to the a and b axes, allow only the B_2 modes, which include the c-axis fluctuations, to be studied. If the beam polarizations are parallel to the c and a or b axes the E modes are similarly isolated in the spectrum. Since in DKDP the spontaneous polarization appears along the former tetragonal c-axis, the soft mode will be one of the B_2 modes.

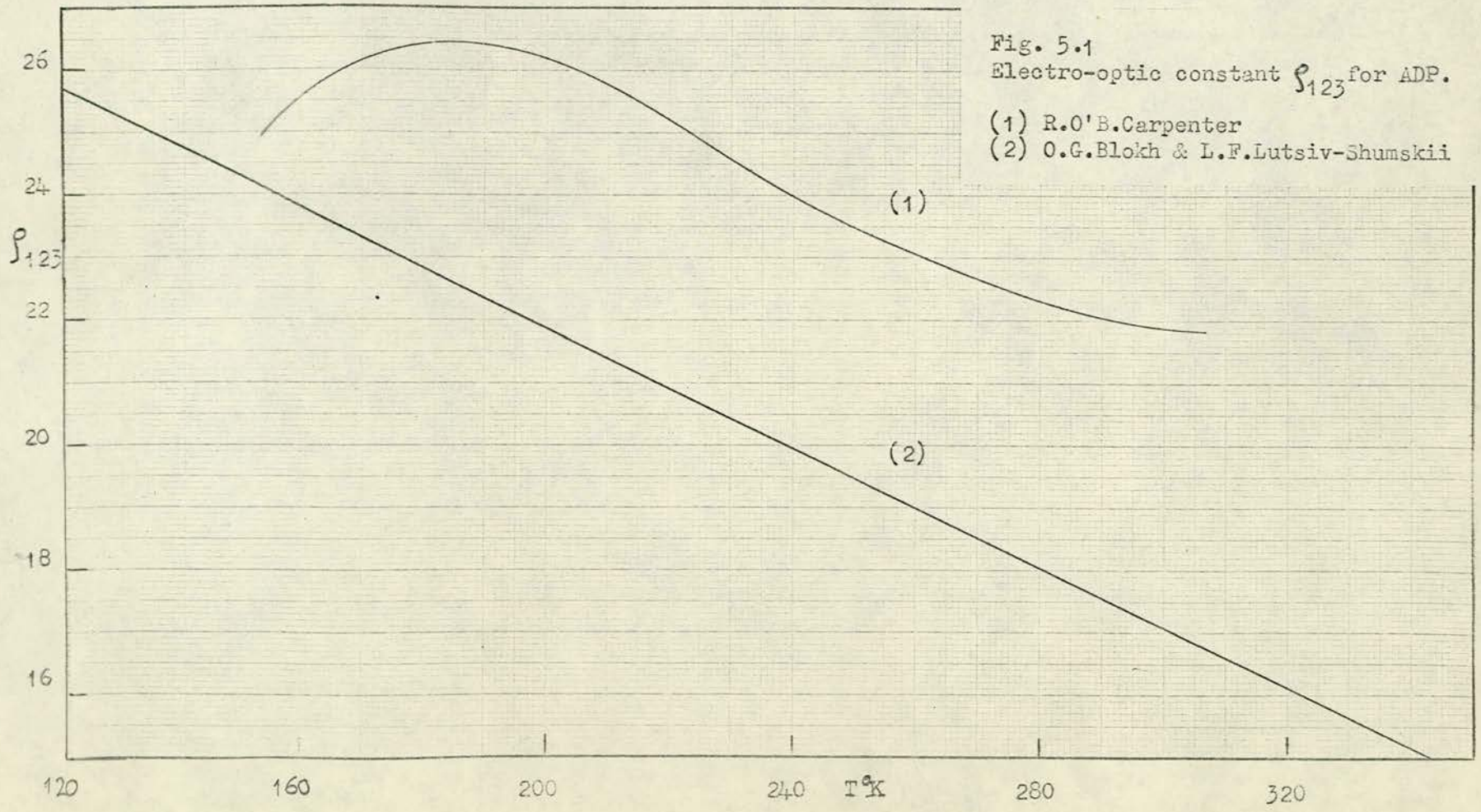

Fig. 5.1
Electro-optic constant ρ_{123} for ADP.

(1) R.O'B.Carpenter
(2) O.G.Blokh & L.F.Lutsiv-Shumskii

With the experimental geometries defined above, the essential temperature and frequency behaviour of the scattered intensity is contained in

$$I(\omega) = n(\omega)\,\chi''(\omega) \qquad (5\cdot3)$$

where the units of $I(\omega)$ are arbitary. The electro-optic constant may contribute some additional temperature dependence.

DATA REDUCTION

This is essentially the problem of obtaining $\frac{\chi''(\omega)}{\omega}$ from the recorded spectra and then finding a model which describes its behaviour. This will be considered first for the results obtained from the grating spectrometer and then for the interferometer.

GRATING SPECTROMETER RESULTS

A typical spectrum is shown in figure (5·8). All the spectra obtained for each of the four modes, appear as a wing on the Rayleigh peak. Stokes and anti-Stokes spectra were obtained over a wide range of temperatures, sometimes at the same temperature on heating and cooling. The spectrometer and chart recorder speeds, the chart recorder and ratemeter sensitivities, the ratemeter time constant and the spectrometer slit width were all set to give a compromise between signal to noise ratio, resolution and the experimental time required to record a set of spectra.

The scattered light frequency is measured from the peak due to elastic scattering. This is recorded during a spectral run by reducing the ratemeter gain and/or inserting a neutral density filter. From each value of the observed intensity, $I_{obs}(\omega)$, measured, a normalised intensity, $I_N(\omega)$, is calculated, where

$$I_N(\omega) = \left[\frac{\exp\left(\frac{hc}{k_B}\frac{\omega}{T}\right) - 1}{\frac{hc}{k_B}\frac{\omega}{T}} \right] I_{obs}(\omega) \qquad (5\cdot4)$$

$$= \frac{k_B}{hc} T \frac{\chi''(\omega)}{\omega} \qquad (5\cdot5)$$

The term in the square brackets is not greatly different from unity for the frequency and temperature ranges studied, but it does remove the Stokes/anti-Stokes assymmetry. This allows $I_N(\omega)$ and $I_N(-\omega)$ to be directly averaged so that small errors in determining the frequency origin and small laser power fluctuations cancel out.

The direct calculation of $\chi''(\omega)$, which is approximately proportional to $\omega.I_{obs}(\omega)$, is best avoided since it gives prominance to the high frequency points whose intensity measurement is the least accurate. This arises firstly since the intensity of the wing in lowest at high frequencies, and secondly because, apart from the wing, the spectrum includes a small contribution from higher order processes which is proportionately greater at lower wing intensities. Those who calculate $\chi''(\omega)$ directly from the recorded spectra usually fail to account for this background contribution.

The results of many spectra for all four modes, showed that for all or much of the wing beyond the Rayleigh peak, a log-log plot of $I_N(\omega) = D\omega^n$ had a best fit for $n \approx -2$. A damped harmonic oscillator has $I_N(\omega) \propto \omega^{-4}$ at high ω, while $I_N(\omega) \propto \omega^{-2}$ for a Debye relaxation function.

By plotting a linear graph of $I_N(\omega) = B + \frac{C}{\omega^2}$, where B and C are constants, a straight line fit is found for the high frequency points at least, verifying the frequency dependence suggested by the earlier log-log graph. The constant $B = I_N(\infty)$ gives the contribution to the

total intensity due to multiphonon scattering and stray light. The higher order scattering is assumed frequency independent in the range of interest. Subtraction of the background contribution, B, leaves the spectral distribution due to the wing alone.

A Debye Relaxation function, having

$$\chi''(\omega) = \frac{A\,\omega\tau}{1 + (\omega\tau)^2} \qquad (5\cdot6)$$

has been found a good fit to the spectra obtained where there is a deviation from $I_N(\omega) \propto \frac{1}{\omega^2}$ at lower frequencies. A non-linear least squares program (5·4) was used to fit either

$$I_N(\omega) = \frac{A\ \tau}{1 + (\omega\,\tau)^2} \qquad (5\cdot7)$$

to the wing intensity alone, or more usually

$$I_N(\omega) = \frac{A\ \tau}{1 + (\omega\ \tau)^2} + B \qquad (5\cdot8)$$

to the total normalised intensity. τ is the relaxation time while A, in arbitary units includes the static susceptibility $\chi(o) \propto \frac{1}{T-Tc}$ and the $\frac{k_B}{hc}$ T term of equation (5·5). Thus A $\propto \frac{T}{T-Tc}$ and is frequency independent. A also includes $\rho^2_{\mu\nu j}$ which, as has been remarked, may have some temperature dependence.

Some experiments involved a temperature, rather than frequency, scan, to obtain I_{obs} (T) at a fixed point on the wing.

FABRY PEROT INTERFEROMETER RESULTS

INTRODUCTION

A typical spectrum is shown in figure (5·10). The spectrum of light scattered by a crystal can be divided into five groups of features. These are:-

(1) The 'Rayleigh' peak due to elastic scattering from surface and bulk imperfections. This can be minimised by good sample preparation and by index matching, but is still the most intense feature of nearly all the spectra. The observed width is almost totally instrumental.

(2) Brillouin scattering. In KDP-type crystals, for the orientations of most interest, the longitudinal acoustic modes appear at $\sim 0{\cdot}5\ cm^{-1}$, while the transverse modes are not selected. Their observed width is largely instrumental. At large free spectral ranges the Rayleigh and Brillouin peaks may not be resolved.

(3) The soft optic mode which appears a wing centred on the Rayleigh line. For some of the modes studied there is some intensity out to $\sim 100\ cm^{-1}$.

(4) Raman scattering from the remaining optic modes observed in that orientation. These peaks occur in the interval $100 \leqslant \omega \leqslant 3000\ cm^{-1}$ with widths in the range between a few and several hundred cm^{-1}.

(5) Higher order Raman scattering from multiphonon processes. This gives a broad featureless background to the first order scattering.

These features combine to form the entire spectrum scattered by the sample - $S(\omega)$. The recorded spectrum, $I(\omega)$, results from the simultaneous transmission of all the orders of interference, n, of the Fabry-Perot interferometer. Thus

$$I(\omega) = \sum_{n=-\infty}^{\infty} S(\omega + n_{\cdot} f) \qquad (5\cdot9)$$

Neglecting the slight asymmetry introduced by $n(\omega)$, unique values of $I(\omega)$ occur only for $0 \leqslant \omega \leqslant \frac{f}{2}$ cm^{-1}, since $S(\omega)$ is symmetrical about the origin.

The problem is thus to extract the spectral distribution of the soft mode wing from the total spectrum, which has been folded over on itself at intervals of the free spectral range. This overlapping of the spectrum, inherent in the use of a Fabry-Perot interferometer, is not generally a problem since the entire feature of interest is usually confined to a spectral region less than the free spectral range necessary to observe it. This is the case when Rayleigh linewidths or acoustic mode frequencies are being measured. It is also true for acoustic mode widths even though the mode and Rayleigh peak are of different orders. The overdamped modes which are observed in this experiment often have a region of interest - this usually means temperature dependence - which is very much less than the overall extent of the wing. Since the free spectral range is set to match this region of interest, the wing is itself overlapped by the interferometer. It is therefore not clearly distinguished from the background due to other Raman processes, as an acoustic mode would be, but does itself contribute to that background.

EXPERIMENTAL DETAILS

Spectra were obtained for a number of different temperatures at the same free spectral range. As the spectral region of the wing having most temperature dependence was itself temperature dependent - especially for the B_2 mode in DKDP - a number of free spectral ranges were used. Two runs were obtained at each temperature while heating or cooling, as the case may be, and, often, again while returning to room temperature.

The scan rate used was a compromise between the need for good signal to noise ratio, maintenance of the interferometer stability and the time required to obtain a series of spectra at the same free spectral range. 10 minutes was the usual scan time. The pinhole diameter diameter was chosen to give a balance between intensity and resolution. The ratemeter time constant was selected to provide some smoothing to the signal without appreciable spectral distortion. The values chosen were typically less than 0·5% of the scan time. The ratemeter sensitivity sometimes had to be changed to follow the temperature dependence of the intensity. The relations between ranges of the ratemeter were previously checked.

GRAPHICAL ANALYSIS

Using the frequency calibration curve in the form of a piece of transparent graph paper ruled off in equal, but arbitary, frequency intervals, the intensity is measured at some 50 points on each spectrum. The free spectral range was found in terms of the separation of the Rayleigh peaks on this same scale. [Figure 5·2].

These intensities, for all spectra obtained under the same conditions, are plotted on a single graph in the range 0 to f/2 cm^{-1}. (Figure 53). Since the contributions to the signal detected at a given point in the scan came alternatively from the Stokes and anti-Stokes spectrum, there is a much smaller Stokes/anti-Stokes asymmetry than was the case for the grating spectrometer. The best fit to the graph of figure 5·3 averages this asymmetry and thus gives the overlapped normalised intensity, $I_N(\omega)$. In order to extract that part of the total intensity due to the wing, use was made of the result of the spectrometer experiments that at high frequencies the intensity had a $\frac{1}{\omega^2}$ frequency dependence. It can be shown that the output from a Fabry-Perot interferometer, for a wing having $I(\omega) \propto \frac{1}{\omega^2}$ for all ω, is independent of the free spectral range used, apart from a constant of proportionality. Such an imaginary spectrum is denoted by $I(\omega) \propto \sum \frac{1}{2}$, where $\sum$ indicates the overlap. By plotting $I_N(\omega)$ against $\sum_{\omega}^{\infty} \frac{1}{\omega^2}$ in the range $0 \leqslant \omega \leqslant \frac{f}{2}$, a straight line portion is found if the onset of the $\frac{1}{\omega^2}$ behaviour occurs for ω much less than $\frac{f}{2}$. [Figure 5·4] That is, the straight line represents

$$I_N(\omega) = A \sum \frac{1}{\omega^2} + B \qquad (5\cdot10)$$

where A and B are constants. Since most Raman lines apart from the wing are broader than many of the free spectral ranges used, overlapping of these modes and the multiphonon components is assumed to give a flat contribution to the Fabry-Perot spectrum. The smooth shape of spectra recorded at high temperatures where the wing is weakest supports this assumption. The constant B, of equation (5·10), represents this background. Subtraction of B from $I_N(\omega)$ for all ω up to $\frac{f}{2}$ gives the spectrum due to an overlapped wing only.

Fig. 5.2

Raw data with schematic example of measuring grid.

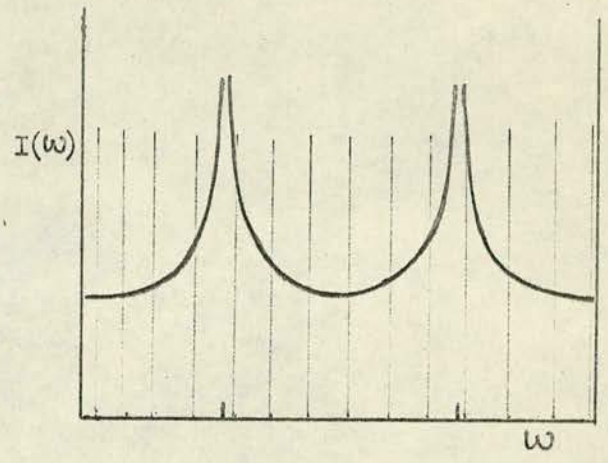

Fig. 5.3

$I_N(\omega)$ with overlap, from Stokes and anti-Stokes spectra of all similar runs.

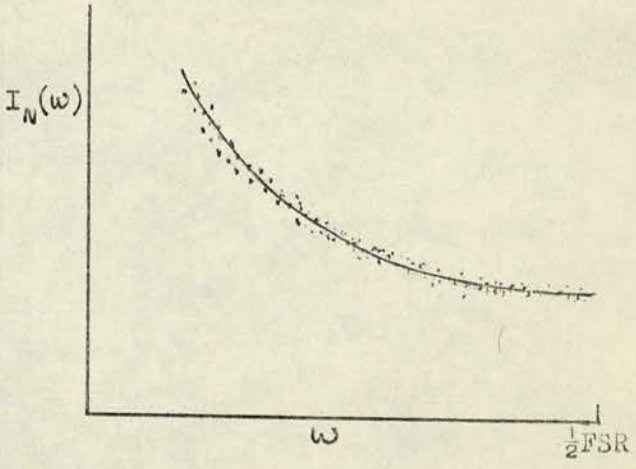

Fig. 5.4

Determination of background contribution from straight line portion, whose equation is:-

$$I_N(\omega) = A \sum \frac{1}{\omega^2} + B$$

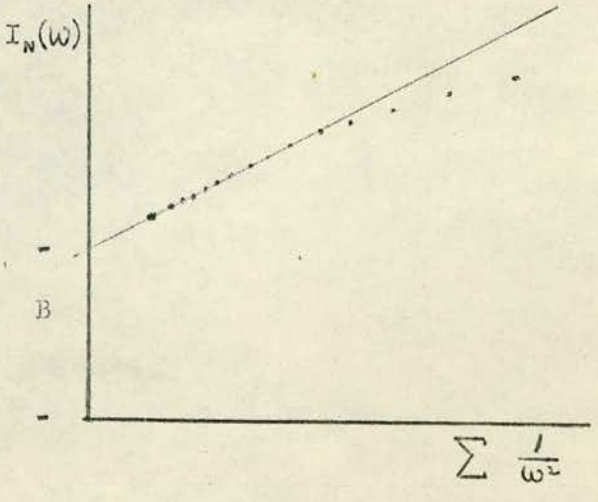

Since the presence of the straight line portion of figure (5·4) indicated that the $\frac{1}{\omega^2}$ dependence extended from some frequency less than $\frac{f}{2}$, that contribution to the spectrum arising from the overlapping of an $I(\omega) \propto \frac{1}{\omega^2}$ wing for $\frac{f}{2} \leqslant \omega \leqslant \infty$ can be found by using the constant of proportionality, A, in equation (5·10). Thus, by further subtraction, the wing intensity for $\omega < \frac{f}{2}$ could be obtained without any overlap or background contribution.

By repeating this process for many free spectral ranges and a wide range of temperatures it was hoped to obtain $I(\omega,T)$ for all the runs together. Only at this stage was fitting of the data to a particular model envis aged. Although a single Debye relaxation time had proved adequate for the limited amount of spectrometer data, this would not necessarily be the best fit at the lower frequencies investigated by the interferometer. It was felt that by considering the spectra en masse rather than singly, that the best fit could be found.

The graphical method of overlap removal described above is subject, however, to uncertainties and limitations. It requires that a portion of the wing for $\omega < \frac{f}{2}$ has a $\frac{1}{\omega^2}$ dependence. Since this part of the spectrum has least curvature, there may be appreciable uncertainty regarding which points in figure (5·4) contribute to the straight line portion and what is the best line through them. If the $\frac{1}{\omega^2}$ behaviour is extensive enough to give a confident straight line fit, there are only a few points between the end of the Rayleigh-Brillouin peak and the beginning of the $\frac{1}{\omega^2}$ portion. It is these points which are most important in distinguishing between the models. The uncertainties involved in making the subtractions necessary to obtain the wing without overlap are necessarily cumulative and render the

Fig. 5.5

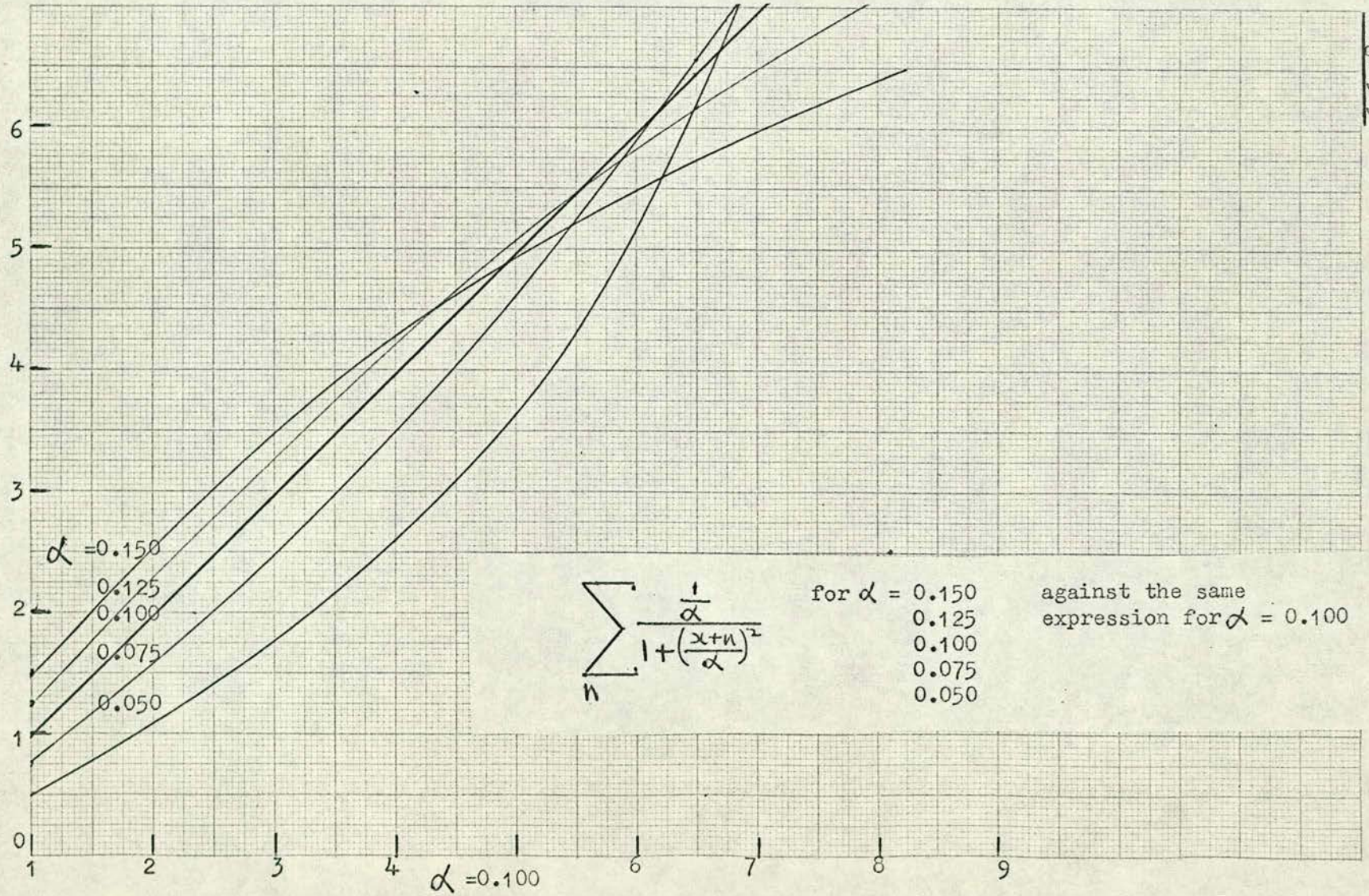
6
5
4
3
2
1
0
α =0.150
0.125
0.100
0.075
0.050
1
2
3
4
α =0.100
6
7
8
9
$\sum_{n} \frac{\frac{1}{\alpha}}{1+\left(\frac{x+n}{\alpha}\right)^2}$
for α = 0.150
0.125
0.100
0.075
0.050
against the same expression for α = 0.100

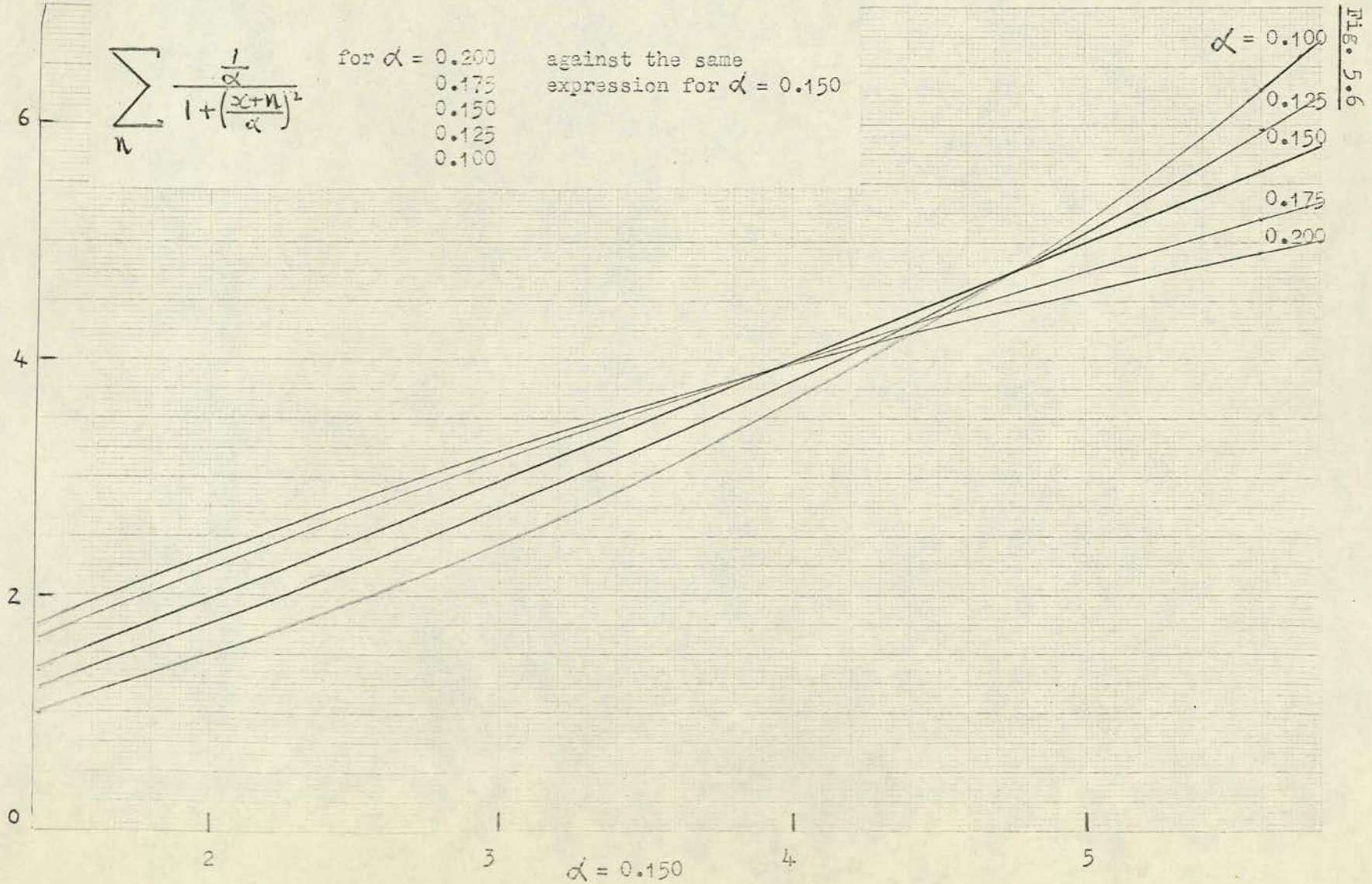
$\sum_n \frac{\frac{1}{\alpha}}{1+\left(\frac{x+n}{\alpha}\right)^2}$
for α = 0.200
0.175
0.150
0.125
0.100
against the same expression for α = 0.150
α = 0.100
0.125
0.150
0.175
0.200
0
2
4
6
2
3
4
5
α = 0.150

Fig. 5.6

Fig. 5.7

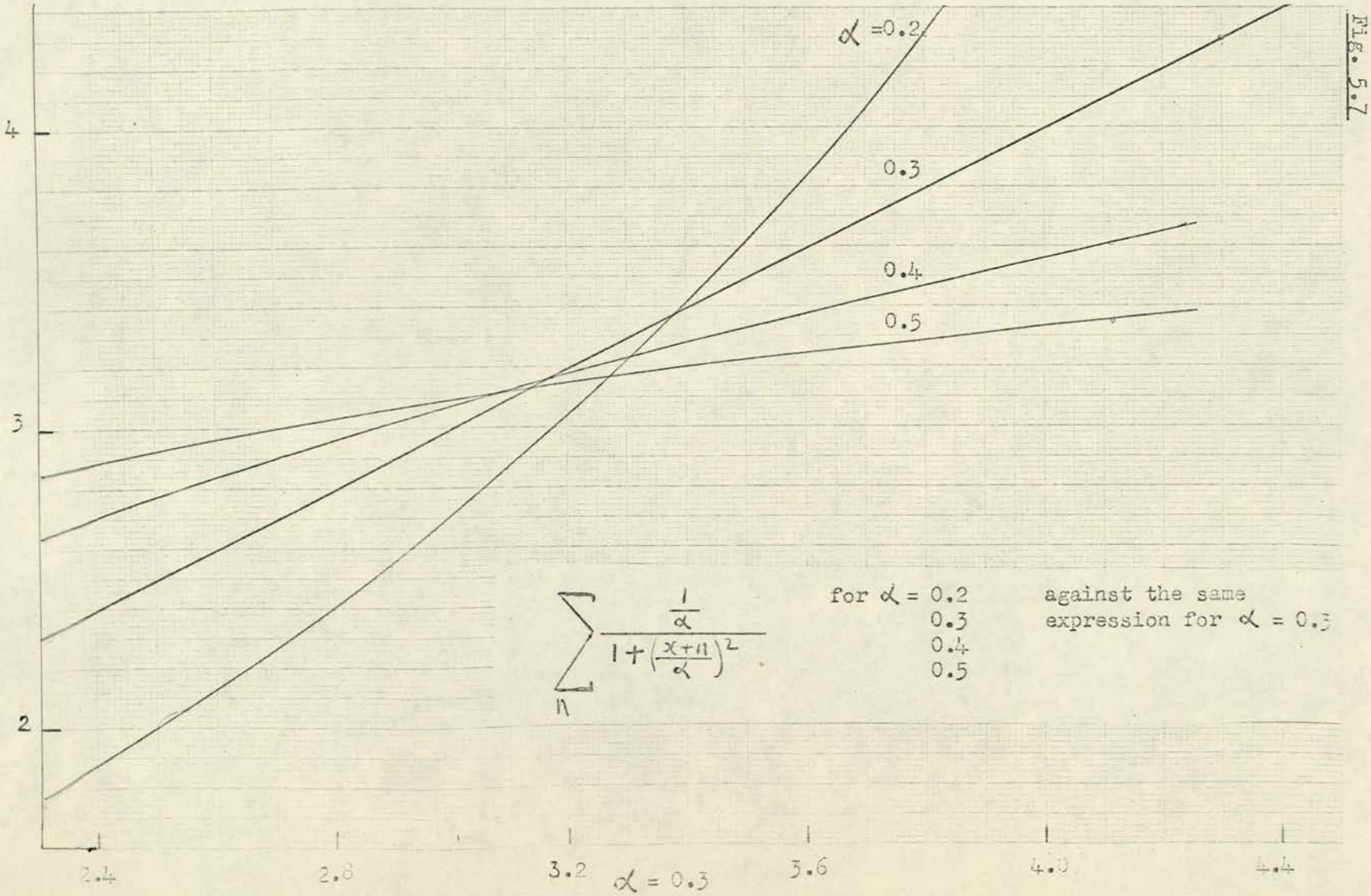
α =0.2
0.3
0.4
0.5
4
3
2
2.4
2.8
3.2
3.6
4.0
4.4
α = 0.3
$\sum_{n} \frac{\frac{1}{\alpha}}{1+\left(\frac{x+n}{\alpha}\right)^2}$
for α = 0.2
0.3
0.4
0.5
against the same expression for α = 0.3

points finally obtained open to some doubt. Further problems also arise in accurately reducing the results of different series of spectra to a common, but arbitary, intensity scale. Another disadvantage of this method was the considerable labour it involved. Thus, while in principle this seems an attractive way of removing the background intensity and the overlap, using only the result that the high frequency part of the wing had a $\frac{1}{\omega^2}$ frequency dependence for the intensity, it was discarded as a practical method.

COMPUTER ANALYSIS

The next approach was to use a non-linear least square program to fit to the data, in the form $I_N(\omega)$, a function formed by overlapping a Debye relaxation function at intervals of the free spectral range and adding a frequency independent parameter. Viz:-

$$I_N(\omega) = \sum_{n=-m}^{m} \left(\frac{A\tau}{1 + \tau^2(\omega + n.f)^2} \right) + C \qquad (5\cdot11)$$

The first term represents the wing and the second the background contributions. The sum over n is such that $m.f$ is approximately the extent of the wing - ~ 100 cm^{-1}. A similar fitting procedure was performed for the Gaussian distribution of relaxation times proposed by Hill and Ichiki (3·103).

Fitting was carried out individually for a number of spectra at various temperatures and free spectral ranges. As both models gave equally good fits, it was decided to take the simpler, single Debye relaxation time to represent the soft mode within the accuracy with which the data was obtained.

Since the units of intensity are arbitary, the function given by equation (5·11) has essentially two independent parameters - τ and $\frac{C}{A}$. The accuracy of the fitting procedure is limited by the extent to which the parameters can be varied to give calculated spectra which lie within the noise fluctuations on the observed signal. To investigate this, a series of spectra, for overlapped wings only, were generated by

$$I(\omega) = \sum_{n=-m}^{m} \frac{A\tau}{1 + \tau^2(\omega + n.f)^2} \qquad (5·12)$$

with

$$A = f$$

$$\tau = (\alpha . f)^{-1}$$

$$\omega = x . f$$

The use of these reduced variables enabled the spectra, due to wings whose half width at half maximum - $\omega_{\frac{1}{2}} = \frac{1}{\tau}$ - were different fractions of the free spectral range, to be compared most easily. Figures 5·5-5·7 show graphs of the right hand side of equation(5·12) for a particular value of α, plotted against the same expression but with different values of α for the frequency range between the Rayleigh-Brillouin peak and $\frac{f}{2}$ ie. $0·06 \leqslant x \leqslant 0·50$. The nearer a graph is to a straight line, the smaller is the difference in profile for spectra having the values of α appropriate to the functions on the abscissa and ordinate. As α is increased, the spectral profile becomes less sensitive to changes in α itself. For instance, the points on the spectra produced by $\alpha = 0·3$ and $\alpha = 0·4$ differ by only a few percent although $\omega_{\frac{1}{2}}$ varies by $\sim 30\%$.

The effect of the presence of a background component in the spectrum is to increase the noise fluctuations on the signal, since the signal itself is bigger, and to reduce proportionately the effect of a given change in α on the spectral profile. Further, in the fitting program, changes in the estimated values of α and the background compensate one another to give only small net variations to the shape of the calculated spectrum. For example, for a spectrum having a background contribution comparable to the minimum of the overlapped wing. Changing α from 0·125 to 0·150 - a ~ 20% variation in half width - causes intensity changes of less than 6%. 6% noise fluctuations occur typically on a 300 count/second signal which is, if anything, above average for this experiment. Thus, as $\omega_{\frac{1}{2}}$ becomes a smaller fraction of the free spectral range the fit becomes more reliable, but this reliability decreases as the magnitude of the background component is increased. For data of a given quality, it may, in certain cases, be impossible in principle to obtain any reasonable estimate of $\omega_{\frac{1}{2}}$ in the presence of an unknown background due to other Raman processes.

Two other points are worth noting. Firstly, if $\omega_{\frac{1}{2}}$ is very much less than the free spectral range, such that most of the wing beyond the Rayleigh peak has the $\frac{1}{\omega^2}$ behaviour, the fit will again be unreliable since it will be difficult to distinguish a Debye relaxation function from a purely $\frac{1}{\omega^2}$ profile. Secondly, at lower temperatures where the $\frac{1}{\omega^2}$ behaviour extends to lower frequencies, and thus smaller free spectral ranges are used, the background becomes a smaller fraction of the total intensity, so increasing the reliability of the fit.

A possible way of resolving the above problem is to use a narrowband interference filter which would reject the background to a greater extent than the wing. Apart from the 50% loss of valuable signal even at peak transmission, the spectral profile of the filter destroys the $\frac{1}{\omega^2}$ intensity dependence at high frequencies which is essential in order to carry out the spectral analysis. Also the filter behaved in a strange manner by intermittently rejecting the Brillouin lines even though they occur at ~3% of the filter's half width. The use of interference filters does not seem very profitable.

FOURIER TRANSFORM ANALYSIS

As the spectral output of the interferometer is a periodic function, it may be possible to extract that part of the spectrum due to the wing by Fourier analysis.

The total signal for $0 \leqslant \omega \leqslant \frac{f}{2}$, $I(\omega)$, can be expressed as a Fourier series:-

$$I(\omega) = \sum_{n=0}^{\infty} An \cos\left(\frac{2\pi n \omega}{f}\right) \qquad (5\cdot14)$$

The sin terms are omitted because $I(\omega)$ is an even function. The $\{An\}$ can be determined from:-

$$\left.\begin{aligned} A_{n \geqslant 1} &= \frac{4}{f} \int_0^{\frac{f}{2}} I(\omega) \cos\left(\frac{2\Pi n \omega}{f}\right) d\omega \\ Ao &= \frac{2}{f} \int_0^{\frac{f}{2}} I(\omega)\, d\omega \end{aligned}\right\} \qquad (5\cdot15)$$

The Fourier transform of $I(\omega)$, $I(t)$, is defined by

$$I(t) = \int_0^\infty I(\omega) \cos (2\pi t \omega) \, d\omega \qquad (5\cdot16)$$

If the limits of integration in equations (5·15-5·16) can be made equivalent, then the $\{A_n\}$ give the values of $I(t)$ for $t = \frac{n}{f}$, apart from a constant of proportionality. It is necessary to consider the contributions to the total values, for the $\{A_n\}$ from each class of spectral features, and whether or not they can be separated.

(1) The Rayleigh-Brillouin system for a single acoustic mode has a spectral distribution in the region $0 \leqslant \omega \leqslant \frac{f}{2}$ given by

$$I_{RB}(\omega) = \frac{I_R(0)\,\Gamma^2}{\omega^2 + \Gamma^2} + \frac{I_B(\omega_B)\,\Gamma^2}{(\omega-\omega_B)^2 + \Gamma^2} \qquad (5\cdot17)$$

The subscripts R, B denote parameters appropriate to the Rayleigh and Brillouin peaks. Each peak is assumed to have the instrumental Lorentzian profile having half width at half height Γ. ω_B is the acoustic mode frequency.

Application of equation (5·15) yields

$$\left.\begin{aligned} (A_{n\geqslant 1})_{RB} &= \frac{\pi}{F}\left\{I_R(0) + I_B(\omega_B)\cos\left(\frac{2\pi n \omega_B}{f}\right)\right\} e^{-\frac{\pi n}{F}} \\ (A_o)_{RB} &= \frac{\pi}{2F}\left\{I_R(0) + I_B(\omega_B)\right\} \end{aligned}\right\} \qquad (5\cdot18)$$

where the finesse F has been defined by $F = \frac{f}{2\Gamma}$ and use has been made of the fact that the Rayleigh-Brillouin scattering has negligible intensity beyond $\frac{f}{2}$, allowing the limits of equations (5·15) to be extended to infinity. The $\{A_n\}_{RB}$ thus lead directly

to the Fourier transform of these peaks. Since the Rayleigh and Brillouin peaks are localised in ω-space, their Fourier transform is likely to be spread out in t-space. This is verified by equations (5·18) for the typical values of F found in this experiment.

(2) The overlapped wing intensity I_W obs (ω) is related to the un-overlapped intensity $I_W(\omega)$ by

$$I_W \text{ obs}(\omega) = \sum_{m=-\infty}^{\infty} I_W(\omega + m.f) \qquad (5\cdot19)$$

Evaluation of equations (5·15) gives

$$\left.\begin{aligned} (A_{n\geq 1})_W &= \frac{4}{f}\int_0^{\infty} I_W(\omega)\cos\left(\frac{2\pi n\omega}{f}\right) d\omega \\ (A_o)_W &= \frac{2}{f}\int_0^{\infty} I_W(\omega)\, d\omega \end{aligned}\right\} \qquad (5\cdot20)$$

That is, the integral from 0 to $\frac{f}{2}$ for an overlapped wing is equivalent to the integral to infinity for an un-overlapped wing. Thus the Fourier Transform of the wing can be obtained from the appropriate integration of the overlapped wing from 0 to $\frac{f}{2}$.

As an example, for a Debye relaxation time

$$I_W(\omega) = \frac{A\tau}{1 + (\omega\tau)^2} \qquad (5\cdot21)$$

$$\left.\begin{aligned} (A_{n\geq 1})_W &= \frac{2A\pi}{f} e^{-\frac{2\pi n}{f}\frac{1}{\tau}} \\ (A_o)_W &= \frac{A\pi}{f} \end{aligned}\right\} \qquad (5\cdot22)$$

The $\{A_n\}$ will vary appreciably when $t = \frac{n}{f}$ is comparable to τ.

(3) The flat Raman Background contribution has

$$I_{RBS}(\omega) = \text{Constant} \qquad (5\cdot23)$$

$$\left.\begin{aligned} (A_{n\geq 1})_{RBS} &= 0 \\ (A_o)_{RBS} &= \frac{2.\text{constant}}{f} \end{aligned}\right\} \qquad (5\cdot24)$$

Thus the background only contributes to A_o and equivalently $I(t=0)$.

This method of analysis appears attractive at first sight because the Raman background contribution is isolated in one term, A_o, and it is the <u>un</u>-overlapped wing that contributes to the total Fourier transform. However, in Fourier space the Rayleigh-Brillouin system is spread out widely having much the same effect as the Raman background in real space. The problems involved in separating a wing from a background have already been discussed and apply equally in the Fourier case. An alternative procedure would be to remove the Rayleigh peak from the raw data by estimating the wing intensity at $\omega = 0$. However since the wing is usually steepest where it 'disappears' into the Rayleigh peak, the extrapolation to zero frequency is highly uncertain.

There are also difficulties caused by the need to reduce the results for spectra obtained under different conditions to some arbitary scale and the problems involved in calculating A_n for larger values of n where the cos term is varying rapidly across the free spectral range. Evaluation of the integrals is then a lengthy process.

Thus both direct and Fourier fitting procedures are fraught with difficulties due to background - which is either Raman scattering for direct fitting or the Rayleigh-Brillouin contribution for Fourier fitting - and the uncertainty in the intensity due to noise which limits the distinguishability of fits having different parameters.

This reflects the fact that the information contained in the data is limited and cannot be increased by the use of a particular analysis, but only by an improvement in the quality of that data.

The least complicated fitting procedure, that of fitting an overlapped Debye relaxation function plus constant background to the spectrum beyond the Rayleigh peak, was the one used.

THE REMOVAL OF THE ACOUSTIC MODES

In the orientations used in this experiment only one pair of Brillouin peaks can be observed. When the acoustic modes are clearly resolved from the Rayleigh peak it is simplest to remove them by estimating the wing profile under them from that on either side. As a way of reducing their effect, the two peaks can be overlapped at the centre of the free spectral range or even concealed under a nearby Rayleigh peak. These methods can only be used at small free spectral ranges. The limit to the smallest free spectral range that can usefully be employed is set by the laser linewidth, since reduction of the spectral width of the pinhole much below the laser linewidth will result in a sharp drop in intensity with only a modest increase in observed finesse. Even if a finesse of only 25 is adequate, the free spectral range is limited to $\sim 0{\cdot}9\ cm^{-1}$. The acoustic mode present in the B_2 spectrum of DKDP has a shift of $\sim 0{\cdot}45\ cm^{-1}$, so modes of adjacent orders can be

overlapped at the centre of the free spectral range. As the wing intensity varies most slowly in this region, estimation of the wing profile below the acoustic modes is not difficult. Although this longitudinal mode frequency depends on the anomalous elastic constant C_{66} through $\Delta\omega \sim \sqrt{C_{11} + C_{12} + C_{66}}$, C_{12} is an order of magnitude greater than the other two constants so that there is little total temperature dependence .

EXPERIMENTAL RESULTS

The crystals used were nominally of 100% deuteration. The DKDP sample was a 1 cm cube, while the DADP crystal measured 2·0 x 0·6 x 0·6 cms. Spectra obtained both on the spectrometer and interferometer for each of the four wings will be discussed in turn.

DKDP B_2 WING

SPECTROMETER RESULTS

A room temperature spectrum for $0 < \omega < 1000$ cm^{-1} showed that a wing on the Rayleigh linewas the strongest feature. The next appreciable peak was at 382 cm^{-1}.

Using the x(yx)y orientation, spectra were obtained at five temperatures between 295°K and 374°K, at ratemeter sensitivities of 0-3000 counts/sec for $0 < \omega < 20$ cm^{-1} and 0-300 counts/sec for $12 < \omega < 100$ cm^{-1}. No temperature dependence was noted for this latter set of spectra; this was verified by recording the intensity at 15 cm^{-1} as a function of temperature. The spectral distribution was found to be $I_N(\omega) \propto \frac{1}{\omega^2}$ with a weak multiphonon background of ~ 5 counts/sec.

Figure (5·8) shows the spectra obtained on the less sensitive range, superposed for comparison. The Rayleigh peak is shown with reduced sensitivity. The 'resolution', in the caption, is the full width of the Rayleigh peak at half maximum intensity. Compared to the spectral range under study, the resolution of 1·35 cm^{-1} is only moderate, but attempts to improve it resulted in a severe loss of intensity. The spectra were fitted by a Debye relaxationfunction plus constant background - as in equation (5·8) - for the region beyond the tail of the Rayleigh peak, $\omega \geq 3{\cdot}5$ cm^{-1}. The results, listed in table (5·1), comprise the temperature, parameter A and half width $\omega_{\frac{1}{2}}$ (cm^{-1}) which is related to the relaxation time τ (seconds) by $\omega_{\frac{1}{2}} = \frac{1}{\tau 2\pi c}$. The halfwidth is given in preference to the relaxation time as it is more readily comparable with the spectra.

TABLE 5·1

$T^{o}K$	$\omega_{\frac{1}{2}}$ cm^{-1}	A
374	5·65	2249
353	4·61	2634
333	3·79	3039
315	3·11	3547
295	2·28	4594

The accuracy of these results is limited by the noise on the signal, especially for the lower intensities recorded at higher temperatures, and by parameter interaction in the fitting program. This is greatest at lower temperatures where the spectrum is not much different from $I_N(\omega) \propto \frac{1}{\omega^2}$ and thus the A and τ in $\frac{A\tau}{1 + (\omega\tau)^2}$ are no longer totally independent parameters.

Discussion of these results will be delayed until after the interferometer data has been presented.

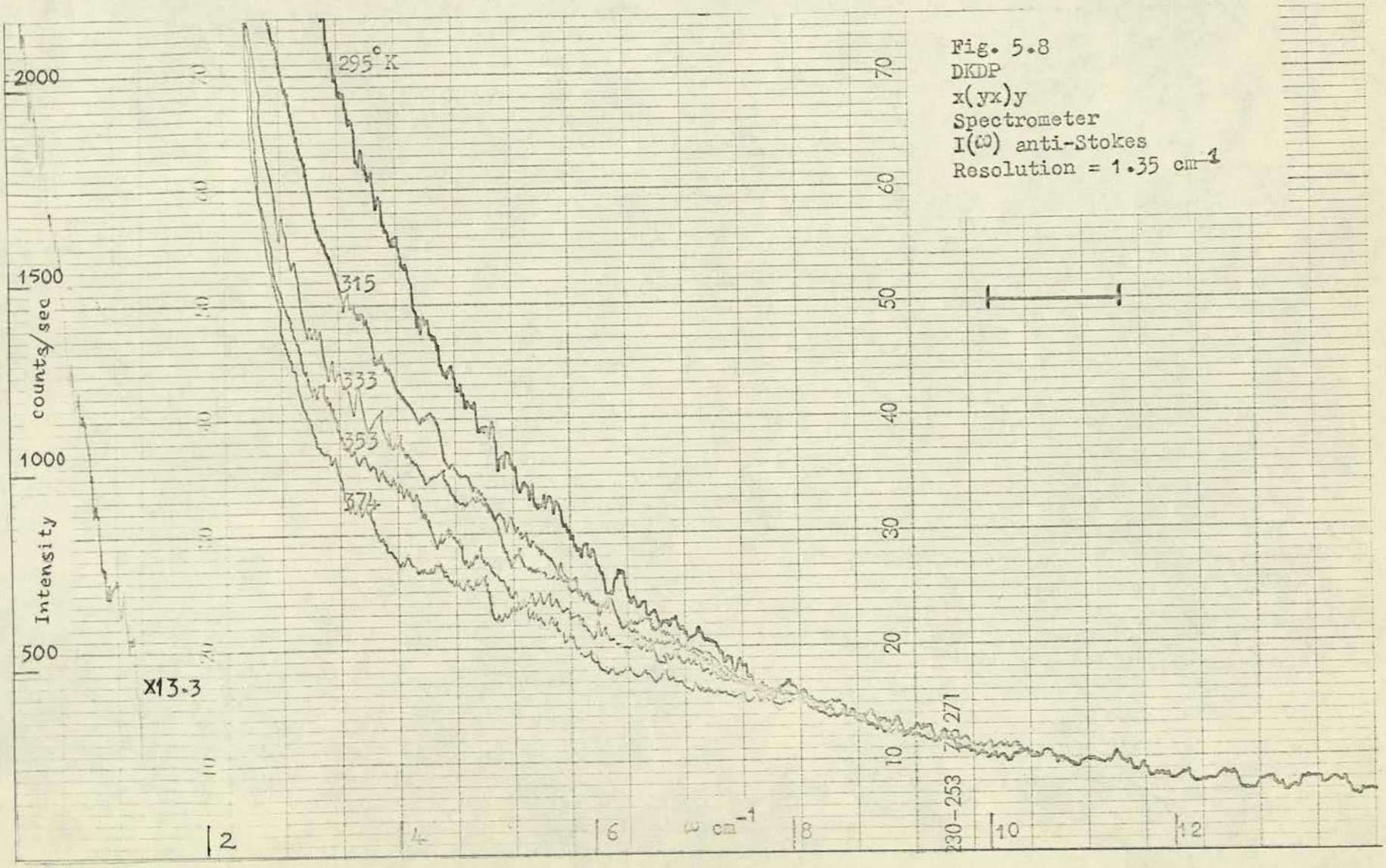

Fig. 5.8
DKDP
x(yx)y
Spectrometer
I(ω) anti-Stokes
Resolution = 1.35 cm^{-1}

Since for much of the spectral region that could be studied, the room temperature wing had approximately a $\frac{1}{\omega^2}$ behaviour, it was thought unprofitable to investigate temperatures below room temperature in detail. An earlier set of spectra having poorer resolution but recorded at 225°K, 295°K and 373°K for $\omega \geq 12$ cm^{-1} had shown no temperature dependence.

INTERFEROMETER RESULTS

From the results of experiments listed in the introduction to this chapter it was postulated that there would be a B_2 wing having a halfwidth of $\sim 0{\cdot}5$ cm^{-1} at room temperature. Initial experiments performed with a free spectral range of 5 cm^{-1} failed to show any wing. It was only by comparing the spectra for KDP and DKDP recorded both with and without a narrow band interference filter that the presence of a wing in DKDP similar to that in KDP, but at lower frequencies, could be deduced. The flat signal between the two Rayleigh peaks - which was largely dark current from the noisy EMI photomultiplier tube - was reduced more by the filter for KDP than DKDP, indicating that the bulk of the scattered intensity was at lower frequencies in the latter crystal.

As a result of these initial experiments, the interferometer was modified to increase, by a factor of 10, its maximum free spectral range to ~ 70 cm^{-1}. Also, the low noise ITT photomultiplier tube was ordered. Some preliminary spectra where then recorded on the grating spectrometer; these have been discussed in the previous section.

Interferometer spectra were obtained for free spectral ranges from 60·8 cm^{-1} to 0·89 cm^{-1}, and at temperatures from 220°K to 370°K. Higher temperatures were not used as an earlier crystal had shown a 'paraelectric to powder transition' at about 390°K. Typical spectra are shown in figures 5·9 - 5·20, while the results of fitting a Debye relaxation function plus background - equation (5·11) - are given in table 5·2.

Spectra obtained above room temperature for free spectral ranges of 60·8 cm^{-1}, figure (5·9), and 35·4 cm^{-1}, figure (5·10), have the general appearance of the spectrometer traces. Many of the remarks made for these apply here also. Spectra obtained at the smaller free spectral range have better resolution, 0·7 cm^{-1}, and approach the Rayleigh line more closely, ~1·5 cm^{-1}. The wing appears temperature independent for $\omega \geq 8$ cm^{-1} but weakens on heating at lower frequencies. At 60·8 cm^{-1}, spectra were recorded with ratemeter sensitivities of 1000 and 2000 counts/sec, full scale deflection. The differences in the results obtained in the two cases gives an estimate of the uniqueness of the fit to the data. The half widths have on average a 10% difference. There was a high A-τ correlation at the lowest temperature because the spectral distribution is little different from a $\frac{1}{\omega^2}$ wing, while at higher temperatures small changes in the estimated background can give large changes to τ. At these spacings the background is estimated to form about 70% of the minimum signal.

It should be remembered that, while the values of τ, or equivalently $\omega_{\frac{1}{2}}$, obtained for different sets of spectra are directly comparable, this is not so for A, which contains an unknown intensity factor.

At free spectral ranges of 31·0 cm^{-1} and 14·3 cm^{-1}, figures (5·11), (5·12), data was obtained over the range $220 < T^{\circ}K < 360$. No temperature dependence was noted below $\sim 270^{\circ}K$ for the wing at the smaller spacing, as the $\frac{1}{\omega^2}$ behaviour extended from $\sim 1{\cdot}5$ cm^{-1}, while for the 14·3 cm^{-1} setting, a slight increase in intensity at frequencies just greater than that of the acoustic mode was observed.

Of interest was the marked increase in intensity of the Rayleigh peak itself below room temperature. This indicated that the temperature dependent part of the wing occurred at frequencies below ~ 1 cm^{-1}. However, fitting the $I(\omega = 0)$ temperature behaviour is not possible for three reasons. Firstly, the contribution to $I(\omega = 0)$ from surface scattering is unknown and varies due to the temperature dependence of the liquid - crystal refractive index difference. Secondly, the intensity due to other orders of interference is not easily estimated. Thirdly, at high temperatures where the half width of the wing is much greater than the spectral width of the detector, the wing intensity detected around $\omega = 0$ is indeed $I(\omega = 0)$, but at low temperatures, at the same free spectral range, the half width of the wing may well be less than the detector width and so the measured intensity is an average over a portion of the wing.

At 14·3 cm^{-1} free spectral range, the wing intensity decreases markedly above room temperature to give little curvature to the observed spectrum. Over much of the temperature range 220-365°K, the background is estimated at about 50% of the minimum signal, but at higher temperatures the fit attributes a larger portion to the background, thus giving greatly enhanced values for τ.

Spectra obtained at 10·96 cm^{-1} free spectral range, figure 5·13, show the low frequency strengthening of the wing on cooling more clearly. Similar results but at higher resolution were obtained at a free spectral range of 7·28 cm^{-1}, figure 5·14. Here the longitudinal acoustic modes are resolved from the Rayleigh peak. The same acoustic modes appear in the x(zz)y orientation where they are more distinct since the wing is not present. The separation of these modes can be measured relative to the sodium D line splitting and then used to calibrate subsequent, smaller free spectral ranges. The mode frequency was found to be 0·445 cm^{-1}. It is of interest to contrast the rapid gain in intensity at this frequency with the minimal temperature dependence of the intensity at the centre of the free spectral range.

The 5·44 cm^{-1} data, figure 5·15, clearly shows the lack of curvature on the room temperature spectrum that was initially a puzzling feature.

Figures 5·16-5·17, for the 1·90 cm^{-1} setting, show the strong temperature dependence at low frequencies which becomes very marked near the transition. The wing has little curvature at frequencies lower than the acoustic mode for temperatures above 245°K. This is to be expected, since, for frequencies much less than the half width, a Debye relaxation function has little frequency dependence. As the temperature is lowered the wing intensity increases dramatically until the transition is reached, figure 5·17, where there is a sharp drop in intensity. The Rayleigh peak fell to 1000 counts/sec. Due to the decrease in specific heat below the transition, the temperature also drops rapidly - by about 10 degrees in as many minutes during the recording of trace d on figure 5·17. The crystal was not poled in the ferroelectric phase nor was the temperature dependence of the wing studied.

The behaviour of the wing at frequencies lower than the acoustic modes is shown in figures 5·18-5·20 . The variation of intensity with temperature is so rapid near the transition that many of the traces have either too little curvature to allow any reasonable estimate of the background to be determined or else are almost entirely of the $\frac{1}{\omega^2}$ form. The long thermal time constant due to the specific heat anomaly at the transition, makes stability of the crystal temperature difficult to achieve in precisely that region where the intensity varies most strongly with temperature. Figure 5·20 illustrates a spectrum obtained on passing slowly through the transition at an estimated temperature of 219·4°K.

In order to obtain a moderate finesse of 24, a smaller pinhole was used at this spacing. There is a severe loss of intensity compared to the spectra obtained at 1·90 cm^{-1}.

It is of interest to examine the behaviour of the ratio of the background intensity to minimum wing signal, which, for a wing having a $\frac{1}{\omega^2}$ behaviour from at least $\omega = \frac{1}{2}$ FSR cm^{-1}, is proportional to the free spectral range. Figure 5·27 shows a graph of this data for some free spectral ranges. There is a large spread in the points especially at large free spectral ranges where the background is proportionally greater and thus the fitting procedure more uncertain. For some sets of data obtained at the larger spacings the spectra went from having little curvature to being almost entirely of the $\frac{1}{\omega^2}$ form over the temperature range studied. Due to uncertainties on the fitted values, the ratio of background to wing varied widely. There is, however, a trend to follow the predicted behaviour.

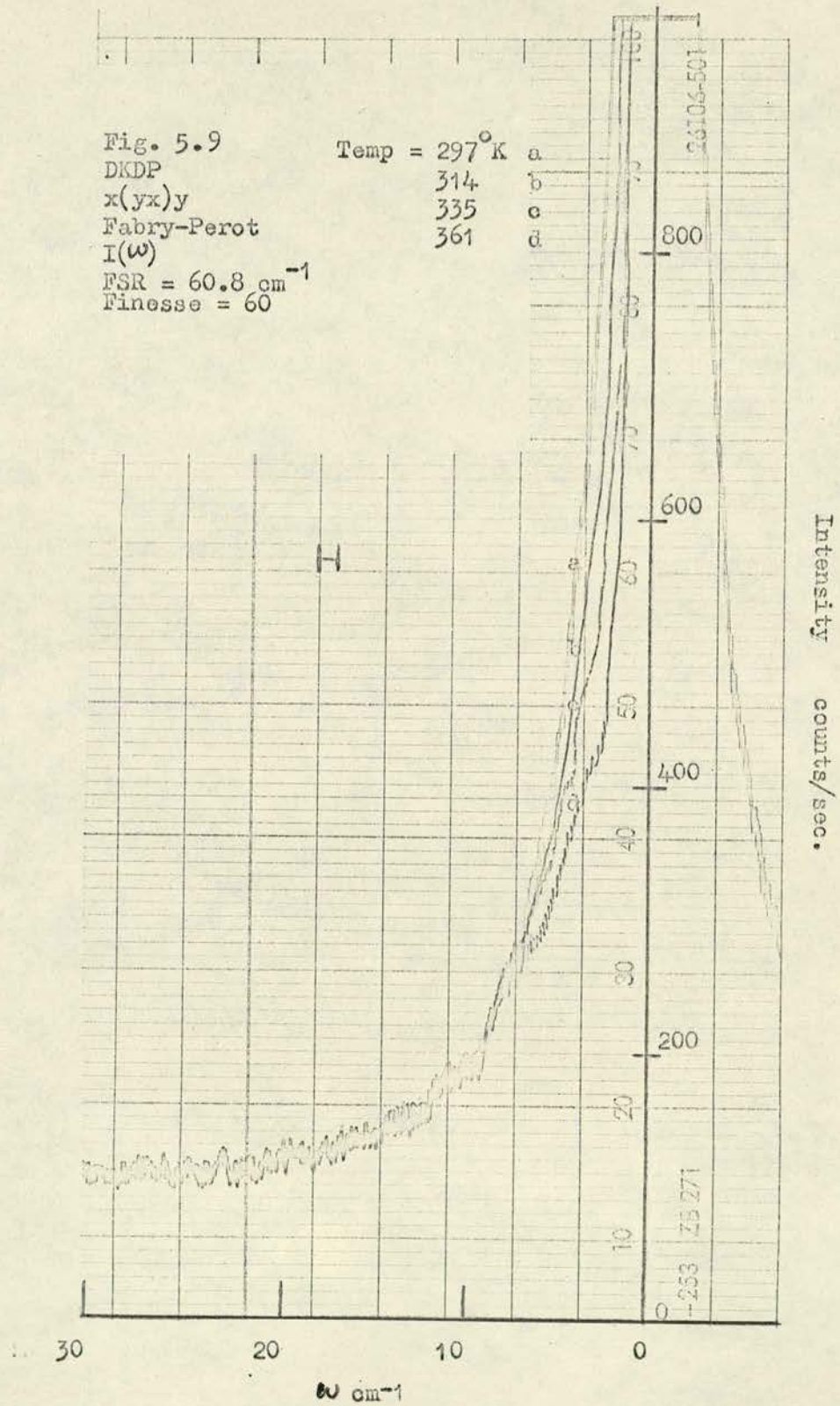
Fig. 5.9
DKDP
x(yx)y
Fabry-Perot
I(ω)
FSR = 60.8 cm⁻¹
Finesse = 60
Temp = 297°K a
314 b
335 c
361 d
Intensity counts/sec.
800
600
400
200
0
30
20
10
0
ω cm⁻¹

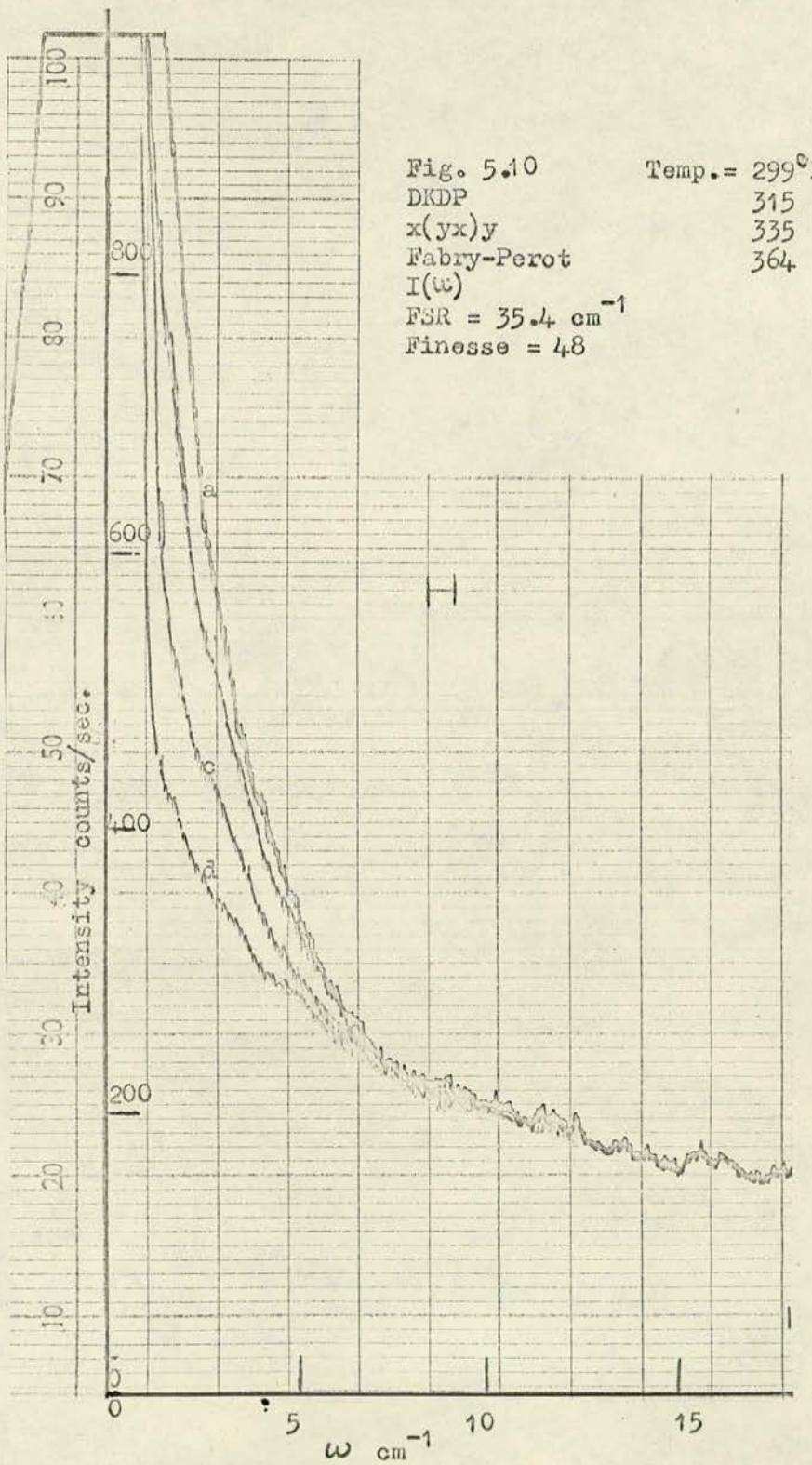

Fig. 5.10
DKDP
x(yx)y
Fabry-Perot
I(ω)
FSR = 35.4 cm^{-1}
Finesse = 48

Temp.= 299°K a
315 b
335 c
364 d

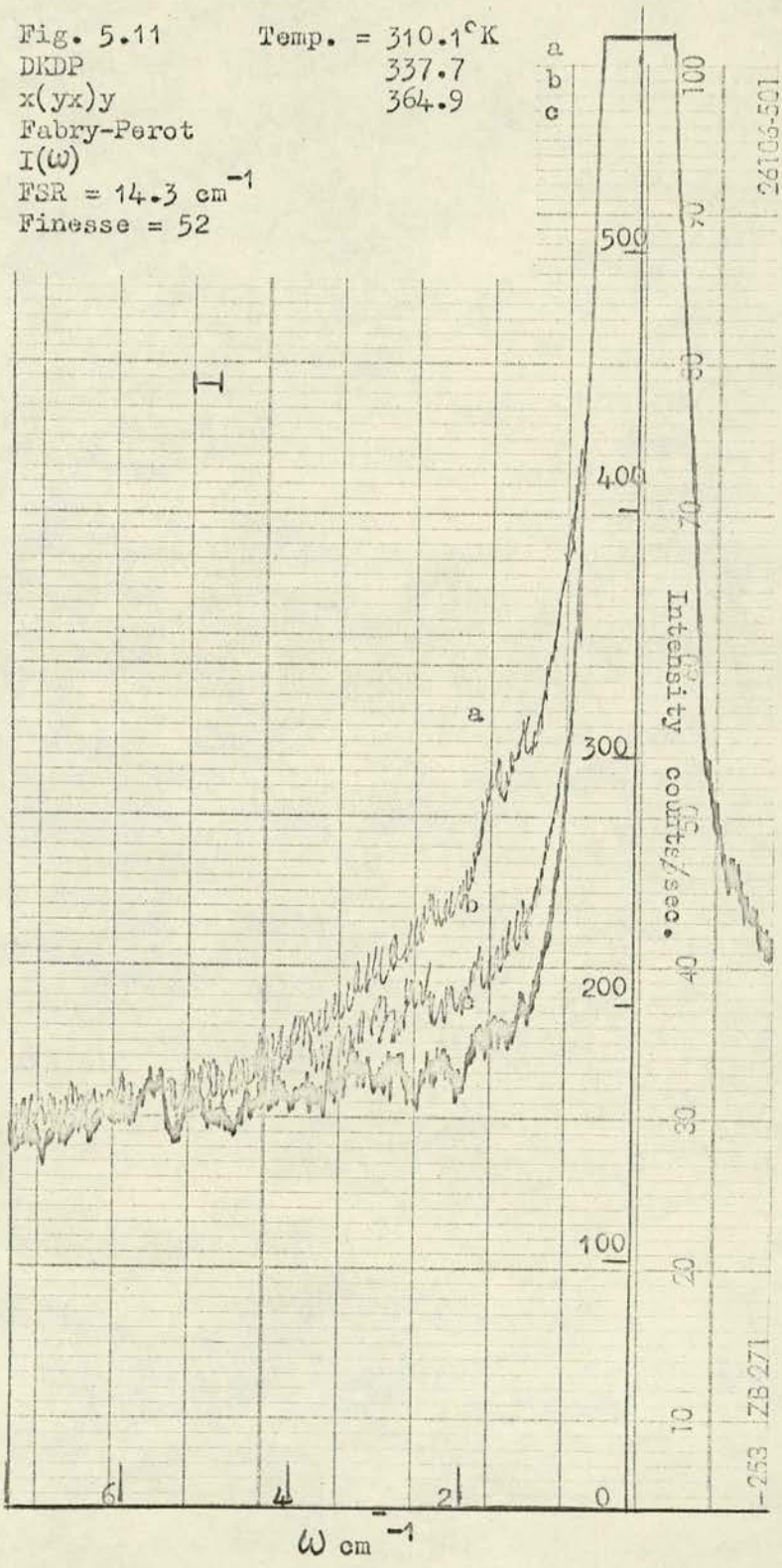
Fig. 5.11
DKDP
x(yx)y
Fabry-Perot
I(ω)
FSR = 14.3 cm⁻¹
Finesse = 52
Temp. = 310.1°K
337.7
364.9
a
b
c
500
400
300
200
100
0
Intensity counts/sec.
100
50
30
20
10
6
4
2
ω cm⁻¹
26106-501
ZB 271
-253

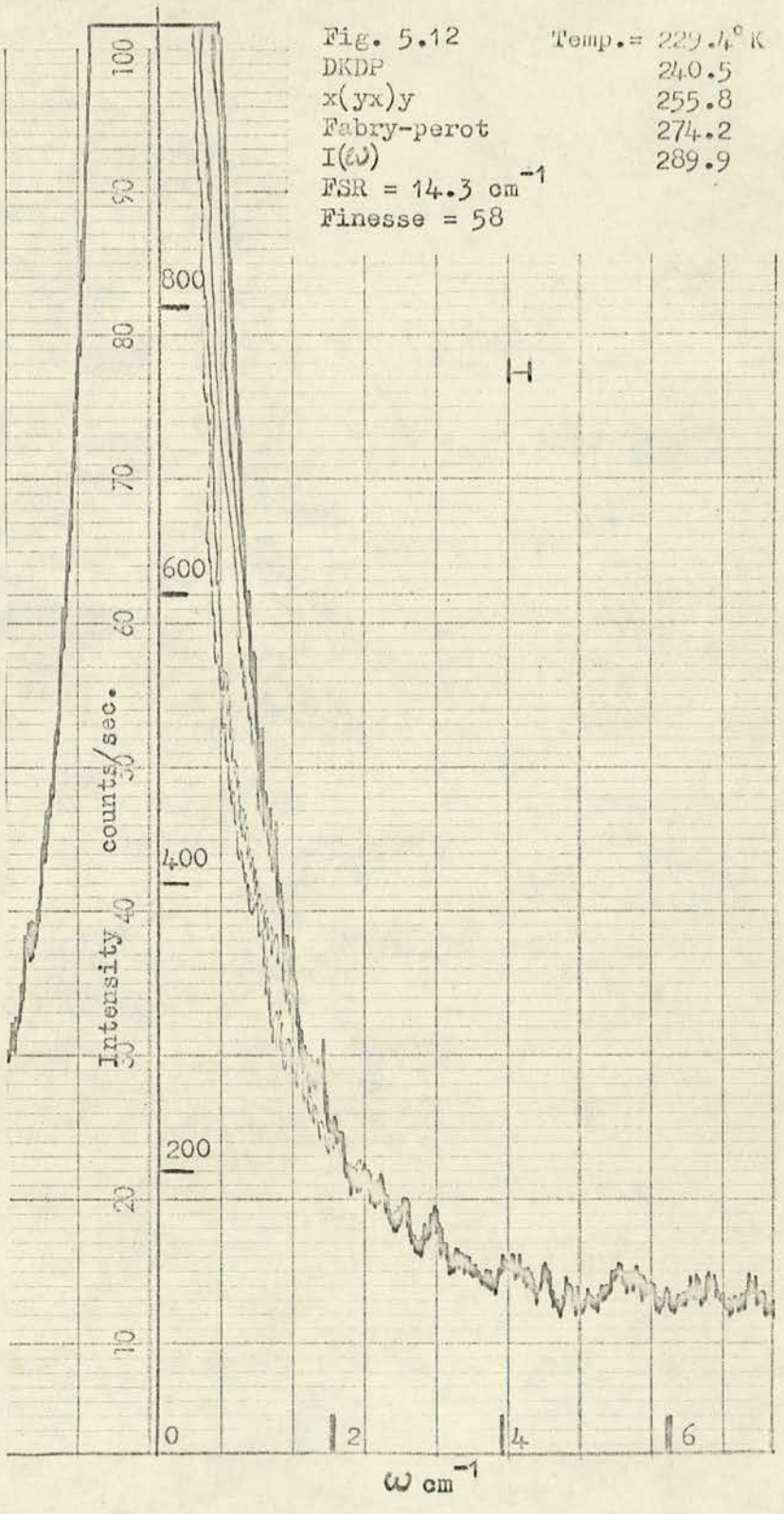
Fig. 5.12
DKDP
x(yx)y
Fabry-perot
I(ω)
FSR = 14.3 cm⁻¹
Finesse = 58
Temp.= 229.4° K
240.5
255.8
274.2
289.9
Intensity counts/sec.
100
90
80
70
60
50
40
30
20
10
800
600
400
200
0
2
4
6
ω cm⁻¹

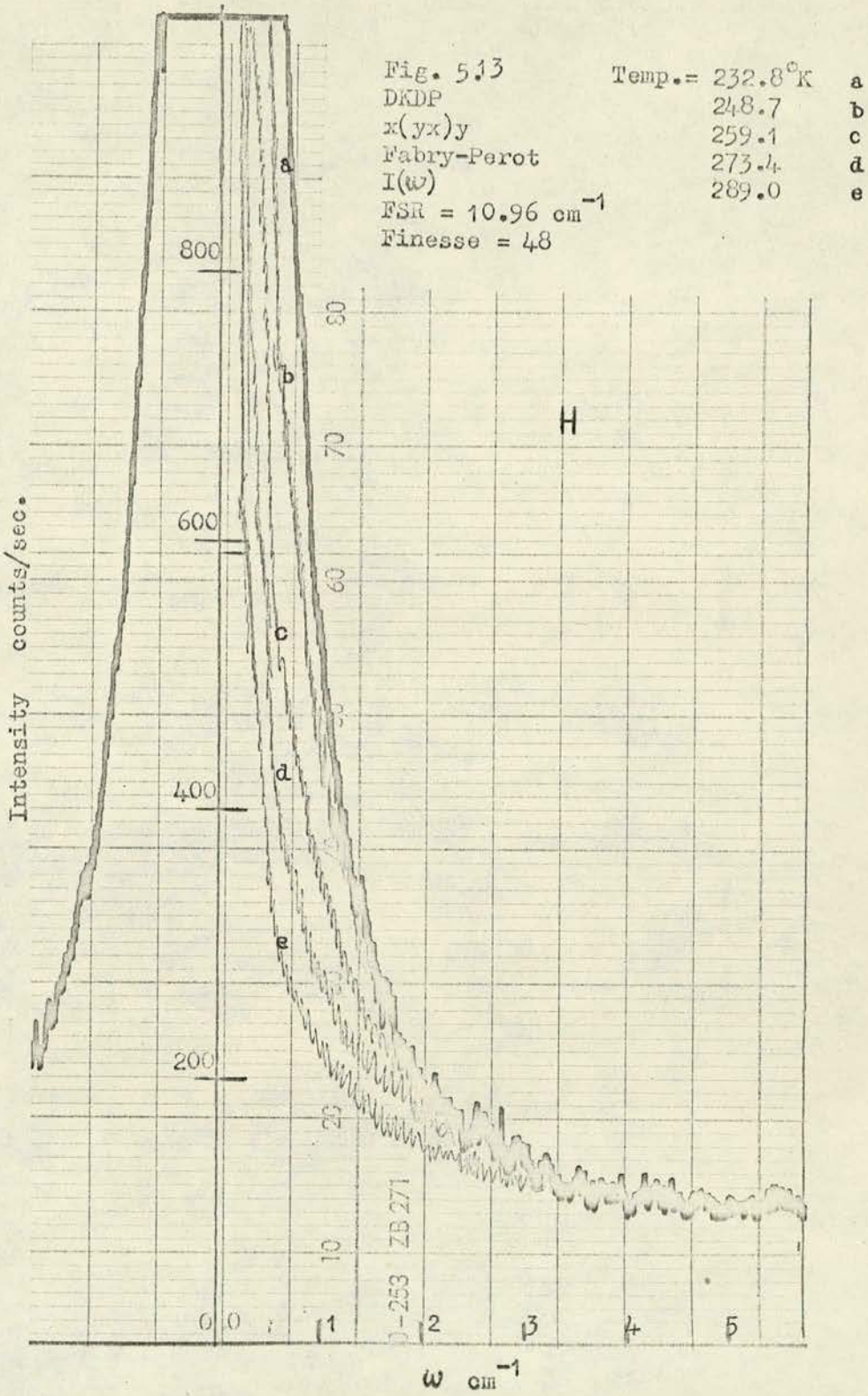
Fig. 5.13
DKDP
x(yx)y
Fabry-Perot
I(ω)
FSR = 10.96 cm⁻¹
Finesse = 48
Temp.= 232.8°K a
248.7 b
259.1 c
273.4 d
289.0 e
H
Intensity counts/sec.
800
600
400
200
0
ω cm⁻¹
ZB 271
D-253

Fig. 5.14 DKDP I(ω)
x(yx)y FSR = 7.28 cm^{-1}
Fabry-Perot Finesse = 50

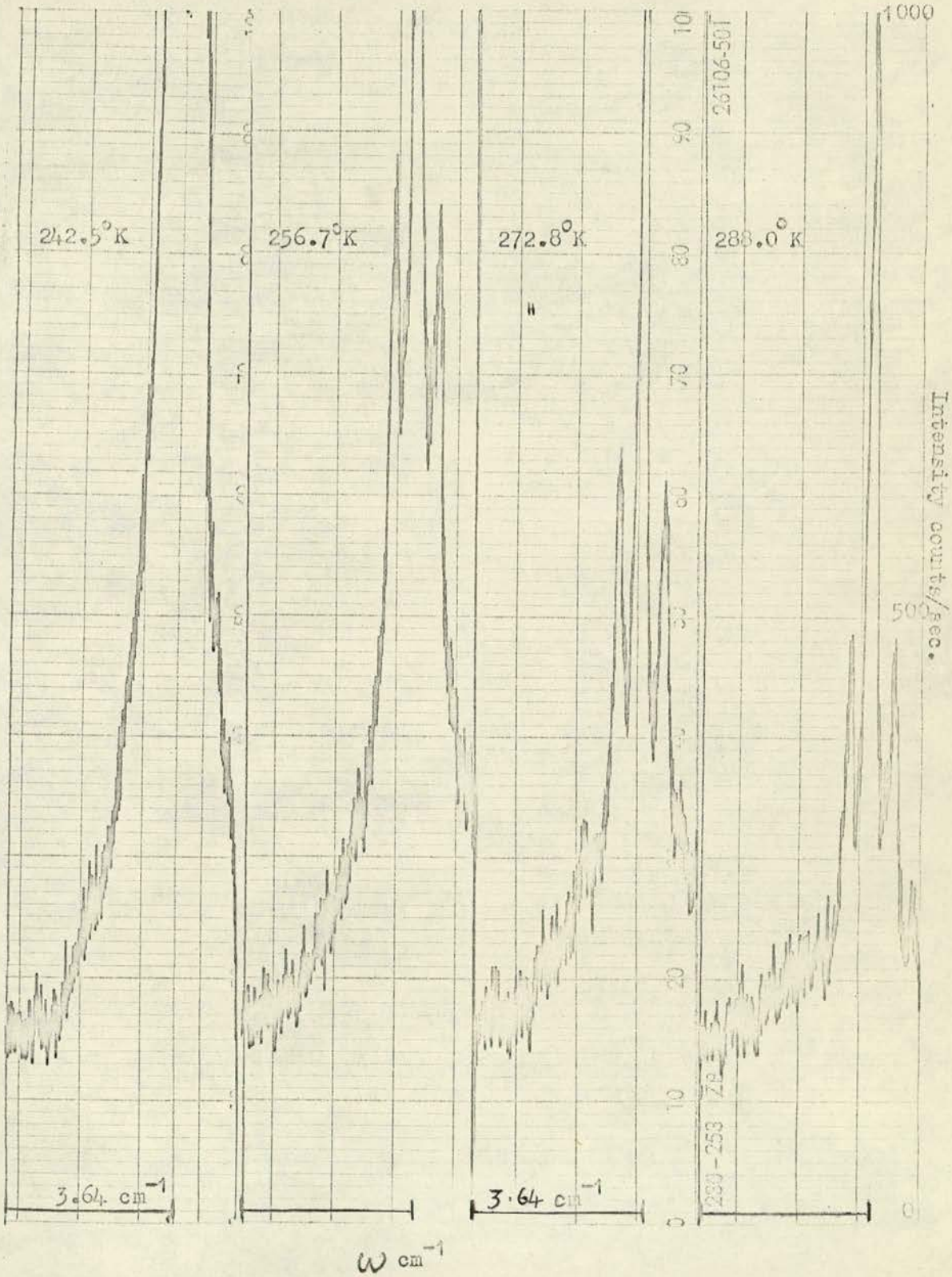

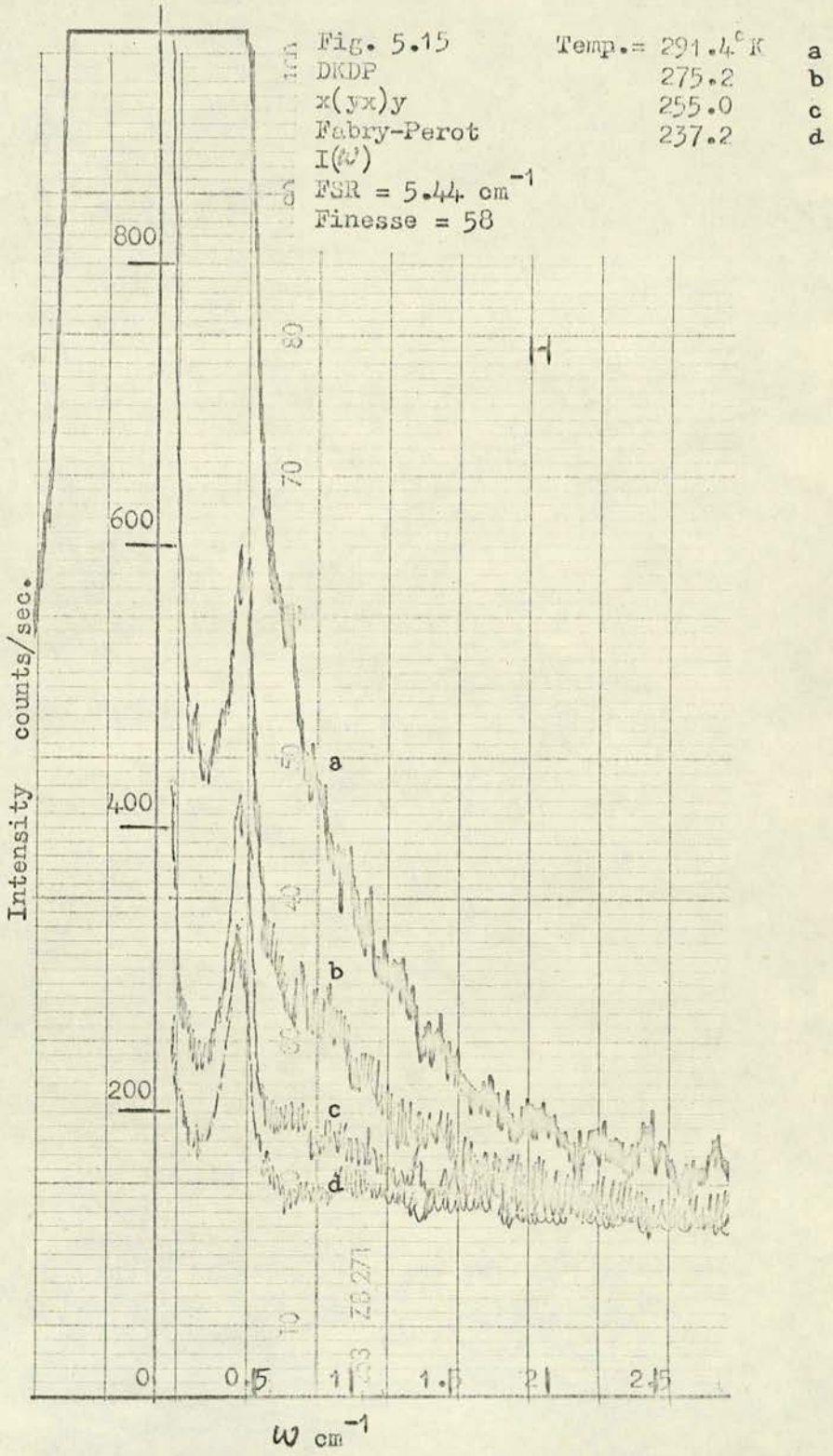
Fig. 5.15
DKDP
x(yx)y
Fabry-Perot
I(ω)
FSR = 5.44 cm⁻¹
Finesse = 58
Temp.= 291.4°K a
275.2 b
255.0 c
237.2 d
Intensity counts/sec.
800
600
400
200
0
0.5
1
1.5
2
2.5
a
b
c
d
ω cm⁻¹

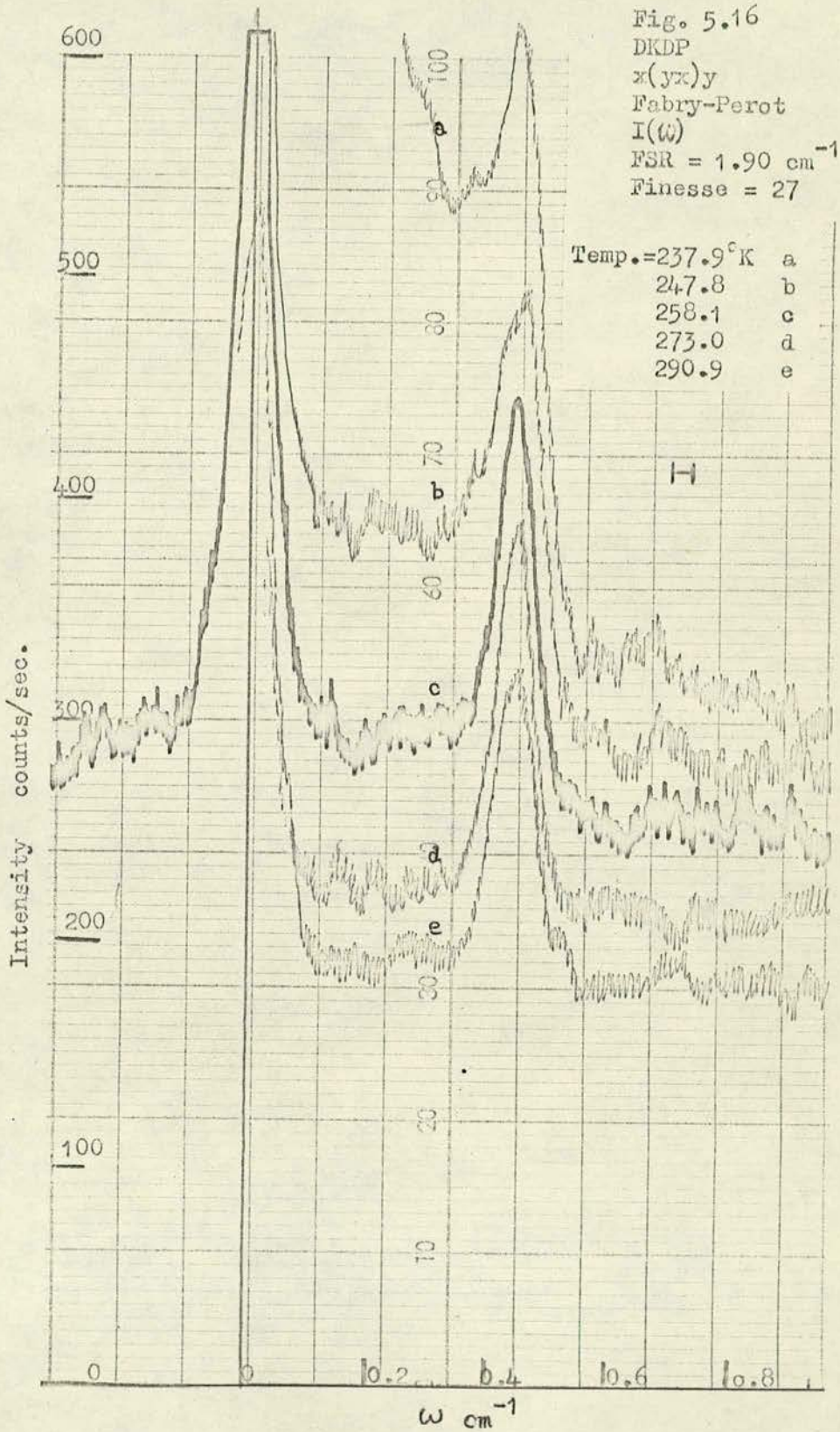
Fig. 5.16
DKDP
x(yx)y
Fabry-Perot
I(ω)
FSR = 1.90 cm⁻¹
Finesse = 27
Temp.=237.9°K a
247.8 b
258.1 c
273.0 d
290.9 e
Intensity counts/sec.
600
500
400
300
200
100
0
0
0.2
0.4
0.6
0.8
ω cm⁻¹
a
b
c
d
e

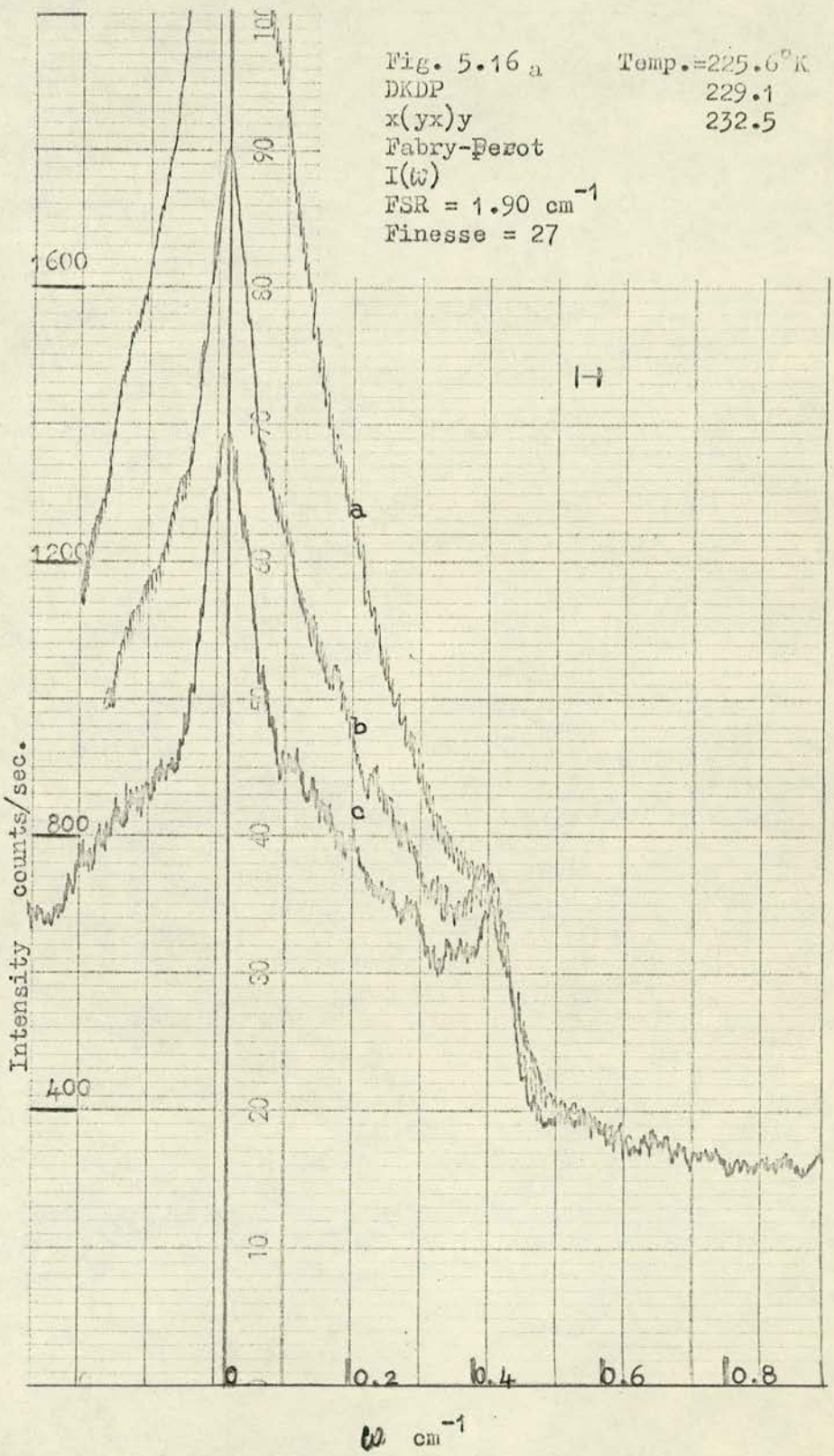
Fig. 5.16 a
DKDP
x(yx)y
Fabry-Perot
I(ω)
FSR = 1.90 cm⁻¹
Finesse = 27
Temp.=225.6°K a
229.1 b
232.5 c
1600
1200
800
400
Intensity counts/sec.
100
90
80
70
60
50
40
30
20
10
a
b
c
0
0.2
0.4
0.6
0.8
ω cm⁻¹

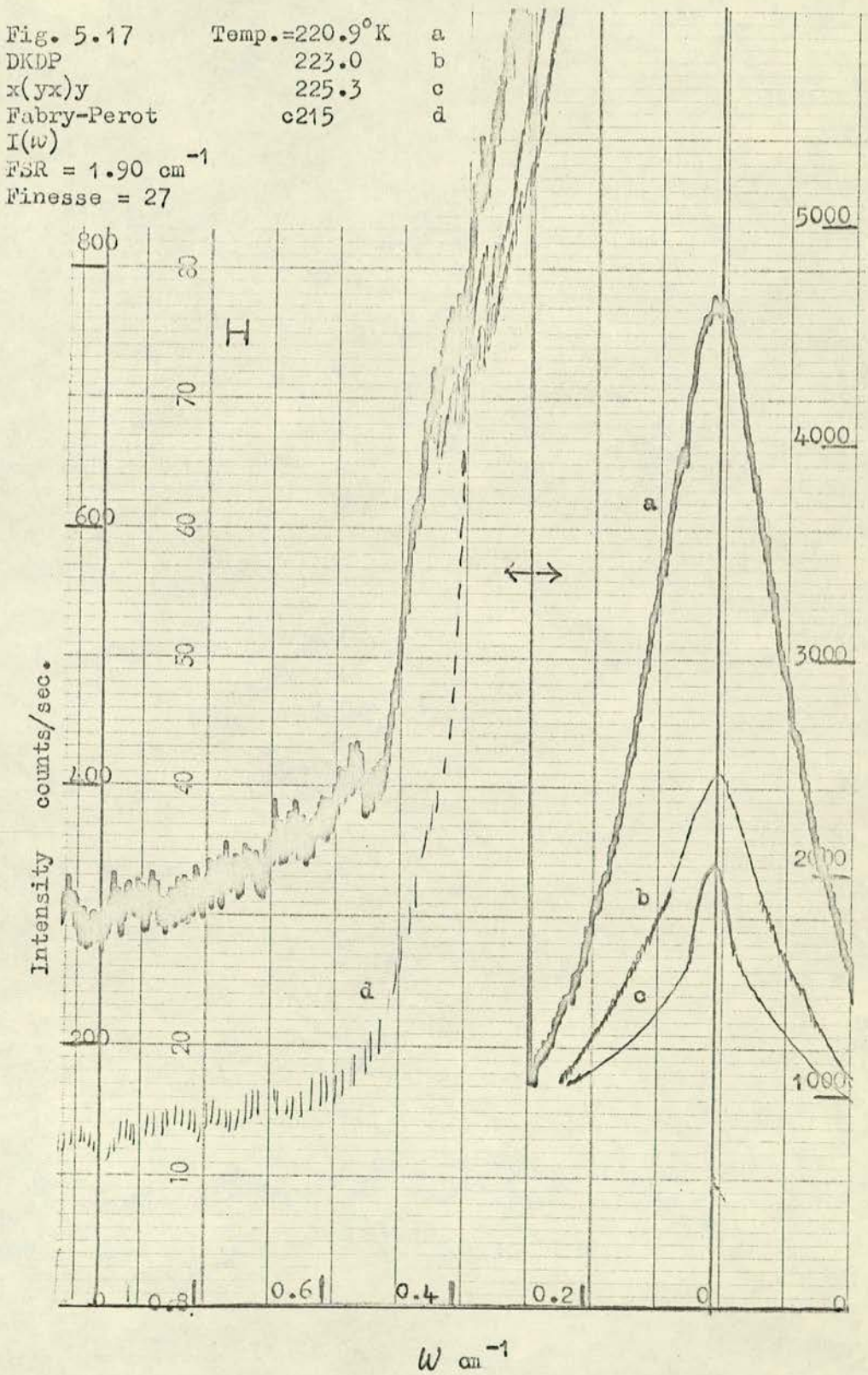
Fig. 5.17
DKDP
x(yx)y
Fabry-Perot
I(ω)
FSR = 1.90 cm⁻¹
Finesse = 27
Temp.=220.9°K a
223.0 b
225.3 c
c215 d
H
Intensity counts/sec.
800
600
400
200
80
70
60
50
40
20
10
5000
4000
3000
2000
1000
a
b
c
d
0.8
0.6
0.4
0.2
0
ω cm⁻¹

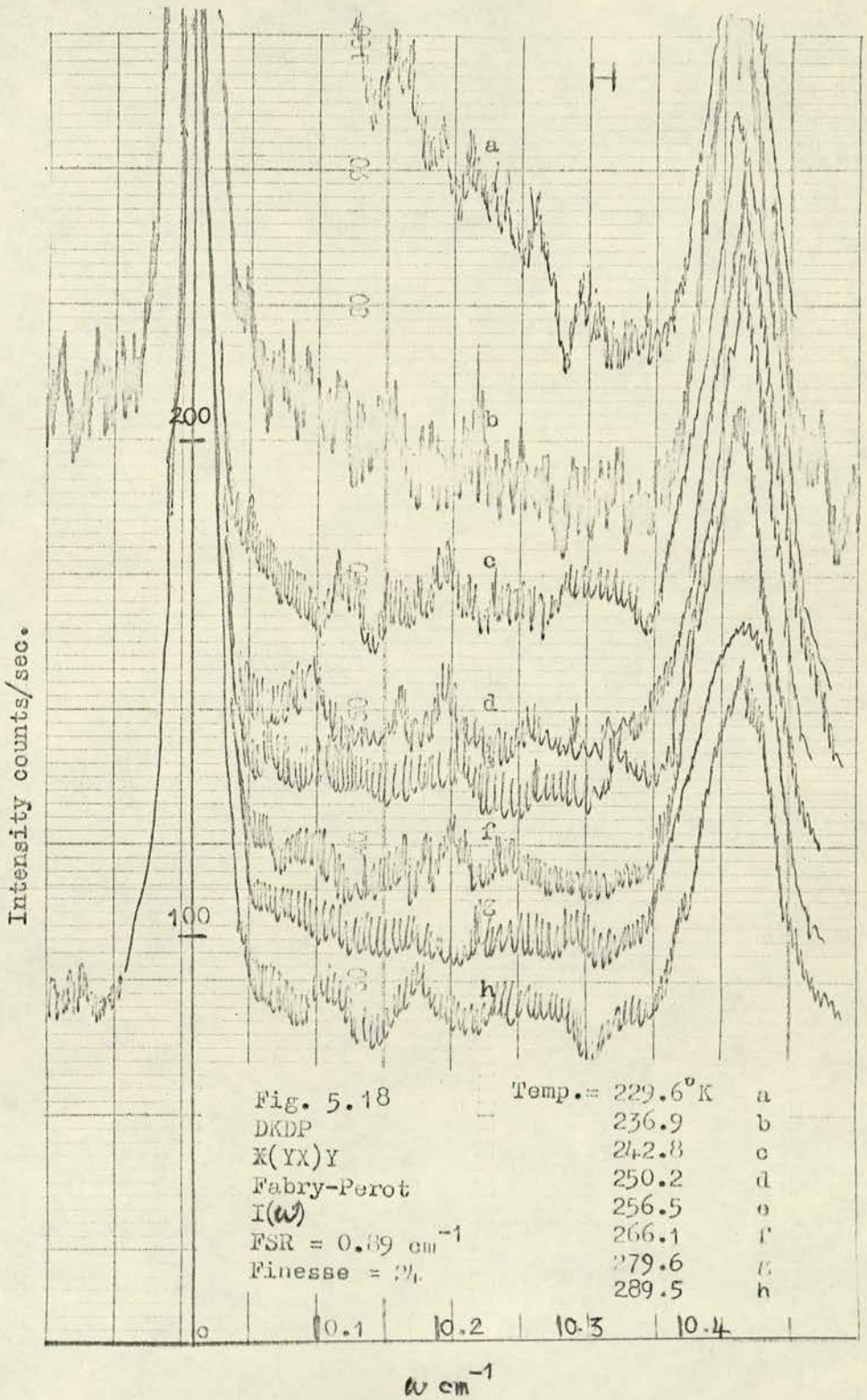

Fig. 5.18
DKDP
X(YX)Y
Fabry-Perot
I(ω)
FSR = 0.89 cm^{-1}
Finesse = 24

Temp. =		
	229.6°K	a
	236.9	b
	242.8	c
	250.2	d
	256.5	e
	266.1	f
	279.6	g
	289.5	h

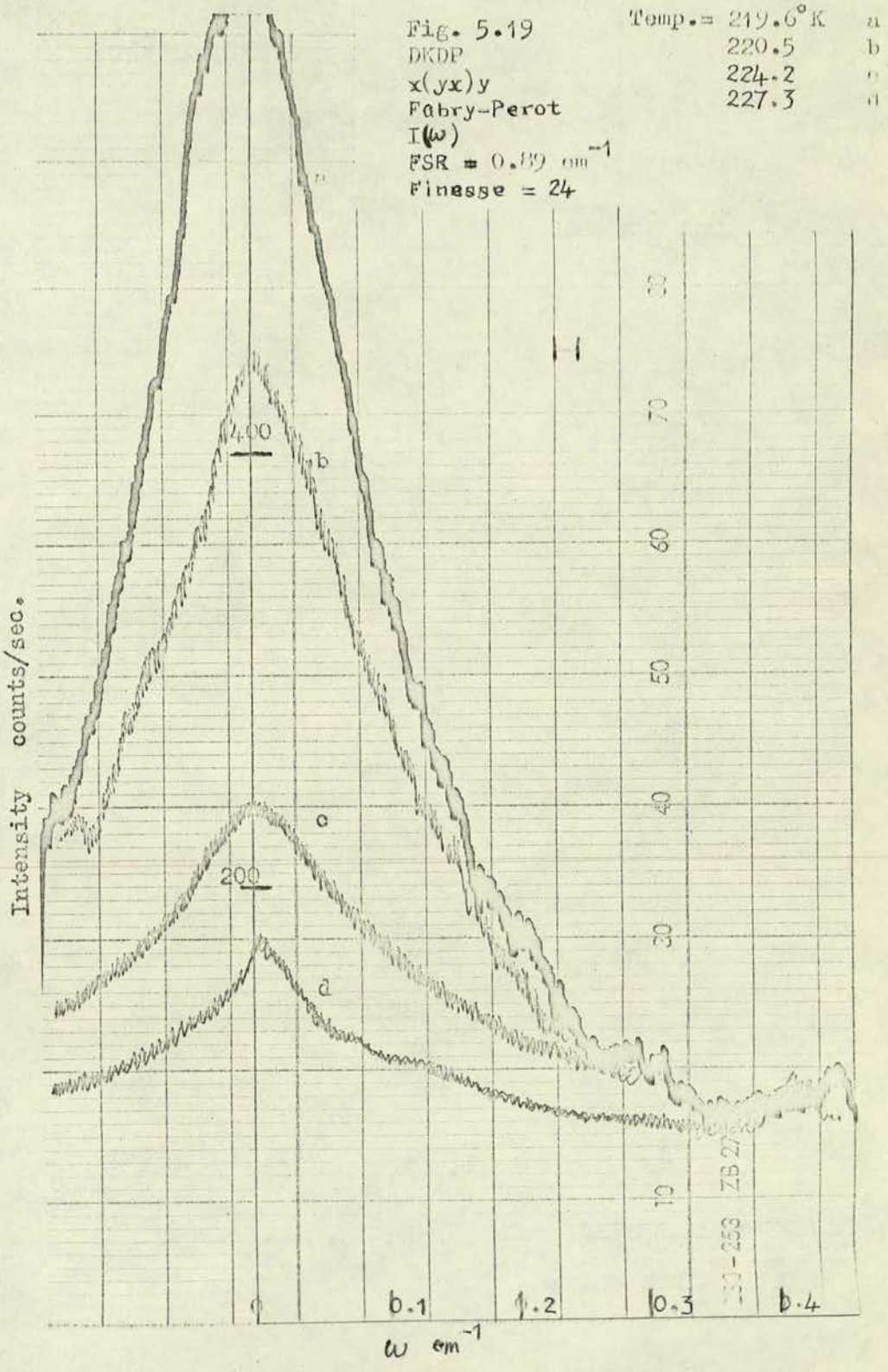
Fig. 5.19
DKDP
x(yx)y
Fabry-Perot
I(ω)
FSR = 0.89 cm⁻¹
Finesse = 24
Temp.= 219.6°K a
220.5 b
224.2 c
227.3 d
Intensity counts/sec.
400
200
a
b
c
d
0.1
0.2
0.3
0.4
ω cm⁻¹

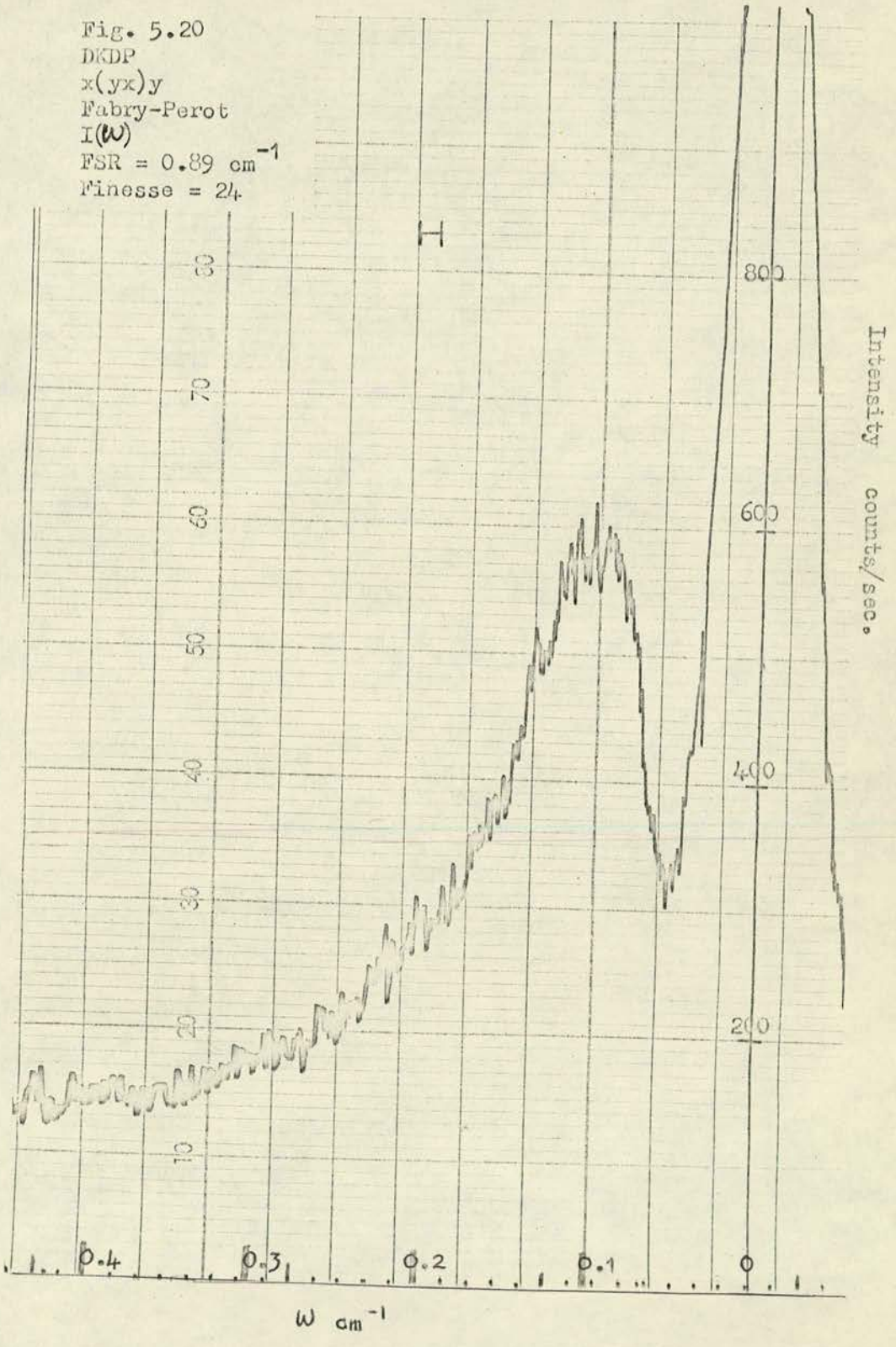
Fig. 5.20
DKDP
x(yx)y
Fabry-Perot
I(ω)
FSR = 0.89 cm⁻¹
Finesse = 24
H
80
70
60
50
40
30
20
10
800
600
400
200
0
Intensity counts/sec.
0.4
0.3
0.2
0.1
0
ω cm⁻¹

There appears little coupling between the longitudinal acoustic mode at 0·445 cm^{-1} and the transverse optic wing at any temperature. Similarly, none of the other optic modes of B_2 symmetry are near enough to the wing to give any noticeable coupling.

CONCLUSIONS

There are several general features of the results. The intensity at high frequencies is temperature independent, with a $\frac{1}{\omega^2}$ frequency behaviour. As the temperature is lowered, the onset of the $\frac{1}{\omega^2}$ portion shifts to lower frequencies. The effect on the intensity at a given point on the wing, is that it increases as the temperature is lowered until the $\frac{1}{\omega^2}$ behaviour descends to that frequency, after which the intensity remains constant on further cooling. In order that the above behaviour satisfies the Debye relaxation function, which appears to be a reasonable fit to the data, the parameters A and τ are required to have the same temperature behaviour. It is likely, from what has been said in earlier sections, that their temperature dependence will be either $\frac{Tc}{T-Tc}$ or $\frac{T}{T-Tc}$.

The values of A and τ, obtained from the Debye fit to the data, are listed in table 5·2 and plotted against the above variables of figures 5·21-5·26. The uncertainties in the results of the fitting procedure are evident in the wide spread of the points on these graphs. It is thus not immediately obvious which of the two temperature dependences gives the better straight line fit. Although $\frac{1}{A} \sim T^{o}K$ and $\frac{1}{A} \sim \frac{10^3}{T^{o}K}$ appear equally likely when considering the values obtained below room temperature, (figures 5·22 and 5·24) it is at high temperatures that the functions differ most. In this region the data favours $A \propto \frac{Tc}{T-Tc}$ against $A \propto \frac{T}{T-Tc}$, since the extrapolated Curietemperature

TABLE 5·2

f cm^{-1}	Temp $T^{o}K$	$\omega_{\frac{1}{2}}$ cm^{-1}	A	f cm^{-1}	Temp $T^{o}K$	$\omega_{\frac{1}{2}}$ cm^{-1}	A
60·8	297	2·46	779·5	14·3	290·7	1·16	106·1
	314	3·28	656·2		278·0	1·71	158·6
	335	4·00	558·1		265·8	1·28	173·8
	361	5·36	472·9		254·0	1·22	223·6
	297	2·88	402·8		290·4	1·71	170·1
	314	3·41	309·4		278·4	1·61	205·4
	335	4·65	274·2		264·2	1·37	256·3
	361	5·50	221·0		255·8	0·788	322·3
35·4	275·1	1·37	607·7		289·9	1·61	143·9
	282·8	1·67	498·1		273·3	1·39	154·2
	291·6	2·02	411·8		255·5	0·842	238·7
	299·0	2·04	395·4		240·5	0·660	271·4
	281	2·37	722·1		289·4	1·37	75·86
	290	2·30	633·9		274·0	1·07	91·44
	299	2·48	586·3		257·3	0·845	114·5
	315	2·89	472·2		244·1	0·748	160·3
	335	2·54	385·7				
	364	4·05	275·2		244·1	0·560	53·15
					234·4	0·399	64·28
31·0	220·7	NO UNIQUE FIT			220·9	0·465	214·6
	239·0	1·33	983·3				
	257·1	1·63	814·4	10·96	290·0	1·85	64·84
	274·4	1·91	752·1		268·7	1·22	86·45
	286·9	2·06	608·0		250·6	0·83	134·20
					238·6	0·64	179·20
	278·4	1·84	797·2				
	291·5	2·10	693·6		289·0	1·73	78·32
	308·5	2·77	551·0		273·4	1·28	106·20
	320·2	3·06	492·8		259·1	1·00	141·10
	338·1	3·18	405·5		248·7	0·822	176·3
	351·9	3·41	335·0		232·8	0·461	289·4
14·3	364·9	0·51	73·23	7·28	288·0	1·51	123·6
	351·4	1·18	63·61		272·8	1·35	215·7
	337·0	1·48	84·98		256·7	1·09	317·6
	323·3	2·32	138·1		242·5	1·804	409·5
	310·0	1·76	164·4		232·7	0·626	499·4
	293·8	2·00	235·6		220·8	0·237	1088

f cm^{-1}	Temp $T^{o}K$	$\omega_{\frac{1}{2}}$ cm^{-1}	A	f cm^{-1}	Temp $T^{o}K$	$\omega_{\frac{1}{2}}$ cm^{-1}	A
5·44	291·4	1·44	58·52	0·89	227·5	0·214	14·32
	275·2	0·799	80·00		225·5	0·219	25·51
	255·0	0·881	197·8		224·2	0·212	24·52
	237·2	0·630	250·0		223·7	0·180	22·05
					223·3	0·148	18·15
	275·2	1·26	109·4				
	255·0	0·749	178·4		221·1	0·154	35·96
	237·2	0·530	345·4		220·9	0·144	36·11
	225·3	0·392	501·2		220·7	0·145	29·05
					220·7	0·144	36·06
1·90	232·5	0·352	18·20		220·5	0·137	34·41
	229·1	0·296	22·05				
	225·5	0·228	27·06		220·0	0·139	46·98
	224·3	0·238	28·47		219·7	0·124	54·20
	224·0	0·188	26·86		219·5	0·121	61·11
	223·8	0·195	30·26				
	223·2	0·179	30·87				
	221·6	0·184	33·22				
	221·1	0·175	35·84				
	229·4	0·290	18·06				
	225·1	0·254	24·94				
	223·0	0·207	28·13				
	221·2	0·140	39·67				
	220·9	0·132	39·92				
0·89	236·9	0·258	9·095				
	229·6	0·224	25·64				
	224·1	0·222	71·98				
	229·0	0·264	19·41				
	226·9	0·145	22·10				
	222·1	0·152	52·52				
	225·9	0·216	15·77				
	221·1	0·148	29·64				
	220·2	0·102	29·74				
	234·4	0·155	3·01				
	227·4	0·221	22·18				

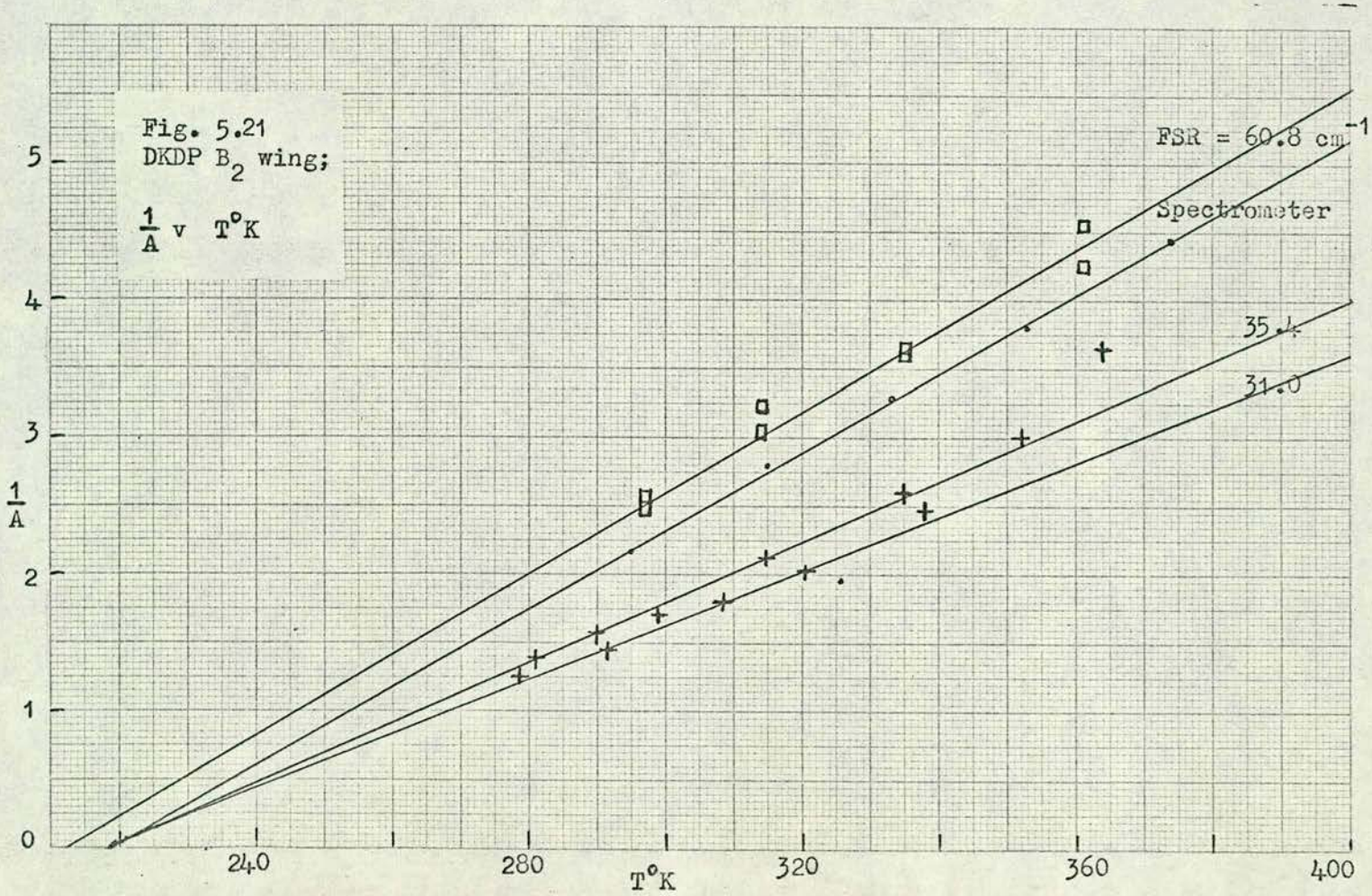
Fig. 5.21
DKDP B_2 wing;
$\frac{1}{A}$ v T°K
FSR = 60.8 cm^{-1}
Spectrometer
35.4
31.0
$\frac{1}{A}$
T°K
0
1
2
3
4
5
240
280
320
360
400

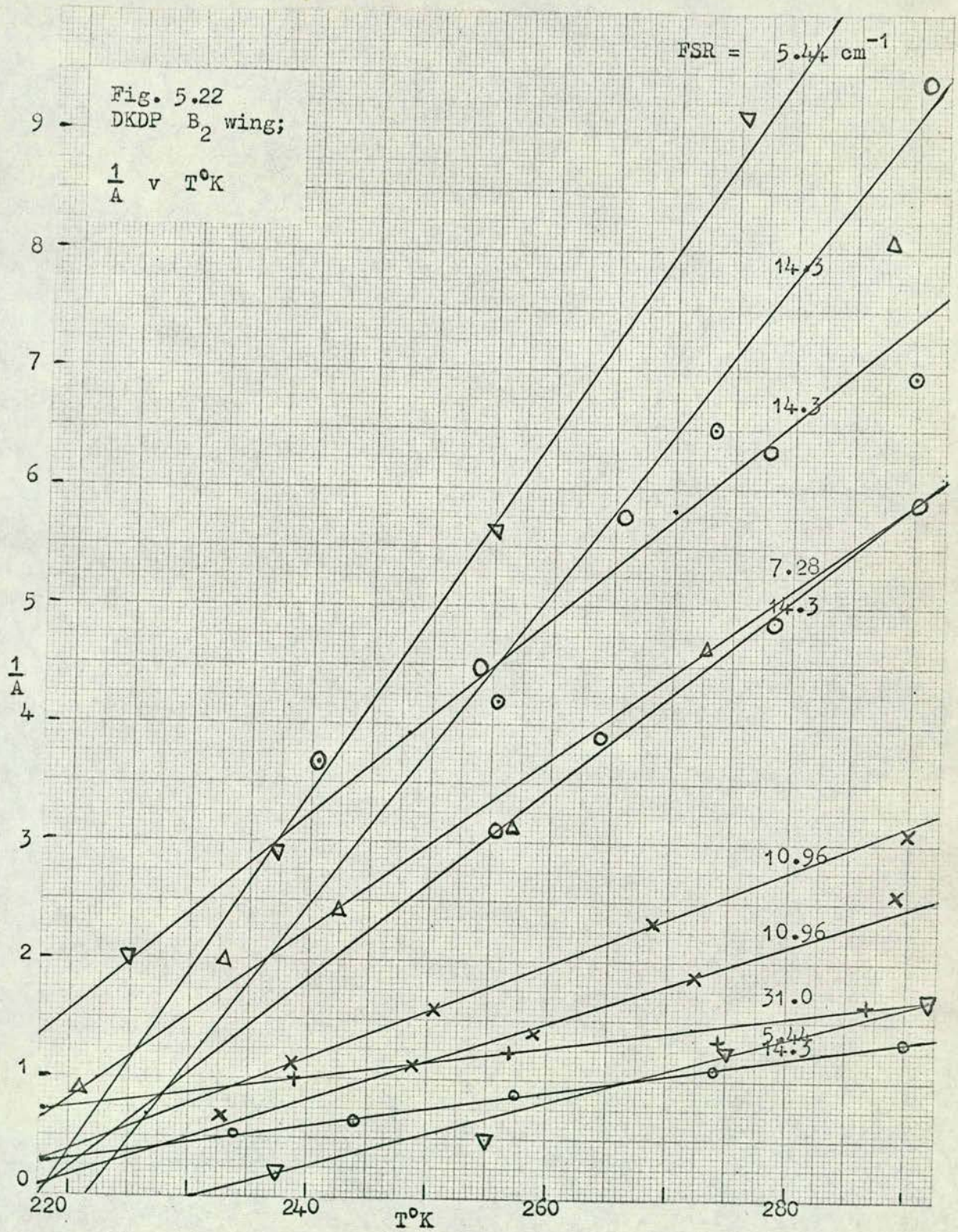
Fig. 5.22
DKDP B_2 wing;
$\frac{1}{A}$ v T^oK
FSR = 5.44 cm^{-1}
14.3
14.3
7.28
14.3
10.96
10.96
31.0
5.44
14.3
$\frac{1}{A}$
T^oK
0
1
2
3
4
5
6
7
8
9
220
240
260
280

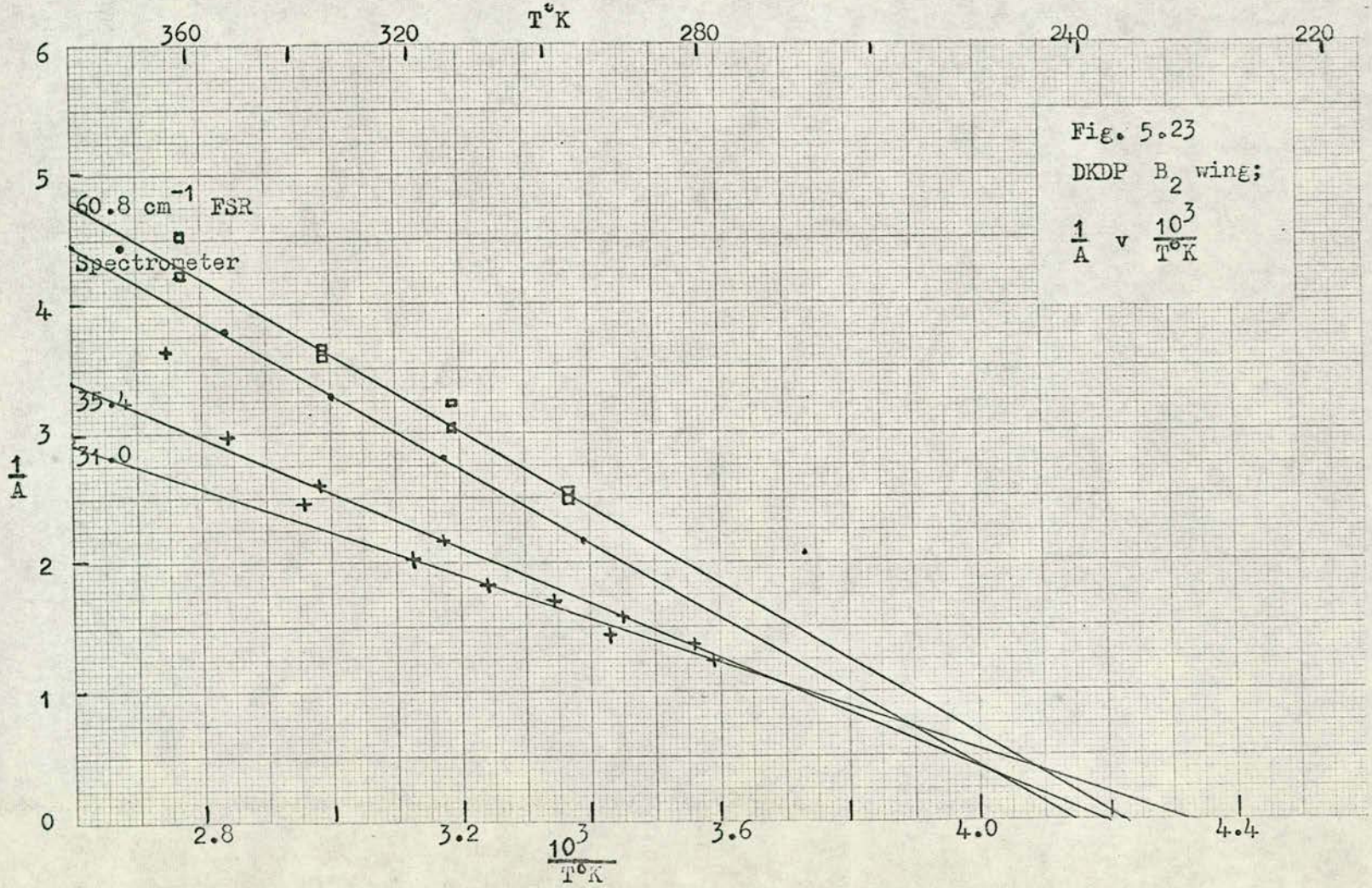
T°K
360
320
280
240
220
6
5
4
3
2
1
0
1/A
60.8 cm⁻¹ FSR
Spectrometer
35.4
31.0
2.8
3.2
3.6
4.0
4.4
10³/T°K
Fig. 5.23
DKDP B2 wing;
1/A v 10³/T°K

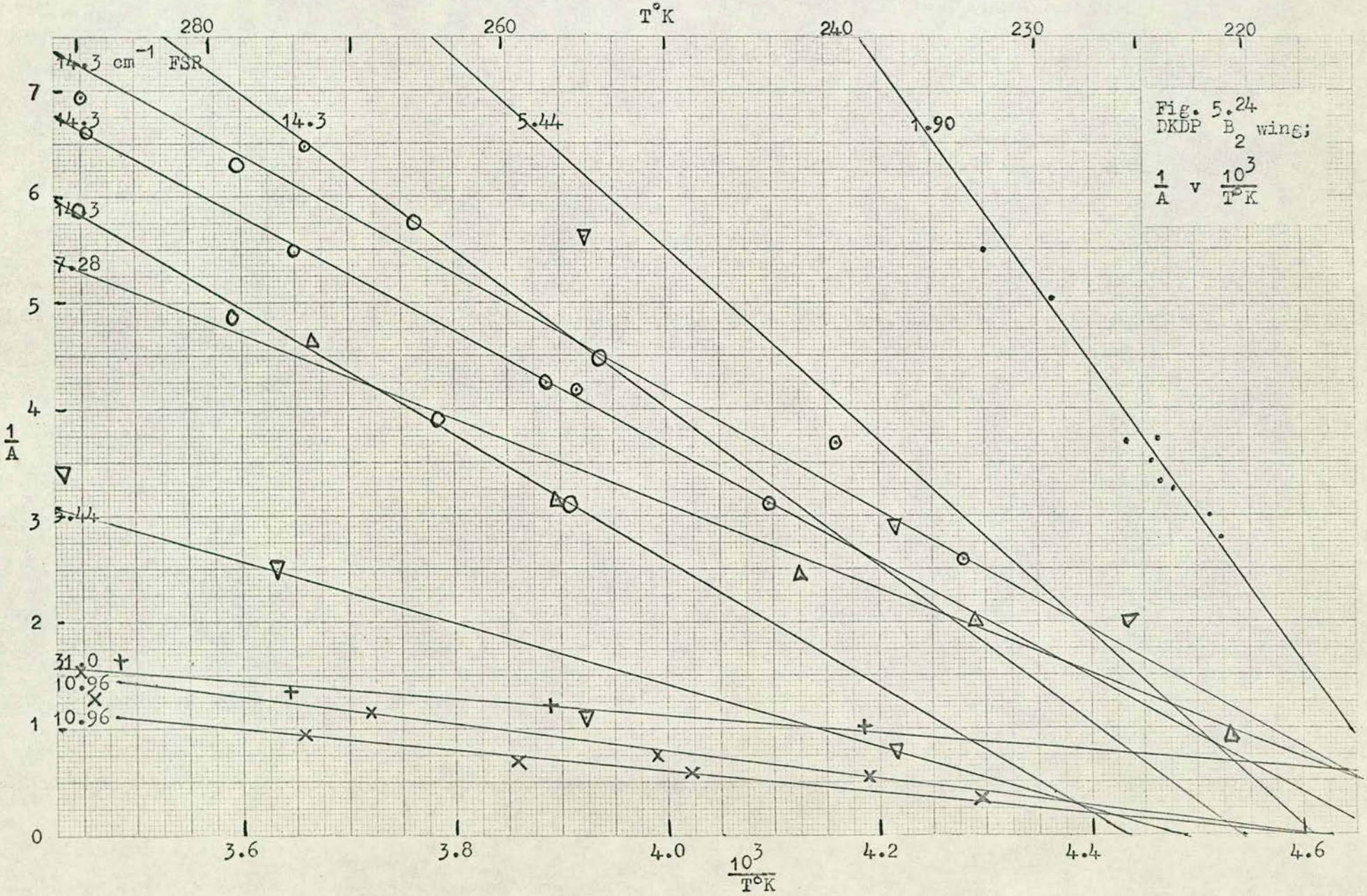
T°K
280
260
240
230
220
14.3 cm⁻¹ FSR
14.3
14.3
14.3
7.28
5.44
5.44
1.90
31.0
10.96
10.96
1/A
0
1
2
3
4
5
6
7
3.6
3.8
4.0
4.2
4.4
4.6
10³/T°K
Fig. 5.24
DKDP B2 wing;
1/A v 10³/T°K

Fig. 5.25
DKDP B_2 wing;
Half-width ~ Temperature

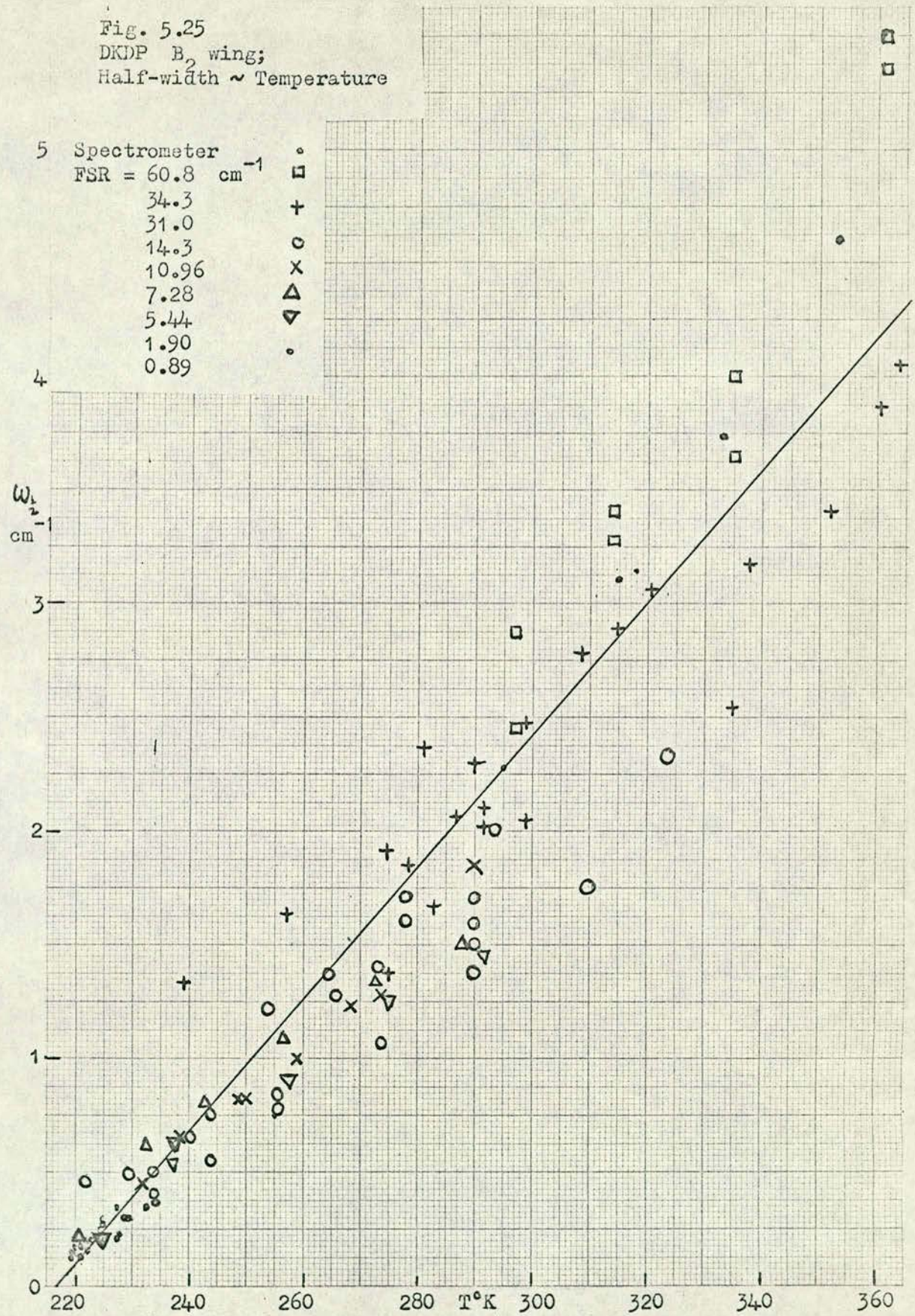

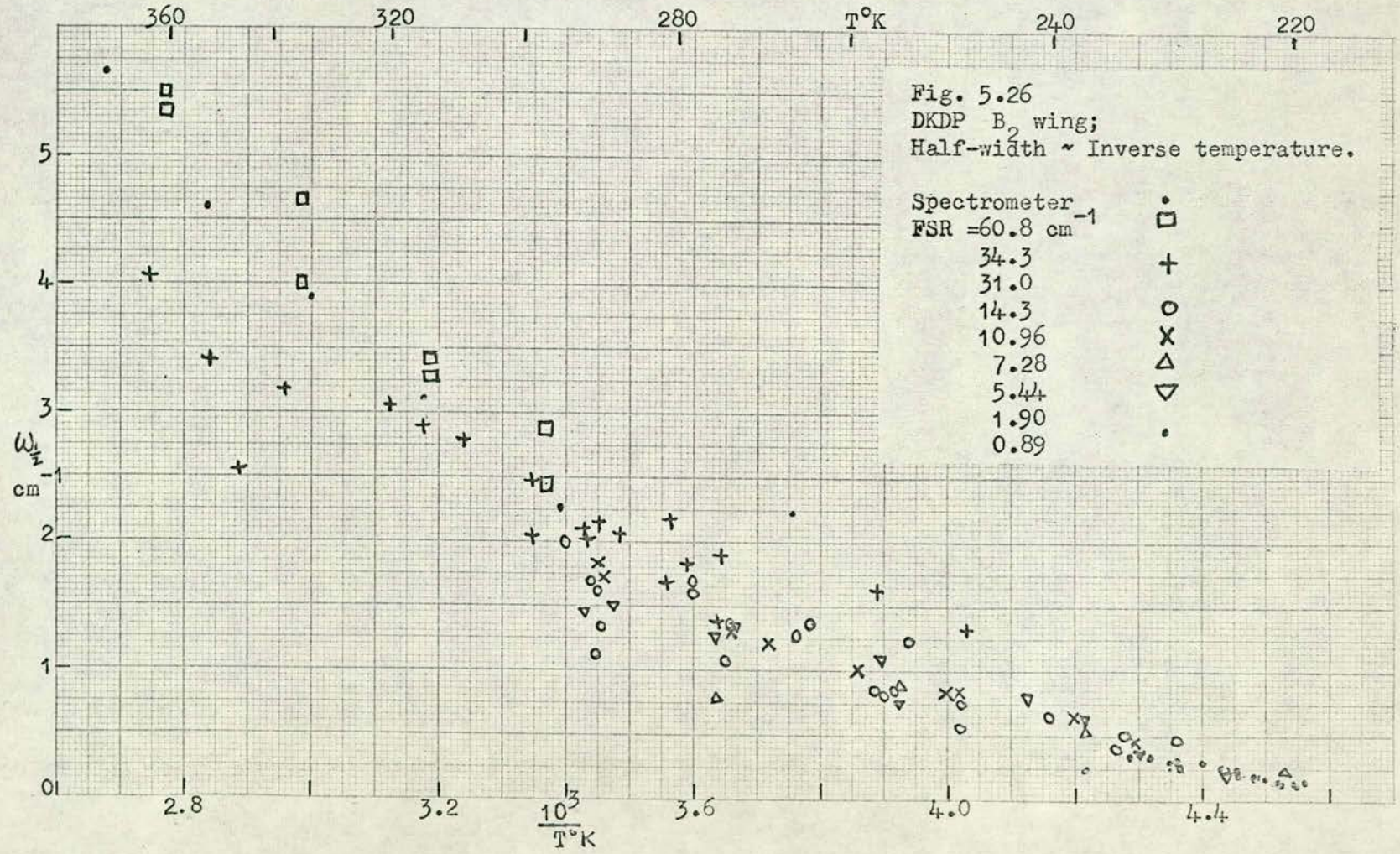

Fig. 5.26
DKDP B_2 wing;
Half-width ~ Inverse temperature.

Spectrometer FSR (cm^{-1})	
60.8	□
34.3	+
31.0	○
14.3	×
10.96	△
7.28	▽
5.44	·
1.90	
0.89	

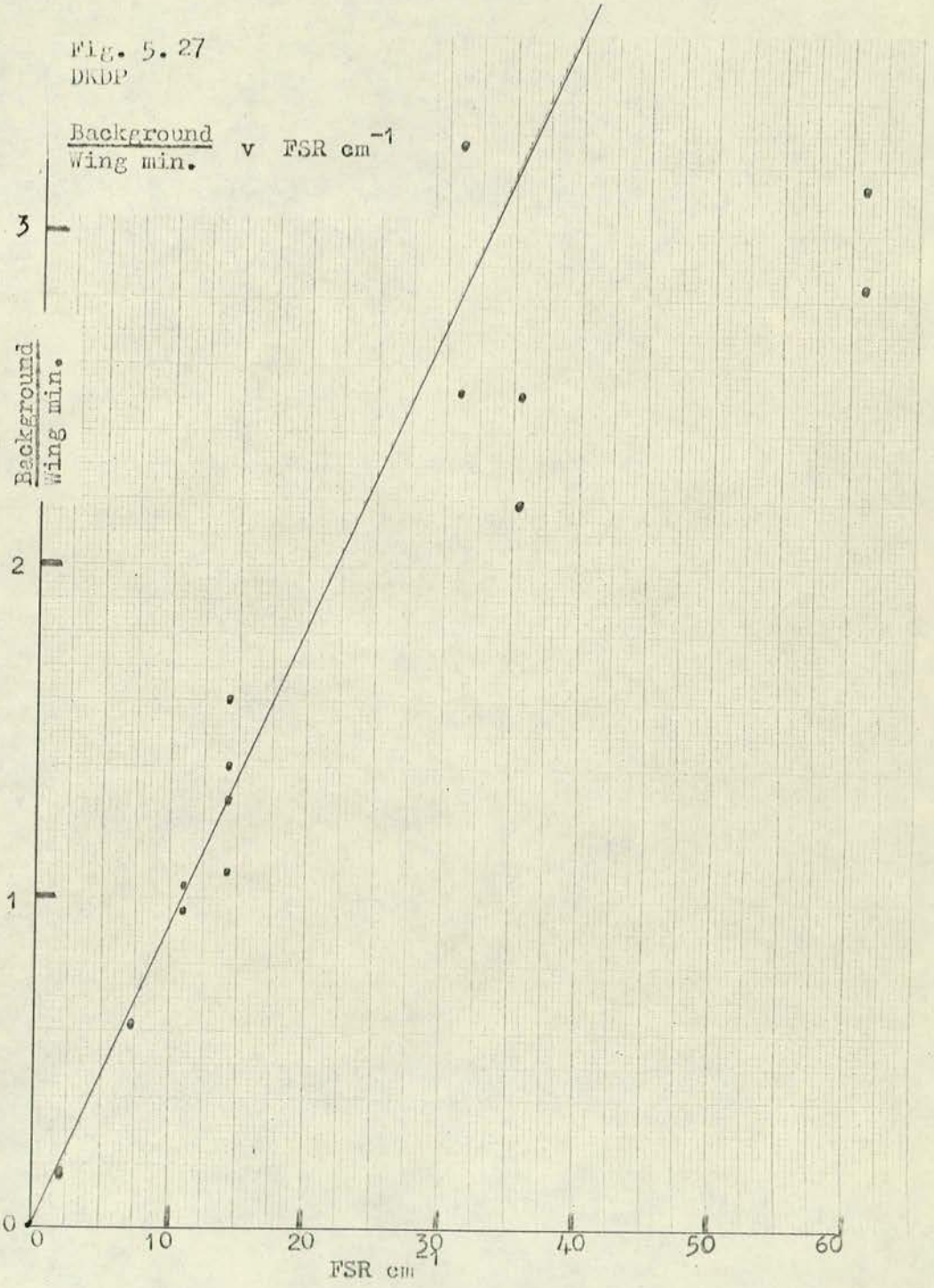
Fig. 5.27
DKDP
Background / Wing min. v FSR cm⁻¹
Background / Wing min.
3
2
1
0
0
10
20
30
40
50
60
FSR cm⁻¹

for the former is just below the transition temperature, as in KDP, while it is some 20 degrees higher for the latter. Since $A \propto \frac{Tc}{T-Tc}$ and as it is known that $\chi(o) \propto \frac{1}{T-Tc}$, it is likely that the decrease of the phonon population factor, $n(\omega)$, on cooling is cancelled by an increase in the electro-optic tensor component $\mathcal{J}_{123}$ - some evidence for this behaviour in ADP was given earlier (5·3).

Of the two possibilities, the half width does seem better fitted by $\omega_{\frac{1}{2}} \propto (T-Tc)$ although the uncertainties are large. Thus A and τ are found to have the same temperature dependence in agreement with the temperature independent intensity behaviour at high frequencies. The values obtained are:-

$$\omega_{\frac{1}{2}} = 0{\cdot}029\ (T-Tc)\ cm^{-1} \qquad (5{\cdot}25)$$

or $$\tau = \frac{1{\cdot}83 10^{-10}}{T-Tc} \quad secs$$

with $Tc = 216{\cdot}5^{o}K$

while $To = 219{\cdot}4^{o}K$, the transition temperature.

The uncertainty in $\omega_{\frac{1}{2}}$ is about $\pm$ 15%.

DKDP E WING

SPECTROMETER RESULTS

Using the x(zx)z orientation, the Stokes and anti-Stokes intensities were recorded at a number of temperatures above room temperature. Typical spectra for this mode, which appeared as a wing on the Rayleigh line, are shown in figure 5·28. This wing is much weaker than the B_2 mode, although similar in extent. There is a suggestion of some temperature variation, with the intensity at high frequencies increasing with temperature while that at low frequencies decreases.

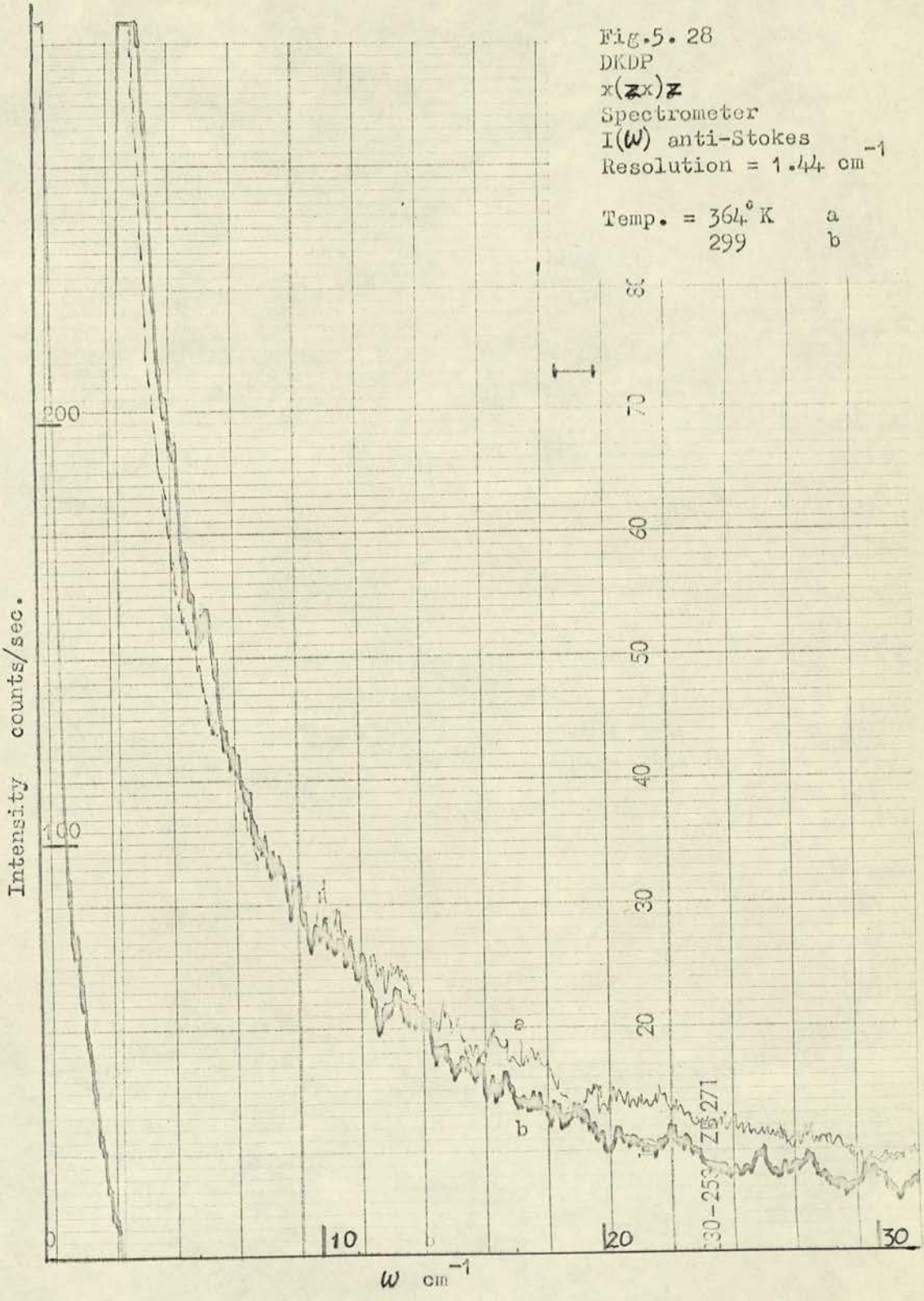
Fig.5. 28
DKDP
x(zx)z
Spectrometer
I(W) anti-Stokes
Resolution = 1.44 cm⁻¹
Temp. = 364° K a
299 b
Intensity counts/sec.
200
100
0
10
20
30
W cm⁻¹
80
70
60
50
40
30
20
a
b
30-253 Z65 271

The increase in intensity is probably due to the increase in phonon population, while the decrease at lower frequencies may be due to moving away from a thwarted a-axis instability linked to the high dielectric constant $\epsilon_a(o)$. However, the temperature dependence of the intensity is small - being comparable to the noise fluctuations on the signal. The intensity at 11·75 cm^{-1} remained constant on varying the temperature in the range 295°K-360°K. Since the observed temperature variations were weak, it was decided that little additional information would be obtained from spectra recorded below room temperature.

A Debye relaxation function plus background - equation (5·8) - was found to give a reasonable fit. Although both A and τ tended to decrease slightly on heating, the values obtained differed by about their uncertainty. Only the mean value for spectra at all temperatures is really meaningful since the extrapolated Curie temperature varied widely indeed. The fitting procedure gives

$$\omega_{\frac{1}{2}} = 8{\cdot}45 \text{ cm}^{-1} \qquad (5{\cdot}26)$$

or $\tau = 6{\cdot}29\ 10^{-13}$ secs

with an uncertainty of ± 15%. The multiphonon background is about 6 counts/sec.

Since the wing intensity is negligible at 100 cm^{-1}, it does not couple to the two other modes of E symmetry which occur in that region of the spectrum.

INTERFEROMETER RESULTS

Spectra, shown in figures 5·29, 5·30, were obtained at several temperatures at a free spectral range of 70·3 cm^{-1}, both with and

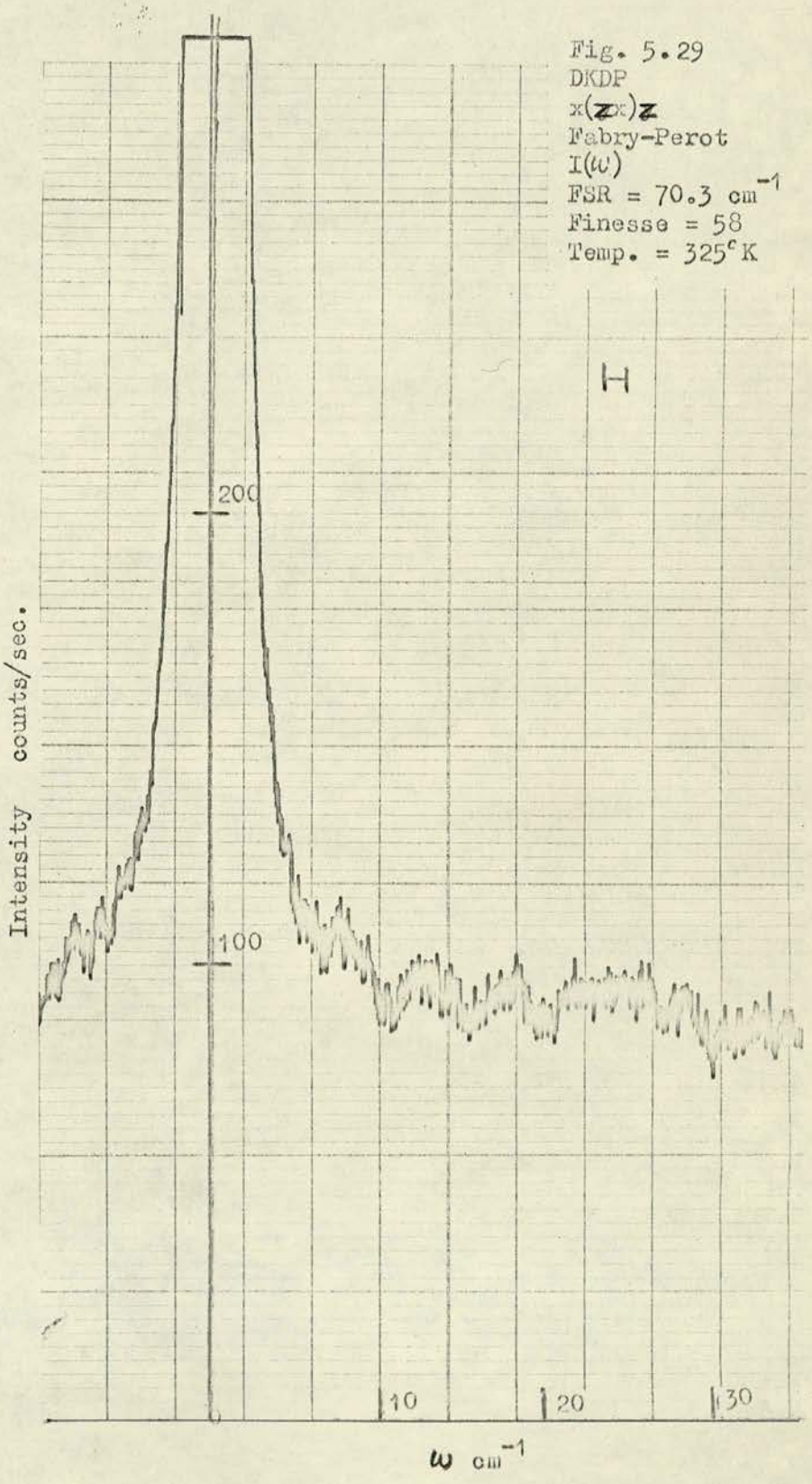
Fig. 5.29
DKDP
x(zx)z
Fabry-Perot
I(ω)
FSR = 70.3 cm⁻¹
Finesse = 58
Temp. = 325°K
H
200
100
Intensity counts/sec.
10
20
30
ω cm⁻¹

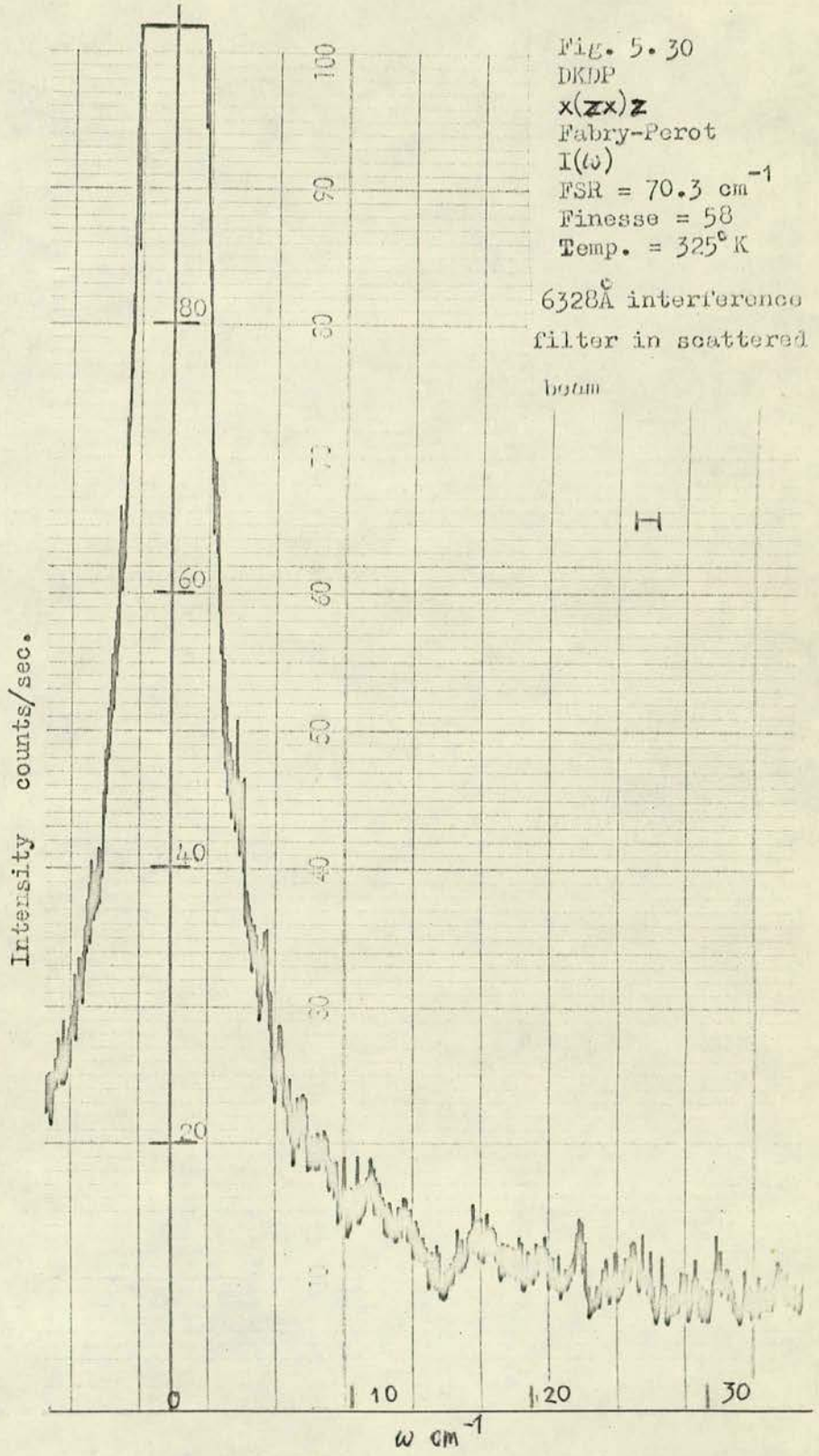
Fig. 5.30
DKDP
x(zx)z
Fabry-Perot
I(ω)
FSR = 70.3 cm-1
Finesse = 58
Temp. = 325° K
6328Å interference
filter in scattered
beam
Intensity counts/sec.
100
80
60
40
20
0
10
20
30
ω cm-1

without an interference filter of half width $\pm$ 55 cm^{-1} in the beam. The traces obtained without the filter showed a very weak wing on a stronger background, but the total signal was less than 100 counts/sec. The use of the filter caused higher frequency modes to be rejected and revealed a wing of average intensity about 15 counts/second. No definite temperature dependence was noted in the presence of large noise fluctuations. The distortion of the wing caused by the spectral response of the filter precluded the use of the usual fitting procedure.

No additional information can be obtained by the use of smaller free spectral ranges since even the filtered signal becomes flatter.

ANISOTROPY

Since in the x(zx)z orientation used to study the E symmetry wing, the scattering phonon is not travelling parallel or perpendicular to the C-axis there may be some effects present due to crystal anisotropy. Unfortunately no time was available on the spectrometer apparatus to perform the experiment carefully in the preferable x(yz)y orientation once this discrepancy was found. However some rough experiments had been performed in this orientation earlier, although these were of limited usefulness due to large fluctuations in laser power and a wide Rayleigh peak - the wing intensity could only be determined for $\omega > 20$ cm^{-1}. The observed wing appeared to have the $\frac{1}{\omega^2}$ behaviour. This is consistent with a half width of 8·45 cm^{-1} determined above in the x(zx)z setting. Monitoring the intensity as a function of temperature showed a slight increase in intensity at high frequencies with no temperature dependence at low frequencies. Again this is in general agreement with the previous data.

Reference to Wilson's work on KDP (3·85) shows that frequency shifts due to anisotropy are negligible. Thus the x(zx)z data on DKDP are taken to be a good representation of E mode behaviour.

DADP B_2 WING

The x(yx)y Stokes spectrum was obtained over the range 0-1560 cm^{-1}. The strongest feature was a wing on the Rayleigh peak extending towards 100 cm^{-1}. The next mode was a broad weak band around 216 cm^{-1}, but there was some Raman intensity at all frequencies.

The Stokes and anit-Stokes spectra were obtained at several temperatures above room temperature but no variation was detected. A typical trace is shown in figure 5·31. Monitoring the intensity at 12 cm^{-1} as a function of temperature confirmed the above result.

The Debye Relaxation function plus background again proved a good fit to the average of all the traces obtained, with fitted values of

$$\omega_{\frac{1}{2}} = 10{\cdot}6 \text{ cm}^{-1} \qquad (5{\cdot}27)$$

on $\tau = 5{\cdot}01\ 10^{-13}$ secs

with about a ± 10% uncertainty. The multiphonon background contributes about 5 counts/second.

FABRY-PEROT INTERFEROMETER RESULTS

Spectra were obtained at a free spectral range of 70·3 cm^{-1}, at several temperatures, and both with and without the interference filter in the scattered beam. A weak wing is apparent in figure 5·32 which is more clearly seen in figure 5·33 where the filter has rejected higher frequency modes. No temperature-dependence could be detected in any spectrum.

Fig. 5.31
DADP
Spectrometer
$I(\omega)$ Stokes
Resolution = 1.32 cm^{-1}
Temp. = 379°K
x(yx)y

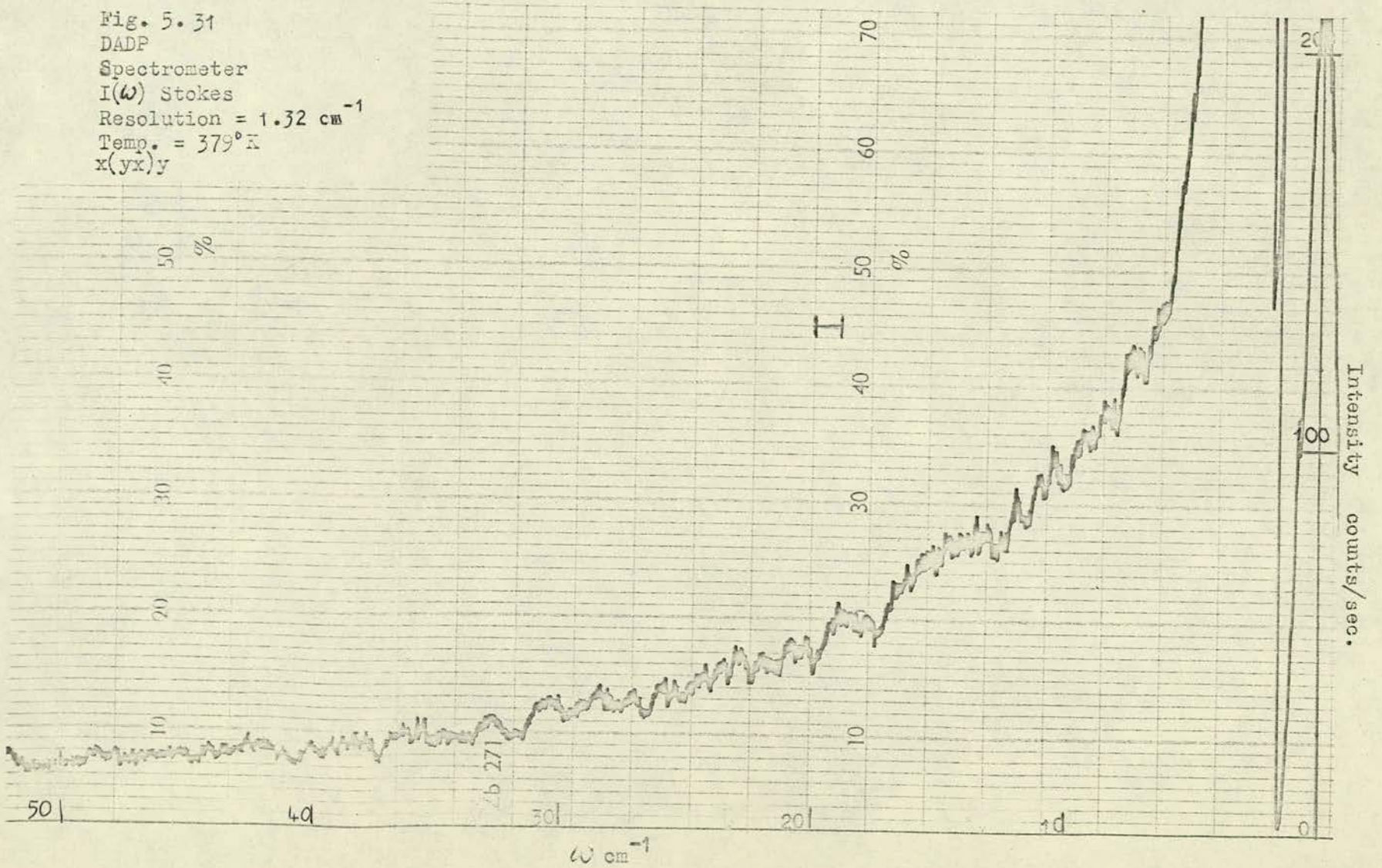

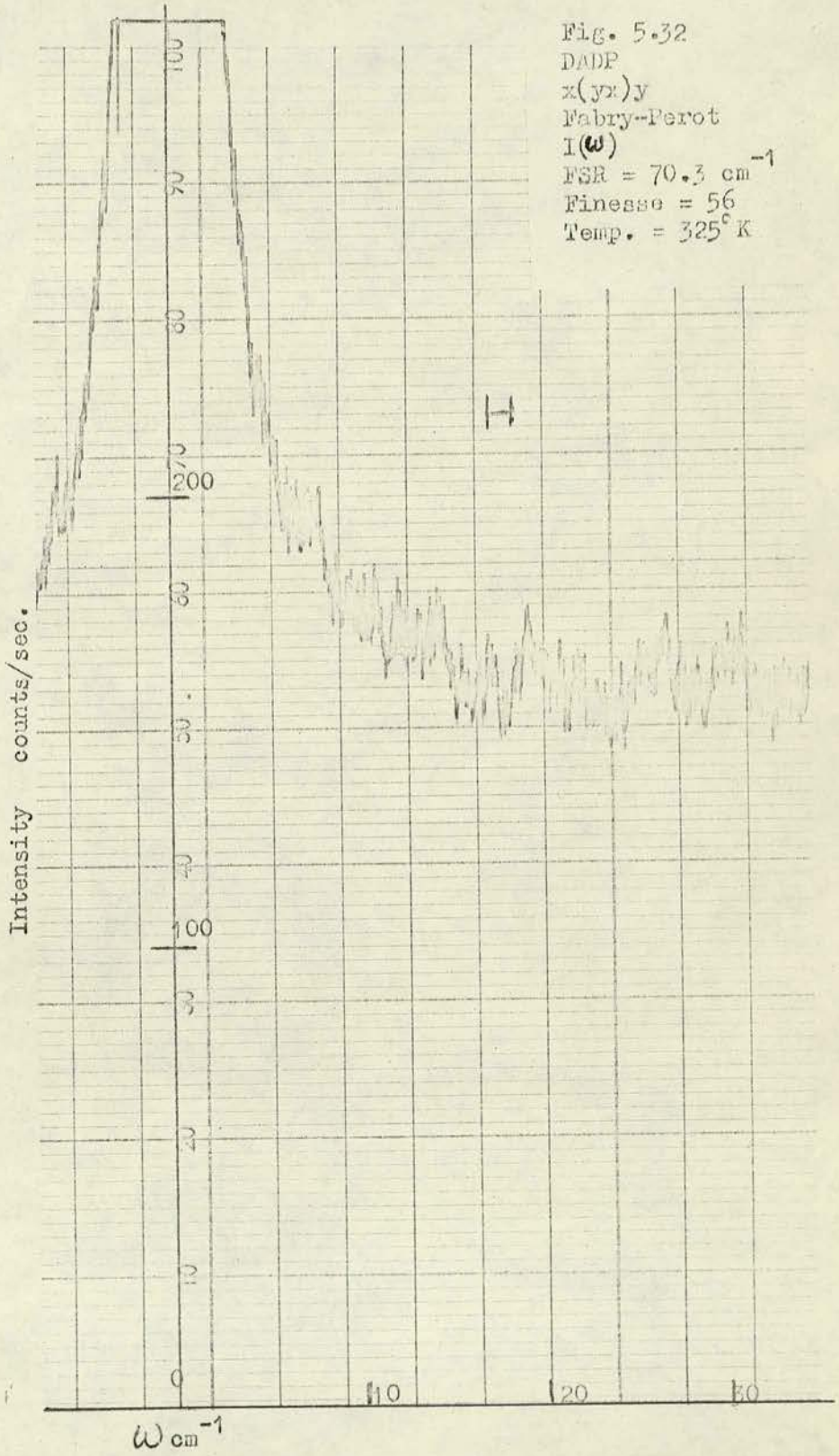
Fig. 5.32
DADP
x(yx)y
Fabry-Perot
I(ω)
FSR = 70.3 cm⁻¹
Finesse = 56
Temp. = 325° K
Intensity counts/sec.
200
100
0
10
20
30
ω cm⁻¹

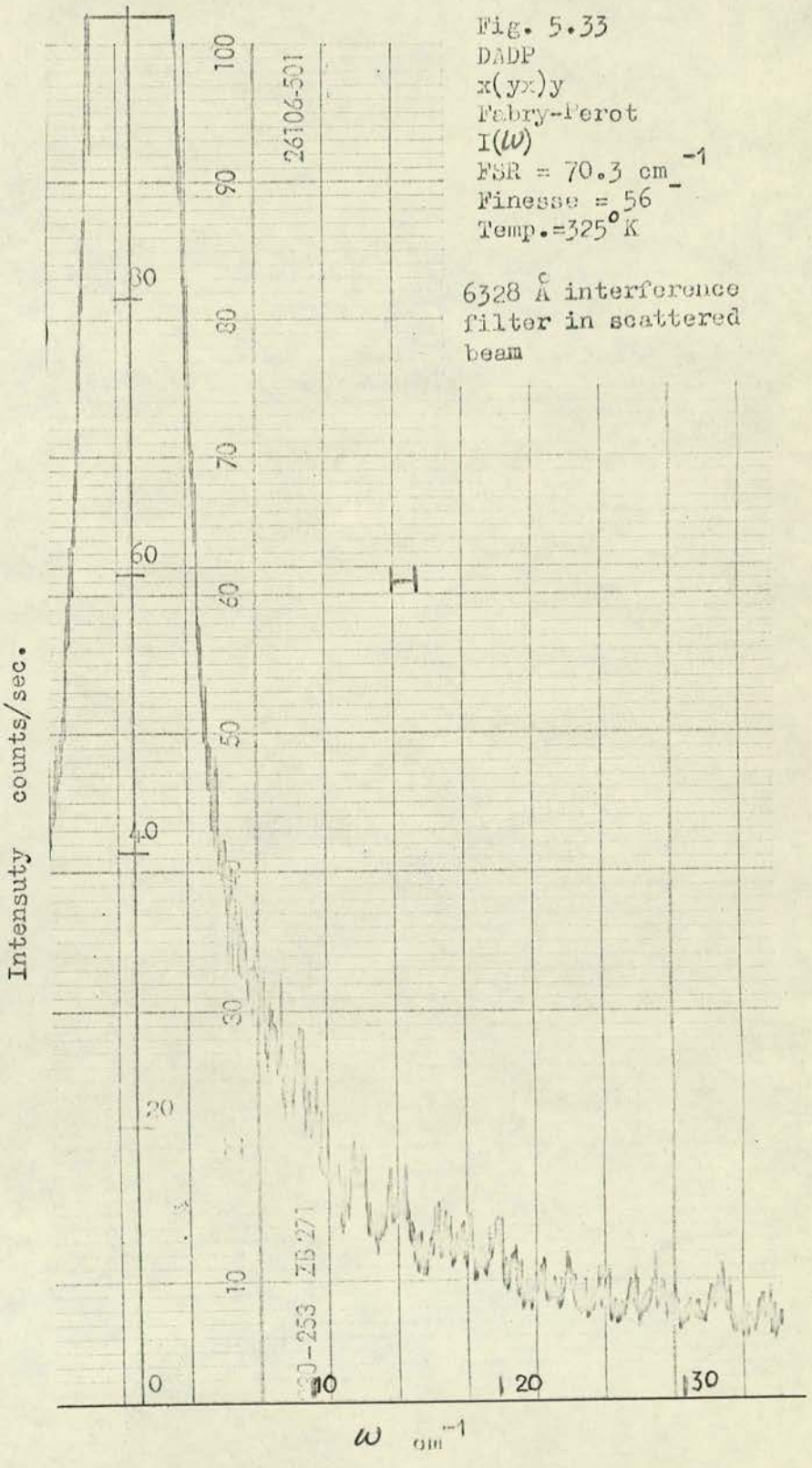
Fig. 5.33
DADP
x(yx)y
Fabry-Perot
I(ω)
FSR = 70.3 cm⁻¹
Finesse = 56
Temp.=325°K
6328 Å interference filter in scattered beam
Intensuty counts/sec.
ω cm⁻¹
26106-501
ZB 271
0
10
20
30
40
50
60
70
80
90
100

The large background and noise fluctuations on the spectra obtained without the filter, and the spectral distortion caused by the filter for those obtained with it, meant that the usual Debye fit could not reliably be performed. The wing intensity, for spectra obtained with the filter, is only 10 counts/second at the half width of the wing - 10·6 cm^{-1}. This is indeed a weak signal.

Since no new information would be obtained at smaller free spectral ranges where the overlapped wing would have negligible curvature, none were used.

CONCLUSIONS

It is of interest that it is not only the wing which is temperature independent, but also all the optic modes which go to make up the background to the unfiltered interferometer spectra. The possibly temperature dependent parameters which affect the intensity of all modes are the appropriate electro-optic tensor component and the phonon population factor. That there is no net temperature dependence indicates that a change in temperature affects these two parameters oppositely. The same behaviour was noted for the B_2 modes in DKDP where the background contribution from higher frequency modes is found to be temperature independent. Evidence for a decrease, with increasing temperature, for the corresponding electro-optic tensor in ADP has alreadybeen given (5·3). The magnitude of this decrease is such as to approximately cancel the increase in intensity due to increasing phonon population. It should be noted that, weak though the signals are, an increase in intensity due solely to the Bose factor would be detectable on the unfiltered interferometer spectra for DADP.

From the above, the parameter A in the Debye function must have the temperature dependence $A \propto \chi_c(o) \propto \frac{1}{T-Tc}$, where Tc is the extrapolated Curie temperature of a frustrated a-axis instability associated with the low frequency wing mode. For the spectra to be temperature independent at high frequencies, τ must have the same behaviour. Thus for frequencies much less than the half width, say 1 cm^{-1}, the wing intensity is frequency independent and is given by

$$I(o) = A\ \tau \propto \left(\frac{1}{T-Tc}\right)^2 \qquad (5\cdot28)$$

Since the temperature function appears squared, it is possible that, provided (T-Tc) is not too large in the paraelectric phase, a significant change in the low frequency intensity could be produced, leading to a determination of Tc. However, due to the multiple overlapping of the wing for small ω even when using an interference filter, which has a flat response in this region, to remove the other modes, it is not possible to make accurate observations on the low frequency part of the wing alone.

DADP E WING

SPECTROMETER RESULTS

A spectrum obtained using the x(zx)z orientation over the range 0-200 cm^{-1} showed a strong wing on the Rayleigh peak extending to ~ 100 cm^{-1} with much less intense underdamped modes at 67 cm^{-1}, having full width at half maximum intensity of 10 cm^{-1}, 114 cm^{-1}, having width 23 cm^{-1}, and a broad band centred on 150 cm^{-1}. While the mode at 67 cm^{-1} is the strongest of the three, it has a peak intensity coresponding only to that of the wing at 30 cm^{-1}.

Stokes and anti-Stokes spectra were obtained at six temperatures in the range 296°K-364°K. (Figure 5·34). At low frequencies the wing intensity decreased somewhat on heating, but at high frequencies no temperature dependence was noted. Monitoring the intensity at 7·5 cm^{-1} while cooling from 360°K to 310°K showed an increase in intensity corresponding to the intensities measured on each of the individual runs. A similar experiment at 19·8 cm^{-1} gave an essentially temperature independent trace.

The usual Debye function, equation (5·8), provided a good fit to the data in the range $\omega < 45$ cm^{-1} where the profile was not complicated by the presence of the other modes. The fitted values are given in the following table - 5·3.

TABLE 5·3

Temp T°K	$\omega_{\frac{1}{2}}$ cm^{-1}	A
296·5	8·20	5818
309·5	9·21	5575
324·0	9·70	5424
339·0	10·09	5193
354·5	10·63	5005
364·0	12·20	5171

The multiphonon background at ~ 60 counts/sec was much stronger than that found in the other three cases.

Figure 5·35 shows the actual spectrum for $\omega < 140$ cm^{-1} compared to the Debye function fitted to the data for $\omega < 45$ cm^{-1}. There appears to be negligible coupling between the lattice modes at 67 cm^{-1} and 114 cm^{-1}, and the wing. This is to be expected since the wing half-width of ~10 cm^{-1} is much lower than either mode, both of which are very much weaker than the wing.

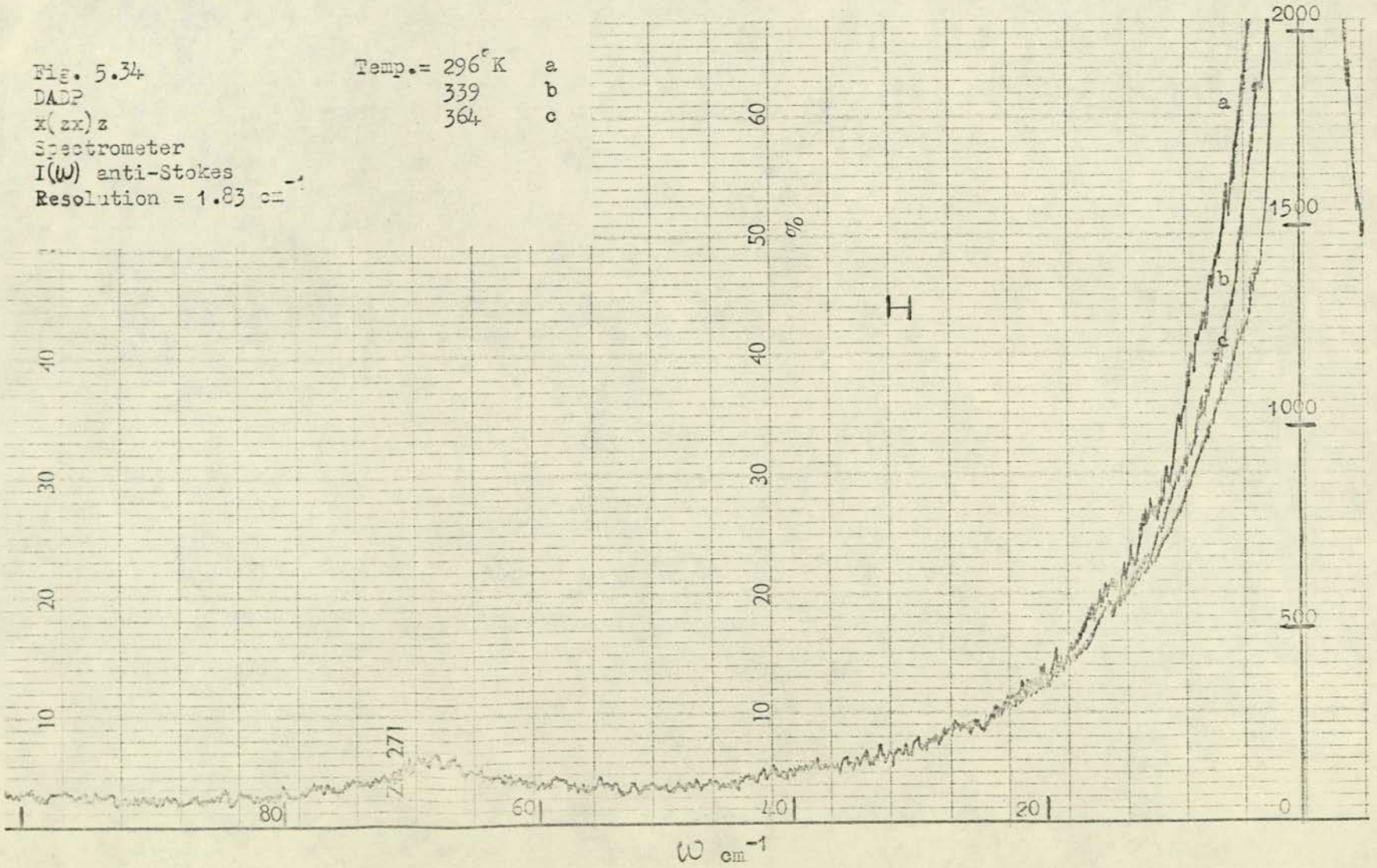
Fig. 5.34
DADP
x(zx)z
Spectrometer
I(ω) anti-Stokes
Resolution = 1.83 cm⁻¹
Temp.= 296°K a
339 b
364 c
2000
1500
1000
500
0
a
b
c
60
50
%
40
30
20
10
H
271
80
60
40
20
ω cm⁻¹
Intensity counts/sec.

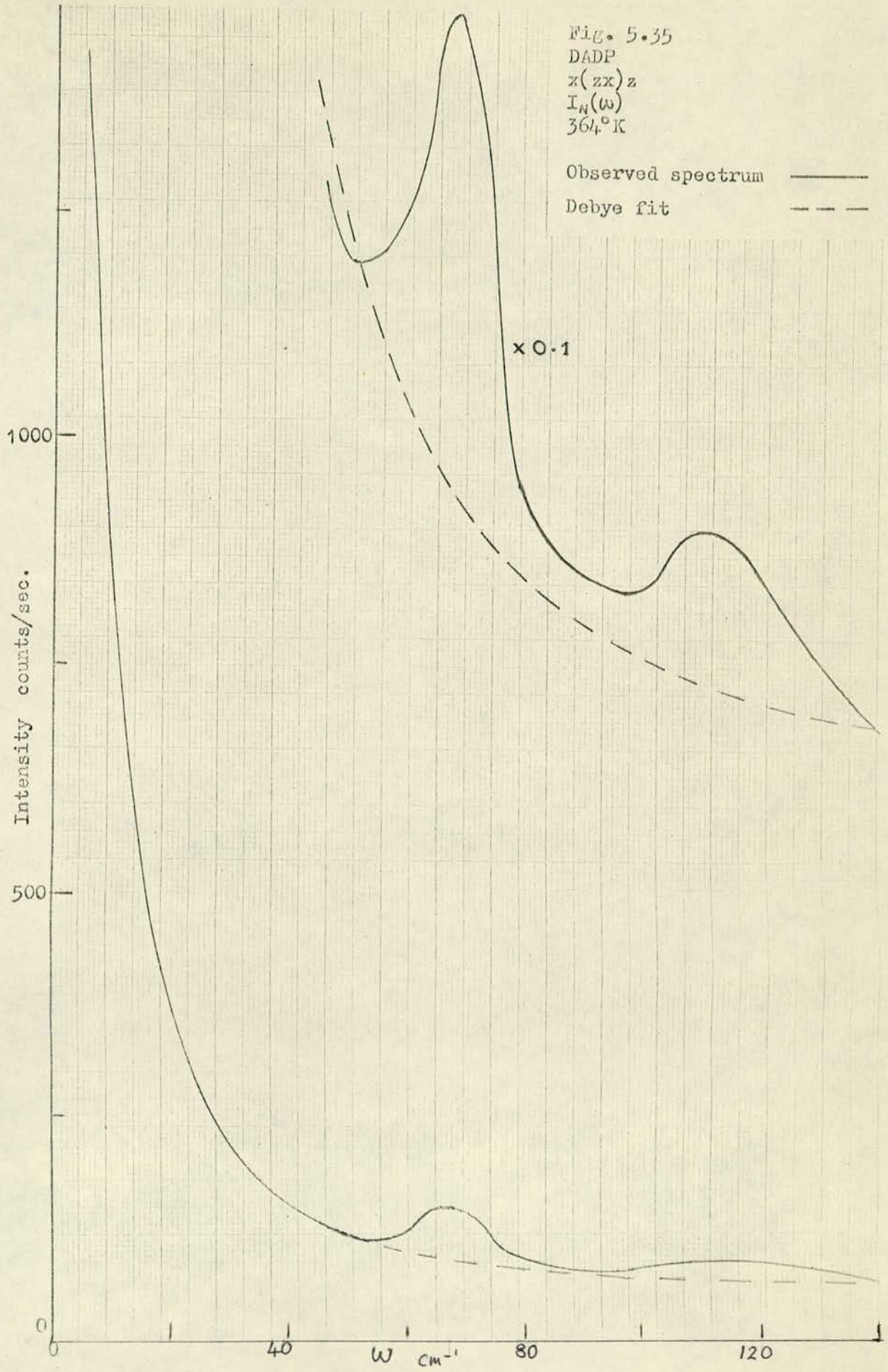
Fig. 5.35
DADP
x(zx)z
$I_N(\omega)$
364°K
Observed spectrum
Debye fit
×0·1
1000
500
0
Intensity counts/sec.
0
40
ω cm⁻¹
80
120

As DADP undergoes an antiferroelectric transition near 245°K, at which the crystal is likely to shatter, and since the temperature dependence of the wing is not strong, it was not thought profitable to investigate the limited region below room temperature.

INTERFEROMETER RESULTS

Spectra, typical of those obtained above room temperature at a free spectral range of 70·3 cm^{-1}, are shown in figure 5·36-5·37. Even without the filter, the wing is evident on top of a strong background. The filter, figure 5·37, removes this background to reveal the wing more clearly. As with the spectrometer traces, the wing becomes weaker at low frequencies on heating. The minimum signal on the unfiltered spectrum, which is due mainly to other Raman lines, does show some increase with increasing temperature, indicating that the phonon population factor is not cancelled by the electro-optic tensor component in this orientation.

Due to the large background, fitting the Debye model plus background was impossible with any reasonable certainty. Figure 5·37 shows two possible fits to a spectrum which lie within the noise fluctuations of that spectrum yet differ in half width by over 100%.

The use of smaller free spectral ranges only makes matters worse by introducing more overlaps into the spectra, and reducing their curvature.

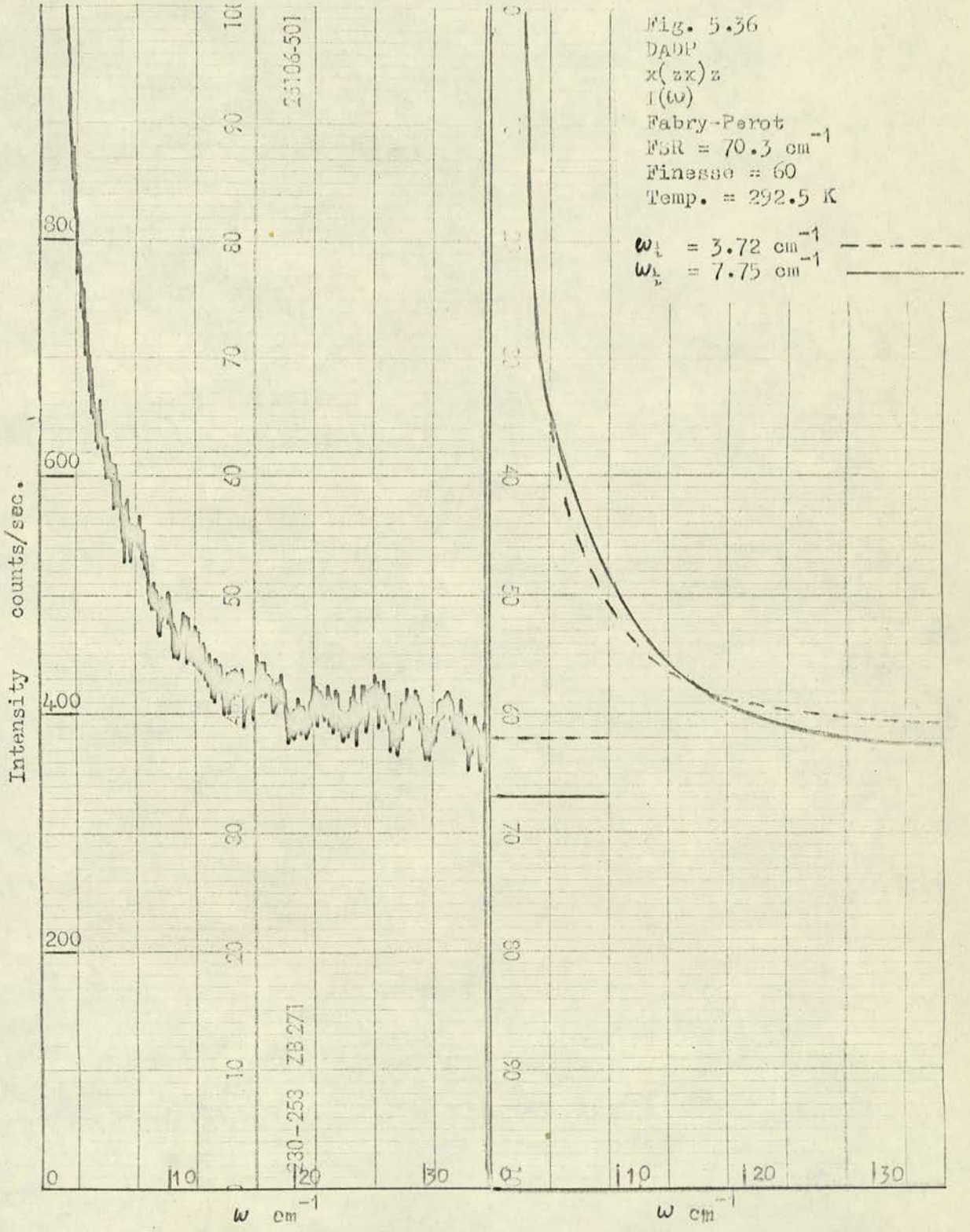
Fig. 5.36
DADP
x(zx)z
I(ω)
Fabry-Perot
FSR = 70.3 cm⁻¹
Finesse = 60
Temp. = 292.5 K
ω₁ = 3.72 cm⁻¹
ω₂ = 7.75 cm⁻¹
Intensity counts/sec.
800
600
400
200
0
10
20
30
ω cm⁻¹
25106-501
230-253 ZB 271

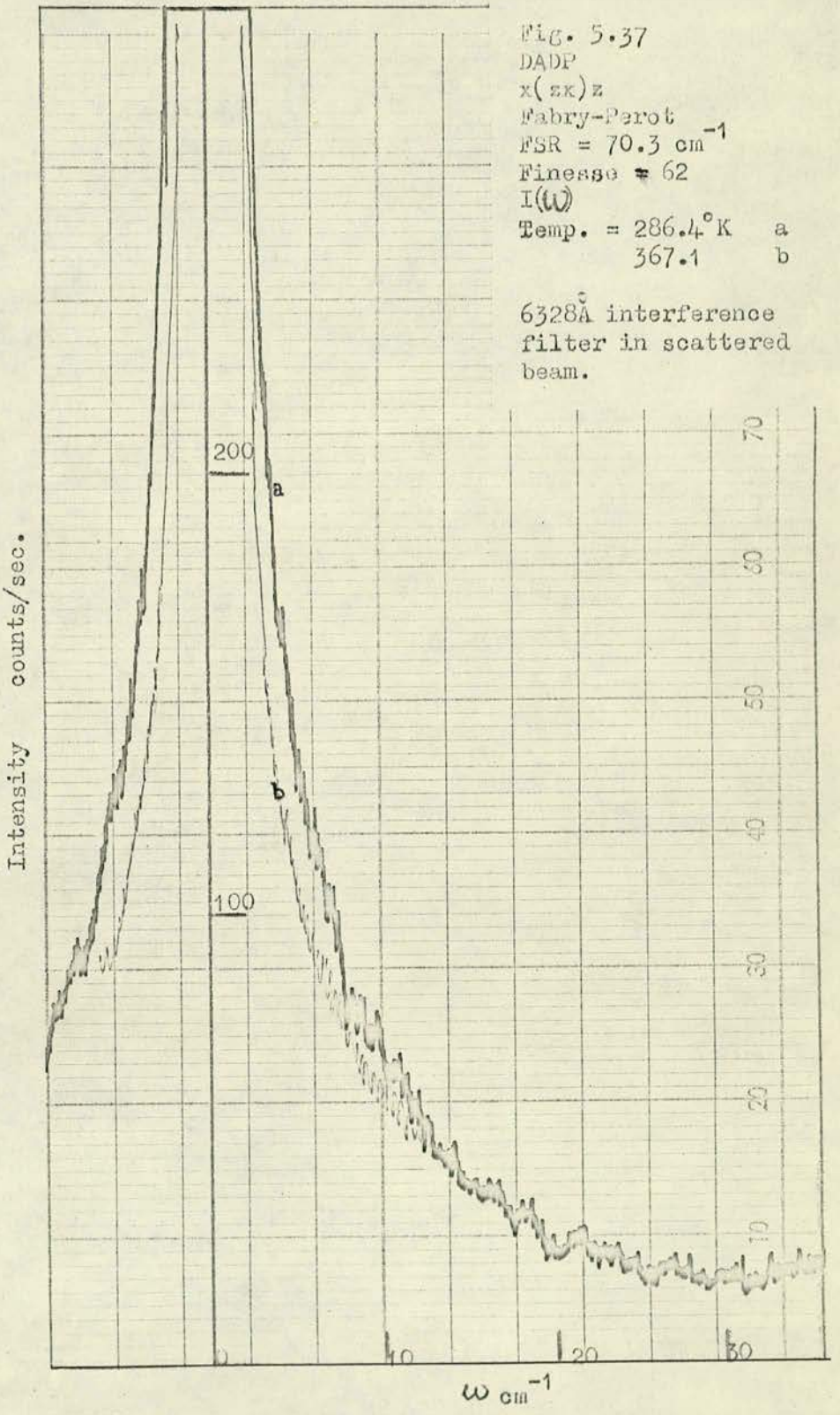

Fig. 5.37
DADP
x(zx)z
Fabry-Perot
FSR = 70.3 cm^{-1}
Finesse = 62
$I(\omega)$
Temp. = 286.4°K a
367.1 b

6328Å interference filter in scattered beam.

CONCLUSIONS

Figures 5·38-5·41 show the values of $\omega_{\frac{1}{2}}$ and $\frac{1}{A}$ obtained on the spectrometer plotted against both T and $\frac{1}{T}$. Apart from the points corresponding to the highest temperature spectrum, all four graphs can be fitted by straight lines; viz

$$A = \frac{3020\ T}{T-143} \qquad (5\cdot28)$$

$$A = \frac{2\cdot17\ 10^{6}}{T + 77} \qquad (5\cdot29)$$

$$\omega_{\frac{1}{2}} = 20\cdot3\ \frac{T-169}{T}\ \text{cm}^{-1} \qquad (5\cdot30)$$

$$\omega_{\frac{1}{2}} = 0\cdot030\ (T-1\cdot8)\ \text{cm}^{-1} \qquad (5\cdot31)$$

The extrapolated values of Tc in the above formulae have uncertainties of typically $\pm$ 8°K.

Although from the quality of fit the two possible temperature dependences for both A and $\omega_{\frac{1}{2}}$ are equally likely, that there was a general rise in the Raman background on heating, for the interferometer results, suggests that A depends on the Bose factor and $\chi(o)$ and is thus given by Equation (5·28), while the apparent temperature independence of the high frequency portion of wing indicates that τ has the same behaviour as A, namely that of equation (5·30). The Curie temperatures obtained from these fits are in better agreement than those from the other pair.

Thus $A = \frac{3020\ T}{T - 143}$ (5·28)

$\omega_{\frac{1}{2}} = 20\cdot3\ \frac{T-169}{T}\ \text{cm}^{-1}$ (5·30)

or $\tau = 2\cdot62\ 10^{-13}\ \frac{T}{T-169}$ secs .

with Tc $\approx$ 156 °K

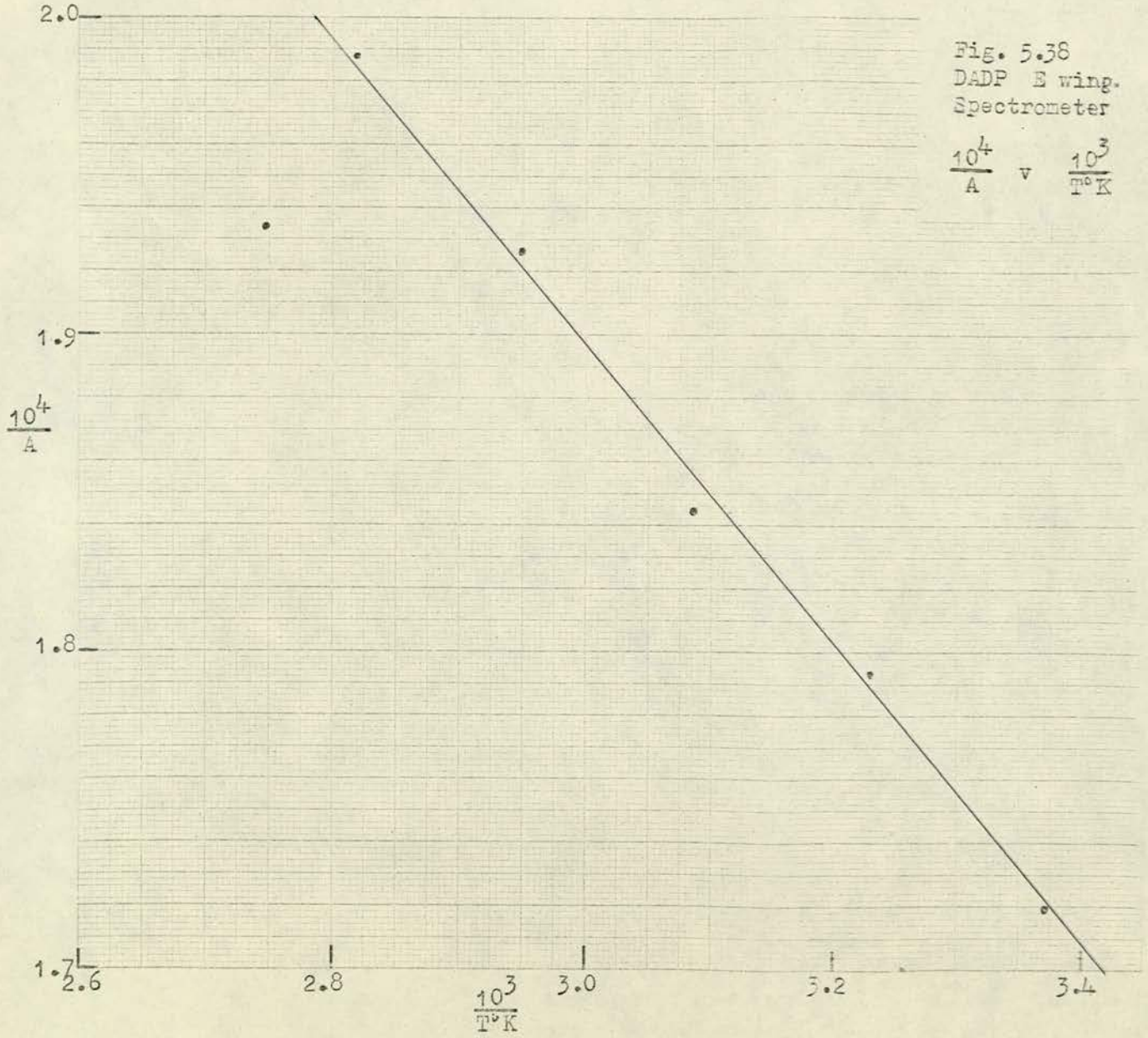

Fig. 5.38
DADP E wing.
Spectrometer

$\frac{10^4}{A}$ v $\frac{10^3}{T°K}$

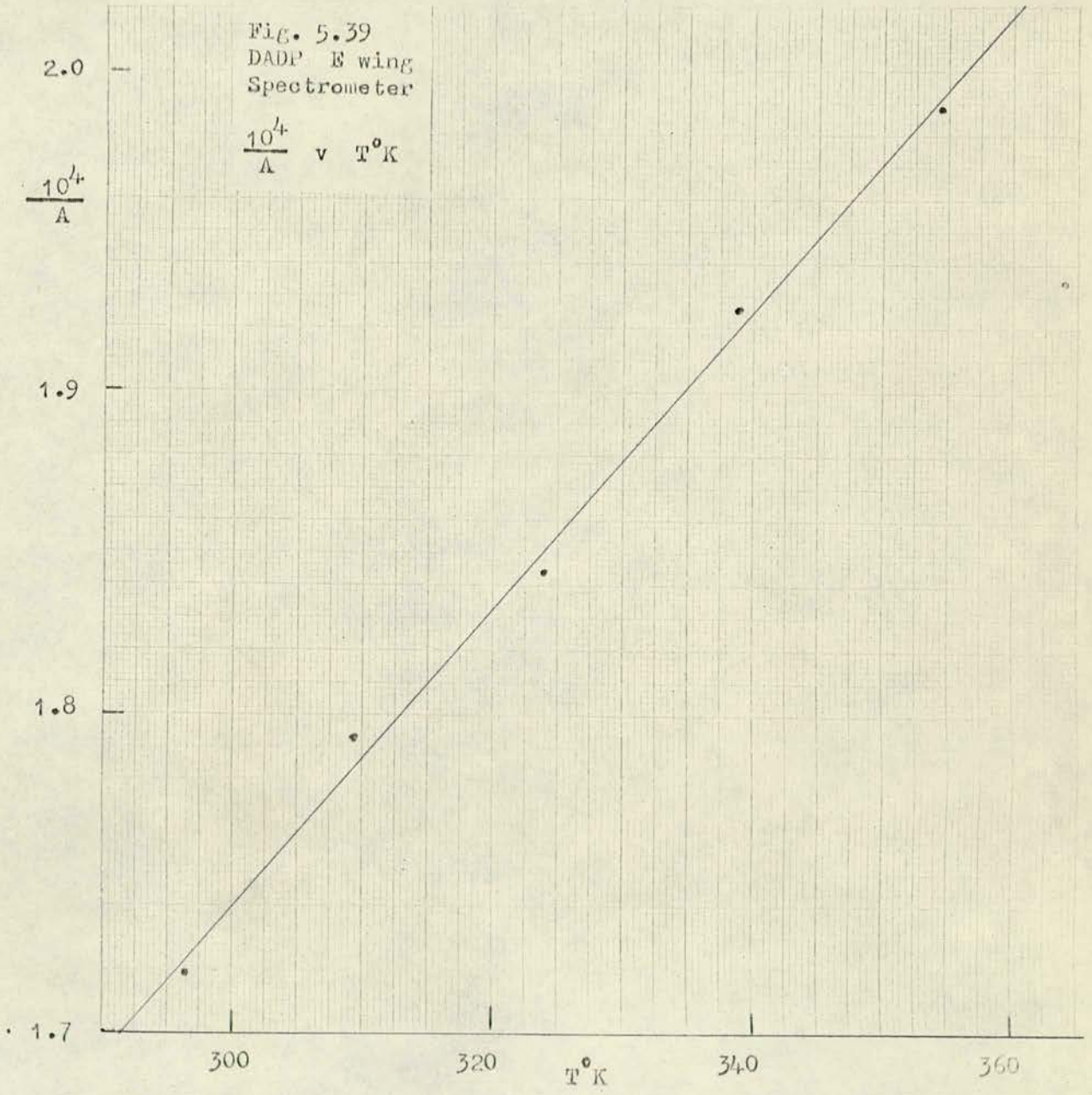
Fig. 5.39
DADP E wing
Spectrometer
$\frac{10^4}{A}$ v T°K
2.0
1.9
1.8
1.7
$\frac{10^4}{A}$
300
320
340
360
T°K

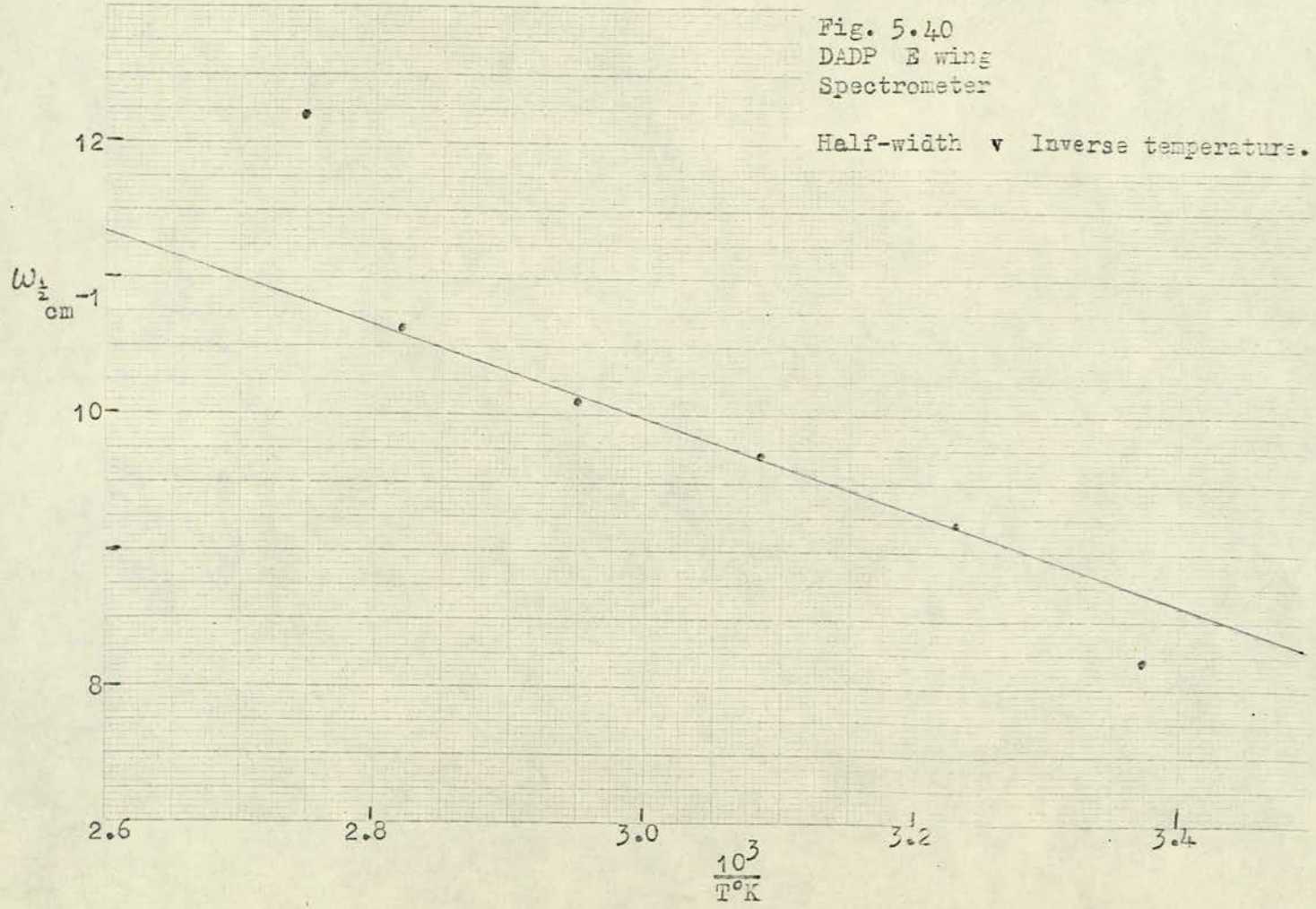

Fig. 5.40
DADP E wing
Spectrometer

Half-width v Inverse temperature.

Fig. 5.41
DADP E wing
Spectrometer

Half-width v Temperature.

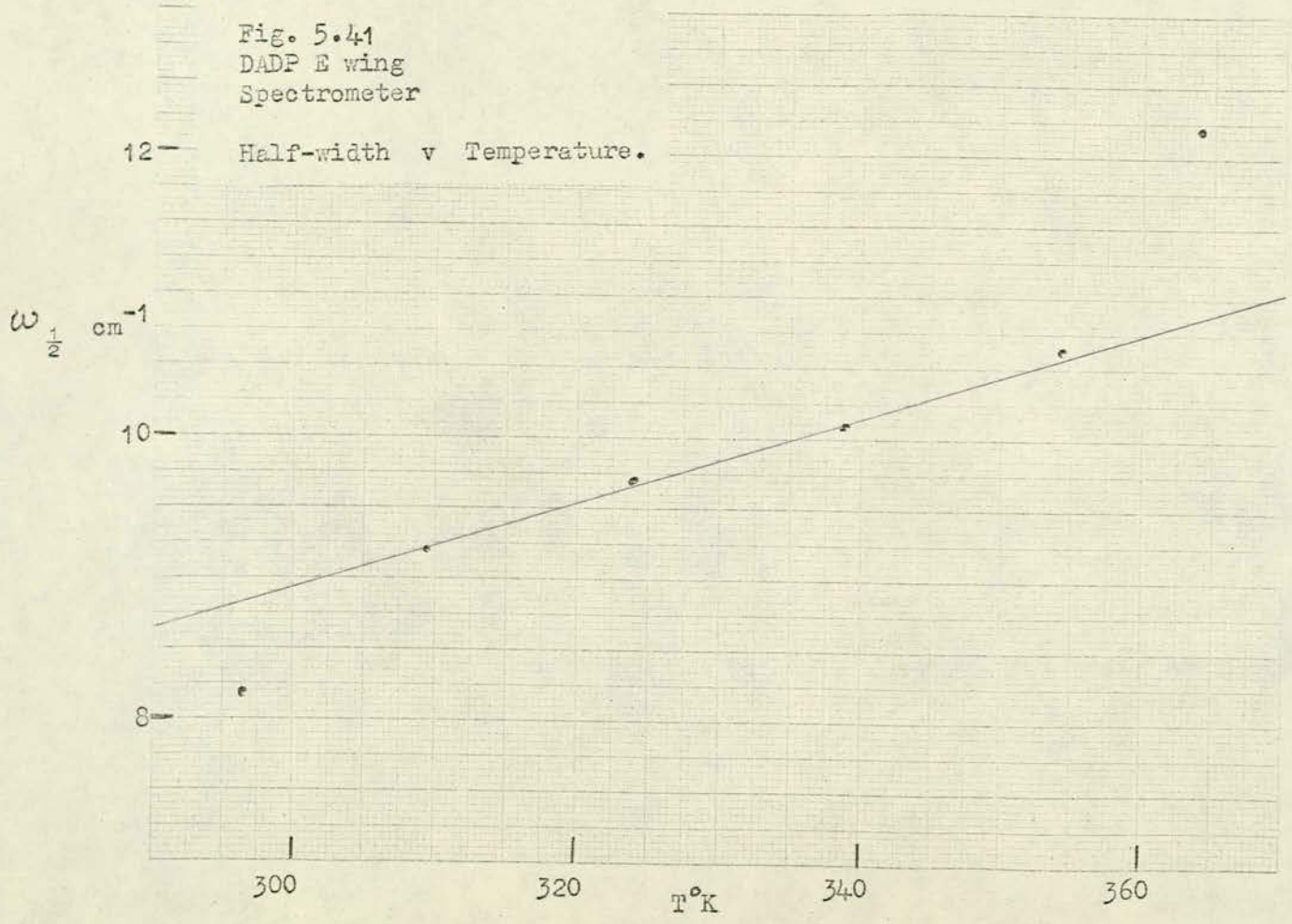

CHAPTER SIX

In this chapter the results of the present experiment are compared with those of other studies and with theoretical predictions.

STATIC DIELECTRIC CONSTANT MEASUREMENTS

In a series of experiments (1·45, 1·47), Mason and Matthias have measured the temperature dependence of the free low frequency a and c-axis dielectric constants ($\epsilon_a(o)$, $\epsilon_c(o)$) of KDP, ADP and DADP. Such data can be fitted by the relation

$$\epsilon(o) = \epsilon_1 + \frac{C}{T-Tc} \qquad (6\cdot1)$$

where ϵ_1 denotes the contribution to $\epsilon(o)$ for all modes other than the soft mode, which itself gives the Curie-Weiss term. The result of Mason's fit of the $\epsilon_c(o)$ data of KDP to the above equation is given in table 6·1 together with my own fittingto the other five sets of data taken from Mason's published work. The results of a similar analysis for ADP by Nagamiya (1·46) are included for completeness. Sliker and Burlege's (6·1) figures for $\epsilon_c(o)$ in DKDP are also listed. They assumed that ϵ_1 was negligible in their fitting procedure.

In most cases, the extrapolated Curie temperature lies well below the region in which measurements are possible - the paraelectric phase - and the change of $\epsilon(o)$ with temperature is not large. It is difficult to obtain a unique fit to the data since ϵ_1, C and Tc may all be varied to produce little difference to the quality of the fit. The fitting program usually failed to converge if all 3 parameters were allowed vary simultaneously unless the initial values chosen were

close to the 'best' values. This problem was circumvented by finding C and Tc for each of a series of fixed values of ϵ_1. Definite minima to the least squares sum could be found in all cases.

A number of points emerge on studying the table of results

(1) There is fair agreement with the values obtained by Nagamiya from Masons ADP data. It is not clear what fitting procedure he used. Mason has a graph of $\frac{1}{\epsilon(o)}$ against T. While for $\epsilon_c(o)$ in KDP, C and Tc may be obtained from a straight line fit in the region near the transition, this is not possible in ADP where the relevant transition temperature is not approached.

(2) Figures 6·1 and 6·2 show $\epsilon(o)$ as a function of temperature for the a and c axes of ADP and DADP. The DADP data has been off set on the temperature axis to aid comparison. The main effect of deuteration on $\epsilon_c(o)$ is to increase Tc by about 100 degrees. ϵ_1 is a little stronger in DADP than ADP but the two graphs have the same basic shape. This is similar to the behaviour of $\epsilon_c(o)$ in KDP where the isotope effect is restricted to Tc only. On the other hand, for $\epsilon_a(o)$ in ADP, deuteration causes all three parameters to change. That this is not a spurious result of the fitting procedure can be seen from figure 6·2 where the graphs for ADP and DADP do have a different curvature which is consistent with the large increase of ϵ_1 and Tc, and decrease of C, on deuteration.

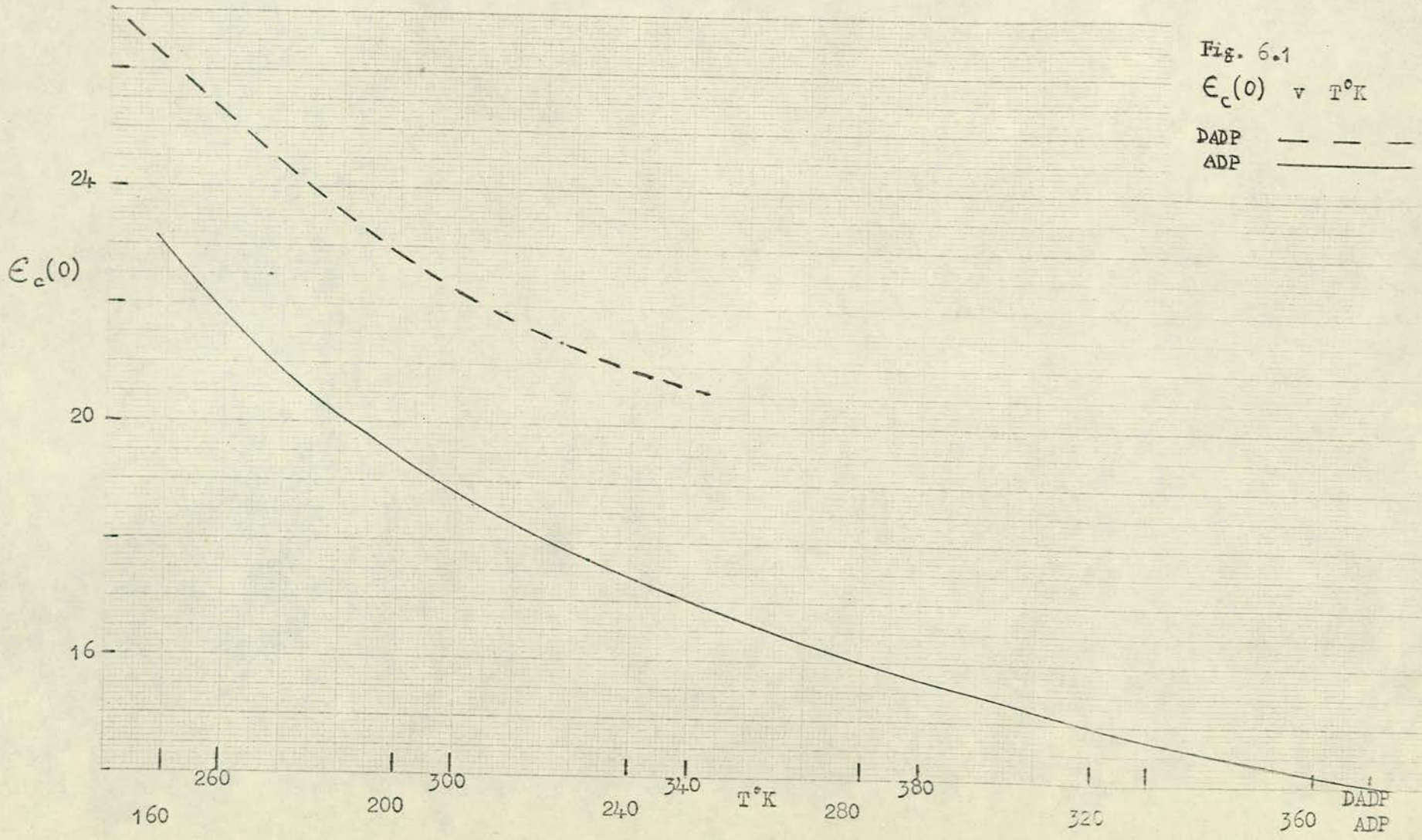
Fig. 6.1
$\epsilon_c(0)$ v T°K
DADP
ADP
24
20
16
$\epsilon_c(0)$
160
200
240
260
300
340
T°K
280
380
320
360
DADP
ADP

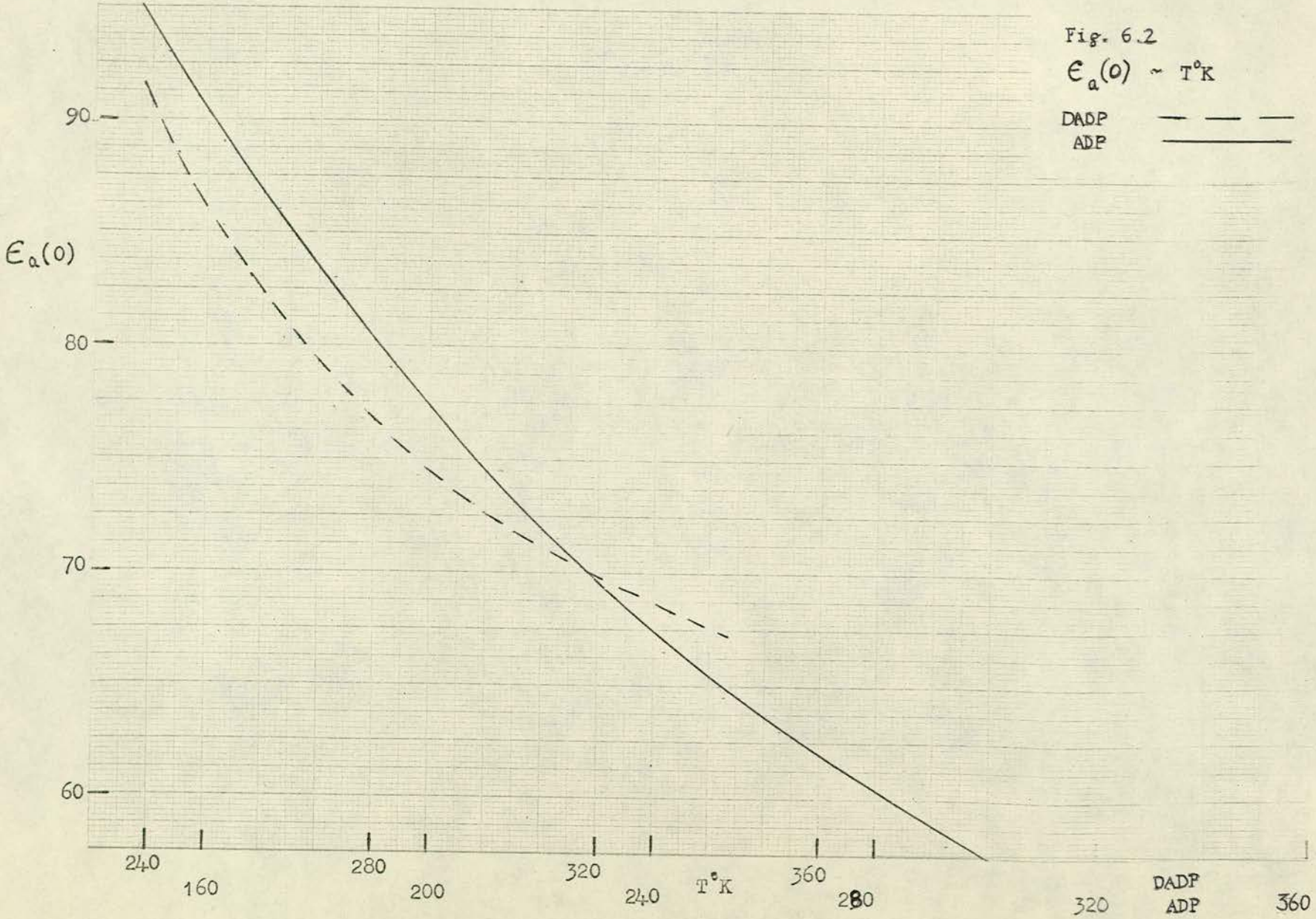
Fig. 6.2
$\epsilon_a(0)$ ~ T°K
DADP
ADP
$\epsilon_a(0)$
90
80
70
60
240
160
280
200
320
240
T°K
360
280
DADP
ADP
320
360

(3) Mason determined the free dielectric constants in his experiment but it is the clamped ones that are appropriate in a Raman experiment. While the difference between the c-axis free and clamped Curie temperatures in KDP and DKDP is about 4 degrees, Mason estimated, using the value of the piezoelectric constant, that the difference is nearer 50 degrees in ADP. No figures are given for the a-axis Curie temperatures for ADP or KDP but the clamped values will be somewhat lower than the free ones.

(4) Only for the B_2 wing of DKDP could the previously known transition temperature be used to confirm the best fit to the temperature dependence of the parameter A, obtained from the Debye function. This could not be done for the other three wings since they are not related to an actual transition. However the Curie temperature for the a-axis dielectric constant in DADP obtained from Masons data is in good agreement with that obtained from the present Raman experiment, considering the uncertainties involved. This tends to verify that the fit to the dielectric constant data and the choice of temperature dependence for A and τ for the light scattering experiment are in fact valid. $\epsilon_c(o)$ in DADP and $\epsilon_a(o)$ in KDP, and presumably so in DKDP, also, are only weakly dependent on temperature. This is in agreement with the similar lack of temperature dependence of the corresponding wing spectra.

(5) While for KDP, DKDP and ADP the c-axis Curie temperature is above the a-axis one, the opposite is possibly true for DADP, although the uncertainties arelarge. A possible way of resolving

this point would be to investigate that part of the wing where the temperature dependence is strongest - namely, at frequencies much lower than the half-width where

$$I(\omega \approx o) = A\tau \tag{6·2}$$

and $A\tau$ is likely to be

$$A\tau = \left(\frac{T}{T-Tc}\right)^2 \tag{6·3}$$

$$\text{or} \quad A\tau = \left(\frac{1}{T-Tc}\right)^2 \tag{6·4}$$

Since $T-Tc \geqslant 100^{o}K$ in DADP for both wings, measurements at $\sim 1\ cm^{-1}$ will give the required intensity, equation (6·2), at a point accessible to a well aligned tandem grating spectrometer, (which would avoid overlap problems) which is also resolved from the Rayleigh and Brillouin peaks. The temperature dependence of the product $A\tau$ may be strong enough to give both a more reliable estimate for Tc and better differentiation between the models, of equation (6·3) (6·4).

As the isotope effect on KDP is likely to take Tc for the E wing in DKDP to around $0^{o}K$ a similar study of that mode could be used to distinguish betwen equation (6·3) which would give a temperature independent $I(\omega \approx o)$ and equation (6·4) which would not.

TABLE 6·1

rystal	Free Dielectric Constant	ϵ_1	C ^{O}K	Tc ^{O}K	$\epsilon(o) = x$ at $T = y\ ^{O}K$		Source of fit
					x	y	
KDP	ϵ_c (o)	4·5	3122	122			Mason
KDP	ϵ_a (o)	15·9 ± 4·5	13390 ± 3370	-150 ± 46	42 63·5	363 123	Self
DKDP	ϵ_c (o)		3760 ± 60	222 ± 1			Sliker and Burlage
ADP	ϵ_c (o)	9·4 ± 0·6	1487 ± 213	52 ± 12	13·9 23·2	373 161	Self
ADP	ϵ_a (o)	12·5 ± 2·0	14740 ± 1030	- 28 ± 9	49 97	373 148	"
DADP	ϵ_c (o)	14·1 ± 1·7	1299 ± 476	141 ± 24	20·6 27·2	343 239	"
DADP	ϵ_a (o)	52·6 ± 1·5	2447 ± 291	176 ± 6	67·3 91·4	343 239	"
ADP	ϵ_c (o)	7	2690	- 17			Nagamiya
ADP	ϵ_a (o)	7	18000	- 55			"

Hill and Ichiki[3·103] fit their data for the complex c-axis dielectric constants of DKDP for $10^{-3} < \omega < 1\ cm^{-1}$ and $T < 260^{o}K$, to a Gaussian distribution of Debye relaxation times. While this fits most of their data for $\epsilon'(\omega)$ well, it is a poor fit to $\epsilon''(\omega)$, with measured and fitted values differing by as much as 100%, although this is not immediately obvious since their results are presented on a log-log graph.

I found that their data had an alternative interpretation. The graph they draw is of $\log\left(\frac{\epsilon''(\omega)}{\frac{C}{T-Tc}}\right) \sim \log(\omega\,\tau_o)$, where τ_o is the half width of the Gaussian distribution, while $\frac{C}{T-Tc}$ is the contribution to the static dielectric constant, $\epsilon(o)$, from the soft mode. In the temperature range of Hill and Ichiki's experiment $\epsilon(o) \approx \frac{C}{T-Tc}$. In the high and low frequency regions, their data lies on straight lines of gradients -1 and +1 respectively. That is

$$\frac{\epsilon''(\omega)}{\epsilon(o)} = \alpha \frac{1}{\omega\tau_o} \quad \text{for } \omega\tau_o >> 1 \tag{6·5}$$

$$\frac{\epsilon''(\omega)}{\epsilon(o)} = \beta\ \omega\tau_o \quad \text{for } \omega\tau_o << 1 \tag{6·6}$$

where α and β are constants determined by that fit to the data. These formulae, however, are precisely the high and low frequency limits of a single Debye relaxation time, τ, given by

$$\frac{\epsilon''(\omega)}{\epsilon(o)} = \frac{\omega\tau}{1 + (\omega\tau)^2} \tag{6·7}$$

Ignoring for the moment the data obtained below 3.10^{-2} cm^{-1}, the straight line fits to Hill and Ichiki's data yield values for α and β which both give the inverse single relaxation time $\omega_{\frac{1}{2}} = \frac{1}{\tau 2\pi c}$ as

$$\omega_{\frac{1}{2}} = 1{\cdot}82\ 10^{-2}\ (T-Tc)\ cm^{-1} \qquad (6{\cdot}8)$$

on using Hill and Ichiki's result that $\frac{1}{\tau_o} = 7{\cdot}3 10^{-3}\ (T-Tc)\ cm^{-1}$. That all the points, and not just those for $\omega\tau_o >>$ or $<<$ 1, fit the same single relaxation function can be seen from the fact that the peak of $\frac{\epsilon''(\omega)}{\epsilon(o)} \sim (\omega\tau_o)$ occurs for $\omega\tau_o = 2{\cdot}47$ ie $\omega\tau = 1$, and has a value of 0·5 - both these features are required by this function.

The points for $\omega < 3.10^{-2}$ cm^{-1}, while lying on a straight line of gradient +1, have a different value for β compared to the points for $\omega = 7.10^{-2}$ cm^{-1} and 13.10^{-2} cm^{-1}. This corresponds to an enhancement of the relaxation time at low frequencies to give

$$\omega_{\frac{1}{2}} = 1{\cdot}11\ 10^{-2}\ (T-Tc)\ cm^{-1} \qquad (6{\cdot}9)$$

This result is in line with the predictions of Cowley etal. (3·90) mentioned earlier, with regard to the effects of the difference between high and low frequency response in piezoelectric ferroelectrics. The frequency region in which this behaviour is evident in Hill and Ichiki's work, is below the limit of the present experiment.

Thus, over the same frequency range, both Hill and Ichiki's experiment which gives $\epsilon''(\omega)$, and my own, which yields $I(\omega) \propto \frac{\epsilon''(\omega)}{\omega}$, can be fitted by the same function with the same temperature dependence for the relaxation time.

While in the former $\omega_{\frac{1}{2}} = 1{\cdot}82\ 10^{-2}\ (T-Tc)\ cm^{-1}$

in the latter $\omega_{\frac{1}{2}} = 2{\cdot}9\ 10^{-2}\ (T-Tc)\ cm^{-1}$

Although Hill and Ichiki's results for $\epsilon''(\omega)$ are better fitted by a single relaxation time, which increases stepwise for $\omega \leqslant 3{\cdot}10^{-2}\ cm^{-1}$, than by a Gaussian distribution of relaxation times, this is not so for $\epsilon'(\omega)$ which has a $(\frac{1}{\omega\tau})$ high frequency behaviour whereas a relaxation function has $(\frac{1}{\omega\tau})^2$.

The formula for $\epsilon(\omega)$ fitted to Hill and Ichiki's data by Ishibashi et.al.(3·10) does not readily give analytical expressions for $\epsilon'(\omega)$ and $\epsilon''(\omega)$ separately. Direct comparison with the present data has not been attempted.

It is worth noting that Hill and Ichiki's work on $\epsilon''(\omega)$ in TGS, which they fit by distribution of relaxation times, is also much better represented by a single relaxation time.

INFRA-RED REFLECTIVITY EXPERIMENTS

Barker and Tinkham (3·95) predicted the presence of a low frequency B_2 mode in DKDP to give agreement between the strengths of the modes they observed and the known value of $\epsilon c(o)$. The wing spectra of the present experiment form a direct observation of this mode and the corresponding mode in DADP, together with the lowest frequency modes associated with $\epsilon a(o)$ in these crystals.

INELASTIC NEUTRON SCATTERING

The large gain in the quasi-elastic intensity in DKDP observed in the neutron experiments (3·98, 3·99) has been shown, by the higher resolution available in the present Raman experiment, to be due to a soft, highly overdamped, low frequency mode. It is perhaps surprising that no contribution to the neutron instrumental half width of 2 cm^{-1} from the soft mode was noted, since this mode's half width is given by $\omega_{\frac{1}{2}} = 2{\cdot}9 10^{-2}$ (T-Tc) cm^{-1}. Compared to the observed half width near the transition, a 30% increase is to be expected at 240°K - a temperature at which the quasi-elastic intensity is still appreciable.

LIGHT SCATTERING EXPERIMENTS

(a) KDP B_2 Wing

While Kaminow (6·2) states that he determined $\chi(o), \omega_o^2(o)$ and Γ by a least squares fit of equation (3·3) tothe spectra at each temperature individually and then found the temperature dependence of these parameters, rather than inserting postulated temperature dependences into equation (3·3) and then fitting the resultant formula to all the spectra simultaneously, Cochran (6·3) questions the uniqueness of Kaminow and Damen's analysis which gives the $\frac{T-Tc}{T}$ dependence for ω_o^2 (o) predicted by Kobayashi in contrast to the (T-Tc) dependence generally found in displacive ferroelectrics. The point in question can be seen most clearly by considering two explicit sets of temperature dependences and substituting them into equation (3·3), viz:-

$$(1)\quad \omega_o^2(o) = A^2\,\frac{T-Tc}{T}\quad ;\quad \Gamma = D \quad ;\quad \chi_\delta(o) = \frac{C}{T-Tc} \qquad (6\cdot10)$$

$$(2)\quad \omega_o^2(o) = A^2\,\frac{T-Tc}{Tc}\quad ;\quad \Gamma = D\,\frac{T}{Tc} \quad ;\quad \chi_\delta(o) = \frac{C}{T-Tc} \qquad (6\cdot11)$$

This latter behaviour has been predicted by Maradudin and Fein (6·4) for a weakly anharmonic crystal. Substitution of the above in equation (3·3) gives:-

$$\chi''(\omega) = \frac{2A^2\,CD\quad \omega\,T}{\left[A^2(T-Tc) - T^1\,\omega^2\right]^2 + \left[2DT\omega\right]^2} \qquad (6\cdot12)$$

where T^1 = T in case (1)

= Tc in case (2)

On fitting the two forms of equation (6·12) to Kaminow and Damen's published data (3·73), I have been unable to distinguish one giving a better fit than the other. This is understandable since it is only for large T that T and Tc are significantly different, and only at high ω is the term $T^1\,\omega^2$ appreciable. This is precisely the region of least accurate results due to the low intensity and uncertain contribution from multiphonon processes.

Not only was it impossible to distinguish between these two forms of the damped harmonic oscillator, but, near the transition, neither could be distinguished from a Debye relaxation function. Kaminow and Daman claim 10% noise fluctuations on their signal. The difference between a damped harmonic oscillator and a Debye function can be seen by considering the ratio formed by equation (3·3), for the damped harmonic oscillator, with and without the ω^4 term in the denominator. Using the

parameter values found by Kaminow and Damen, this indicates that the two formulae differ by less than 10% for $\omega < 65$ cm^{-1} and less than 5% for $\omega < 45$ cm^{-1}. Thus near the transition where the bulk of the intensity appears at low frequencies, the damped harmonic oscillator and Debye relaxation function are indistinguishable within the accuracy of the measurements.

Even at higher temperatures and frequencies, when fitting the damped harmonic oscillator of equation (3·3), I did not obtain a relatively constant value for Γ as Kaminow and Damen did. I found a strong interaction between $\omega_o^2(o)$ and Γ. The choice of initial parameter values, which non-linear least squares programs usually require, may thus lead to only a local minimum for the least squares sum and hence give a spurious fit.

Inspection of the $\chi''(\omega) \sim \omega$ curves in Kaminow and Damen's paper shows that, for frequencies less than 90 cm^{-1}, the envelope of all these curves is a straight line of gradient -1. As this is a log-log plot, the envelope has $\chi''(\omega) \propto \frac{1}{\omega}$ and thus $I_N(\omega) \propto \frac{1}{\omega^2}$. This is the high frequency limit of a Debye relaxation function

$$\chi''(\omega) = \frac{\chi_o(o)\,\omega\,\tau}{1 + (\omega\,\tau)^2} \qquad (6·13)$$

By plotting $\frac{\omega}{\chi''(\omega)} \sim \omega^2$ for all spectra within 100 degrees of the transition, the Debye function was shown to be a good fit. Since, on the graph of $\chi''(\omega) \sim \omega$ all the spectra taken below 220°K have a common envelope, given from equation (6·13) by

$$\chi''(\omega) = \frac{\chi_o(o)}{\omega\tau} \qquad (6·14)$$

$\chi_o(o)$ and τ thus have the same temperature dependence - namely $\frac{1}{(T-Tc)}$. Since $\chi''(\omega)$ and $\chi_o(o)$ are given on the same but arbitary scale, it is possible to calculate τ from Kaminow and Damen's published graphs to give

$$\omega_{\frac{1}{2}} = 0{\cdot}304\ (T-Tc)\ cm^{-1} \qquad (6{\cdot}13)$$

In their infra-red experiment (3·97), Sugawara and Nakamura have obtained $\epsilon''c(\omega)$ for KDP. There is good agreement between their data and that of Kaminow and Damen, as is evident since the Debye half width similarly obtained from the infra-red data is

$$\omega_{\frac{1}{2}} = 0{\cdot}288\ (T-Tc)\ cm^{-1} \qquad (6{\cdot}14)$$

The question remains as to why the wing beyond $\sim 90\ cm^{-1}$ has less intensity than would be expected from a $\frac{1}{\omega^2}$ dependence. While Kaminow and Damen find that $\chi''(\omega) \propto \omega^{-3}$ at high frequencies, Sugawara and Nakamura obtain -8 for the exponent. In CsDA (3·88) the effect of coupling between the wing and lowest frequency phonon mode was seen to be a depletion of wing intensity below the phonon peak and an enhancement above. Inspection of more extensive data published later by Kaminow (3·84) shows that a similar but smaller effect may be present in KDP too. Certainly, the 186 cm^{-1} mode has a lineshape which is steeper on the low frequency side. The opposite would be true of an isolated lightly damped harmonic oscillator.

Wilson's result (3·85) that the temperature dependence of the damped harmonic oscillator parameters depended on the temperature range considered, could be interpreted as arising from the increased coupling between the modes as the undamped soft mode frequency approaches that of the 186 cm^{-1} mode, as the temperature is raised. This would agree with Wilson's further observation that the damped harmonic oscillator became a less good fit at higher temperatures, since the increased coupling on heating takes the wing lineshape further from a Debye relaxation function rather than closer to a damped harmonic oscillator.

I think that an analysis of the KDP B_2 wing spectra by the treatment of Katiyar, Ryan and Scott (3·88) willreveal that the uncoupled soft mode has a Debye relaxation function profile, as in CsDA, and that deviations of the observed spectra from this are due to coupling to the 186 cm^{-1} mode. Although a damped harmonic oscillator may fit a region of the observed spectrum, it does not represent a single mode.

It is likely that at frequencies far from the 186 cm^{-1} mode, the observed wing intensity will closely approximate to the undamped mode profile since in this region the coupling will be weak. It is in precisely this region that I fitted the Debye function to Kaminow and Damen's data to obtain the half width expressed earlier in equation (6·13).

This half width has the same temperature dependence as found in the present experiment for the corresponding wing in DKDP. At a given value of (T-Tc) the half width is an order of magnitude less in DKDP compared with KDP. It seems reasonable

to find that the soft mode analytically uncoupled in KDP has the same general behaviour as that physically uncoupled by deuteration in DKDP.

Kaminow and Damen make no mention of any temperature dependence of the electro-optic tensor, invoked while discussing the present results for DKDP. Since they plot a graph of $\frac{1}{\chi_o(o)} \sim T^oK$ for all their data together, they must have used some standard of scattered intensity since $\chi_o(o)$ is in arbitary units. It is likely that they used the intensity of the strong narrow line at 395 cm^{-1} as a reference. If this was so, since any temperature dependence of the electro-optic tensor affects all B_2 modes similarly, their data is automatically compensated for changes in this variable.

(b) KDP E Wing

In the light of the observation of an E symmetry wing in DKDP, it is instructive to ask if a similar wing, though of greater half-width, would explain the flat response observed by Wilson (3·85) to extend from 0 cm^{-1} to the region of the 97 cm^{-1} and 115 cm^{-1} modes. An estimate of the half width of such a mode can be found, on assuming that the B_2 and E wings are affected similarly on deuteration, from

$$\left(\frac{\omega_{\frac{1}{2}}\ \text{KDP}}{\omega_{\frac{1}{2}}\ \text{DKDP}}\right)_E = \left(\frac{\omega_{\frac{1}{2}}\ \text{KDP}}{\omega_{\frac{1}{2}}\ \text{DKDP}}\right)_{B_2} \qquad (6\cdot15)$$

Using the values for DKDP obtained in the present experiment, equation (5·25, 5·26), and that obtained above for KDP from

Kaminow and Damen's data, equation (6·13), and evaluating the right hand side of (6·15) at the same value of (T-Tc), gives the half width of an E mode wing in KDP as

$$\omega_{\frac{1}{2}} = 88{\cdot}5 \text{ cm}^{-1} \qquad (6{\cdot}16)$$

An attempt was made to fit a Debye relaxation function (for the flat feature) and two damped harmonic oscillators (for the two modes ~ 100 cm^{-1}) to Wilson's spectrum. This was only moderately successful, presumably due to the neglect of coupling between these three modes. However a Debye function of ~ 90 cm^{-1} half width is clearly compatible with the observed spectrum especially in conjunction with appreciably damped 97 cm^{-1} mode which gives a tail extending to lower frequencies in that region in which the Debye function is descending from its initially constant value. The net effect accounts well for the flat response recorded. The observed spectrum and interpretation proposed above are illustrated in figure 6·3.

That Wilson observed little temperature dependence for this mode is in agreement with the corresponding spectrum in DKDP and the lack of a marked anomaly in the a-axis dielectric constant.

(c) DKDP B_2 Wing

Reese, Fritz and Cummins (6·5) have observed this wing at three temperatures. They fit a Debye relaxation function to the spectrum recorded 0·5°K above the transition. The relaxation time they obtain is 1·1 10^{-9} seconds, which corresponds to a half width of 0·0048 cm^{-1} since $\omega_{\frac{1}{2}} = \frac{1}{2\pi c \tau}$ cm^{-1} where τ is in seconds.

Fig. 6.3
DKDP
Spectrometer x(yz)y -after Wilson (3.85)

Spectrum and proposed interpretation.

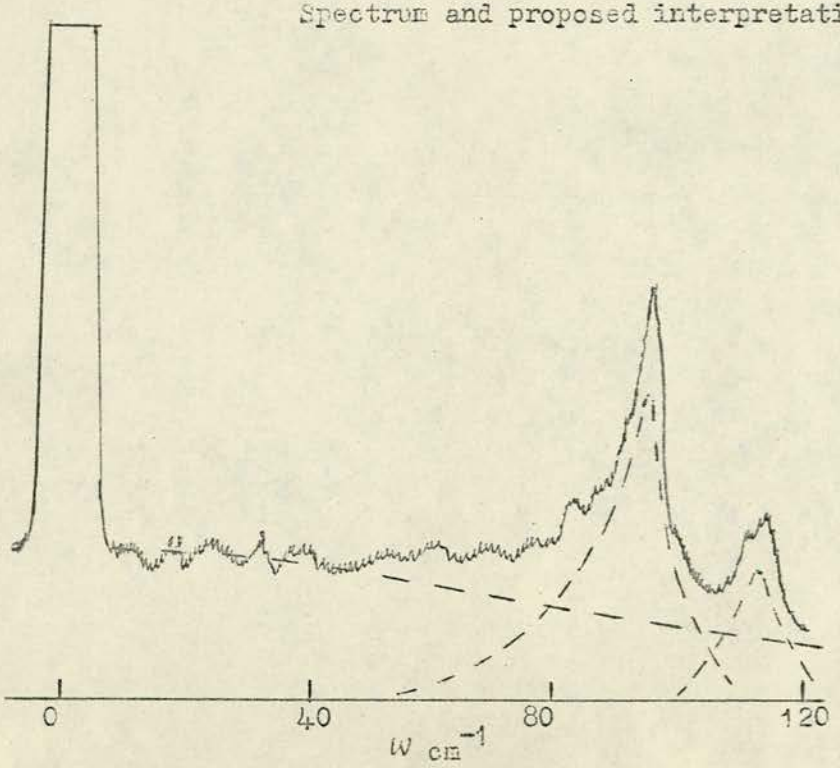

This is much less than the corresponding result in the present experiment - 0·12 cm^{-1}. I am surprised that they were able to determine this half-width, since at the free spectral range (1·667 cm^{-1}) and finesse (25) that they used, the wing profile could have differed little, if at all, from a purely $\frac{1}{\omega^2}$ form. They claim reasonable agreements with Hill and Ichiki's experiment (3·103), as I do. The paradox may be resolved if it is assumed that Reese, Fritz and Cummins took T-Tc = 0·5°K in Hill and Ichiki's results instead of 6·5°K, since Tc is the clamped Curie temperature, which Hill and Ichiki found to be 6° below the transition temperature, and Reese, Fritz and Cummins made their measurements 0·5°K above the transition.

Reese, Fritz and Cummins repeated their observations in an orientation which revealed both the soft optic wing mode and the soft acoustic mode related to the anomalous elastic constant c_{66}.

(d) B_2 and E Wings in ADP

Ryan, Katiyar and Taylor (6·6) have determined the half width of a Debye fit to the uncoupled softmodes in ADP as

$$\omega_{\frac{1}{2}} = 164 \left(\frac{T-29}{T}\right) \text{ cm}^{-1} \text{ for the } B_2 \text{ wing}$$

$$\omega_{\frac{1}{2}} = 85 \left(\frac{T-29}{T}\right) \text{ cm}^{-1} \text{ for the E wing}$$

The corresponding results in the present experiment on DADP were given in equations (5·27) and (5·30) as

$$\omega_{\frac{1}{2}} = 10·6 \text{ cm}^{-1} \text{ for the } B_2 \text{ wing}$$

$$\omega_{\frac{1}{2}} = 20·3 \frac{T-169}{T} \text{ cm}^{-1} \text{ for the E wing}$$

Thus both half-widths are substantially reduced on deuteration, the B_2 mode by a factor of 15, the E mode by one of 4. This is to be compared with the order of magnitude reduction for the B_2 mode in KDP and DKDP.

ULTRASONIC EXPERIMENTS

The polarization relaxation times have been found for KDP and DKDP in several experiments (3·105-3·108). It is perhaps useful to list the values of the parameter

$$\left(\frac{\partial \frac{1}{\tau}}{\partial T}\right)_{T=Tc}$$

for these and other experiments. This is done in table 6·2. With the exception of the KDP figures for $T < Tc$ there is reasonable agreement among the various results in each section. Of particular note is the order of magnitude increase in relaxation time on deuteration in the paraelectric phase.

COMPARISON WITH KOBAYASHI'S THEORY

(1) On Kobayashi's theory, the coupled tunnelling soft mode frequency, $\omega_-(o)$, is proportional to Ω, the tunnelling frequency of an isolated proton, and should decrease on deuteration. The half width, $\omega_{\frac{1}{2}}$, obtained by the Debye fit to the data is related to the undamped mode frequency, $\omega(o)$, and damping constant, Γ, of a damped harmonic oscillator by

$$\omega_{\frac{1}{2}} = \frac{\omega_-(o)^2}{2\Gamma} \qquad (6\cdot17)$$

$$= \frac{1}{2\Gamma}\left(\frac{2\Omega}{\hbar}\right)^2 \frac{T-T_2}{T} \qquad (6\cdot18)$$

on using equation (1·63).

TABLE 6·2

stal	$\frac{\partial(\frac{1}{\tau})}{\partial T}$ (sec deg)$^{-1}$	Temp dependence of $\frac{1}{\tau}$	Experiment	Source
xis Tc	$5{\cdot}74\ 10^{10}$	(T-Tc)	Raman	My fit to Kaminow and Damen (3·73)
	9·30 ±	$(\frac{T-Tc}{T})$	"	Kaminow and Damen (3·73)
	6·91 ±	$(T-Tc)^{0{\cdot}76}$	"	Wilson (3·85)
	16·80 ±	$(T-Tc)^{0{\cdot}63}$	"	"
	4·2	(T-Tc)	Ultrasonic	Garland and Novotny (3·105)
	2·8	(T-Tc)	"	Garland and Litov (3·106)
	8·5		Microwave Transmission	Gauss and Happ (3·102)
	5·43	(T-Tc)	IR	My fit to Sugawara and Nakamura (3·97)
	$1{\cdot}6\ 10^{10}$	(T-Tc)	Ultrasonic	Garland and Litov (3·106)
xis Tc	24·5	(T-Tc)	Raman	Wilson (3·85)
P xis	$0{\cdot}55\ 10^{10}$	(T-Tc)	Raman	Present experiment
Tc	0·41	(T-Tc)	Ultrasonic	Litov and Uehling (3·107)
	0·35	(T-Tc)	Microwave	My fit to Hill and Ichiki (3·103)
P xis Tc	$3{\cdot}1\ 10^{10}$	(T-Tc)	Ultrasonic	Litov and Uehling (3·108)

Assuming τ on Debye function is approximately $\frac{2\Gamma}{\omega_o^2}$ on damped harmonic oscillator function.

Neglecting the possibility of an isotope effect on the damping constant, which is not discussed by the Kobayashi theory since torques acting on pseudo-spins are omitted, and assuming $\Gamma \propto \frac{1}{T}$ to agree with the observed temperature dependence, the measured reduction of $\omega_{\frac{1}{2}}$ for the B_2 wing in KDP on deuteration (equations 6·13 and 5·25) gives

$$\Omega_{KDP_{B_2}} = 3{\cdot}2 \quad \Omega_{DKDP_{B_2}} \qquad (6{\cdot}19)$$

A similar isotope effect on the E wing in KDP was shown to be plausible. Comparison between the present experiment and that of Ryan, Katiyar and Taylor (6·6) shows that these wing frequencies are likewise reduced on deuteration in ADP.

The strong isotope effect on the frequencies of these modes, which are responsible for the high dielectric constants in these crystals, is a good indication that they are partly of tunnelling origin.

(2) The temperature dependence found for the half-width of the B_2 wing in DKDP was (T-Tc), equation (5·25), while for the E wing in DADP it was $(\frac{T-Tc}{T})$, equation (5·30). The two other wings had little temperature dependence. Whether these agree with Kobayashi's theory, equation (6·18), depends on the temperature dependence, if any, of Γ. The wings observed in the present experiment are overdamped to such an extent that Γ cannot be determined directly.

(3) The change in Curie temperature on deuteration can be expressed, using equation (1·62) as

$$\frac{\Omega_p}{\Omega_D}\,\frac{(J + J_L(o))_D}{(J + J_L(o))_p} = \frac{\tanh\left[\dfrac{\Omega_p}{k_B . Tc_p}\right]}{\tanh\left[\dfrac{\Omega_D}{k_B . Tc_D}\right]} \qquad (6\cdot20)$$

where p and D denote the protonated and deuterated crystals respectively. Assuming the coupling terms, J, are the same in either case, gives, for the B_2 wing in KDP and DKDP

$$\frac{2\Omega_D}{\hbar} = 90\ \text{cm}^{-1}$$

$$\frac{2\Omega_p}{\hbar} = 290\ \text{cm}^{-1} \qquad (6\cdot21)$$

$$\Gamma \approx 500\ \text{cm}^{-1} \text{ at } 300^{\circ}\text{K}$$

The values are quite plausible, giving the highly overdamped modes observed in these crystals and showing that Kobayashi's theory could account for the isotope effect on Tc.

(4) It is of interest to study the validity of some of the approximations used when discussing Kobayashi's theory in chapter one, in the light of some results obtained in this experiment.

(a) The approximation tank x ≈ x where $x = \frac{\Omega}{k_B T}$. While for the B_2 wing in DKDP $\tanh \frac{\Omega}{k_B T} \leqslant \tanh 0{\cdot}42 = 0{\cdot}40$ and the approximation is good, in KDP it is poor since, $\tanh \frac{\Omega}{k_B T} \leqslant \tanh 1{\cdot}7 = 0{\cdot}94$.

(b) The assumption that the coupling between the tunnelling and optic phonon mode is weak requires of equation (1·55) that

$$\frac{16\Omega \left| G_j(o) \right|^2 \langle S^o \rangle}{\hbar^2 (\omega_j^2(o) - \Omega^2(o))^2} \ll 1 \qquad (6\cdot22)$$

Using equations (1·28) and (1·65), and neglecting $\Omega^2(o)$ compared to $\omega_j^2(o)$ gives

$$2 \frac{(\frac{2\Omega}{\hbar})^2}{\omega_j^2(o)} \cdot \frac{T_2 - T_1}{T} \ll 1 \qquad (6\cdot23)$$

where T_2 and T_1 are the Curie temperatures of the proton system with and without coupling to the lattice. Since to give the observed Curie-Weiss behaviour for $\chi(o)$, equation (2·81), we require $T_2 - T_1 >> T - T_2$, $T_2 - T_1$ and T are likely to be comparable. Since in DKDP, for the B_2 wing, $(\frac{2\Omega}{\hbar}) = 90 cm^{-1}$ and the first lattice mode has $\omega_1(o) \approx 200\ cm^{-1}$, the weak coupling approximation is only just valid. In KDP both the fact that $(\frac{2\Omega}{\hbar})$ is larger than in DKDP and that $\Omega^2(o)$ can no longer be neglected in comparison the lowest lattice mode frequency, the approximation implied by equation 6·22 is no longer applicable. It was mentioned earlier that there was evidence for coupling to the 186 cm^{-1} mode for the B_2 wing in KDP but not DKDP.

Thus, while the approximations made in Kobayashi's theory are reasonable in DKDP, the higher frequencies involved in KDP require the full theory.

(c) The approximation $\omega_-^2(o) + \beta^2 >> \omega_a^2(o)$ (1·74)

Using equation (1·28, 1·63, 1·68, 1·81) the left hand side of the above equality is found to have the minimum value of $2\left(\frac{2\Omega}{\hbar}\right)^2\left[\frac{T_3-T_2}{T}\right] \approx 300\ (cm^{-1})^2$ for DKDP B_2 wing. This inequality is very well satisfied for DKDP and KDP, since the acoustic mode frequency is around 0·5 cm^{-1}.

(d) The requirement that the coupling between the coupled optic tunnelling mode, $\omega_-(o)$, and the acoustic mode, $\omega a(o)$, is weak requires in equation (1·71) that

$$\frac{2\beta^2\ \omega_a^2(o)}{\left(\omega_-^2(o) - \omega_a^2(o) + \beta^2\right)^2} << 1 \qquad (6·24)$$

Use of equations (1·28, 1·68, 1·81) reduces the above inequality to

$$2\ \frac{\omega a^2(o)\ T(T_3-T_2)}{\left(\frac{2\Omega}{\hbar}\right)^2\left[T + T_3 - 2T_2\right]^2} << 1 \qquad (6·25)$$

This is well satisfied by both KDP and DKDP.

CHAPTER SEVEN

This chapter contains a few suggestions both on the type of apparatus best suited to the study of low frequency wing spectra and also on some further experiments which could prove interesting.

The central experimental problem of the present work has been the extraction of the required information from the overlapped spectrum produced by the Fabry-Perot interferometer. Possible ways of reducing this problem are listed below.

(1) High resolution grating spectrometers

Although gratings do in principle have an overlap problem because there are several orders of interference, these are widely spaced compared to the extent of the wings and, also, by correct choice of the blaze angle most of the diffracted light can be channelled into one order.

At the smallest free spectral range used in this experiment - 0.89 cm^{-1} - the observed finesse was ~ 25 giving a resolving power of $\sim 4.10^5$. The use of a laser operating in a single longitudinal mode would have doubled this value. Such a value of resolving power can also be obtained with a grating. A 5 inch wide grating having 60,000 lines / inch has a resolving power of $1.2 10^5$ in first order. The use of gratings in tandem gives increased dispersion, contrast and suppression of ghosts. The practical resolution limit of double grating spectrometers is set by the relative precision with which the gratings are scanned, rather than their ultimate resolving power. Commercial spectrometers are designed with a compromise between resolution and the spectral range that can be studied. The requirement in the present case is for high resolution over a

limited spectral range. This might best be met by having a tandem spectrometer, of appreciable focal length, in which the photomultiplier tube and exit slit scanned the spectrum produced by fixed gratings, thus avoiding problems due to faulty tracking. The use of piezo-electric elements could achieve and maintain the accurate alignment of the gratings so necessary when the highest resolving powers are sought.

Such an arrangement would successfully remove the overlap problem, and it probably represents the best way of studying the required spectra. There is the added advantage when using a grating spectrometer that the entrance slit will collect light from a much greater length of beam than does the pinhole of a Fabry-Perot.

(2) Tandem Fabry-Perot Interferometers

The use of two Fabry-Perot's of different free spectral ranges results in an instrument having the free spectral range of the smaller interferometer spacing and the resolution of the larger. Separation ratios of over 100:1 are practicable provided the light is passed through the interferometers twice, in order to suppress the tail on the instrumental profile of the large free spectral range etalon which could be transmitted by the other along with the peak signal. The main problem with such a system would be synchronization, since the scanning rate required of each interferometer is proportional to its spacing.

A novel variation on the tandem system would be to use three mirrors, with the outer two both scanning towards the centre flat whose reflecting surface faced the smaller spacing. This arrangement would allow all the light transmitted by the first interferometer

to pass into the second. Coupling between the two interferometers might give rise to some distortion of the transmitted intensity which would be undesirable. Synchronous scanning would remain a severe problem however.

The tandem combination of a grating spectrometer and Fabry-Perot interferometer likewise requires that the scan rates be maintained with precision.

If it were only frequency shifts of narrow spectral lines that were required, then the requisite information could be obtained by scanning the Fabry-Perot through the peak transmitted by a stationary spectrometer or interferometer, since the spectral transmission of the pre-disperser does not affect the frequency of transmitted light. It is the present requirement for a measurement of intensity as a function of frequency that imposes the severe restriction that both instruments scan in step.

(3) Light Beating Techniques

When a single mode laser is used, light beating experiments do give a spectrum without overlap. The width of the Rayleigh peak has been determined for some liquids using a forward scattering geometry. A typical value is $10^3\ (\theta^\circ)^2$ Hz. This is seven orders of magnitude less than the halfwidth of the B_2 mode in DKDP near the transition. The 90° scattering angle needed for these wings means that light is collected from a much smaller length of beam than in a forward scattering arrangement. The increased halfwidth and decreased collection efficiency both act so as to reduce the homodyne signal.

During some weeks spent at the Royal Radar Establishment, Malvern, attempts were made to observe the B_2 wing of DKDP using light beating techniques but, almost as expected, without success.

A number of possible experiments which might prove profitable are listed below.

(1) KDP isomorphs

(a) It is important to establish with greater certainty the temperature dependence of the half-width of wing modes in these crystals, in order that comparison with Kobayashi's theory be more complete. For instance, can either the T-Tc or $\frac{T-Tc}{Tc}$ temperature dependencies be assigned without any doubt? Is their any evidence that the approximation $\tanh \frac{\Omega}{kT} \approx \frac{\Omega}{kT}$ is invalid in the protonated materials, thus giving a more complex temperature behaviour for these modes? By monitoring the intensity of a number of other modes of the same symmetry as the wing in question, the temperature dependence due to the phonon population factor and electro-optic tensor can be determined. Any additional temperature dependence of the wing can then be attributed to its soft behaviour. It would be unwise to use a single mode near the wing as a reference of intensity since it might have some temperature dependence due to coupling to the soft mode. Monitoring the intensity of a number of modes would reveal this.

(b) In chapter 6 it was suggested that the B_2 and E wings in KDP and DKDP were similar, except that for KDP the higher frequencies involved led to some distortion of the spectral profile on coupling to the nearest lattice mode. It would be of interest to see if, for a wider range of KDP isomorphs, the behaviour of the wings, which in deuterated crystals are separated physically from the lattice modes, is similar to that of the wings of the protonated crystals after analytical decoupling by the process of Katiyar, Ryan and Scott (3·88).

(c) The study of tritium substituted KDP isomorphs would be of general interest in the study of this type of ferroelectric. Since in ADP, (table 6·1) the a-axis Curie temperature appears to be rising faster than the anti-ferroelectric transition temperature, it is possible that TADP might be a ferroelectric with a-axis polarization.

(2) TGS - Triglycine Sulphate

Hill and Ichiki (3·103) have obtained data for TGS similar to that for DKDP. By analysing their $\epsilon''(\omega)$ data as I did for their DKDP experiment, I predict a Debye wing having half width given by

$$\omega_{\frac{1}{2}} = 0{\cdot}045\ (T-Tc)\ cm^{-1} \qquad (7{\cdot}1)$$

$$Tc = 321{\cdot}4^{\circ}K$$

For a given value of (T-Tc), such a wing is somewhat wider than that in DKDP. Gammon and Cummins (7·1) have performed a Brillouin scattering study of TGS but do not report observing a wing.

TGS and DTGS are interesting because they are hydrogen bonded ferroelectrics in which deuteration seems less important - the transition temperature rising only a few degrees on deuteration. The observation of a wing mode consistent with Hill and Ichiki's data would form a useful experiment as would the study of a possible isotope effect on the half-width of such a wing.

(3) $Na\ H_3\ (SeO_3)_2$ - Sodium Trihydrogen Selenite

This is a hydrogen bonded ferroelectric for which neutron measurements (7·2) indicate the possibility of a weak double minimum well as in KDP. Peercy (3·72) has studied the Raman spectra of this crystal without finding a low frequency wing or any soft behaviour. Peercy's published spectra, which are for $\omega \geq 15\ cm^{-1}$, do show what could either be the tail of a wing or just the Rayleigh peak. The study of the 0-20 cm^{-1} region in sodium trihydrogen selenite and its deuterated counter-part might reveal a soft mode. It would be interesting to see to what extent the behaviour of KDP crystals was general for hydrogen bonded ferroelectrics.

APPENDIX 1

Some properties of KDP

Property	$T > Tc$	$T < Tc$
Space group	$I\bar{4}2d$ (Tetragonal)	Fdd_2 (Orthorhombic)
Point group	D_2d $\bar{4}2m$	C_2r mm
Unit cell dimensions	a = 7·453 Å b = 7·453 c = 6975 (at 296°K)	10·455 Å 10·540 6·918 (at 77°K)
Bond length	2·49 Å at 293°K	2·49 Å at 77°K
Formula units per unit cell	4 (2 in primitive cell)	8
Refractive index	n_o = 1·508 n_e = 1·467	

APPENDIX 2

PHYSICS LETTERS PAPER

This paper was written after a few early experiments on DKDP were performed. The analysis used was the graphical method described in chapter five. This gives uncertain results if the $\frac{1}{\omega^2}$ behaviour does not extend to sufficiently low frequencies. The later, more complete, data obtained using a least squares program to fit an overlapped Debye function, did in fact show that this was a good fit within the accuracy with which the spectra had been obtained.

RAMAN SCATTERING BY THE FERROELECTRIC MODE IN KD_2PO_4

K.I. WHITE, W. TAYLOR, R.S. KATIYAR and S.M. KAY *
University of Edinburgh, Edinburgh, UK

Received 16 September 1970

Raman scattering by the temperature dependent ferroelectric mode in KD_2PO_4 has been observed. Comparison is made with neutron and microwave experiments on KD_2PO_4, and with Raman scattering from the corresponding mode in KH_2PO_4.

Raman scattering has been observed from a low frequency, temperature dependent, highly overdamped mode in a deuterated single crystal of potassium dihydrogen phosphate - KD_2PO_4. This mode, which is responsible for the ferroelectric properties of the crystal, has B_2 symmetry and was studied using the $x(yx)y$ configuration [1] with a helium-neon laser as the light source. KD_2PO_4 undergoes a ferroelectric phase transition near 222°K - the precise temperature depending on the percentage deuteration.

The spectral distribution of the light scattered at room temperature was observed with a double grating spectrometer and is shown in fig. 1 where it is compared with that obtained from KH_2PO_4 in a similar experiment [1]. In both cases the Raman scattering is a wing on the central Rayleigh peak. Although both wings are comparable in extent, the bulk of the intensity in the case of KD_2PO_4 is at much lower frequencies than for KH_2PO_4. Kaminow and Damen showed that the spectrum for KH_2PO_4 was best fitted by a damped simple harmonic oscillator giving a high frequency behaviour for the spectral distribution of $I(\omega) \sim \omega^{-4}$. However, for KD_2PO_4 the high frequency end of the wing behaves as ω^{-2} and is temperature independent apart from the small increase in intensity with increasing temperature which arises from the changing phonon population.

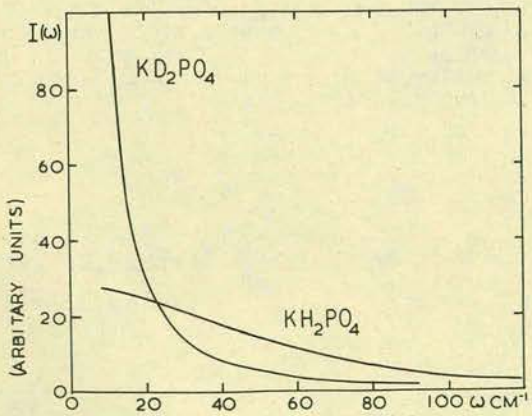

Fig. 1. The room temperature spectral distribution for KD_2PO_4 and KH_2PO_4. Average of Stokes and anti-Stokes.

The low frequency end of the spectrum was investigated using a scanning Fabry-Perot interferometer having a free spectral range variable from a maximum of 70 cm^{-1}. In the range $\omega > 2$ cm^{-1} the intensity was found to increase on cooling from 370°K in such a way that the high frequency ω^{-2} behaviour extended to lower frequencies as the temperature was reduced, until at about 260°K the entire wing beyond 2 cm^{-1} followed a ω^{-2} dependence. No additional change in intensity was observed on cooling further. Investigation of the region $\omega < 2$ cm^{-1} was complicated by the presence of the longitudinal acoustic modes at $\omega = 0.45$ cm^{-1} and by the multiple overlap of the wing (an effect inherent in this instrument) which gives rise to a flat background making analysis of the spectrum complex. As the transition is approached closely from above, a rapid increase in intensity was observed at frequencies less than that of the acoustic mode. This disappeared abruptly on passing into the ferroelectric phase, reappearing as before on returning to the paraelectric phase.

Inelastic neutron scattering measurements on KD_2PO_4 [2,3] have shown a rapid gain in intensity of the quasi-elastic scattering within the

* Now at Royal Holloway College, London.

3 cm^{-1} resolution of the spectrometer, as the transition is approached from above. This is consistent with the low frequency gain in intensity observed in the present experiment.

Since the spectral distribution, $I(\omega)$, and the imaginary part of the dielectric susceptibility, $\chi''(\omega)$, are related according to the fluctuation dissipation theorem, $I(\omega)$ and $\chi''(\omega)/\omega$ being proportional in the classical region $\hbar\omega \ll kT$, the results of the present experiment are plotted on fig. 2 in the form $\chi''(\omega)/\omega \sim T$. In a microwave experiment on KD_2PO_4 Hill and Ichiki [4] obtained the real and imaginary parts of the dielectric susceptibility in the range $10^{-3} < \omega < 1$ cm^{-1}. For comparison, their results for $\chi''(\omega)/\omega$ are also plotted on fig. 2. This shows clearly the close agreement between the two experiments in the range $\omega < 2$ cm^{-1} where there is a rapid increase in $\chi''(\omega)/\omega$ as the transition is approached, and also the fact that once

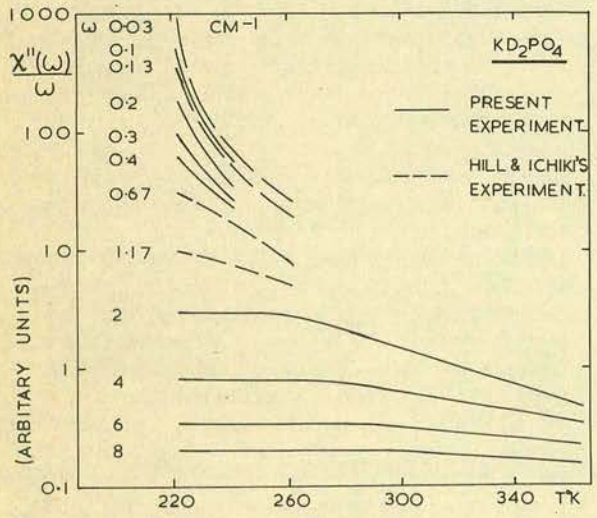

Fig. 2. $\chi''(\omega)/\omega$ as a function of temperature for various frequencies.

$\chi''(\omega)/\omega$ has become proportional to ω^{-2} it remains constant on further reducing the temperature.

Reese et al. [5] have also observed Raman scattering from the ferroelectric mode in KD_2PO_4 and have fitted the spectrum at 0.5°K above the transition and in the frequency range up to 0.5 cm^{-1} by a Debye relaxation time. However, we have found that over the wider frequency and temperature ranges used in the microwave and present Raman measurements, a Debye relaxation time gives a poor fit. Hill and Ichiki used a Gaussian distribution of relaxation times. This results in a ω^{-2} behaviour at high frequencies - as do all distributions of relaxation times - but although it fits their results for $\chi'(\omega)$ well it gives a poorer fit to $\chi''(\omega)$ and is also unsatisfactory in the present experiment.

Although further distributions of relaxation times and a recent analysis of Hill and Ichiki's results for TGS and KD_2PO_4 by Ishibashi et al. [6] are being studied, a satisfactory model to fit the dielectric and Raman measurements over their entire frequency and temperature range has yet to be found.

We wish to acknowledge many helpful discussions with Professor W. Cochran and are grateful to the Science Research Council for financing the experiment.

References

[1] I. P. Kaminow and T. C. Damen, Phys. Rev. Letters 20 (1968) 1105.
[2] G. Paul, W. Cochran, W. J. L. Buyers and R. A. Cowley, J. Phys. Soc. Japan 28 (1970) 278.
[3] J. Skalyo, B. C. Frazer and G. Shirane, Phys. Rev. B1 (1970) 278.
[4] R. M. Hill and S. K. Ichiki, Phys. Rev. 130 (1963) 150.
[5] R. L. Reese, I. J. Fritz and H. Z. Cummins, to be published.
[6] Y. Ishibashi, A. Sawada and Y. Takagi, J. Phys. Soc. Japan 28 (1970) 1488.

* * * * *

REFERENCES.

(1.1) H.D.Megaw 'Ferroelectricty in Crystals' Methuan London (1957)

(1.2) W.Känzig Solid State Physics 4(1957) 1-197.

(1.3) F.Jona and G.Shirane 'Ferroelectric Crystals' Pergammon New York,(1962).

(1.4) C.B.Sawyer andC.H.Tower Phys. Rev. 35(1930) 269.

(1.5) L.D.Landau and E.M.Lifshitz 'Statistical Physics' Ch14 Pergammon.

(1.6) A.F.Devonshire Adv. Phys. 3(1954)85.

(1.7) D.A.Daegert and S.Singh Solid State Commun. 9(1971)595.

(1.8) W.Cochran Phys. Rev. Letters 3(1959)412.

" Adv.Phys. 9(1960)387.
10(1961)401.

(1.9) W.Cochran NATO Advanced Study Institute, Norway 1971.

(1.10) C.V.Raman and T.M.K.Negungadi Nature 145(1940)147.

(1.11) V.L.Ginzburg J.E.T.P. 19(1949)36.

(1.12) H.Fröhlich 'Theory of Dielectrics' (Oxford Univ. Press 1949)

(1.13) R.H.Lyddane, R.G.Sachs andE.Teller Phys.Rev.59(1941)673.

(1.14) P.W.Anderson 'Fizika Dielectrikov' ed. G.I.Skanavi p290 Acad.Nauk. SSSR. Moscow.

(1.15) G.S.Pawley, W.Cochran, R.A.Cowley and G.Dolling Phys. Rev. Letters 17(1966)753.

(1.16) E.F.Steigmeier and G.Harbeke Solid State Commun. 8(1970)1275

(1.17) M.Born and K.Huang 'Dynamical Theory of Crystal Lattices' Oxford Univ.Press, 1954.

(1.18) B.G.Dick and A.W.OverHauser Phys. Rev. 112(1958)90.

(1.19) W.Cochran and R.A.Cowley J.Chem.Phys. Solids 23(1962)447.

(1.20) G.Busch and P.Scherrer Naturwiss 23(1935)737.

(1.21) J.West Z.Krist. 74(1930)306.

(1.22) B.C.Frazer and R.Pepinsky Acta Cryst. 6(1953)273.

(1.23) G.E.Bacon and R.S.Pease Proc. Roy. Soc. A220(1953)397.
A230(1955)359.

(1.24) H.Baumgartner, F.Jona and W.Kanzig Ergeb. Exakt.Naturwiss
23(1950)235.

(1.25) J.C.Slater J.Chem. Phys. 9(1941)16.

(1.26) Y.Takagi J.Phys. Soc. Jap. 3(1948)271.

(1.27) M.E.Senko Phys. Rev. 121(1961)1599.

(1.28) H.B.Silsbee,E.A.Uehling and V.H.Schmidt Phys. Rev. A133(1964)165.

(1.29) J.Pirenne Physica 12(1949)1019.
21(1955)219.

(1.31) P.G.deGennes Solid State Commun. 1(1963)132.

(1.30) R.Blinc J.Phys.Chem.Solids 13(1960)204.

(1.32) R.Brout, K.A.Muller and H.Thomas Solid State Commun.
4(1966)507.

(1.33) J.Villain and C.Stamenkovic Phys. Status Solidi 15(1966)585.

(1.34) M.Tokunaga and T.Matsubara Progr. Theor. Phys. 35(1966)581.

" " 36(1966)857.

(1.35) L.Novakovic J.Phys.Chem.Solids 27(1966)1469.

(1.36) K.K.Kobayashi Phys.Letters 26A(1967)55.

J.Phys.Soc.Japan 24(1968)497.

(1.37) W.Cochran Adv. Phys. 18(1969)157.

(1.38) T.Matsubara and M.Tokunaga Symposium 'Phase Transitions
and Ferroelectrics'I.S.S.P. Japan.

(1.39) Y.Yamada and T.Yamada J.Phys.Soc.Jap. 21(1966)2167.

(1.40)W.Cochran and R.A.Cowley 'Handbuch der Physik' Vol.25/1a, p65.

(1.41) R.J.Elliot NATO Advanced Study Institute, Norway 1971.

(1.42) G.J.Coombs Private Communication.

(1.43) G.Busch Helv. Phys. Acta 11(1938)269.

(1.44) E.A.Wood, J.Merz and B.T.Matthias Phys. Rev. 87(1952)544.

(1.45) W.P.Mason and B.T.Matthias Phys. Rev. 88(1952)477.

(1.46) T.Nagamiya Progr. Theor. Phys. 7(1952)275.

(1.47) W.P.Mason Phys. Rev. 69(1946)173.

(2.1) Lord Rayleigh — Phil.Mag. 41(1871)107,274,447. 47(1899)375.

(2.2) M. von Smoluchowski — Ann.d.Physik. 25(1908)205.

(2.3) A.Einstein — Ann.d.Physik. 38(1910)1275.

(2.4) P.Debye — Ann.d.Physik. 39(1912)789.

(2.5) L.Brillouin — Compt.Rend. 158(1914)1331.

Ann.Phys. 17(1922)88.

(2.6) E.Gross — Nature 126(1930)201,400,602. 129(1932)722.

(2.7) L.Landau and G.Placzek — Phys.Z.Soviet Union 5(1934)172.

(2.8) A.Smekal — Naturwiss 11(1923)873.

(2.9) H.A.Kramers and W.Heisenberg — Zeit.Phys. 31(1925)681.

(2.10) C.V.Raman — Ind.J.Phys. 2(1928)387.

C.V.Raman and K.S.Krishnan — Nature 121(1928)501.

(2.11) G.Landsberg and L.Mandlestam — Naturwiss 16(1928)57.

(2.12) G.Placzek — Marx's Handbuch der Radiologie vi 2(1934)209.

(2.13) G.B.Benedek and K.Fritsch — Phys.Rev. 149(1966)647.

(2.14) A.Griffin — Rev.Mod.Phys. 40(1968)167.

(2.15) M.Born and K.Huang. — 'Dynamical Theory of Crystal Lattices' Oxford Univ. Press 1954.

(2.16) R.Louden — Adv.Phys. 13(1964)423.

(2.17) D.L.Mills and E.Burnstein — Phys.Rev. 188(1969)1465.

(2.18) L.Mandel and E.Wolf — Rev.Mod.Phys. 37(1965)231.

W.B.Davenport and W.Root — 'An Introduction to the Theory of Random Signals and Noise. Ch.6 McGraw-Hill 1958

C.Kittel — 'Elementary Statiatical Physics' p136 John Wiley 1958.

F.Reif — 'Fundamentals of Statistical Physics' p585 McGraw-Hill 1965.

(2.19) T.C.Damen, S.P.S.Porto and B.Tell — Phys.Rev. 142(1966)570.

(2.20) J.F.Nye — 'Physical Properties of Crystals' Oxford Univ.Press 1969.

(2.21) W.Cochran and R.A.Cowley Handbuch der Physik Vol.25/1a p.59

W.Cochran Adv.Phys. 18(1969)157.

(2.22) L.D.Landau and E.M.Lifshitz 'Statistical Physics' p397 Pergammon.

(2.23) R.A.Cowley Adv.Phys. 12(1963)421.

(2.24) A.S.Barker Phys.Rev. 136(1964)1290.

(2.25) R.Brout 'Phase Transitions' Benjamin 1965.

(2.26) B.D.Silverman Phys.Rev.Letters 25(1970)107.

(3.1) P.A.Fleury and J.M.Worlock Phys.Rev.Letters 18(1967)665.

(3.2) " " Phys.Rev. 174(1968)613.

(3.3) G.Shirane, R.Nathans and V.J.Minkiewiez Phys.Rev. 157(1967)376.

(3.4) C.H.Perry and T.F.McNelly Phys.Rev. 154(1967)456.

(3.5) S.Wemple Phys.Rev. 137A(1965)1575.

(3.6) J.M.Worlock and P.A.Fleury Phys.Rev.Letters 19(1967)1176.

(3.7) T.G.Davies J,Phys,Soc.Jap. 28(1971) Suppl.

(3.8) H.Granicher Helv.Phys.Acta 29(1956)210.

(3.9) K.A.Müller Helv.Phys.Acta 31(1958)173.
Phys.Rev.Letters 2(1959)341.

(3.10) L.Rimai and G.A.de Mars Phys.Rev. 127(1962)702.

(3.11) R.O.Bell and G.Rupprecht Phys.Rev. 125(1962)1915.
129(1963)90.

(3.12) F.W.Lyttle J.App.Phys. 35(1964)2212.

(3.13) W.G.Nilsen andJ.G.Skinner J.Chem.Phys. 48(1968)2240.

(3.14)D.C.O'Shea, R.V.Kolluri and H.Z.Cummins Solid State Commun. 5(1967)387.

(3.15) R.F.Schaufele and M.J.Weber J.Chem.phys. 46(1967)2859.

(3.16) L.Rimai and J.L.Parsons Solid State Commun. 5(1967)381.

(3.17) H.Unoki and T.Sakudo J.Phys.Soc.Jap. 23(1967)546.

(3.18) K.A.Müller, W.Berlinger and F.Waldner Phys.Rev.Letters 21(1968)814.

(3.19) P.A.Fleury. J.F.Scott and J.M.Worlock Phys.Rev.Letters 21(1968)16.

(3.20) V.L.Ginzburg Sov.Phys.Usp. 5(1963)649.

(3.21) L.D.Landau and E.M.Lifshitz 'Statistical Physics' Pergammon.

(3.22) G.Shirane and Y.Yamada Phys.Rev. 177(1969)858.

(3.23) R.A.Cowley, W.J.L.Buyers and G.Dolling Solid State Commun. 7(1969)181.

(3.24) K.Otnes, T.Riste, G.Shirane and J.Feder Solid State Commun. 9(1971)1103.

(3.25) W.Kaiser and R.Zurek Phys.Letters 28(1966)668.

(3.26) B.Berre and K.Fossheim NATO Advanced Study Institute Norway 1971.

(3.27) W.Cochran and A.Zia Phys.Status Solidi 25(1968)273.

(3.28)V.Plakhty and W.Cochran Phys.Status Solidi 29(1968)K81

(3.29) J.F.Scott Phys.Rev. 183(1969)823.

(3.30) J.D.Axe, G.Shirane and K.A.Müller Phys.Rev. 183(1969)820.

(3.31) V.J.Minkiewicz and G.Shirane J.Phys.Soc.Jap. 26(1968)624.

(3.32) W.J.Burke and R.J.Pressley Solid State Commun. 7(1969)1187.

(3.33) L.S.Wall, M.Rokui and A.L.Schawlow Solid State Commun. 9(1971)573.

(3.35) F.Jona and G.Shirane 'Ferroelectric Crystals' Macmillan.

(3.36) M.DiDomenico, S.P.S.Porto and S.H.Wemple Phys.Rev.Letters 19(1967)855.

(3.37) M.DiDomenico, S.P.S.Porto, S.H.Wemple andR.P.Bauman Phys.Rev. 174(1968)522.

(3.38) A.Pinczuk, W.Taylor, E.Burnstein and I.Lefkowitz Solid State Commun.5(1967)429.

(3.39) A.S.Barker Phys.Rev. 145(1966)391.

(3.40) J.M.Ballantyne Proc.Int.Meeting on Ferroelectricty Prague, 1966.

(3.41) A.Pinczuk, E.Burnstein andS.Ushioda Solid State Commun. 7(1968)139.

(3.42) J.L.Parsons and L.Rimai Solid State Commun. 5(1967)423.

(3.43) G.Shirane, B.C.Frazer, V.J.Minkiewicz, J.A.Leake and A.Linz
Phys.Rev.Letters 19(1967)234.

(3.44) G.Shirane, J.Axe, J.Harada and A.Levy Phys.Rev. 2B(1970)3651.

(3.45) P.A.Fleury and P.D.Lazay (to be published)

(3.46) E.M.Brody and H.Z.Cummins Phys.Rev.Letters 25(1970)169.

(3.47) A.S.Barker and J.J.Hopfield. Phys.Rev. 135A(1964)1732.

(3.48) G.Burns and B.A.Scott Phys.Rev.Letters 25(1970)167.

(3.49) " " " 25(1970)1191.

(3.50) G.Shirane, K.Suzaki and A.Takeda J.Phys.Soc.Jap. 7(1952)12.

(3.51) G.Burns and B.A.Scott Solid State Commun. 9(1971)813.

(3.52) W.D.Jonston and I.P.Kaminow Phys.Rev. 168(1967)104.

(3.53) V.L.Ginzburg Sov.Phys.Usp. 5(1963)649.

(3.54) D.A.Kleinman and W.S.Spitzer. Phys.Rev. 125(1962)16.

(3.55) P.K.Narayanaswang Proc.Ind.Acad.Sci. A28(1948)417.

(3.56) S.M.Shapiro, D.C.O'Shea and H.Z.Cummins. Phys.Rev.Letters
19(1967)361.

(3.57) J.F.Scott Phys,Rev.Letters 21(1968)907.

(3.58) J.D.Axe and G.Shirane Phys.Rev. 61(1970)342.

(3.59)J.F.Scott Phys.Rev.Letters 24(1970)1107.

(3.60) A.Kikuchi, K.Sakata, S.Hasagawa, G.O'hara, M.Wada and M.Nishizawa
Jap.J.App.Phys. 8(1969)692.

(3.61) C.H.Perry and D.K.Agrawal Solid State Commun. 8(1969)225.

(3.62) E.V.Chisler, I.T.Savatinova and V.M,Friakin
Sov.Phys.Solid state 12(1971)2327.

(3.63) G.Harbeke, E.F.Steigmeier and R.Welmer Solid State Commun.
8(1970)1765.

(3.64) J.R.Sandercock Optics Commun. 2(1970)73.

(3.65) G.S.Pawley, W.Cochran, R.A.Cowley and G.Dolling
Phys.Rev.Letters 17(1966)753.

(3.66) E.F.Steigmeier and G.Harbeke Solid State Commun. 8(1970)1275.

(3.67) K.Aizu J.Phys.Soc.Jap 27(1969)387.

(3.68) J.D.Axe, B.Dorner and G.Shirane Phys.Rev.Letters 26(1971)519.

(3.69) E.Pytte (to be published)

(3.70) P.A.Fleury Solid State Commun 8(1970)601.

(3.71) L.A.Cross, A.Fouskova and S.E.Cummins
Phys.Rev.Letters 21(1968)812.

(3.72) P.S.Peercy Optics Commun. 2(1970)270.

(3.73) I.P.Kaminow and T.C.Damen Phys.Rev.Letters 20(1968)1105.

(3.74) J.Chapelle J.Chem.Phys. 46(1949)30.
Compt.Rend. 228(1949)755.

(3.75) G.S.Landsberg and F.S.Baryshanskaya Doklad.Acad.Nauk. USSR.
61(1948)1027.

(3.76) P.S.Narayanan Proc.Ind.Acad.Sci. A28(1948)469.
A33(1951)240.

(3.77) I.M.Aref'ev a nd P.A.Bazhulin. Soviet Phys. Solid State
7(1965)326.

(3.78) A.I.Stekhanova and E.A.Popova Soviet Phys.Solid State
7(1966)2849.

(3.79) I.P.Kaminow, R.C.C.Leite and S.P.S.Potro
Bull.Am.Phys.Soc. 9(1964)660.

(3.80) I.P.Kaminow, R.C.C.Leite and S.P.S.Porto
J.Phys.Chem.Solids 26(1965)2086.

(3.81) A.S.Barker and M.Tinkham J.Chem.Phys. 38(1963)2257.

(3.82) I.M.Aref'ev, P.A.Bazhulin and T.V.Mikhal'teva
Sov.Phys.Solid State 7(1966)1948.

(3.83) I.P.Kaminow and G.O.Harding Phys.Rev. 129(1963)1562.

I.P.Kaminow Phys.Rev. 138A(1965)1539.

(3.84) I.P.Kaminow Light Scattering Spectra of
Solids. ed. G.B.Wright
Springer-Verlag. N.Y.

(3.85) C.M.Wilson Thesis, The Johns Hopkins Univ.
1971.

(3.86) B.Lavrencic, I.Levstek. B.Zaks andR.Blinc and D.Hazdi
Chem.Phys.Letters 52(1970)2891.

(3.87) R.Blinc. Theory of Condensed Matter I.A.E.A. Vienna p395 1968.

(3.88) R.S.Katiyar, J.F.Ryan and J.F.Scott Proc. Int. Conf. on Light Scattering, Paris 1971.

(3.89) A.Zawdowski and J.Ruvalds Phys.Rev.Letters 24(1970)1111.

(3.90) R.A.Cowley. G.J.Coombs, R.S.Katiyar, J.F.Ryan and J.F.Scott J.Phys.C. 4(1971)L203.

(3.91) A.A.Maradudin and A.A.Fein Phys.Rev. 128(1962)2589.

(3.92) E.M.Brody and H.Z.Cummins Phys.Rev.Letters 21(1968)1263.

(3.93) W.P.Mason Phys.Rev. 69(1946)173.

(3.94) E.M.Brody and H.Z.Cummins Phys.Rev.Letters 23(1969)1039.

(3.95) A.S.Barker and M.Tinkham J.Chem.Phys. 38(1963)2257.

(3.96) T.Kawamura, A.Mitsuishi and H.Yoshinaga J.Phys.Soc.Japan 28(1970)227 Suppl.

(3.97) F.Sugawara and T.Nakamura J.Phys.Soc.Jap. 28(1970)157 Suppl.

(3.98) G.L.Paul, W.Cochran, W.J.L.Buyers and R.A.Cowley Symp. on Inelastic Scattering of Neutrons I.A.E.A. Vienna p265 vol.1 1969.

Phys.Rev. B2(1970)4603.

(3.99) J.Skalyo, B.C.Frazer and G.Shirane Phys.Rev. B1(1970)150.

(3.100) H.Meister, J.Skalyo, B.C.Frazer and G.Shirane Phys.Rev. 184(1969)550.

(3.101) W.P.Mason and B.T.Matthias Phys.Rev. 88(1952)477.

W.P.Mason Phys.Rev. 69(1946)173.

(3.102) I.P.Kaminov and G.O.Harding Phys.Rev. 129(1963)1562.

I.P.Kaminow Phys.Rev.138A(1965)1539.

(3.103) R.M.Hill and S.K.Ichiki Phys.Rev. 128(1962)1140.
130(1963)150.
132(1963)1603.

(3.104) Y.Ishibashi and A.Sawada and Y.Takagi J.Phys.Soc.Jap. 28(1970)1488.

(3.105) C.W.Garland and D.B.Novotny Phys.Rev. 177(1969)971.

(3.106) E.Litov and C.W.Garland Phys.Rev.B2(1970)4592.

(3.107) E.Litov and E.A.Uehling Phys.Rev.Letters 21(1968)809.

(3.108) E.Litov and E.A.Uehling Phys.Rev. B1(1970)3713.

(3.109) L.D.Landau and I.M.Khalatnikov Sov.Phys.Doklady 96(1954)469.

(3.110) S.Y.Geguzina and M.A.Krivoglaz Sov.Phys.Solid State 9(1968)2441.

(3.111) M.Shimshoni and E.Harnik Physics Letters 29A(1969)620.
32A(1970)322.

(3.112) M.Inoue Physics Letters 27A(1968)242.
J.Phys.Soc.Jap. 26(1969)420.

(3.113) W.Reese and L.F.May Phys.Rev. 162(1967)510.
167(1968)504.
181(1969)905.

(3.114) M.Burnstein, J.Grinzberg, I.Pelah and E.Weiner
Solid State Commun. 8(1970)1211.

(4.1) F.A.Jenkins and H.E.White Fundamentals of Optics, McGraw-Hill N.Y.

(4.2) Am.Inst.Phys.Handbook.

(4.3) J.Tschunko J.Opt.Soc.Am.55(1965)1.

M.Born and E.Wolf Principles of Optics, Macmillan N.Y.

(5.1) R.A.Phillips J.Opt.Soc.Am. 56(1966)629.

(5.2) M.Beck and H.Granicher Helv.Phys.Acta 23(1950)522.

(5.3) R.O'B.Carpenter Thesis,Harvard Univ. 1951.

O.G.Blokh and L.F.Lutsiv-Shumskii Sov.Phys.Cryst. 12(1967)380.

(5.4) An Oak Ridge Fortran Program Translated into Atlas Autocode by G.S.Pawley.

(6.1) T.R.Sliker and S.R.Burlage J.App.Phys. 34(1963)1837.

(6.2) I.P.Kaminow Private communication to W.Cochran.

(6.3) W.Cochran Private communication.

(6.4) A.A.Maradudin and A.F.Fein Phys.Rev. 128(1962)2589.

(6.5) R.L.Reese, I.J.Fritz and H.Z.Cummins
Solid State Commun. 15(1971)327.

(6.6) J.F.Ryan, R.S.Katiyar and W.Taylor Second European Meeting on Ferroelectricty, Dijon, 1971.

(7.1) R.W.Gammon and H.Z.Cummins Phys.Rev.Letters 17(1966)193.

(7.2) S.F.Kaplan, M.I.Kay and B.Morosin. Ferroelectrics 1(1970)31.